THE ROLE OF OMICS CHARACTERISTICS IN THE DIAGNOSIS, TREATMENT, AND PROGNOSIS OF AUTOIMMUNE DISEASES

EDITED BY: Zhangran Chen, Ming Zhao, Qinglong Wu and Kang Ning
PUBLISHED IN: Frontiers in Immunology

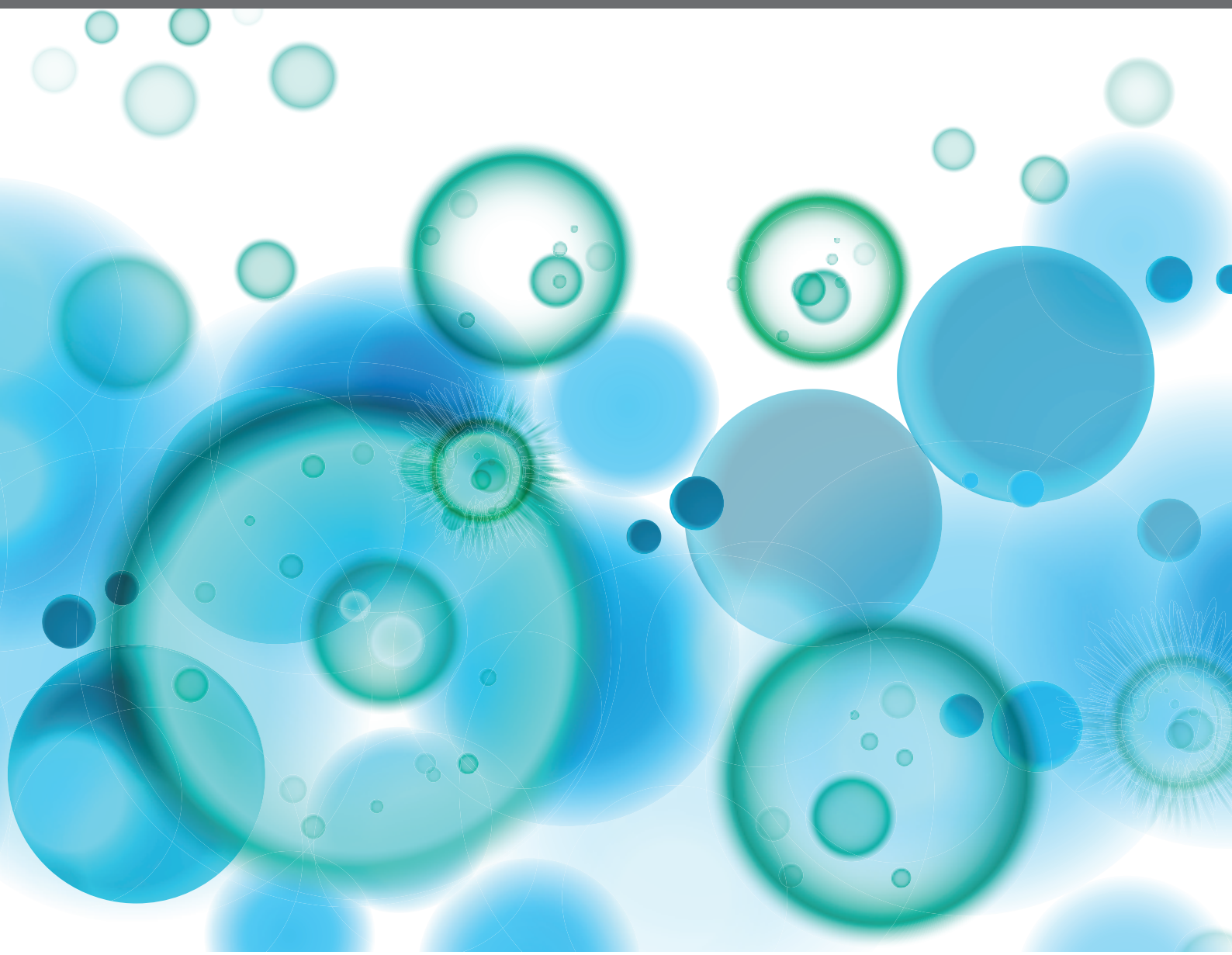

frontiers Research Topics

frontiers

ISSN 1664-8714
ISBN 978-2-83250-803-9
DOI 10.3389/978-2-83250-803-9

About Frontiers

Frontiers is more than just an open-access publisher of scholarly articles: it is a pioneering approach to the world of academia, radically improving the way scholarly research is managed. The grand vision of Frontiers is a world where all people have an equal opportunity to seek, share and generate knowledge. Frontiers provides immediate and permanent online open access to all its publications, but this alone is not enough to realize our grand goals.

Frontiers Journal Series

The Frontiers Journal Series is a multi-tier and interdisciplinary set of open-access, online journals, promising a paradigm shift from the current review, selection and dissemination processes in academic publishing. All Frontiers journals are driven by researchers for researchers; therefore, they constitute a service to the scholarly community. At the same time, the Frontiers Journal Series operates on a revolutionary invention, the tiered publishing system, initially addressing specific communities of scholars, and gradually climbing up to broader public understanding, thus serving the interests of the lay society, too.

Dedication to Quality

Each Frontiers article is a landmark of the highest quality, thanks to genuinely collaborative interactions between authors and review editors, who include some of the world's best academicians. Research must be certified by peers before entering a stream of knowledge that may eventually reach the public - and shape society; therefore, Frontiers only applies the most rigorous and unbiased reviews.
Frontiers revolutionizes research publishing by freely delivering the most outstanding research, evaluated with no bias from both the academic and social point of view. By applying the most advanced information technologies, Frontiers is catapulting scholarly publishing into a new generation.

What are Frontiers Research Topics?

Frontiers Research Topics are very popular trademarks of the Frontiers Journals Series: they are collections of at least ten articles, all centered on a particular subject. With their unique mix of varied contributions from Original Research to Review Articles, Frontiers Research Topics unify the most influential researchers, the latest key findings and historical advances in a hot research area! Find out more on how to host your own Frontiers Research Topic or contribute to one as an author by contacting the Frontiers Editorial Office: frontiersin.org/about/contact

THE ROLE OF OMICS CHARACTERISTICS IN THE DIAGNOSIS, TREATMENT, AND PROGNOSIS OF AUTOIMMUNE DISEASES

Topic Editors:
Zhangran Chen, Xiamen University, China
Ming Zhao, Central South University, China
Qinglong Wu, Baylor College of Medicine, United States
Kang Ning, Huazhong University of Science and Technology, China

MW, YL and ZC were employed by Inner Mongolia Shuangqi Pharmaceutical Co.Ltd. XZ, FL, LC and ZC were employed by Shenzhen Wedge Microbiology Research Co.Ltd.

Citation: Chen, Z., Zhao, M., Wu, Q., Ning, K., eds. (2022). The Role of Omics Characteristics in the Diagnosis, Treatment, and Prognosis of Autoimmune Diseases. Lausanne: Frontiers Media SA. doi: 10.3389/978-2-83250-803-9

Table of Contents

frontiers | Frontiers in Immunology

TYPE Editorial
PUBLISHED 02 November 2022
DOI 10.3389/fimmu.2022.1069918

OPEN ACCESS

EDITED AND REVIEWED BY
Adolfo Andrade-Cetto,
National Autonomous University of Mexico, Mexico

*CORRESPONDENCE
Zhangran Chen
zhangran22105@163.com
Ming Zhao
zhaoming307@csu.edu.cn
Jinmiao Chen
chen_jinmiao@immunol.a-star.edu.sg

†These authors have contributed equally to this work

SPECIALTY SECTION
This article was submitted to Autoimmune and Autoinflammatory Disorders : Autoimmune Disorders, a section of the journal Frontiers in Immunology

RECEIVED 14 October 2022
ACCEPTED 24 October 2022
PUBLISHED 02 November 2022

CITATION
Wu Q, Ning K, Zhao X, Liao F, Wang M, Chang L, Liu Y, Chen J, Zhao M and Chen Z (2022) Editorial: The role of omics characteristics in the diagnosis, treatment, and prognosis of autoimmune diseases. *Front. Immunol.* 13:1069918. doi: 10.3389/fimmu.2022.1069918

Editorial: The role of omics characteristics in the diagnosis, treatment, and prognosis of autoimmune diseases

Qinglong Wu[1†], Kang Ning[2†], Xiaoxiao Zhao[3†], Feng Liao[3], Min Wang[3,4], Longgang Chang[3], Yanmin Liu[4], Jinmiao Chen[5,6*], Ming Zhao[7*] and Zhangran Chen[3,4,8*]

[1]Texas Children's Microbiome Center, Baylor College of Medicine, Houston, TX, United States, [2]School of Life Science and Technology, Huazhong University of Science and Technology, Wuhan, China, [3]Shenzhen Wedge Microbiology Research Co.Ltd, Shenzhen, China, [4]Inner Mongolia Shuangqi Pharmaceutical Co.Ltd, Huhhot, China, [5]Singapore Immunology Network (SIgN), Agency for Science, Technology and Research (ASTAR), Singapore, Singapore, [6]Immunology Translational Research Program, Yong Loo Lin School of Medicine, Department of Microbiology and Immunology, National University of Singapore (NUS), Singapore, Singapore, [7]The Second Xiangya Hospital, Central South University, Changsha, China, [8]Department of Gastroenterology, Zhongshan Hospital Affiliated to Xiamen University, Xiamen, China

KEYWORDS

autoimmune diseases, biomarker, microRNAs, fecal microbiota, rheumatoid arthritis, omics technology

Editorial on the Research Topic
The role of omics characteristics in the diagnosis, treatment, and prognosis of autoimmune diseases

Autoimmune diseases (ADs) represent a type of disease that causes damage to the body due to the disorder of autoantigen immune tolerance and host immune responses to autoantigens. Such defects could affect any part of the body, i.e. weakening bodily function and even turning life-threatening consequences. The incidence of ADs has increased over the past decade, affecting 5% to 8% of the world population and posing great challenge to the healthcare system. Up to now, more than eighty types of autoimmune diseases have been clinically identified. In addition to protect the host against infections, cancers and other diseases, the immune system also produces elevated levels of inflammatory cytokines and auto-antibodies that could induce complex autoimmune disorders (AIDs), such as Type I diabetes (T1D), primary biliary cirrhosis (PBC), rheumatoid arthritis (RA), multiple sclerosis (MS), autoimmune liver disease (ALD), systemic lupus erythematosus (SLE), ankylosing spondylitis (AS), Sjogren syndrome (SS), and polymyositis/dermatomyositis, etc. However, the pathogenesis of ADs and many other diseases, especially certain types of cancers, still remains elusive and needs to be illuminated systematically.

This current Research Topic brings nine articles together presenting and summarizing the most recent research updates, which give us a better understanding of new potential diagnostics and therapeutics for some ADs.

With the increasing attention to the disease and the improvement of diagnostic techniques, the perception of ADs has been gradually improved. The IgG4-RD is an immune-mediated disorder with diverse autoimmune features. Wu et al. identified four major cell types and twenty-one subtypes in IgG4-RD peripheral blood monocytes (PBMCs) by using single-cell RNA-sequencing.Such findings are of great relevance for clinical characterization of IgG4-RD patients. SLE is a chronic systemic inflammatory disease that can affect many organs including kidney, lung, and skin. The CDC27 gene was uniquely found in 24 lupus lineages by using whole-exome sequencing (WES) in combination with multiple analytical methods. This work by Shang et al. revealed that CDC27 gene may serve as a biomarker for the diagnosis of SLE. Of note, WES analytics showed as a useful methodology that might screen causative genes for other diseases through small pedigrees, especially among non-close relatives. RA is an ADs characterized by chronic erosive arthritis. Using comprehensive proteomic analysis, Hu et al. discovered that Orosomucoid 1 (ORM1) in the serum is differentially expressed between healthy subjects and RA patients. ORM1 is correlated with disease activity, $CD56^{dim}$ natural killer cell, effector memory CD8 T cell and natural killer cell in the pathological mechanism, highlighting future research on its role in RA pathogenesis. Psoriatic arthritis (PsA) is a chronic ADs characterized by both joint inflammation and skin psoriasis. Wang et al. identified differential metabolites among PsA patients, RA patients and healthy subjects by using ultra-high-performance liquid chromatography coupled with hybrid triple quadrupole time-of-flight mass spectrometry (UHPLC-Q-TOF-MS). Potential biomarkers including α/β-turmerone, glycerol 1-hexadecanoate, dihydrosphingosine, pantothenic acid and glutamine differentiate PsA from both HC and RA. Given the fact that joint inflammation occurrs in both PsA and RA patients, this study demonstrated the utility of metabolomics for early diagnosis of PsA and even for monitoring host response during treatment. Existing evidence suggests that both dysregulated innate and adaptive immune pathways contribute to the aberrant intestinal inflammatory response in patients with inflammatory bowel disease (IBD), while the exact etiology remains unclear. Using the Transcriptome and Metatranscriptome Meta-Analysis (TaMMA) framework and Cell-type Identification By Estimating Relative Subsets Of RNA Transcripts (CIBERSORT) method, Bai et al. identified and enumerated the composition of twenty-two immune cell types, demonstrating disease-specific (ulcerative colitis vs. Crohn's disease) and lesion-specific immune cell features in IBD. These results would advance further development of precision immunotherapies for IBD.

Blood and serum circulating miRNAs have been explored as important biomarkers for early diagnosis, prognosis and prediction of drug response. Sun et al. profiled exosome miRNAs for early determination of the sensitivity of intravenous glucocorticoid therapy (ivGCs) in graves ophthalmopathy (GO) patients. Mir-885-3p was identified as a biomarker of ivGCs sensitive circulation through miRNA sequencing. This finding provides a scientific basis for the choice of treatment for GO patients and is of great clinical importance for ensuring a good prognosis in patients. Recently, accumulating studies have demonstrated that miRNAs play a key role in various cancers and ADs including RA, LSE, SS and systemic sclerosis. Chang et al. emphasized the important role of miRNA in RA susceptibility, pathogenesis and efficacy evaluation, providing a comprehensive summary to support precision medicine research in RA. Apart from conventional therapeutics, greater attention has also been focused on fecal microbiota transplantation in treating T1DM. He et al. conducted a 1-year follow-up study in two independent pediatric cohorts of T1DM disease, and found that patients in both cohorts showed better glycemic control, improved insulin resistance and no adverse effects post fecal transplantation. This study provides strong evidence for exploring fecal microbiota transplantation to treat T1DM. However, the clinical effectiveness of fecal microbiota transplantation relies on the input microbiota composition from the screened healthy donors. Interestingly, Cheng et al. found long-term travelling significantly changed the enterotype of individuals, i.e. great shifts in gut microbiota composition. Such shifts have been linked to the changes in the environment and diets that would likely account for switching their enterotypes. These results opened new avenues for probing the effects of diet and environment on human gut microbiota composition, as well as the implications of different human gut enterotypes in modelling host immunity and for treating patients with microbiota transplantation procedure.

Overall, this Research Topic provides readers with new ideas for the diagnosis and treatment of ADs. We could already understand from these works that the advancement of researches have promoted the understanding of pathogenesis of ADs. We believe the translation of these findings into clinics could largely improve the diagnosis and treatment of ADs. However, this Research Topic mainly focuses on RA, while less on other ADs. We look forward to more new studies to illustrate the disease-related mechanisms and the application of novel treatments to ADs for the health and wellness of ADs patients.

Author contributions

QW, KN, XZ, FL, MW, LC, YL, ZC wrote and revised this article. QW, KN, JC, MZ and ZC co-edit the Research Topic.

All authors made a substantial, direct, and intellectual contribution to this work and approved it for publication.

Funding

This work is supported by grants from the National Natural Science Foundation of China (Grant No. 81900541).

Acknowledgments

We greatly appreciate the contributions to this Research Topic by all authors and reviewers. We thank all the guest associated editors of the Research Topic, and the editorial board of the journal of Frontiers, for their support. We also appreciate Canhui Lan, from Beijing Rexinchang Biotechnology Research Institute Co. Ltd for his help in promoting this current Research Topic.

Conflict of interest

MW, YL and ZC were employed by Inner Mongolia Shuangqi Pharmaceutical Co.Ltd. XZ, FL, LC and ZC were employed by Shenzhen Wedge Microbiology Research Co.Ltd.

The remaining authors declare that the research was conducted in the absence of any commercial or financial relationships that could be construed as a potential conflict of interest.

Publisher's note

frontiers in Immunology

ORIGINAL RESEARCH
published: 21 February 2022
doi: 10.3389/fimmu.2022.819680

Plasma Exosomes Transfer miR-885-3p Targeting the AKT/NFκB Signaling Pathway to Improve the Sensitivity of Intravenous Glucocorticoid Therapy Against Graves Ophthalmopathy

*Jingxue Sun[1], Jiaxing Wei[1], Yaguang Zhang[1], Jingjing Li[1], Jian Li[1], Jiazhuo Yan[2], Min Guo[3], Jun Han[3] and Hong Qiao[1]**

[1] Department of Endocrinology and Metabolism, The Second Affiliated Hospital of Harbin Medical University, Harbin, China, [2] Department of Gynecological Radiotherapy, Harbin Medical University Cancer Hospital, Harbin, China, [3] Department of Endocrinology and Metabolism, The Fourth Affiliated Hospital of Harbin Medical University, Harbin, China

OPEN ACCESS

Edited by:
Kang Ning, Huazhong University of Science and Technology, China

Reviewed by:
Jialiang Yang, Genesis (Beijing) Co., Ltd., China
Xiuli Peng, Huazhong Agricultural University, China

***Correspondence:**
Hong Qiao
qiaohong@hrbmu.edu.cn

Specialty section:
This article was submitted to Autoimmune and Autoinflammatory Disorders, a section of the journal Frontiers in Immunology

Received: *22 November 2021*
Accepted: *20 January 2022*
Published: *21 February 2022*

Citation:
Sun J, Wei J, Zhang Y, Li J, Li J, Yan J, Guo M, Han J and Qiao H (2022) Plasma Exosomes Transfer miR-885-3p Targeting the AKT/NFκB Signaling Pathway to Improve the Sensitivity of Intravenous Glucocorticoid Therapy Against Graves Ophthalmopathy. Front. Immunol. 13:819680. doi: 10.3389/fimmu.2022.819680

Graves ophthalmopathy (GO), a manifestation of Graves' disease, is an organ-specific autoimmune disease. Intravenous glucocorticoid therapy (ivGCs) is the first-line treatment for moderate-to-severe and active GO. However, ivGCs is only effective in 70%–80% of GO patients. Insensitive patients who choose 12-week ivGCs not only were delayed in treatment but also took the risk of adverse reactions of glucocorticoids. At present, there is still a lack of effective indicators to predict the therapeutic effect of ivGCs. Therefore, the purpose of this study is to find biomarkers that can determine the sensitivity of ivGCs before the formulation of treatment, and to clarify the mechanism of its regulation of ivGCs sensitivity. This study first characterized the miRNA profiles of plasma exosomes by miRNA sequencing to identify miRNAs differentially expressed between GO patients with significant improvement (SI) and non-significant improvement (NSI) after ivGCs treatment. Subsequently, we analyzed the function of the predicted target genes of differential miRNAs. According to the function of the target genes, we screened 10 differentially expressed miRNAs. An expanded cohort verification showed that compared with NSI patients, mir-885-3p was upregulated and mir-4474-3p and mir-615-3p were downregulated in the exosomes of SI patients. Based on statistical difference and miRNA function, mir-885-3p was selected for follow-up study. The *in vitro* functional analysis of exosomes mir-885-3p showed that exosomes from SI patients (SI-exo) could transfer mir-885-3p to orbital fibroblasts (OFs), upregulate the GRE luciferase reporter gene plasmid activity and the level of glucocorticoid receptor (GR), downregulate the level of inflammatory factors, and improve the glucocorticoid sensitivity of OFs. Moreover, these effects can be inhibited by the corresponding miR inhibitor. In addition, we found that high levels of mir-885-3p could inhibit the AKT/NFκB signaling pathway, upregulate the GRE plasmid activity and GR level, and downregulate the level of inflammatory factors of OFs. Moreover, the improvement of glucocorticoid sensitivity by mir-885-3p transmitted by SI-exo can also be inhibited by the AKT/NFκB agonist. Finally, through

the *in vivo* experiment of the GO mouse model, we further determined the relationship between exosomes' mir-885-3p sequence, AKT/NFκB signaling pathway, and glucocorticoid sensitivity. As a conclusion, plasma exosomes deliver mir-885-3p and inhibit the AKT/NFκB signaling pathway to improve the glucocorticoid sensitivity of OFs. Exosome mir-885-3p can be used as a biomarker to determine the sensitivity of ivGCs in GO patients.

Keywords: Graves ophthalmopathy, glucocorticoid sensitivity, plasma exosomes, miR-885-3p, AKT/NFκB signaling pathway

INTRODUCTION

Graves ophthalmopathy (GO) is an organ-specific autoimmune disease associated with Graves' disease (1). 25%–50% of Graves' disease is accompanied by varying degrees of GO. GO significantly affects the appearance of patients. In severe cases, the patient's eyeball is fixed, resulting in corneal ulcer, total ophthalmia, and even blindness. Even mild GO will also lead to a significant decline in the psychological state and quality of life (2).

IvGCs is the first-line treatment for moderate-to-severe active GO. For mild GO, ivGCs is also recommended when the quality of life is seriously affected (3). In other words, most of active GO needs ivGCs treatment. However, ivGCs is only effective in 70%–80% of GO patients (3, 4), which means that at least one GO patient is insensitive to ivGCs in five patients. Insensitive patients who choose 12-week ivGCs not only delay treatment but also bear the risk of adverse reactions of glucocorticoids, such as cortical hyperfunction, severe infection, and organ dysfunction. Therefore, it is very important to find an appropriate method to determine the ivGCs sensitivity of GO patients.

Studies found that the clinical signs of GO patients (5), the duration of eye symptoms and restoration of euthyroidism (6), the response to ivGCs during treatment (7), ocular MRI alone (8, 9), or combined with clinical activity score (CAS) (10) may be helpful to determine the sensitivity of ivGCs. However, some of these methods are subjective and cannot be quantified, and some are expensive and difficult to popularize. Moreover, the time of judging sensitivity by these methods is relatively lagging. Therefore, there is still a lack of effective biomarkers that are convenient to detect and determine the sensitivity of ivGCs before making treatment plans.

The biomarkers that can predict the sensitivity of ivGCs in GO patients mainly include proteins, nucleic acids, and lipids. It is generally believed that the nucleotide sequence change of GR can change the sensitivity of glucocorticoid sensitivity. However, this phenomenon seems not to be found in GO patients treated with ivGCs. A study of 58 GO patients treated with ivGCs found that the 3 GR gene polymorphisms, ER22/23EK, N363s, and BCL1 do not influence the therapeutic effect of steroids (11). Li found that patients with high IgG4 levels responded better to ivGCs treatment (12). However, this does not mean that patients with normal or low IgG4 levels are less sensitive to ivGCs. It has also been confirmed that patients with baseline LDL >193.6 mg/dl may have poor response to ivGCs treatment (13). However, this phenomenon can be ameliorated by lipid-lowering therapy. Studies have shown that serum miR-224-5p may predict whether GO patients are sensitive to ivGCs (14).

Exosomes are 30–150-nm membrane vesicles secreted by almost all types of human cells. In 1983, exosomes were first found in sheep reticulocytes. After nearly 40 years of research, exosome detection technologies are becoming more and more mature, and independent databases of exosomes such as exoRBase (http://www.exorbase.org/exoRBaseV2/toIndex) and exocorta (http://exocarta.org/index.html) were established. However, serum miRNAs are fragile and very sensitive to RNA enzymes in the air, and its level will fluctuate with physical factors. Under the protection of the double-layer membrane structure, plasma exosome miRNAs remain stable without degradation. More importantly, exosome miRNAs can be easily and stably extracted even in long-term frozen samples. Plasma exosome miRNAs may be helpful to determine the sensitivity of ivGCs.

Therefore, the purpose of this study is to search for exosome miRNAs that can early determine the sensitivity of ivGCs in GO patients and to clarify the mechanism of exosome miRNAs regulating glucocorticoid sensitivity. In order to solve this problem, miRNA sequencing was performed on plasma exosomes of SI and NSI patients, and differential expression of exosome miRNAs was analyzed. Candidate miRNAs were screened according to the function of target genes and validated by PCR of the extended cohort. We found that plasma exosome mir-885-3p levels were upregulated in ivGCs-sensitive GO patients. Finally, through *in vitro* and *in vivo* functional analyses of exosome mir-885-3p, we confirmed that SI-exo delivered mir-885-3p into OFs and upregulated the level of mir-885-3p. The upregulated mir-885-3p targeted the inhibition AKT/NFκB signaling pathway and improved the glucocorticoid sensitivity of OFs.

MATERIALS AND METHODS

Patients

A total of 17 patients diagnosed as moderate-to-severe activity GO according to NOSPECS score (**Table S1**) and CAS score (**Table S2**) were included. The above patients were from the Department of Endocrinology and Metabolic Diseases of the Second and Fourth Affiliated Hospitals of Harbin Medical University. According to EUGOGO (3), ivGCs was their first

choice of treatment. The exclusion criteria included the following: 1) inactive or mildly active GO; 2) patients who received orbital radiation therapy, orbital decompression, or other immunosuppressive therapy within the last 3 months; and 3) contraindications of glucocorticoid therapy.

Baseline plasma was obtained before treatment. After 12 weeks of treatment, according to the grouping criteria of enrolled patients (**Table 1**), the patients were divided into SI (n = 11) and NSI (n = 6) groups. This experiment was reviewed by the Ethics Committee of the Second Affiliated Hospital of Harbin Medical University, China (no. KY2016-046).

Exosome Isolation and Identification

Exosomes were isolated from plasma according to the instructions for the Plasma Exosome Extraction Kit (Invitrogen, Carlsbad, CA, USA). The particle size distribution and concentration of exosomes were detected by a NOT analyzer (Zeta View PMX 110, Particle Metrix, Meerbusch, Germany). Exosome morphology was observed by transmission electron microscopy (Hitachi, Tokyo, Japan). Exosome protein concentrations were determined by BCA protein quantification (Beyotime, Shanghai, China). Finally, exosome-specific marker proteins CD9, CD81, and TSG101 were detected by Western blot.

Screening Differentially Expressed Exosome miRNAs

Three patients in both SI and NSI groups were randomly selected for exosome miRNA sequencing. Sequencing data were analyzed, and the differentially expressed exosome miRNAs were defined as miRNAs with p value <0.05 and log2(fold change) ≠ 0.

The target genes of miRNA identified in differential exosomes were predicted by miRanda (15)and RNAhybrid (16), and the intersection of target genes was obtained by the two methods for subsequent analysis. The target gene was enriched and analyzed by Kyoto Encyclopedia of Genes and Genomes (KEGG) and Gene Ontology (Go) to predict the function of the target gene. One KEGG pathway and two Go function target genes related to glucocorticoid pharmacological action were selected, and the intersection was taken to obtain the candidate miRNA target genes. Corresponding miRNAs were screened according to target genes. Finally, expanded cohort verification of differential miRNA was performed on the remaining 11 secrete samples.

TABLE 1 | Grouping criteria of enrolled patients.

	Indicator
1	Exophthalmos decreased by at least 2 mm.
2	The width of palpebral fissure is reduced by at least 3 mm.
3	Gorman diplopia score decreased by at least one grade.
4	Any two items in the NOSPECS score reduced by two grades.
5	Visual acuity improved, and visual acuity chart improved by at least one line.

SI: patients whose CAS score is reduced by at least two points and finally less than 3 points, and who have more than two of the above indicators at the same time; NSI: patients with CAS reduced by less than 2 points or still in active stage; patients with no more than 2 improvements in the above indicators.

Plasmid Construction

The possible sites of mir-885-3p predicting AKT intervention were queried in the miRNA database. Two pairs of DNA single strands (**Table S3**) were designed according to the sequence around the miRNA-binding prediction site gctgcca. After annealing, the DNA single strand was linked to pmirglo (Promega, Madison, WI, USA) plasmid digested with sac I and Xho I, and AKT2 3-UTR and mut-AKT2 3-UTR plasmids were constructed.

Establishment and Treatment of the GO Animal Model

The GO animal model was established by Balb/c female mice aged 8–10 weeks. The establishment method of the model group was the same as our previous study (17), and the control group was given the same amount of PDF. After modeling, 3 mice in the model group and control group were randomly sacrificed. The left orbital tissue of each mouse was used for histological analysis, and the right orbital tissue was resected under aseptic conditions for primary culture OFs.

Other mice in the model group were randomly divided into 6-week treatment group, 9-week treatment group, 12-week treatment group, and corresponding control group. In the first 6 weeks of treatment, mice in the treatment group were given methylprednisolone 1 mg/kg intraperitoneal injection once a week. From the 7th week, the dose of methylprednisolone was adjusted to 0.5 mg/kg. The control group was given the same amount of normal saline. The mice were sacrificed at the 6th, 9th, and 12th weeks of treatment, and their plasma and orbital tissue were collected for analysis. All mice were provided by the Experimental Animal Center of the Second Affiliated Hospital of Harbin Medical University, raised in an environment free of specific pathogens and operated in accordance with the humane animal care standards stipulated by Harbin Medical University. Animal experiment was reviewed by the Ethics Committee of the Second Affiliated Hospital of Harbin Medical University, China (no. KY2017-110).

Primary Cell Culture and Identification

GO mouse extraocular muscle was obtained under aseptic conditions, and primary OFs were cultured. The OFs were cultured in Dulbecco's modified Eagle medium (Corning, Tewksbury, MA, USA) with 10% fetal bovine serum (ExCell Bio, Montevideo, Uruguay) and incubated in a constant 37°C, 5% CO_2-humidified environment. The cells were identified by immunofluorescence.

Immunofluorescence Staining of Exosomes and Cells

500 μg purified exosome suspension was taken and diluted to a volume of 500 μl with sterile 1× PBS. According to the instructions, exosomes were labeled with PKH26 staining kit (Maokangbio, Shanghai, China). After staining, the concentration of the stained exosome suspension was quantified by the BCA method (Beyotime, Shanghai, China), and then aseptic 1× PBS adjusted the exosomes to the appropriate concentration.

5×10^4 OFs were spread to a 24-well plate containing sterile slides. Cells were adjusted to a bottling rate of 50%, and a complete culture medium containing 25 μg/ml PKH26-labeled exosomes was added for 24 h. After PBS cleaning, fixation was performed with 4% formaldehyde solution, room temperature peroxidation with 0.5% Triton X-100 solution (Solarbio, Beijing, China), cytoskeleton staining with FITC working solution (Sigma, San Francisco, CA, USA), and nucleus staining with DAPI (Solarbio, China). Finally, they were observed and photographed by a fluorescence microscope.

miRNA Transfection

The day before transfection, OFs were inoculated into T-25 culture vials in a quantity of 5×10^5 per vial. 10-μl miRNA plasmids (**Table S3**) and Lipofectamine 3000 (Invitrogen, USA) were diluted in the medium and mixed. Each mixed medium was added to OFs for incubation, and the culture was continued for 8 h in the incubator. Complete medium was replaced and expanded to the number required for the experiment.

Western Blotting

The proteins of suspensions OFs, exosomes, and tissues were obtained and quantified by the BCA method (Beyotime, Shanghai, China). Protein lysates were transferred to the PVDF membrane by 8% SDS-PAGE (Beyotime Biotechnology, China). The PVDF membrane was cleaned with TBST and sealed with 5% skim milk powder for 2 h. The cut film was incubated overnight in the primary antibody dilution solution and 2 h in the secondary antibody dilution solution. Finally, the film was scanned. The main antibodies used included HRP-binding GAPDH monoclonal antibody (ProteinTech, Wuhan, China), AKT polyclonal antibody (ProteinTech, China), NFκB P65 polyclonal antibody (ProteinTech, China), Rabbit Anti-phosphorylated NFκB P65 (Ser276) Antibody (Bioss, Beijing, China), Rabbit Anti-phosphorylated AKT (Ser473) antibody (Bioss, China), IL-1α polyclonal antibody (ProteinTech, China), ICAM1 polyclonal antibody (ProteinTech, China), CD9 monoclonal antibody (ProteinTech, China), TSG101 polyclonal antibody (ProteinTech, China), CD81 monoclonal antibody (ProteinTech, China), Goat Anti-mouse IgG (H+L) (ProteinTech, China), Goat anti-rabbit IgG (H+L) (ProteinTech, China), and glucocorticoid receptor polyclonal antibody (ProteinTech, China).

Real-Time Quantitative PCR

TRIzol (Thermo Fisher Scientific, Waltham, MA, USA) extracted total RNA from OFs, exosomes, and tissues. 1 μg RNA was reversed transcribed using the transcript first-strand cDNA synthesis Kit (Roche Diagnostics GmbH, Mannheim, Germany). Thermal cycling conditions were as follows: pre-denaturation at 95°C for 3 min, 95°C for 20 s, and 60°C for 45 s for 40 cycles. Fluorescence was measured at the end of each cycle. Primers were synthesized by Shanghai Tianhao Biotechnology Co., Ltd., China. Detailed sequences information of primers are shown in **Table S4**.

Double Luciferase Activity Detection

The OFs transfected with pGRE-luc (Beyotime, Shanghai, China) and pRL-TK (Beyotime, Shanghai, China) were incubated with lysate, and 300-μl samples were taken into the chemiluminescence detection tube. 500 μl 1× firefly luciferase reaction solution (Solebo Technology Co., Ltd., China) was added to the reaction tube. The Junior LB 9509 chemiluminescence detector detected the luminescence value for 10 s. 500 μl 1× Aquin luciferase reaction solution (Sobibor Technology Co., Ltd., China) was added and gently blown and mixed. The luminescence value was detected by a Junior LB 9509 chemiluminescence detector for 10 s. Relative luciferase activity was calculated based on the two luminescence obtained in each group.

RESULTS

Compared With NSI, Plasma Exosome mir-885-3p Was Upregulated, and mir-4474-3p and mir-615-3p Were Downregulated in SI Patients

In this study, three patients in the SI and NSI groups were randomly selected to extract plasma exosomes (hereinafter referred to as SI-exo, NSI-exo). Transmission electron microscopy, Western blot, and nanoparticle tracking analysis (NTA) were used to verify that the extract was plasma exosome. Transmission electron microscopy showed that there was no significant difference in the morphology of plasma exosomes between SI and NSI, with a diameter of about 100 nm and a typical concave disc-like structure (**Figure 1A**). Western blot showed a positive expression of plasma exosome-specific marker proteins CD9, CD81, and TSG101 (**Figure 1B**). NTA analysis showed that the vesicles at about 100 nm in the SI and NSI groups accounted for more than 95% (**Figure S1**). These results indicated that exosomes were extracted successfully from plasma exosomes. In addition, the BCA quantification of plasma exosome protein in SI and NSI groups was 1.51 ± 0.02 and 1.52 ± 0.01 mg/ml, respectively. There was no statistical difference between the two groups, indicating that there was no significant difference in the concentration of exosome between the two groups.

Subsequently, miRNA expression profiles of 6 plasma exosomes were analyzed by miRNA-seq. A total of 50 differentially expressed exosome miRNAs were screened. Compared with the NSI group, there were 26 upregulated miRNAs and 24 downregulated miRNAs in the SI group (**Figures 1C, D**). The scatter plot of KEGG enrichment (**Figure 1E**) showed the 10 most significant KEGG enrichment signaling pathways, including the cytokine–cytokine receptor interaction, chemokine signaling pathway, ribosome signaling pathway, amino sugar and nucleotide sugar metabolism, etc. 35 target genes enriched in chemokine signaling pathways related to GC pharmacological action were selected for the follow-up study. Bar chart of Go enrichment analysis is shown in **Figure 1F**. A total of 83 Go target genes enriched in cytokine receptor activity and reaction to lipopolysaccharide were selected. The 83 miRNAs and 35 target genes screened from KEGG were intersected, and 12 differentially expressed exosome miRNAs target genes were obtained: *CCR7/CX3CR1/CXCR2/CXCR3/CXCR5/AKT1/CCL5/CXCL1/CXCL2/CXCL3/MAPK3/NFκB1* (**Figure 1G**).

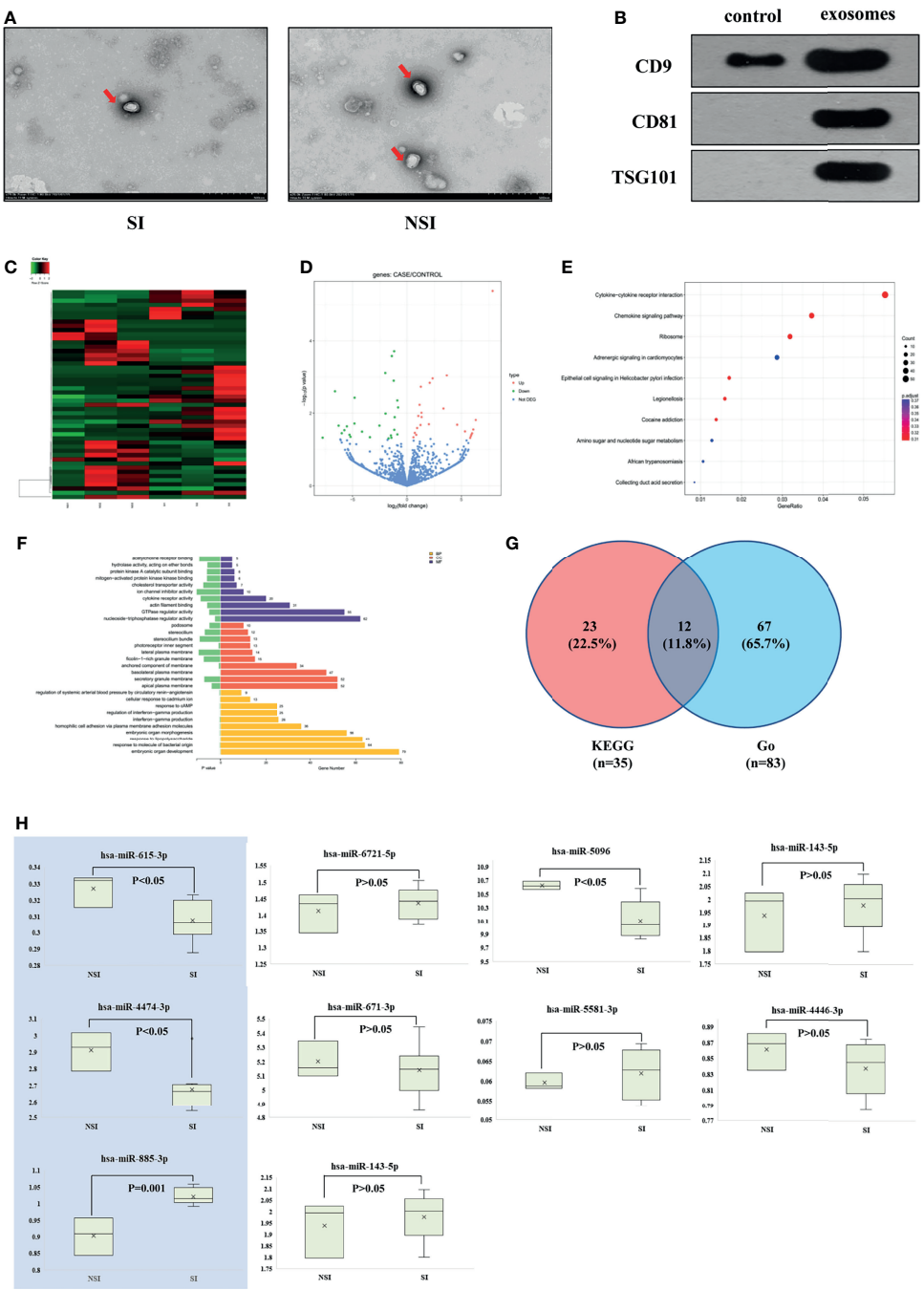

FIGURE 1 | Screening differentially expressed exosome miRNAs. **(A)** Transmission electron microscopy of plasma exosomes of the SI and NSI groups. **(B)** Western blot detected exosome-labeled proteins CD9, CD81, and TSG101. **(C)** Heat map of the cluster analysis of differentially expressed miRNAs among 6 random samples from the SI and NSI groups. **(D)** Volcano map of differentially expressed miRNAs among 6 random samples from the SI and NSI groups. **(E)** Scatter plot of KEGG enrichment in differential exosome miRNA target genes. **(F)** Bar chart of Go enrichment analysis of differential exosome miRNA target genes. **(G)** Veen analysis of differential exosome miRNA target genes. **(H)** PCR results of candidate exosome miRNAs among the remaining samples.

The above 12 target genes correspond to 10 candidate miRNAs. Compared with the NSI group, there were 6 miRNAs upregulated (*miR-6721-5p/miR-5096/miR-4446-3p/miR-885-3p/miR-4433b-3p/miR-671-3p*) and 4 miRNAs downregulated (*miR-615-3p/miR-4474-3p/miR-143-5p/miR-5581-3p*) in the SI group. The levels of the above miRNA in plasma exosomes of the remaining 11 patients were detected by PCR. Compared with the NSI group, the expression of mir-885-3p was highly

expressed ($p = 0.001$), and mir-4474-3p ($p < 0.05$) and mir-615-3p ($p < 0.05$) were low expressed (**Figure 1H**) in exosomes of the SI group. KEGG functional enrichment results showed that *AKT*, the predicted target gene of mir-885-3p, was a classic molecule of the chemokine signaling pathway. NFκB was a downstream protein of the chemokine signaling pathway, and it could regulate the expression of GR to some extent. Meanwhile, the difference of mir-885-3p between the two groups was the most significant ($p = 0.001$). Thus, mir-885-3p was selected for follow-up mechanism research.

SI-exo Improves the GC Sensitivity of OFs

In the above experiments, we observed that patients with upregulation of plasma exosome mir-885-3p at baseline were sensitive to ivGCs. However, it was still unclear whether there was a clear causal relationship and intrinsic association between them. To explore the exact mechanism, it was necessary to confirm that the increased glucocorticoid sensitivity was caused by exosomes.

At first, we cultured primary OFs from GO mice and identified them and then screened the optimal DEX, exosome intervention concentration, and time of OFs. The GO mice used in this project were derived from our recently reported study (17). It could be seen that the eyes of the mice in the model group are obviously prominent, bulbar conjunctival edema, tears, and increased periocular secretions (**Figure 2A**). Pathological results showed the fat infiltration between the optic nerve and muscles and the extraocular myositis cell infiltration of the model mice (**Figure 2B**). The primary culture of OFs was performed on GO mouse extraocular muscle. The immunofluorescence results showed that vimentin staining was positive, confirming that the extracted cells were OFs (**Figure 2C**). We treated with OFs at 0.1, 1, and 10 μM DEX conditions for 1, 12, and 24 h, respectively. It could be seen that the OFs under 24-h treatment with 0.1 μM DEX and the GR expression level were the highest (**Figure 2D**), and GRE luciferase reporter plasmid activity was the highest (**Figure 2E**). Therefore, the intervention concentration and time point of DEX were selected as 0.1 μM for 24 h. Subsequently, we used exosomes with protein concentrations of 0, 1.5, 3, 6.25, 12.5, and 25 μg/ml to intervene OFs 24 h. CCK8 found that exosomes had the greatest influence on cells under the condition of 25 μg/ml acting on OFs for 24 h. Therefore, 25 μg/ml for 24 h was selected as the intervention concentration and time point of exosomes (**Figure 2F**).

In order to explore the effect of exosome miRNAs on OFs, it was necessary to confirm that exosomes could enter into OFs. We cocultured 25 μg/ml plasma exosomes labeled with PKH26 (red fluorescence under the microscope) with OFs for 24 h. The merged image of immunofluorescence showed that the plasma exosomes were endocytosed by OFs (**Figure 2G**). Subsequently, we explored the effect of exosomes on the glucocorticoid sensitivity of OFs. We treated OFs with 25 μg/ml SI-exo and NSI-exo at 0.1 μM DEX for 24 h. It was found that SI-exo significantly upregulated the GRE luciferase reporter plasmid activity of OFs compared with NSI-exo ($p < 0.001$) (**Figure 2H**). At the same time, after SI-exo treatment, GR protein and mRNA levels were significantly upregulated ($p < 0.01$), and the protein ($p < 0.01$) and mRNA ($p < 0.001$) levels of inflammatory factors interleukin-1 (IL-1) and intercellular cell adhesion molecule-1 (ICAM-1) were significantly downregulated (**Figures 2I, J**). It could be seen that SI-exo can improve the glucocorticoid sensitivity of OFs.

SI-exo Improves the Glucocorticoid Sensitivity of OFs by Transferring mir-885-3p

Previous experiments had confirmed that SI-exo could improve the glucocorticoid sensitivity of OFs, but it still cannot prove that the regulation of SI-exo on glucocorticoid sensitivity was achieved by changing the level of miR-885-3p in OFs. In the following experiments, we confirmed the above hypothesis. We treated OFs with 25 μg/ml SI-exo and NSI-exo, respectively, under 0.1 μM DEX for 24 h. We found that both SI-exo and NSI-exo could upregulate the level of mir-885-3p of OFs. Compared with NSI-exo, SI-exo had a stronger upregulation effect on the level of mir-885-3p of OFs ($p < 0.001$) (**Figure 3A**). Subsequently, we added the miR-inhibitor and inhibitor NC respectively on the basis of the above grouping. It was observed that when the SI-exo and miR-inhibitors intervened in cells at the same time, the level of mir-885-3p was significantly lower than that of SI-exo alone under the condition of 0.1 μM DEX ($p < 0.001$). The same trend results also appeared in the NSI-exo group. This indicates that the miR inhibitor can inhibit well the upregulation of miR-885-3p by exosomes (**Figure 3B**). We also observed the GRE luciferase reporter gene plasmid activity and GR, IL-1, ICAM-1 protein, and mRNA levels in each group. It was found that under the condition of 0.1 μM DEX, compared with that treated with SI-exo alone, the GRE luciferase reporter gene plasmid activity of OFs treated with SI-exo and miR inhibitor was significantly decreased ($p < 0.001$) (**Figure 3C**), the GR protein and mRNA levels were significantly downregulated ($p < 0.001$), and inflammatory factor IL-1 and ICAM-1 protein levels ($p < 0.001$) and mRNA levels ($p < 0.01$) were significantly upregulated (**Figures 3D, E**). In other words, when the upregulation of SI-exo on miR-885-3p was blocked by the miR inhibitor, the effect of SI-exo on improving OF glucocorticoid sensitivity was weakened. That is, SI-exo enhances the glucocorticoid sensitivity of OFs by transferring miR-885-3p.

Mir-885-3p Upregulates Glucocorticoid Sensitivity of OFs

We attempted to explore the relationship between miR-885-3p and glucocorticoid sensitivity. For this purpose, mir-885-mimics and mir-NC were used to treat OFs under 0.1 μM DEX for 24 h. It was found that mir-885-3p levels were upregulated after the addition of mir-885-3p mimics, which confirmed the good upregulation effect of mir-885-mimics on mir-885-3p (**Figure 4A**). Then, we detected the GRE luciferase reporter gene plasmid activity and GR, IL-1, ICAM-1 protein, and mRNA levels of each group of OFs. It was found that when mir-885-3p was upregulated, GRE gene plasmid activity increased ($p < 0.001$)

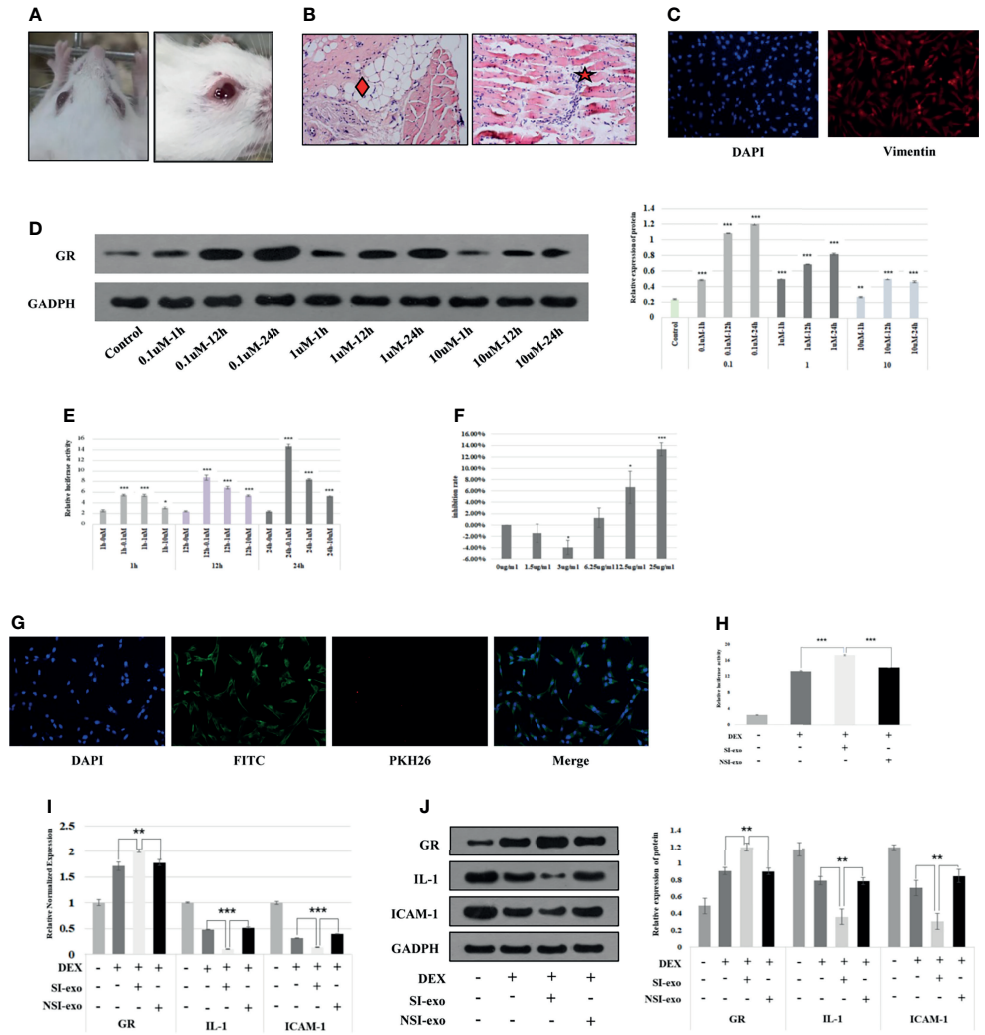

FIGURE 2 | SI-exo improves the glucocorticoid sensitivity of OFs. **(A)** Eye pictures of GO mice. **(B)** HE staining of retrobulbar tissue of GO mice (SP*200); "◆": fat infiltration; "★": inflammatory cell infiltration. **(C)** Results of primary OFs immunofluorescence identification; DAPI: labeling the OF nucleus with blue fluorescence; Vimentin: labeling vimentin with red fluorescence. **(D)** The Western blot result of the GR protein expression level when OFs in DEX at 0.1, 1, and 10 μM for 1, 12, and 24 h, respectively. Compared with the control group: *$p < 0.05$; **$p < 0.01$; ***$p < 0.001$. **(E)** The GRE luciferase reporter plasmid activity result when OFs in DEX at 0.1, 1, and 10 μM for 1, 12, and 24 h. Compared with the 0-μM group: *$p < 0.05$; **$p < 0.01$; ***$p < 0.001$. **(F)** CCK8 results of OFs in exosomes at 1, 1.5, 3, 6.25, 12.5, and 25 μg/ml for 24 h. Compared with the 0-μg/ml group: *$p < 0.05$; ***$p < 0.001$. **(G)** Immunofluorescence results of coculture of plasma exosomes and OFs. DAPI: labeling the OF nucleus with blue fluorescence; PKH26: labeling plasma exosomes with red fluorescence; FITC: labeling cytoskeleton with green fluorescence. **(H)** Plasmid activity of GRE luciferase reporter gene results in each group. DEX: 0.1 μm DEX-treated OFs for 24 h; SI-exo/NSI-exo: 25 μg/ml SI-exo/NSI-exo-treated OFs for 24 h; *$p < 0.05$; **$p < 0.01$; ***$p < 0.001$. **(I)** Statistical chart of PCR detection of GR, IL-1, and ICAM-1 mRNA levels in each group. Grouping and statistical methods are the same as **(I)**. **(J)** Western blot detection of GR, IL-1, and ICAM-1 protein levels and statistical chart in each group. Grouping and statistical methods are the same as **(I)**.

(**Figure 4B**), the GR level was significantly upregulated ($p<0.001$), and inflammatory factors were significantly downregulated (**Figures 4C, D**). The above results suggested that mir-885-3p upregulates the glucocorticoid sensitivity of OFs.

Mir-885-3p Upregulates Glucocorticoid Sensitivity of OFs by Regulating AKT/NFκB

In the following experiments, we explored the endogenous association between mir-885-3p upregulation and increased the glucocorticoid sensitivity. In the previous target gene prediction of differentially expressed exosome miRNAs, we predicted that mir-885-3p might be able to target the regulation of *AKT*. At the same time, *AKT* was also one of the 12 target genes of differential exosome miRNA. Therefore, we constructed AKT2 3′-UTR and mut-AKT2 3′-UTR plasmids by using *AKT* as the downstream target gene of mir-885-3p. 293T cells and OFs were co-transfected with miRNA mimics, miR-NC, recombinant plasmid, and empty plasmid. Compared with the control group, the luciferase activity of the 293T cells co-transfected

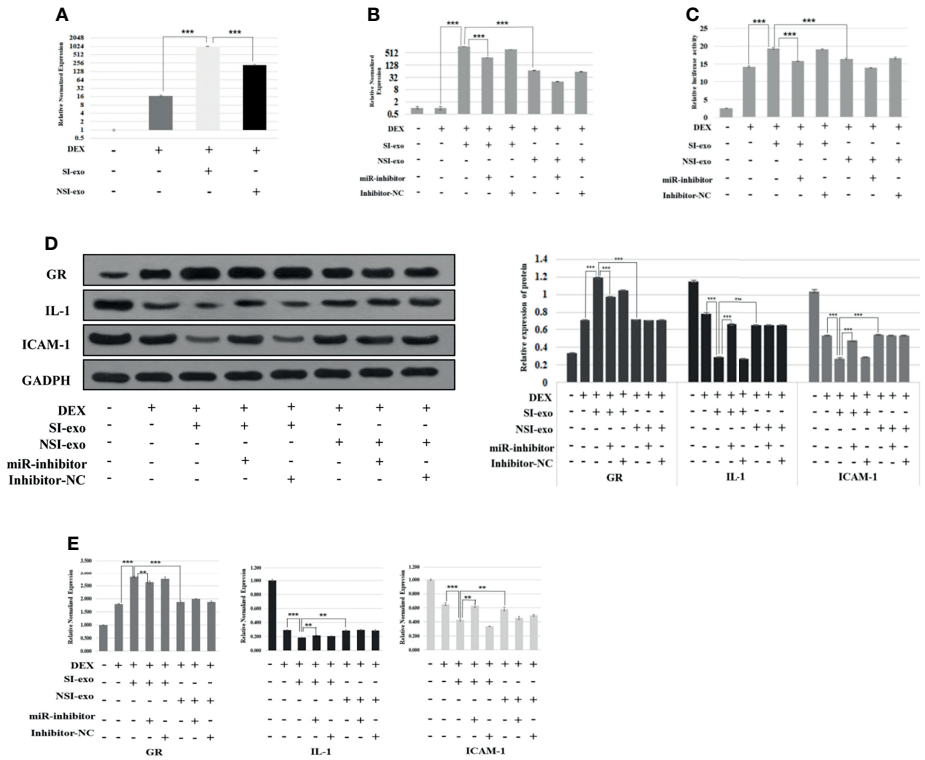

FIGURE 3 | SI-exo improves the glucocorticoid sensitivity of OFs by transmitting mir-885-3p. **(A, B)** Statistical chart of PCR detection of mir-885-3p in each group. DEX: 0.1 μm DEX-treated OFs for 24 h; SI-exo/NSI-exo: 25 μg/ml SI-exo/NSI-exo-treated OFs for 24 h; miR-885-3p: miR-885-mic-treated OFs for 24 h; miR-nc: NC miRNA-treated OFs for 24 h; $^{**}p < 0.01$; $^{***}p < 0.001$. **(C)** Plasmid activity of GRE luciferase reporter gene results in each group; grouping and statistical methods are the same as in **(B)**; **(D)** Western blot detection of GR, IL-1, and ICAM-1 protein levels in each group; grouping and statistical methods are the same as in **(B)**. **(E)** Statistical chart of PCR detection of GR, IL-1, and ICAM-1 mRNA levels in each group; grouping and statistical methods are the same as in **(B)**.

with mir-885-mimics and AKT2 3-UTR recombinant plasmid was significantly decreased after transfection 48 h ($p < 0.001$) (**Figure 4E**). Western blot results showed that the AKT level of OFs significantly decreased after transfection of mir-885-mimics ($p < 0.001$) (**Figure 4F**). The targeted regulation of *AKT* by mir-885-3p was confirmed.

Subsequently, we transfected mir-885-mimic and mir-NC under 0.1-μM DEX conditions and treated OFs for 24 h. Western results showed that the AKT, pAKT, NFκB, and pNFκB protein levels of OFs were changed, especially pAKT ($p < 0.001$) and pNFκB ($p < 0.001$) levels which were significantly downregulated (**Figure 4G**) after transfection with mir-885-mimic compared with that of mir-NC. The trend of AKT and NFκB mRNA levels in each group was consistent with Western blot results (**Figure 4H**). It was confirmed that upregulated mir-885-3p regulates the AKT/NFκB signaling pathway.

On the basis of the above grouping, we added AKT agonist SC79 as mir-885-SC79 group and mir-NC-SC79 group, respectively. We found that the mir-885-3p level in the mir-885-SC79 group was significantly higher than that in the mir-NC-SC79 group after the addition of SC79, indicating that SC79 did not affect the upregulation of mir-885-3p by the mir-885-mimic (**Figure 4I**). Analysis of GRE luciferase reporter gene plasmid activity showed that the GRE gene plasmid activity in the mir-885-3p group was significantly higher than that in the DEX group and the mir-NC group ($p < 0.001$), but the GRE gene plasmid activity was significantly decreased after the addition of SC79 ($p < 0.001$) (**Figure 4J**). Similarly, the protein and mRNA levels of GR in the mir-885 group were significantly higher than those in the mir-NC group ($p < 0.001$), and the protein and mRNA levels of inflammatory factors IL-1 and ICAM-1 were lower than those in the Mir-NC group ($p < 0.001$). After the addition of SC79, the protein and mRNA levels of GR, IL-1, and ICAM1 showed an opposite trend compared with the mir-885-3p group (**Figures 4K, L**). These results suggested that mir-885-3p regulates glucocorticoid sensitivity through the AKT/NFκB pathway.

SI-exo Transmits mir-885-3p to Target AKT/NFκB Upregulates the Glucocorticoid Sensitivity of OFs

In the above experiment, we confirmed that mir-885-3p delivery by SI-exo increases the glucocorticoid sensitivity of OFs and upregulated mir-885-3p targeting regulates AKT/NFκB and improves the glucocorticoid sensitivity of OFs. Next, we

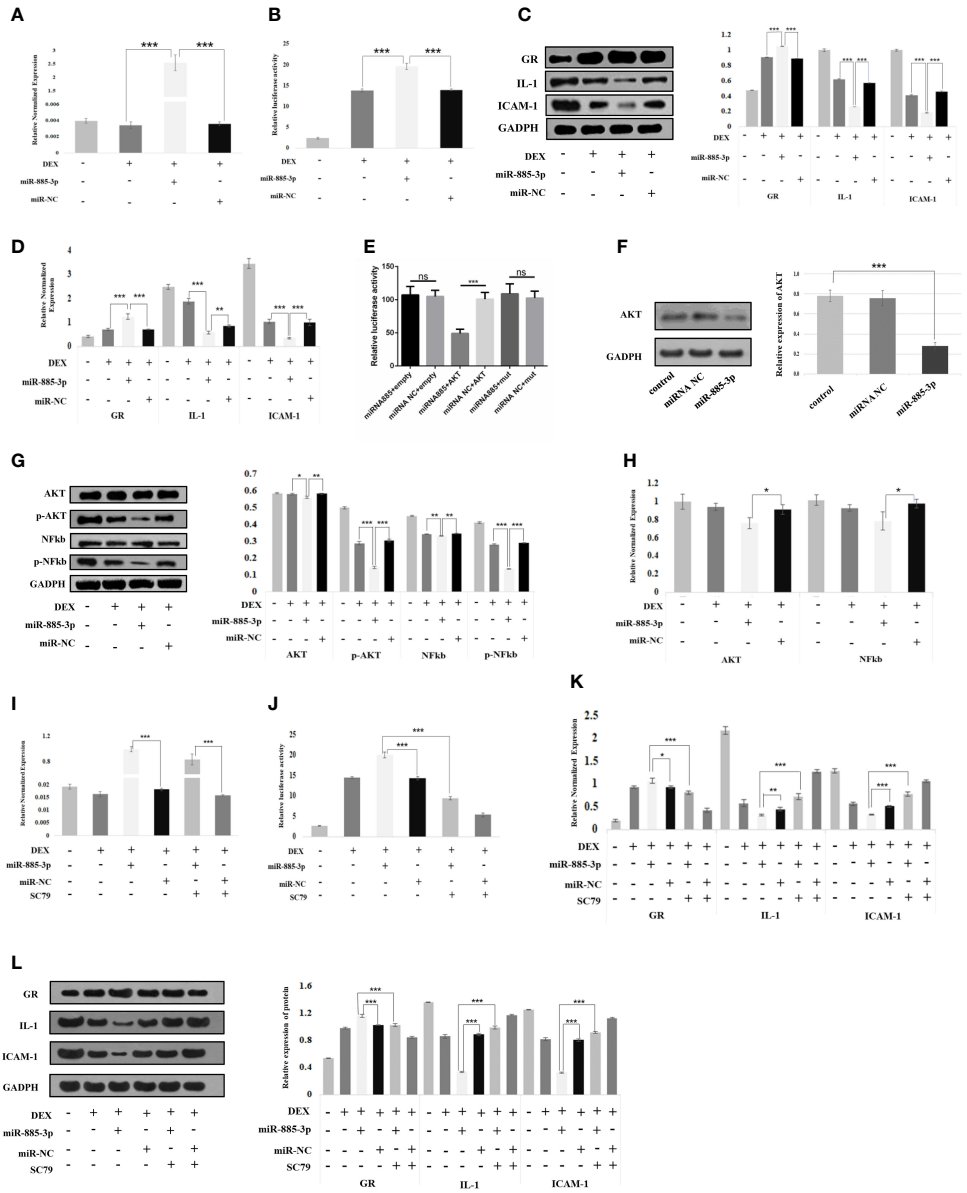

FIGURE 4 | Mir-885-3p regulated the glucocorticoid sensitivity of OFs by targeting AKT/NFκB. **(A)** Statistical chart of PCR detection of mir-885-3p in each group. DEX: 0.1 μm DEX-treated OFs for 24 h; miR-885-3p: miR-885-mic-treated OFs for 24 h; miR-NC: NC miRNA-treated OFs for 24 h; $^{*}p < 0.05$; $^{**}p < 0.01$; $^{***}p < 0.001$. **(B)** Plasmid activity of GRE luciferase reporter gene results in each group; grouping and statistical methods are the same as in **(A)**. **(C)** Western blot detection of GR, IL-1, and ICAM-1 protein levels in each group; grouping and statistical methods are the same as in **(A)**. **(D)** Statistical chart of PCR detection of GR, IL-1, and ICAM-1 mRNA levels in each group; grouping and statistical methods are the same as in **(A)**. **(E)** The results of double luciferase in 293T cells; miRNA-885: miRNA-885-3p mimics co-transfected with plasmid; miRNA NC: corresponding NC miRNA co-transfected with plasmid; empty: co-transfected plasmid was empty; AKT: co-transfected plasmid was AKT2 3′-UTR recombinant plasmid; mut: co-transfected plasmid was mut-AKT2 3′-UTR recombinant plasmid; ns, no statistical significance; $^{***}p < 0.001$. **(F)** Western blot detection of AKT protein levels in each group; grouping and statistical methods are the same as in **(A)**. **(G)** Western blot detection of AKT, pAKT, NFκB, and pNFκB protein levels in each group; grouping and statistical methods are the same as in **(A)**. **(H)** Statistical chart of PCR detection of AKT and NFκB mRNA levels in each group; grouping and statistical methods are the same as in **(A)**. **(I)** Statistical chart of PCR detection of mir-885-3p in each group. DEX: 0.1 μm DEX-treated OFs for 24 h; miR-885-3p: miR-885-mic-treated OFs for 24 h; miR-NC: NC miRNA-treated OFs for 24 h; SC79: AKT agonist-treated OFs for 24 h; $^{*}p < 0.05$; $^{**}p < 0.01$; $^{***}p < 0.001$. **(J)** Plasmid activity of GRE luciferase reporter gene results in each group; grouping and statistical methods are the same as in **(I)**. **(K)** Statistical chart of PCR detection of GR, IL-1, and ICAM-1 mRNA levels in each group; grouping and statistical methods are the same as in **(I)**. **(L)** Western blot detection of GR, IL-1, and ICAM-1 protein levels in each group; grouping and statistical methods are the same as in **(I)**.

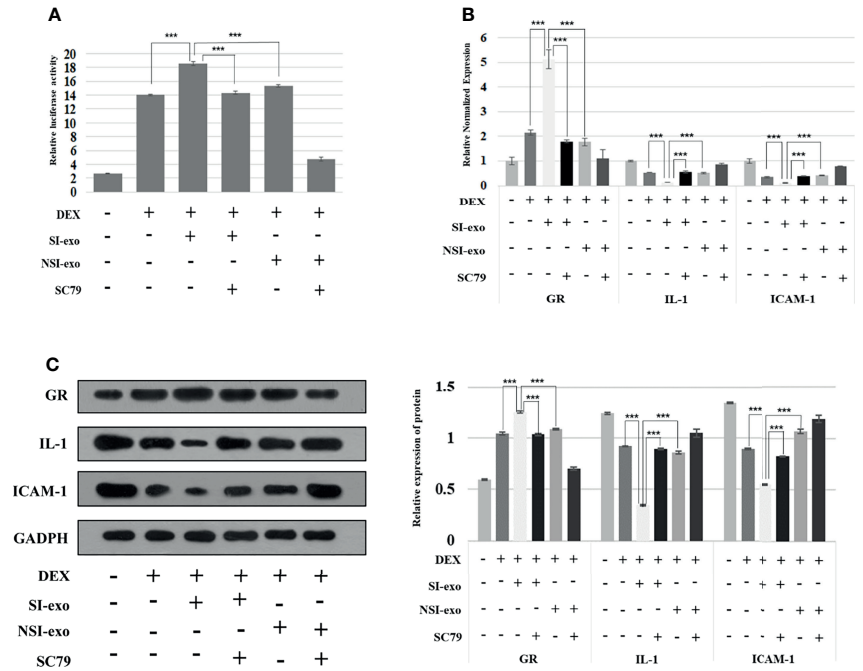

FIGURE 5 | SI-exo transfer miR-885-3p targeting AKT/NFκB improving the glucocorticoid sensitivity of OFs. **(A)** Plasmid activity of GRE luciferase reporter gene results in each group. DEX: 0.1 μm DEX-treated OFs for 24 h; SI-exo/NSI-exo: 25 μg/ml SI-exo/NSI-exo-treated OFs for 24 h; SC79: AKT agonist-treated OFs for 24 h; ***$p < 0.001$. **(B)** Statistical chart of PCR detection of GR, IL-1, and ICAM-1 mRNA levels in each group; grouping and statistical methods are the same as in **(A)**. **(C)** Western blot detection of GR, IL-1, and ICAM-1 protein levels in each group; grouping and statistical methods are the same as in **(A)**.

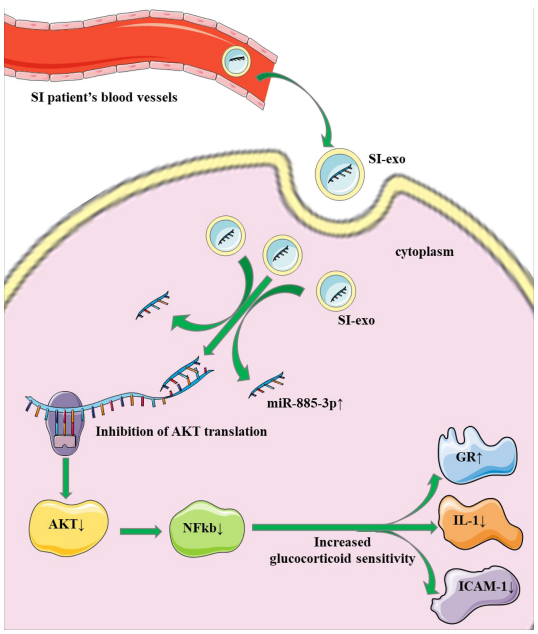

FIGURE 6 | Mechanism pattern of exosome mir-885-3p improving the glucocorticoid sensitivity of OFs.

attempted to link the two conclusions together, confirming that mir-885-3p delivered by SI-exo also improved the glucocorticoid sensitivity of OFs by regulating AKT/NFκB. Under 0.1-μM DEX conditions, SC79 was added into OFs treated with SI-exo and NSI-exo. Compared with OFs treated with SI-exo alone, the plasmid activity of the GRE luciferase reporter gene in the OFs treated with both SI-exo and SC79 decreased significantly ($p < 0.001$) (**Figure 5A**), the levels of GR protein and mRNA decreased significantly ($p < 0.001$), and the levels of protein and mRNA of inflammatory factors IL-1 and ICAM-1 increased significantly ($p < 0.001$). The same trend results also appeared in the NSI-exo group (**Figures 5B, C**). In other words, when the AKT/NFκB signaling pathway was activated, the effect of exosomes on OF glucocorticoid sensitivity weakened. In conclusion, SI-exo delivered mir-885-3p into OFs, upregulated the OF mir-885-3p level, targeted the inhibition AKT/NFκB signaling pathway, and improved the glucocorticoid sensitivity of OFs (**Figure 6**).

The Relationship Between Exosome mir-885-3p Sequence, AKT/NFκB, and Glucocorticoid Sensitivity Exists *In Vivo*

In previous studies, we elucidated the intrinsic association between plasma exosomes with high mir-885-3p levels and glucocorticoid sensitivity. However, the results of *in vitro* experiments could not fully represent the mechanism *in vivo*. Therefore, GO mice were

TABLE 2 | Statistical table of mouse grouping.

Group	6 week(n)	9 week(n)	12 week(n)
Control	2	2	3
Sensitive	6	3	3
Insensitive	7	11	9
Total	15	16	15

treated with glucocorticoid and sacrificed at the 6th, 9th, and 12th weeks of the treatment course, respectively, to observe whether the relationship between mir-885-3p sequence and AKT/NFκB and glucocorticoid sensitivity existed *in vivo*.

The mice sacrificed at each time point were divided into glucocorticoid-sensitive group and insensitive group by orbital tissue histopathology. At the 6th week of treatment, nearly half of the mice had poor response, and at weeks 9 and 12, the proportion of mice with poor response decreased (**Table 2**). HE staining results of the orbital tissues in different groups of mice at each time point showed infiltration of inflammatory cells and connective tissue in the control group and the insensitive group. In contrast, muscle fibers in the sensitive group were smooth, and no such changes were observed in the interfascicles (**Figure 7A**). The sequence levels of plasma exosome mir-883-3p in each group of mice in **Table 2** were detected, and it was found that compared with the glucocorticoid-insensitive group, the sequence levels of plasma exosome mir-883-3p in the glucocorticoid-sensitive group were upregulated at week 6 ($p < 0.01$), week 9 ($p < 0.01$), and week 12 ($p < 0.001$) of the treatment course (**Figure 7B**). Finally, we detected the protein levels of GR, AKT, and NFκB in the orbital tissues of the two groups at 12 weeks after treatment. Compared with the insensitive mice, GR expression in the orbital tissues of the sensitive group was upregulated ($p < 0.001$), while AKT ($p < 0.001$) and NFκB ($p < 0.001$) were downregulated (**Figure 7C**). These results suggested that the relationship between the level of mir-885-3p sequence in exosome, AKT/NFκB, and glucocorticoid sensitivity still existed *in vivo*.

DISCUSSION

As the first-line treatment for GO, ivGCs has a sensitivity rate of only 70%–80%. At present, there is still a lack of biomarkers to effectively predict the curative effect of ivGCs. In this study, biomarkers that can predict the sensitivity of ivGCs before the formulation of diagnosis and treatment were explored by clinical sample sequencing, cell functional experiments, and *in vivo* validation of animal models, and the mechanism of their regulation of ivGCs sensitivity was elucidated.

Exosomes maintain normal physiological processes by acting on target cells and play an important role in the occurrence and development of diseases (18, 19). It has long been established that plasma exosomes are closely related to pathophysiological processes in the body. However, since Salomon et al. found in 2016 that the plasma exosome concentration changes with gestation age and status (20), the discussion on whether the relationship between exosomes and body is caused by the change in the concentration of exosome itself or the change of its contents has been continuing (20–22). In this study, we quantified the protein concentration of exosomes in SI and NSI patients, and the results showed that there was no significant difference in plasma exosomes concentration between the two groups. This suggested that the differences in miRNA levels detected in subsequent sequencing and validation results were caused by changes in corresponding miRNA content in exosomes, rather than changes in exosome concentration per unit volume of plasma.

MiRNAs are known to be associated with many diseases (23–25). In this study, miRNA sequencing technology was used to comprehensively analyze the miRNA expression profiles of ivGCs sensitive and insensitive patients. 50 differentially expressed exosome miRNAs were obtained by bioinformatics. In order to further explore the functions of these exosome miRNAs and screen target miRNAs related to glucocorticoids, we performed KEGG and Go enrichment analyses of different miRNA target genes. The chemokine signaling pathway enriched by KEGG is closely related to the pharmacological action of glucocorticoids (26, 27). The downstream protein of the chemokine signaling pathway is NFκB, and the anti-inflammatory effect of glucocorticoids is mainly achieved through the transcriptional inhibition of NFκB by GR (14, 28). At the same time, NFκB can regulate the expression of GR to some extent (29). Studies have shown that chemokines can affect the central nervous system response to reactive glucocorticoids by mediating T cell directional migration (30), and GR signal transduction caused by endogenous glucocorticoid rhythm changes can also lead to rhythmic fluctuations in chemokine receptor levels (31). Based on the above evidence, 35 differential exosome miRNA target genes enriched by KEGG into the chemokine signaling pathway were selected for follow-up analysis in this study. Go enrichment analysis results showed that differential exosome miRNA target genes were significantly enriched in cytokine receptor activity and response to lipopolysaccharide, which were closely related to the mechanism of glucocorticoids (32–36). Studies have found that increased stress of lipopolysaccharide can lead to GR exon variation (35), and the increase in ITS content is positively correlated with the expression of GR-β (36). GR itself acts as a cytokine receptor, and its ability to respond to glucocorticoids is closely related to cytokine receptor activity. Therefore, 83 target genes enriched in the above two Go functions were selected in this study, and the intersection with the above 35 target genes was obtained to obtain 12 differentially expressed exosome miRNA target genes, which correspond to 10 candidate miRNAs. According to Go and KEGG functional enrichment results, miRNA target genes differentially expressed in SI and NSI groups were mostly enriched in glucocorticoid-related pathways. Thus, the differential exosome miRNAs screened in this study are closely related to ivGCs sensitivity.

To further clarify miRNAs associated with ivGCs sensitivity, 10 candidate exosome miRNAs were verified by qRT-PCR in the extended cohort. Mir-885-3p, mir-4474-3p, and mir-615-3p showed significant differences between the two groups, which can be used as potential biomarkers to determine the sensitivity

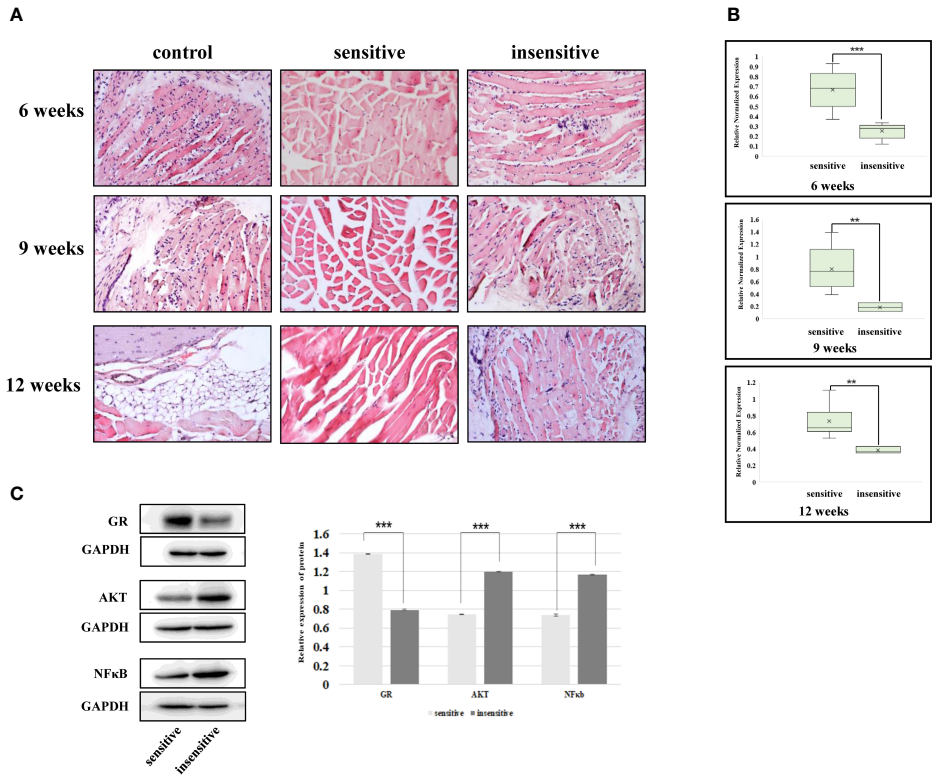

FIGURE 7 | The relationship between exosomes' mir-885-3p sequence, AKT/NFκB, and glucocorticoid sensitivity exists *in vivo*. **(A)** HE staining results of GO mice in the 6th, 9th, and 12th weeks of treatment. **(B)** The level of mir-885-3p sequence in plasma exosomes of mice in the 6th, 9th, and 12th weeks of treatment; $^{**}p < 0.01$; $^{***}p < 0.001$. **(C)** Western blot detection of GR, AKT, and NFκB protein levels; $^{***}p < 0.001$.

of ivGCs in GO patients. Based on statistical differences and miRNA functions, mir-885-3p was selected for follow-up study. To sum up, we only observed that patients with upregulation of plasma exosome mir-885-3p at baseline were sensitive to ivGCs. However, whether there is a clear causal relationship between them and the exact mechanism are still unclear. To explore the relationship between them, we performed cytological function analysis of SI-exo.

Studies have shown that specific miRNAs delivered by exosomes can affect the function of cocultured cells (19, 37). These results indicate that miRNAs in plasma exosomes can be transported to recipient cells through exosomes and then regulate functions of cells, although the parental cells of plasma exosomes selected in this study are not clear. However, exosome miRNA transmission is not a random process; exosomes play a role by binding with target cells through specific mechanisms (38). Therefore, at first, we confirmed that exosomes can be successfully ingested by OFs and upregulated mir-885-3p levels of OFs. These results suggest that plasma exosomes deliver mir-885-3p into OFs.

Next, we investigated the effect of plasma exosomes which transported mir-885-3p on the glucocorticoid sensitivity of OFs. For this purpose, four indicators were selected in this study to reflect the glucocorticoid sensitivity of cells. The IvGCs treatment of Graves ophthalmopathy is mainly because of its anti-inflammatory effects. The mechanism of its receptor GR is in the form of the inactive OF cytoplasm. After the glucocorticoid enters the cells, the cells within the passive diffusion combined with GR form the receptor and the ligand complexes to nuclear transfer, combined with the target gene promoter sequences of GRE, inhibiting inflammatory cytokine gene transcription (39). Therefore, the sensitivity of cells to glucocorticoid can be reflected by the transcriptional activation level of GRE, GR expression level, and inflammatory factor level. In this study, we found that when SI-exo was ingested by OFs, the GRE luciferase reporter gene plasmid activity, GR protein, and mRNA levels were significantly increased, and the levels of inflammatory factors decreased correspondingly. In other words, the glucocorticoid sensitivity of OFs increased. However, when mir-885-3p delivered by SI-exo was inhibited by the mir inhibitor, the effect of SI-exo on the glucocorticoid sensitivity of OFs was weakened. These results confirm that SI-exo enhances the glucocorticoid sensitivity of OFs by delivering mir-885-3p.

Subsequently, we attempted to find the internal relationship between mir-885-3p and OF glucocorticoid sensitivity. Prior to this, we first need to confirm that changes in mir-885-3p levels affect OF glucocorticoid sensitivity. In this study, it was found that when mir-885-3p was upregulated in OFs, the plasmid activity of GRE luciferase reporter gene and the GR protein

and mRNA levels were significantly increased. The levels of IL-1 and ICAM-1 protein and mRNA decreased correspondingly. These results confirmed that the high level of mir-885-3p can increase the glucocorticoid sensitivity of OFs.

Therefore, what is the pathway through which mir-885-3p regulates glucocorticoid sensitivity? Exosome miRNAs can downregulate target protein levels by regulating posttranscriptional translation (40). Current studies have found that mir-885-3p can regulate the functions of multiple target genes such as *HOXB2* (41), *TLR4* (42), and *Aurora A* (43). Among the 12 differential exosome miRNAs target genes obtained by KEGG and Go (*CCR7/CX3CR1/CXCR2/CXCR3/CXCR5/AKT1/CCL5/CXCL1/CXCL2/CXCL3/MAPK3/NFκB1*), we predicted that mir-885-3p targeted the regulation of *AKT*. As a classical molecule of the chemokine signaling pathway, AKT regulates the expression of downstream protein NFκB (44), which is consistent with KEGG functional enrichment results. Therefore, we hypothesized that the mir-885-3p-targeted regulation of the AKT/NFκB signaling pathway enhances the glucocorticoid sensitivity of OFs.

The luciferase activity of mir-885-3p mimics and the AKT2 3′-UTR recombinant plasmid group was significantly reduced by dual luciferase reporter gene assay, confirming that mir-885-3p can target the 3′-UTR of *AKT*. In addition, to further verify the regulatory relationship, Western blot analysis showed that the AKT protein level of OFs was significantly downregulated after transfection with mir-885-3p. These results jointly confirmed that mir-885-3p can target and inhibit AKT expression. Subsequently, we found that when the AKT/NFκB pathway was excited by SC79, the promoting effect of mir-885-3p on glucocorticoid sensitivity disappeared. In other words, mir-885-3p enhances the glucocorticoid sensitivity of OFs by target regulation of AKT/NFκB.

For the sake of rigor, we further investigated whether mir-885-3p delivered by SI-exo also plays a role through AKT/NFκB. The results showed that when the AKT/NFκB pathway was activated by SC79, the promoting effect of mir-885-3p delivered by SI-exo on glucocorticoid sensitivity was also weakened. That is, mir-885-3p delivered by SI-exo improved the glucocorticoid sensitivity of OFs *via* AKT/NFκB.

It is worth mentioning that we found that the NSI-exo group also showed the same trend as SI-exo. NSI-exo can also upregulate the level of mir-885-3p in OFs and affect the levels of GR, IL-1, and ICAM-1. This effect can also be inhibited by the miR-inhibitor. This is because NSI-exo also contains a small amount of miR-885-3p. This also confirmed the effect of exosome mir-885-3p on the glucocorticoid sensitivity of OFs to some extent. However, since miR-885-3p in NSI-exo is not as high as in SI-exo, the effect of NSI-exo on OFs is limited. Similar phenomena have been seen in clinical cases. After ivGCs treatment, NSI group patients also showed a slight improvement. In other words, NSI group patients also have little response to ivGCs. We speculate that these responses are related to the small amount of mir-885-3p in plasma exosomes of NSI group patients. However, these slight improvements do not mean that ivGCs treatment completely alleviates the condition of NSI patients. It also does not mean that NSI patients are sensitive to ivGCs. This may be related to the insufficient amount of mir-885-3p in plasma exosomes of patients with NSI. It can also confirm our conclusion to some extent.

However, the mechanism described above was found *in vitro*. It remains unclear whether the mechanism holds true *in vivo*. In the patients we collected in this study, neither the SI group nor the NSI group received surgical treatment. Therefore, we have no way to obtain the patients' posterior tissue to verify the above mechanism. We solve this problem through animal experiments. We treated GO mice with glucocorticoid and observed the relationship between mir-885-3p sequence level in plasma exosomes, AKT/NFκB level in orbital tissues, and glucocorticoid sensitivity in mice, confirming that our conclusions still hold *in vivo*.

We treated GO mice with glucocorticoid, and the mice were sacrificed at the 6th, 9th, and 12th weeks of the course, respectively. The mice were divided into glucocorticoid-sensitive group and insensitive group according to the pathological manifestations of orbital tissues histopathology. At the 6th week of treatment, about half (6/13) of mice were insensitive to glucocorticoid, while at the 9th and 12th weeks, the proportion of insensitive mice decreased to 3/14 and 3/12, respectively. The proportion of glucocorticoid-insensitive mice was similar at weeks 9 and 12. This result is consistent with the report by Guia that the sensitivity of ivGCs can be judged according to the response of GO patients during 6–8 weeks of treatment (5), which also confirms the accuracy of the results of this study. This suggests that glucocorticoid sensitivity in GO mice may be determined by performance at week 9 of treatment.

Due to the large amount of plasma required for extraction of exosomes and the small body weight of mice, it cannot ensure that mice can still survive when enough plasma is collected. Therefore, the existing technique in this study was unable to detect baseline plasma exosome mir-883-3p sequence levels in mice. We supported the conclusion of this study by detecting the level of plasma exosome mir-883-3p sequence in mice at the 6th, 9th, and 12th weeks of treatment. It was found that compared with the insensitive group, plasma exosome mir-885-3p sequence and GR level were upregulated, and AKT and NFκB levels were downregulated in the sensitive group after glucocorticoid treatment, which was consistent with the results *in vitro* experiment. We confirm that the changes of exosome mir-885-3p sequence, AKT/NFκB, and glucocorticoid sensitivity still existed *in vivo*.

CONCLUSION

In conclusion, this study provided the effective plasma exosome miRNA expression profile of GO patients by miRNA sequencing and searched stable and easily detected circulating biomarkers of ivGCs sensitivity. Meanwhile, the mechanism of exosome mir-885-3p regulating the sensitivity of ivGCs was elucidated: SI-Exo transfer mir-885-3p targeting the AKT/NFκB signaling pathway improves the ivGCs sensitivity of GO patients. Plasma exosome mir-885-3p is expected to become a reliable and feasible biomarker to predict GO patients' sensitivity of ivGCs. It provides a scientific basis for the selection of treatment

methods for GO patients and is of great significance to ensure the good prognosis of patients.

DATA AVAILABILITY STATEMENT

The original contributions presented in the study are publicly available. These data can be found here: https://www.ncbi.nlm.nih.gov/geo/query/acc.cgi?acc=GSE190515.

ETHICS STATEMENT

The studies involving human participants were reviewed and approved by the Ethics Committee of the Second Affiliated Hospital of Harbin Medical University, China (no. KY2016-046). The patients/participants provided their written informed consent to participate in this study. The animal study was reviewed and approved by the Ethics Committee of the Second Affiliated Hospital of Harbin Medical University, China (no. KY2017-110).

AUTHOR CONTRIBUTIONS

HQ conceived the idea of this manuscript. JS performed the experiment. JW, YZ, JjL, JL, JY, MG, and JH collected the data and performed the data analysis. JS wrote the manuscript. All authors contributed to the article and approved the submitted version.

FUNDING

This work was supported by the National Natural Science Fund of China (grant nos. 81872560 and 82073491).

SUPPLEMENTARY MATERIAL

The Supplementary Material for this article can be found online at: https://www.frontiersin.org/articles/10.3389/fimmu.2022.819680/full#supplementary-material

Supplementary Figure 1 | NTA analysis of plasma exosomes. Percentage: the proportion of vesicles with different sizes.

REFERENCES

1. Sadeghi Y, Oberic A, Theintz G, Hamedani M. Graves' Ophthalmopathy in a Paediatric Population. *Klin Monbl Augenheilkd* (2017) 234:591–4. doi: 10.1055/s-0043-100566
2. Wiersinga WM. Quality of Life in Graves' Ophthalmopathy. *Best Pract Res Clin Endocrinol Metab* (2012) 26:359–70. doi: 10.1016/j.beem.2011.11.001
3. Bartalena L, Baldeschi L, Boboridis K, Eckstein A, Kahaly GJ, Marcocci C, et al. The 2016 European Thyroid Association/European Group on Graves' Orbitopathy Guidelines for the Management of Graves' Orbitopathy. *Eur Thyroid J* (2016) 5:9–26. doi: 10.1159/000443828
4. Zang S, Ponto KA, Kahaly GJ. Clinical Review: Intravenous Glucocorticoids for Graves' Orbitopathy: Efficacy and Morbidity. *J Clin Endocrinol Metab* (2011) 96:320–32. doi: 10.1210/jc.2010-1962
5. Ahn HY, Lee JK. Intravenous Glucocorticoid Treatment for Korean Graves' Ophthalmopathy Patients. *J Korean Med Sci* (2020) 35:e177. doi: 10.3346/jkms.2020.35.e177
6. Wang Y, Zhang S, Zhang Y, Liu X, Gu H, Zhong S, et al. A Single-Center Retrospective Study of Factors Related to the Effects of Intravenous Glucocorticoid Therapy in Moderate-to-Severe and Active Thyroid-Associated Ophthalmopathy. *BMC Endocr Disord* (2018) 18:13. doi: 10.1186/s12902-018-0240-8
7. Bartalena L, Veronesi G, Krassas GE, Wiersinga WM, Marcocci C, Marinò M, et al. Does Early Response to Intravenous Glucocorticoids Predict the Final Outcome in Patients With Moderate-to-Severe and Active Graves' Orbitopathy? *J Endocrinol Invest* (2017) 40:547–53. doi: 10.1007/s40618-017-0608-z
8. Hu H, Chen HH, Chen W, Wu Q, Chen L, Zhu H, et al. T2 Mapping Histogram at Extraocular Muscles for Predicting the Response to Glucocorticoid Therapy in Patients With Thyroid-Associated Ophthalmopathy. *Clin Radiol* (2021) 76:159.e151–159.e158. doi: 10.1016/j.crad.2020.09.005
9. Zhai L, Luo B, Wu H, Wang Q, Yuan G, Liu P, et al. Prediction of Treatment Response to Intravenous Glucocorticoid in Patients With Thyroid-Associated Ophthalmopathy Using T2 Mapping and T2 IDEAL. *Eur J Radiol* (2021) 142:109839. doi: 10.1016/j.ejrad.2021.109839
10. Xu L, Li L, Xie C, Guan M, Xue Y. Thickness of Extraocular Muscle and Orbital Fat in MRI Predicts Response to Glucocorticoid Therapy in Graves' Ophthalmopathy. *Int J Endocrinol* (2017) 2017:3196059. doi: 10.1155/2017/3196059
11. Vannucchi G, Covelli D, Campi I, Origo D, Currò N, Cirello V, et al. The Therapeutic Outcome to Intravenous Steroid Therapy for Active Graves' Orbitopathy is Influenced by the Time of Response But Not Polymorphisms of the Glucocorticoid Receptor. *Eur J Endocrinol* (2014) 170:55–61. doi: 10.1530/EJE-13-0611
12. Li Y, Luo B, Zhang J, Zhou X, Shao S, Xu W, et al. Clinical Relevance of Serum Immunoglobulin G4 in Glucocorticoid Therapy of Graves' Ophthalmopathy. *Clin Endocrinol (Oxf)* (2021) 95:657–67. doi: 10.1111/cen.14493
13. Naselli A, Moretti D, Regalbuto C, Arpi ML, Lo Giudice F, Frasca F, et al. Evidence That Baseline Levels of Low-Density Lipoproteins Cholesterol Affect the Clinical Response of Graves' Ophthalmopathy to Parenteral Corticosteroids. *Front Endocrinol (Lausanne)* (2020) 11:609895. doi: 10.3389/fendo.2020.609895
14. Shen L, Huang F, Ye L, Zhu W, Zhang X, Wang S, et al. Circulating microRNA Predicts Insensitivity to Glucocorticoid Therapy in Graves' Ophthalmopathy. *Endocrine* (2015) 49:445–56. doi: 10.1007/s12020-014-0487-4
15. Betel D, Wilson M, Gabow A, Marks DS, Sander C. The microRNA.Org Resource: Targets and Expression. *Nucleic Acids Res* (2008) 36:D149–153 doi: 10.1093/nar/gkm995
16. Rehmsmeier M, Steffen P, Hochsmann M, Giegerich R. Fast and Effective Prediction of microRNA/Target Duplexes. *RNA* (2004) 10:1507–17. doi: 10.1261/rna.5248604
17. Hao M, Sun J, Zhang Y, Zhang D, Han J, Zhang J, et al. Exploring the Role of SRC in Extraocular Muscle Fibrosis of the Graves' Ophthalmopathy. *Front Bioeng Biotechnol* (2020) 8:392. doi: 10.3389/fbioe.2020.00392
18. Jin T, Gu J, Li Z, Xu Z, Gui Y. Recent Advances on Extracellular Vesicles in Central Nervous System Diseases. *Clin Interv Aging* (2021) 16:257–74. doi: 10.2147/CIA.S288415
19. Yang J, Hagen J, Guntur KV, Allette K, Schuyler S, Ranjan J, et al. A Next Generation Sequencing Based Approach to Identify Extracellular Vesicle Mediated mRNA Transfers Between Cells. *BMC Genomics* (2017) 18:987. doi: 10.1186/s12864-017-4359-1
20. Salomon C, Scholz-Romero K, Sarker S, Sweeney E, Kobayashi M, Correa P, et al. Gestational Diabetes Mellitus Is Associated With Changes in the Concentration and Bioactivity of Placenta-Derived Exosomes in Maternal Circulation Across Gestation. *Diabetes* (2016) 65:598–609. doi: 10.2337/db15-0966
21. Salomon C, Scholz-Romero K, Sarker S, Sweeney E, Kobayashi M, Correa P, et al. Gestational Diabetes Mellitus Is Associated With Changes in the Concentration

and Bioactivity of Placenta-Derived Exosomes in Maternal Circulation Across Gestation. *Diabetes* (2016) 65:598–609. doi: 10.2337/db15-0966
22. Liu J, Wang SZ, Wang QL, Du JG, Wang BB. Gestational Diabetes Mellitus is Associated With Changes in the Concentration and Bioactivity of Placental Exosomes in the Maternal Circulation Across Gestation. *Eur Rev Med Pharmacol Sci* (2018) 22:2036–43. doi: 10.26355/eurrev_201804_14733
23. Xu J, Zhu W, Cai L, Liao B, Meng Y, Xiang J, et al. LRMCMDA: Predicting miRNA-Disease Association by Integrating Low-Rank Matrix Completion With miRNA and Disease Similarity Information. *IEEE Access* (2020) 8:80728–38. doi: 10.1109/ACCESS.2020.2990533
24. Xu J, Cai L, Liao B, Zhu W, Wang P, Meng Y, et al. Identifying Potential miRNAs-Disease Associations With Probability Matrix Factorization. *Front Genet* (2019) 10:1234. doi: 10.3389/fgene.2019.01234
25. Yao Y, Ji B, Shi S, Xu J, Xiao X, Yu E, et al. IMDAILM: Inferring miRNA-Disease Association by Integrating lncRNA and miRNA Data. *IEEE Access* (2019) 8:16517–27. doi: 10.1109/ACCESS.2019.2958055
26. Hosoya T, Shukla NM, Fujita Y, Yao S, Lao FS, Baba H, et al. Identification of Compounds With Glucocorticoid Sparing Effects on Suppression of Chemokine and Cytokine Production by Rheumatoid Arthritis Fibroblast-Like Synoviocytes. *Front Pharmacol* (2020) 11:607713. doi: 10.3389/fphar.2020.607713
27. Yang J, Peng S, Zhang B, Houten S, Schadt E, Zhu J, et al. Human Geroprotector Discovery by Targeting the Converging Subnetworks of Aging and Age-Related Diseases. *Geroscience* (2020) 42:353–72. doi: 10.1007/s11357-019-00106-x
28. Liu C, Wei D, Xiang J, Ren F, Huang L, Lang J, et al. An Improved Anticancer Drug-Response Prediction Based on an Ensemble Method Integrating Matrix Completion and Ridge Regression. *Mol Ther Nucleic Acids* (2020) 21:676–86. doi: 10.1016/j.omtn.2020.07.003
29. Shang L, Smith AJ, Reilly CS, Duan L, Perkey KE, Wietgrefe S, et al. Vaccine-Modified NF-kB and GR Signaling in Cervicovaginal Epithelium Correlates With Protection. *Mucosal Immunol* (2018) 11:512–22. doi: 10.1038/mi.2017.69
30. Schweingruber N, Fischer HJ, Fischer L, van den Brandt J, Karabinskaya A, Labi V, et al. Chemokine-Mediated Redirection of T Cells Constitutes a Critical Mechanism of Glucocorticoid Therapy in Autoimmune CNS Responses. *Acta Neuropathol* (2014) 127:713–29. doi: 10.1007/s00401-014-1248-4
31. Besedovsky L, Born J, Lange T. Endogenous Glucocorticoid Receptor Signaling Drives Rhythmic Changes in Human T-Cell Subset Numbers and the Expression of the Chemokine Receptor CXCR4. *FASEB J* (2014) 28:67–75. doi: 10.1096/fj.13-237958
32. Yalinbas EE, Sezgin Evim M, Bor O, Gulbas Z. Cytokine Profile, Apoptosis, Glucocorticoid Receptor, and P-Glycoprotein Expression Before and After Megadose Methylprednisolone Treatment in Children With Acute Immune Thrombocytopenia. *J Pediatr Hematol Oncol* (2019) 41:574–8. doi: 10.1097/MPH.0000000000001366
33. Pap R, Ugor E, Litvai T, Prenek L, Najbauer J, Nemeth P, et al. Glucocorticoid Hormone Differentially Modulates the *In Vitro* Expansion and Cytokine Profile of Thymic and Splenic Treg Cells. *Immunobiology* (2019) 224:285–95. doi: 10.1016/j.imbio.2018.12.002
34. Yuan M, Hu M, Lou Y, Wang Q, Mao L, Zhan Q, et al. Environmentally Relevant Levels of Bisphenol A Affect Uterine Decidualization and Embryo Implantation Through the Estrogen Receptor/Serum and Glucocorticoid-Regulated Kinase 1/Epithelial Sodium Ion Channel Alpha-Subunit Pathway in a Mouse Model. *Fertil Steril* (2018) 109:735–744 e731. doi: 10.1016/j.fertnstert.2017.12.003
35. Green TL, Leventhal SM, Lim D, Cho K, Greenhalgh DG. Lipopolysaccharide Stress Induces Cryptic Exon Splice Variants of the Human Glucocorticoid Receptor. *Shock* (2019) 52:590–7. doi: 10.1097/SHK.0000000000001318
36. Wang SB, Chen SM, Zhu KS, Zhou B, Chen L, Zou XY. Increased Lipopolysaccharide Content Is Positively Correlated With Glucocorticoid Receptor-Beta Expression in Chronic Rhinosinusitis With Nasal Polyps. *Immun Inflamm Dis* (2020) 8:605–14. doi: 10.1002/iid3.346
37. Fu C, Zhang Q, Wang A, Yang S, Jiang Y, Bai L, et al. EWI-2 Controls Nucleocytoplasmic Shuttling of EGFR Signaling Molecules and miRNA Sorting in Exosomes to Inhibit Prostate Cancer Cell Metastasis. *Mol Oncol* (2021) 15:1543–65. doi: 10.1002/1878-0261.12930
38. Zou J, Shi M, Liu X, Jin C, Xing X, Qiu L, et al. Aptamer-Functionalized Exosomes: Elucidating the Cellular Uptake Mechanism and the Potential for Cancer-Targeted Chemotherapy. *Anal Chem* (2019) 91:2425–30. doi: 10.1021/acs.analchem.8b05204
39. Ji JY, Jing H, Diamond SL. Shear Stress Causes Nuclear Localization of Endothelial Glucocorticoid Receptor and Expression From the GRE Promoter. *Circ Res* (2003) 92:279–85. doi: 10.1161/01.RES.0000057753.57106.0B
40. Gou L, Xue C, Tang X, Fang Z. Inhibition of Exo-miR-19a-3p Derived From Cardiomyocytes Promotes Angiogenesis and Improves Heart Function in Mice With Myocardial Infarction *via* Targeting HIF-1alpha. *Aging (Albany NY)* (2020) 12:23609–18. doi: 10.18632/aging.103563
41. Chen X, Li LQ, Qiu X, Wu H. Long Non-Coding RNA HOXB-AS1 Promotes Proliferation, Migration and Invasion of Glioblastoma Cells *via* HOXB-AS1/miR-885-3p/HOXB2 Axis. *Neoplasma* (2019) 66:386–96. doi: 10.4149/neo_2018_180606N377
42. Zhang X, Gu H, Wang L, Huang F, Cai J. MiR-885-3p Is Down-Regulated in Peripheral Blood Mononuclear Cells From T1D Patients and Regulates the Inflammatory Response *via* Targeting TLR4/NF-kappaB Signaling. *J Gene Med* (2020) 22:e3145. doi: 10.1002/jgm.3145
43. Cao J, Geng J, Chu X, Wang R, Huang G, Chen L. MiRNA8853p Inhibits Docetaxel Chemoresistance in Lung Adenocarcinoma by Downregulating Aurora A. *Oncol Rep* (2019) 41:1218–30. doi: 10.3892/or.2018.6858
44. Ranjani S, Kowshik J, Sophia J, Nivetha R, Baba AB, Veeravarmal V, et al. Activation of PI3K/Akt/NF-kB Signaling Mediates Swedish Snus Induced Proliferation and Apoptosis Evasion in the Rat Forestomach: Modulation by Blueberry. *Anticancer Agents Med Chem* (2020) 20:59–69. doi: 10.2174/1871520619666191024115738

Conflict of Interest: The authors declare that the research was conducted in the absence of any commercial or financial relationships that could be construed as a potential conflict of interest.

Publisher's Note: All claims expressed in this article are solely those of the authors and do not necessarily represent those of their affiliated organizations, or those of the publisher, the editors and the reviewers. Any product that may be evaluated in this article, or claim that may be made by its manufacturer, is not guaranteed or endorsed by the publisher.

frontiers in Immunology

ORIGINAL RESEARCH
published: 24 February 2022
doi: 10.3389/fimmu.2022.848994

Microbiome Resilience and Health Implications for People in Half-Year Travel

Mingyue Cheng[1†], Hong Liu[1,2†], Maozhen Han[1†], Shuai Cheng Li[3], Dongbo Bu[4,5], Shiwei Sun[4,5], Zhiqiang Hu[2], Pengshuo Yang[1], Rui Wang[2], Yawen Liu[2], Feng Chen[2], Jianjun Peng[2], Hong Peng[2], Hongxing Song[2], Yang Xia[2], Liqun Chu[2], Quan Zhou[2], Feng Guan[2], Jing Wu[2], Guangming Tan[4,5*] and Kang Ning[1*]*

[1] Key Laboratory of Molecular Biophysics of the Ministry of Education, Hubei Key Laboratory of Bioinformatics and Molecular-Imaging, Center of AI Biology, Department of Bioinformatics and Systems Biology, College of Life Science and Technology, Huazhong University of Science and Technology, Wuhan, China, [2] Beijing Shijitan Hospital, Capital Medical University, Beijing, China, [3] Department of Computer Science, City University of Hong Kong, Hong Kong, Hong Kong SAR, China, [4] Key Lab of Intelligent Information Processing, State Lab of Computer Architecture, Institute of Computing Technology, Chinese Academy of Sciences, Beijing, China, [5] School of Computer and Control, University of Chinese Academy of Sciences, Beijing, China

Travel entail change in geography and diet, both of which are known as determinant factors in shaping the human gut microbiome. Additionally, altered gut microbiome modulates immunity, bringing about health implications in humans. To explore the effects of the mid-term travel on the gut microbiome, we generated 16S rRNA gene and metagenomic sequencing data from longitudinal samples collected over six months. We monitored dynamic trajectories of the gut microbiome variation of a Chinese volunteer team (VT) in their whole journey to Trinidad and Tobago (TAT). We found gut microbiome resilience that VT's gut microbial compositions gradually transformed to the local TAT's enterotypes during their six-month stay in TAT, and then reverted to their original enterotypes after VT's return to Beijing in one month. Moreover, we identified driven species in this bi-directional plasticity that could play a role in immunity modulation, as exemplified by *Bacteroides dorei* that attenuated atherosclerotic lesion formation and effectively suppressed proinflammatory immune response. Another driven species *P. copri* could play a crucial role in rheumatoid arthritis pathogenesis, a chronic autoimmune disease. Carbohydrate-active enzymes are often implicated in immune and host-pathogen interactions, of which glycoside hydrolases were found decreased but glycosyltransferases and carbohydrate esterases increased during the travel; these functions were then restored after VT' returning to Beijing. Furthermore, we discovered these microbial changes and restoration were mediated by VT people's dietary changes. These findings indicate that half-year travel leads to change in enterotype and functional patterns, exerting effects on human health. Microbial intervention by dietary guidance in half-year travel would be conducive to immunity modulation for maintaining health.

Keywords: travel, enterotype, microbiome, bi-directional plasticity, resilience, dietary shift, immunity, health

OPEN ACCESS

Edited by:
Li-Tung Huang, Kaohsiung Chang Gung Memorial Hospital, Taiwan

Reviewed by:
Jialiang Yang, Geneis (Beijing) Co. Ltd., China
Lei Zhang, Shandong University, China

***Correspondence:**
Jing Wu
wujingsjt@gmail.com
Guangming Tan
tgm@ict.ac.cn
Kang Ning
ningkang@hust.edu.cn

†These authors have contributed equally to this work

Specialty section:
This article was submitted to Autoimmune and Autoinflammatory Disorders, a section of the journal Frontiers in Immunology

Received: *05 January 2022*
Accepted: *07 February 2022*
Published: *24 February 2022*

Citation:
Cheng M, Liu H, Han M, Li SC, Bu D, Sun S, Hu Z, Yang P, Wang R, Liu Y, Chen F, Peng J, Peng H, Song H, Xia Y, Chu L, Zhou Q, Guan F, Wu J, Tan G and Ning K (2022) Microbiome Resilience and Health Implications for People in Half-Year Travel. Front. Immunol. 13:848994. doi: 10.3389/fimmu.2022.848994

INTRODUCTION

Human gut microbes form dynamic and interweaved communities (1, 2), shaped by environmental factors such as geography and diet (3, 4). Previous studies have indicated that the human gut microbiome can respond rapidly to short-term environmental changes (5–7). In comparison, during long-term (> 1 year) environmental changes, the composition of an individual's gut microbial community is predominantly determined by dietary habits (8, 9); such dynamics of the gut microbial community are highly variable among individuals (10, 11).

Immigration brings about long-term changes in geography and diet, leading to variation of the human gut microbiome (12). Vangay et al. investigated the dynamics of the gut microbiome during migration from a non-Western country to the United States of America (USA), demonstrating a westernization of an immigrated individual's gut microbiome whose diversity was greatly decreased and that the USA-associated strains became dominated in the gut microbiome (12). Moreover, a study conducted on Irish Traveller revealed that the gut microbiome of Irish Traveler has gradually shifted from the non-industrialized pattern to an industrialized pattern, correlated with the degree to which Travellers have adopted the new non-nomadic lifestyle (13). Furthermore, the westernized or industrialized gut microbiome might increase the risk of obesity (12), and the risk of auto-immune disorders and chronic diseases *via* increasing in the generation of secondary bile acids, LPS biosynthesis, and the ratio of trimethylamine-producing to trimethylamine-consuming bacteria (13).

Traveling abroad, as one of the common activities, entails changes in geography and diet for days or months, whose influences in gut microbiome remain poorly understood. Our previous study investigated gut microbial communities of a Chinese volunteer team (VT) consisting of 10 people who departed from Beijing, stayed for six months in Trinidad and Tobago (TAT) and returned to Beijing. We found the gut microbial communities of VT members switched to the patterns of gut microbial communities of TAT people during their time in TAT and restored to their original patterns after they returned to Beijing in one month (14). However, the 16S rRNA gene sequencing limited the detection of the microbiome at the species and functional level, and their potential health implications for people during this six-month travel.

In this study, we conducted a high-density longitudinal sampling and integrated 16S rRNA gene and metagenomic sequencing data, and dietary records to depict the microbiome variation of VT people in their whole half-year travel to TAT. We tracked the dynamic trajectories of gut microbiome variation in the form of enterotypes. We recognized the driven microbial species and functional changes beneath the switching and restoring of enterotypes in the travel, which were mediated by the change and restoring of the diet. Furthermore, the health implications resulted from the microbiome variation warranted dietary guidance for microbial intervention during half-year travel.

MATERIALS AND METHODS

Collection of Human Fecal Samples and Dietary Information

Fecal samples were collected from each individual of the Chinese VT with a high sampling frequency (**Supplementary Figure S1A**). The collection locations of these samples included Beijing and TAT. Accordingly, these samples were subdivided into three groups, including the Chinese VT (10 individuals) that stayed in Beijing before leaving for TAT (VTC, 15–22 December 2015, 20 samples), the Chinese VT that stayed in TAT (VTT, from 31 December 2015 to June 2016, 109 samples), and the Chinese VT that returned to Beijing after a long stay (VTB, July 2016, 55 samples). These samples were grouped into six phases (**Supplementary Figure S1A**) along the time series, including T1 (20 samples), T2 (28 samples), T3 (60 samples), T4 (21 samples), T5 (35 samples), and T6 (20 samples). T1 represented the pre-travel time; T2, T3, and T4 represented three times during the stay of the VT in TAT; and T5 and T6 represented two times after the VT returned to Beijing, China. T1 belonged to the VTC group; T2, T3, and T4 belonged to the VTT group; and T5 and T6 belonged to the VTB group.

Fecal samples from TTNs (14 individuals, 28 samples; **Supplementary Figure S1B**), TTPs (3 individuals, 6 samples; **Supplementary Figure S1C**), TTCs staying in TAT for more than 1 year (4 individuals, 8 samples; **Supplementary Figure S1C**), and BJNs (10 individuals, 57 samples; **Supplementary Figure S1D**) were used as controls. These fecal samples were kept at -20°C for less than 1 week before transfer to the laboratory of the Beijing Genomics Institute and then stored at -80°C until DNA extraction. Dietary information was collected and recorded for each individual during the long stay.

DNA Extraction and Sequencing

DNA extraction from fecal samples was performed using a PowerSoil DNA Isolation Kit (MoBio, USA) following the manufacturer's instructions. Extracted DNA was dissolved in TE buffer and stored at -20°C until further use. To characterize the taxonomic profile of the gut microbial community, the V4 hypervariable region of the microbial 16S rRNA gene was amplified using the universal bacterial/archaeal primers 515F (5′-GTGCCAGCMGCCGCGGTAA-3′) and 806R (5′-GGACTACHVGGGTWTCTAAT-3′). Fusion primers with dual indexes and adapters were used for a polymerase chain reaction, and the jagged ends of the DNA fragments were converted into blunt ends using T4 DNA polymerase, Klenow fragment, and T4 Polynucleotide Kinase. Then, an 'A' base was appended to each 3′ end to facilitate the addition of adapters. Next, short fragments were removed using Ampure beads. Finally, the qualified libraries were used for sequencing on the Illumina MiSeq platform using paired-end sequencing technology (2 × 250 bp).

To characterize gut microbiome functional profiles, 62 fecal samples were selected for shotgun metagenome sequencing (**Supplementary Figure S1**), including the fecal samples of three individuals: VT3, VT6, and VT10. Metagenomic DNA of

samples was extracted, fragmented randomly to the desired size using a Covaris S/E210 or Bioruptor, and electrophoresed to yield the required lengths of DNA fragments. Subsequently, adapters were ligated to DNA fragments, and these fragments were evaluated for cluster preparation. Sequencing was performed with an insert size of 350 bp on an Illumina Xten platform.

16S rRNA Gene Sequencing Data Processing

All 16S rRNA raw data were preprocessed to obtain clean data, and two paired-end reads were generated using Fast Length Adjustment of Short reads (v1.2.11) (15). Specifically, the threshold of the minimal overlapping length was set to 15 bp, and the mismatch ratio of the overlapped region was no more than 0.1. High-quality paired-end reads were combined into tags based on the overlaps. Putative chimeras were identified using the SILVA database (16) (Release 123) and removed using the 'chimera.uchime' and 'remove.seqs' commands in Mothur (17). Existing tools for analyzing the microbial community include Quantitative Insights Into Microbial Ecology (QIIME) (18), DADA2 (19), and Deblur (20). In this study, QIIME was applied to analyze the 16S amplicon data. All high-quality sequences of human fecal samples (287 samples) were aligned using PyNAST (21) and dereplicated using UCLUST in QIIME (v1.9.1) (18). Finally, the Greengenes database (22) (version 13_8) was applied as the reference database for OTU classification of *de novo* OTUs that were clustered at 97% nucleotide identity threshold. To remove singleton OTUs, the minimum reads per OTU threshold was set to 2. The returned reads per sample varied from 51,837 to 335,665 (average = 124,944 reads per sample). The resulting OTU table containing 287 samples was rarefied to 51,837 reads to remove biases from variations in sample read numbers.

Microbial Diversity Assessment

Microbial alpha- and beta-diversity values were determined using the QIIME (18) pipeline. For alpha-diversity, rarefaction curves were drawn based on the richness metrics, observed OTUs, Chao1 index, the Shannon evenness metric, and the Simpson evenness metric. For beta-diversity analysis, the final OTU table was rarefied to contain 51,837 reads per sample. Pearson correlation, Spearman correlation, and weighted UniFrac distance metrics (23) were adopted to measure community similarity between samples. Microbial community clustering was arrayed by PCoA, visualized using ggplot packages in R, and modified with Adobe Illustrator.

Analysis of Microbial CAGs

The top 109 genera were selected based on the average abundance of the genus, and the associations between individual genera were determined using Kendall's correlation coefficient. The full set of associations was calculated in R with the 'cor' package. The function *pheatmap* in the 'pheatmap' package was used to visualize and cluster these associations in R, whereby the hierarchical clustering was grouped based on the Spearman correlation coefficient, and Ward clustering was applied to capture CAGs at the genus level. All *p* values of these associations were corrected for multiple testing using the Benjamini and Hochberg false discovery rate (FDR)-controlling procedure (24). The cutoff of the FDR-corrected p-value was set at 0.05, and significant associations were imported to Cytoscape (25), which was employed to visualize the resulting networks. The nodes (genera) were grouped based on the results of clustering in pheatmap.

To evaluate the dynamic process of the microbial community, to quantitatively measure the plasticity of the gut microbiome, we proposed the adaptation index. The index was calculated based on **Equation (1)**.

$$D_{1,2} = \sqrt[2]{\Sigma_{i=1}^{n}(x_{1i} - x_{2i})^2/n} \quad (1)$$

In this equation, $D_{1,2}$ is the distance between control (TTN) and the Chinese volunteer team in the different phases (or groups) based on the compositional data of the microbial community. Specifically, x_1 represents the average abundance of the certain genus in top n (109 in this study) genera of the gut microbial community for the volunteer team in one specific phase (out of T1 to T6), and x_2 represents the average abundance of certain genus in top n (109 in this study) genera of the gut microbial community of TTN.

Enterotype Analysis

The enterotype of each fecal sample was analyzed using the PAM method, which analyzes the Jensen-Shannon (JS) distance among samples based on the relative abundance of genera in each community (26). Specifically, before calculating, more abundant genera were selected by setting the threshold of average relative abundance to 10^{-4} (27). JS distances among samples based on the selected genus-level relative abundance were calculated. CH indexes, as previously described, were applied to choose the optimal number of clusters (27, 28).

Functional Profiling Based on the 16S rRNA Datasets

In this study, 62 fecal samples were selected for shotgun metagenomic sequencing. For association studies, we also performed functional predictions for all samples with coarse granularity. We used PICRUSt (29) (version 1.0.0-dev) to make functional predictions based on the 16S rDNA dataset from each sample. In this work, PICRUSt was applied to predict the functional composition of each fecal sample according to the manufacturer's instructions. Specifically, the 'pick_closed_reference_otus.py' command in QIIME was performed on all quality-filtered sequence data to pick OTUs. For clustering the OTUs, 97% nucleotide identity against the Greengenes database (22) (version 13_8) was set as the threshold. The OTU table was normalized using the 'normalize_by_copy_number.py' command. The normalized OTU table was used for functional prediction with the 'predict_metagenomes.py' script, and functional trait abundances were determined for each sample using the KEGG database (30) (version 66.1, May 1, 2013). Finally, the predicted functional content collapsed to level three of the KEGG hierarchy using the 'categorize_by_function.py' script.

Analysis of the Associations Between Diet and Microbial Community Composition

The associations between diet and microbial community composition were calculated based on (i) compositional data, which includes taxonomic composition (relative taxonomic abundances) and functional composition at KEGG module-level three; (ii) dietary information. To preprocess compositional data, the original relative abundance [plus a very small value (1E-20) as suggested by (31)] for each OTU was filtered, and log-transformation was then applied to generate the relative abundances. Similarly, for dietary information, the values of each variable were transformed to *z*-scores. Based on Euclidean distances, the Mantel correlations between compositional data and dietary information (9,999 permutations) were calculated, and the results were obtained in R (version 3.3.1) and visualized in Adobe Illustrator (version 16.0.0). Correlations between taxonomic composition data and functional composition data were determined for each diet using Mantel's tests (31).

Metagenomic Sequence Data Processing

In this study, 62 fecal samples (**Supplementary Figure S1**), obtained from VT3, VT6, and VT10, were selected for metagenomic sequencing. The generated reads were quality filtered and trimmed by removing reads containing 10% or more ambiguous bases (N base), adapter sequences, and 50% or more low-quality (Q < 20) bases. In addition, reads that could be perfectly aligned to the human genome were removed. Finally, 53.23 Gb of high-quality sequences on average for each sample (fastq document) was acquired, producing a total of 3.3 TB of sequence data (fastq document; **Supplementary Table 1**).

Genome Assembly

De novo metagenome assembly was performed for 62 metagenome datasets using MEGAHIT v1.1.1-2-g02102e1 (32), with option –meta-large and with a *k*-mer list of 27, 37, 47, 57, 67, 77, 87, 97, 107, 117, and 127. Contigs larger than 500 bp were kept for further analysis. These contigs exhibited an average N50 length of 6,303 bp and ranged from 910 to 10,685 bp (**Supplementary Table 1**).

Non-Redundant Gene Catalogue Construction

To predict microbial genes and proteins for each of the 62 fecal samples, Prodigal v2.6 (33) in "Meta" mode was applied to recognize open reading frames (ORFs) and proteins in assembled contigs. The program reported an average of 499,729 proteins for each sample (ranging from 207,485 to 1,049,111; **Supplementary Table 1**). Among these proteins, 358,116 were complete proteins for each sample, whereas 141,613 proteins were incomplete (**Supplementary Table 1**). These complete proteins were selected as the nonredundant protein set for each sample, which was built by pairwise comparisons of all predicted proteins of each sample using CD-HIT (34). The redundant proteins were removed using the following criteria: 90% identity over 90% of the short protein length and over 90% of the long protein length. On average, 333,881 unique proteins (ranging from 143,391 to 677,756) for these samples were obtained.

Gene Functional Classification and Ortholog Group Profiling

To identify CAZymes in each sample, CAZyme screening of these nonredundant proteins was performed. According to the manual of dbCAN CAZyme annotation, all completed and putative proteins were annotated by searching against entries in the local CAZy database, which was downloaded from dbCAN (35) (http://csbl.bmb.uga.edu/dbCAN/). The proportion of each component of CAZyme in each sample was computed by dividing the number of each component of the CAZyme by the total number of identified CAZyme components in that sample. Based on the components of CAZyme in each sample, PCA was applied to show the trajectory of each sample, which was colored according to the group information. By using Euclidean distances based on samples' functions, PERMANOVA tests with 9,999 permutations were applied to compare differences among samples grouped by enterotype. Additionally, linear discriminant analysis was used to utilize a linear combination of CAZyme features (top 19 components of CAZyme) to maximize the separation of the groups. Furthermore, based on the top 19 components of CAZyme, heatmap analysis was performed to illustrate the clustering results of CAZyme features and the discernibility of these CAZyme features in different groups.

Shotgun Metagenomics Analysis for Species Composition and Functional Composition

Shotgun metagenomics sequence data of 62 fecal samples were identified at the species level *via* MetaPhlAn2 with default settings (36). Taxonomical information at the species level for these 62 fecal samples was obtained. Functional annotations were identified using the HuMAnN2 (37) pipeline with UniRef50 (38). The functional pathways were annotated by mapping reads to MetaCyc databases (39). Significantly enriched pathways were identified among enterotypes 1 and 2 compared with enterotype 3 with 2-fold changes.

Data Accession

All sequencing data (including 287 16S rRNA data and 62 metagenomic data) for fecal samples were deposited in NCBI's Sequence Read Archive database under Bioproject number PRJNA393237 and can also be viewed in NODE (http://www.biosino.org/node) by pasting the accession (OEP000187) into the text search box or at the URL http://www.biosino.org/node/project/detail/OEP000187.

RESULTS

Study Design and Population

In this work, we collected 287 fecal samples from 41 individuals, including a Chinese VT (10 individuals, 188 samples), Beijing healthy natives (BJNs, 10 individuals, 57 samples), TAT healthy

natives (TTNs, 14 individuals, 28 samples), TAT patients (TTPs, 3 individuals, 6 samples), and TAT Chinese individuals (TTCs, 4 individuals, 8 samples), reflecting high-density longitudinal sampling. We followed individuals for their entire journeys of more than 8 months (including 1 month before and 1 month after travel) and partitioned their journeys into six phases (T1–T6). Specifically, T1 represented the pretravel time; T2, T3, and T4 represented three times during the stay of the VT in TAT; and T5 and T6 represented two times after the VTs returned to Beijing (**Supplementary Figure S1**). Finally, we sequenced the V4 hypervariable region of the microbial 16S rRNA genes and clustered these fecal samples into enterotypes to investigate the relationships between resilience and enterotype. We sequenced 62 of the samples, mostly from VT3, VT6, and VT10, to obtain shotgun metagenomics data for exploring strain-level variations and metabolic differences.

Enterotype-Dependent Resilience Pattern of Taxonomical Structure for Gut Microbial Communities

Microbial communities of the samples collected in Beijing before and after the long stays were indistinguishable ($P = 0.18$ and $P = 0.71$, Wilcoxon test; **Figure 1A**). However, samples collected in Beijing were both distinguishable from their respective samples collected during their stay in TAT ($P = 5.5 \times 10^{-10}$ and $P = 2.7 \times 10^{-10}$, Wilcoxon test; **Figure 1A**).

We also found that the gut microbial communities of VT1, VT2, VT3, VT4, VT6, and VT8 formed one cluster, and the gut microbial communities of VT5, VT7, VT9, and VT10 formed another cluster before they departed from Beijing. The gut microbial communities of VT members gradually transformed to those similar to the natives during their stay in TAT and then reverted to their respective original community structures after returning to Beijing. The dynamic trajectories of VT1, VT2, VT3, VT4, VT6, and VT8 could be regarded as path 1, whereas those of VT5, VT7, VT9, and VT10 could be regarded as path 2. The results revealed that the dynamic changes of resilience had two paths across the PCoA axis for VT members (**Figure 1A**).

To investigate the characteristics of resilience, we performed enterotype analysis on 287 fecal samples and clustered these samples into three enterotypes (**Figure 1B**). The dominant genera in enterotype 1 and enterotype 2 were *Prevotella* and *Bacteroides*, respectively, whereas the enriched genera in enterotype 3 were Ruminococcaceae_unclassified and *Bifidobacterium* (**Figure 1C**). We observed the bidirectional plastic pattern and resilience in the enterotypes of VT members. Specifically, the results of the enterotype analysis revealed that the fecal samples of most of BJNs and all VT members at the T1 phase exhibited two different gut microbial communities, i.e., enterotype 1 and enterotype 2 (26), whereas the fecal samples of most of TTNs belonged to enterotype 3 (**Figure 1D**). During the long stay at TAT, most samples from VT members had enterotypes that evolved towards that of the TAT natives, despite significant differences among their original enterotypes (**Figures 1B, D**). Notably, their enterotypes quickly returned to their respective original enterotypes after the VT members returned to Beijing (**Figures 1B, D**). The results revealed that the bidirectional resilience of human gut microbial communities was specific to enterotype. Based on the grouping strategy in this study, we observed that these alterations in gut microbial communities were triggered immediately after airplane travel, lasting for 1 month, after which the taxonomical structures of microbial communities resemble those of the natives and showed significant stability.

Microbial Drivers at the Genus Level for the Enterotype-Dependent Resilience of Human Microbial Communities

To elucidate the drivers of bidirectional resilience of human gut communities for hosts with different enterotypes, we compared dynamic changes in four representative genera in enterotypes, including their relative abundances (**Figures 2A–D**) and the operational taxonomic units (OTUs) that were maintained in these genera (**Figures 2E–H**). We found that the taxonomical structures of the gut microbial community shifted considerably during the stay. The relative abundances of *Prevotella*, *Bacteroides*, Ruminococcaceae_unclassified, and *Bifidobacterium* showed dramatic changes. The average relative abundances of *Prevotella* and *Bacteroides* decreased when VT members reached TAT and increased when VT members returned to Beijing (**Figures 2A, B**), whereas the average relative abundances of Ruminococcaceae_unclassified and *Bifidobacterium* first increased and then decreased (**Figures 2C, D**). Moreover, by tracing and comparing common OTUs that were present in at least 10% of VT members, we found that individual OTUs within *Prevotella*, *Bacteroides*, Ruminococcaceae_unclassified, and *Bifidobacterium* exhibited distinguished temporal dynamics and showed a plastic pattern during the long stay (**Figures 2E–H**). Many of the OTUs belonging to *Prevotella* displayed plasticity; 71.73% of the OTUs disappeared between the T3 phase and T1 phase, and 39.55% recurred after the VT members returned to Beijing (**Figure 2E**). In contrast, 72.18% of *Bacteroides* OTUs disappeared after arrival to TAT, and 47.75% of *Bacteroides* OTUs recurred after return to Beijing (**Figure 2F**). This plastic pattern was also observable for certain OTUs in Ruminococcaceae_unclassified and *Bifidobacterium* (**Figures 2G, H**). Many Ruminococcaceae_unclassified OTUs (1,101, 56.17%) and *Bifidobacterium* OTUs (79, 75.24%) appeared at the T2 phase and a large proportion of these OTUs (43.05% and 79.75%) still existed in the T3 phase (**Figures 2E–H**).

To gain more insights into the resilience of gut microbial communities, we divided the fecal samples from VTs into two groups according to their enterotypes in Beijing and explored the dynamic changes in these four genera during the long stay. We found that although changes in *Prevotella* and *Bacteroides* differed between enterotype 1 and enterotype 2, the dynamic changes observed in Ruminococcaceae_unclassified and *Bifidobacterium* were similar (**Figure 2I**). Furthermore, we found correlations among the four genera (**Figure 2J**), such as between *Sutterella* and *Bacteroides* (rho = 0.516, $P = 3.34 \times 10^{-14}$) and between *Clostridium* and Ruminococcaceae_unclassified (rho = 0.676, $P = 1.88 \times 10^{-26}$).

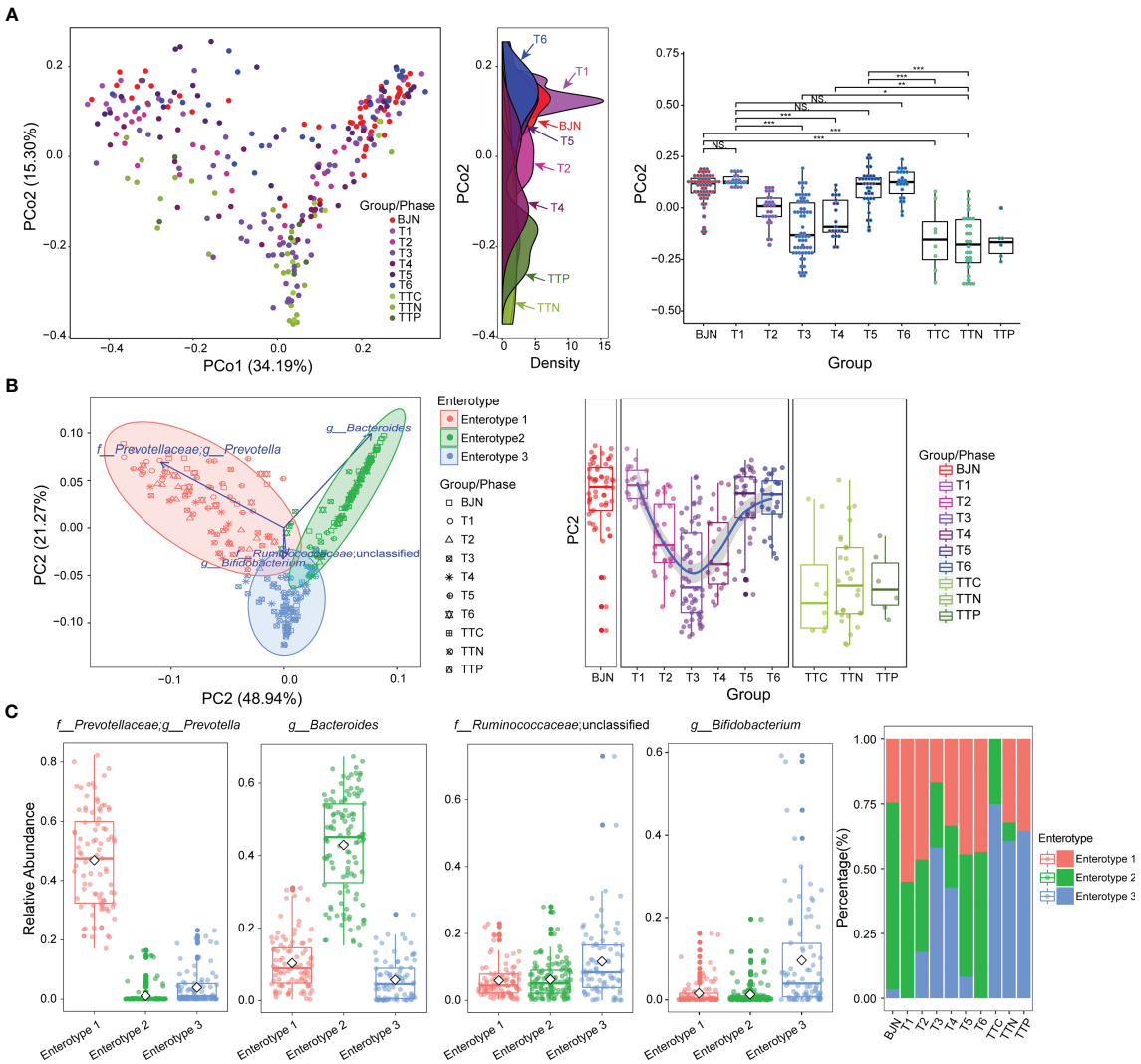

FIGURE 1 | The resilience of human gut microbial communities was bidirectional and was associated with enterotype during the long stay. **(A)** The microbial community compositions of the volunteer team individuals during the study (T1–T6 phases) and those of the control group (BJNs, TTCs, TTNs, and TTPs) plotted in a weighted UniFrac PCoA (left panel). The density curve, which was plotted based on the PCo2 value of each group, showed the distributions of each group of the human gut microbial community (middle panel). The boxplots showed sample distributions against PCo2 of each group (right panel). Statistical significance is tested using Wilcoxon test, ***$P < 0.001$, **$P < 0.01$, *$P < 0.05$, and NS., not significant. **(B)** In total, 287 samples were clustered into three enterotypes based on PCA at the genus level. The majority of samples collected after the VT members returned to Beijing and before departure belonged to clusters of enterotype 1 (pink) and enterotype 2 (green). Together with control fecal samples collected from hosts in Trinidad and Tobago (TTCs, TTNs, and TTPs), the majority of fecal samples collected from TAT (T2–T4) belonged to the cluster of enterotype 3 (blue). **(C)** The major contributors in these three enterotypes were *Prevotella*, *Bacteroides*, Ruminococcaceae_unclassified, and *Bifidobacterium*. **(D)** The distribution of three enterotypes in each group/phase during the stay.

We further investigated the bi-directional plasticity of the gut microbial communities from the aspect of the genera in the ecological network to gain insights into the plasticity. A total of 109 most abundant genera were clustered into 10 co-abundance groups (CAGs) (**Supplementary Figures S2A, B**). These CAGs were annotated according to the dominant genera, including *Prevotella*, *Bacteroides*, Ruminococcaceae_unclassified, Lanchnospiraceae_unclassified, Bacillaceae_unclassified, *Bifidobacterium*, and Enterobacteriaceae_unclassified. The Wiggum plot (6) showed the co-abundance association networks of genera for each phase and each group and revealed unique patterns of abundances for these 10 CAGs from T1 to T6 phases (**Supplementary Figure S3**). Specifically, during the T1 to T6 phases, the relative abundances of six CAGs showed profound changes, including *Prevotella*, *Bacteroides*, Ruminococcaceae_unclassified, Lanchnospiraceae_unclassified, Bacillaceae_unclassified, and Enterobacteriaceae_unclassified CAGs. The relative abundances of *Prevotella* and *Bacteroides* CAGs were suppressed when the VT members stayed in TAT and reverted after returning to Beijing. In contrast, the relative abundances of

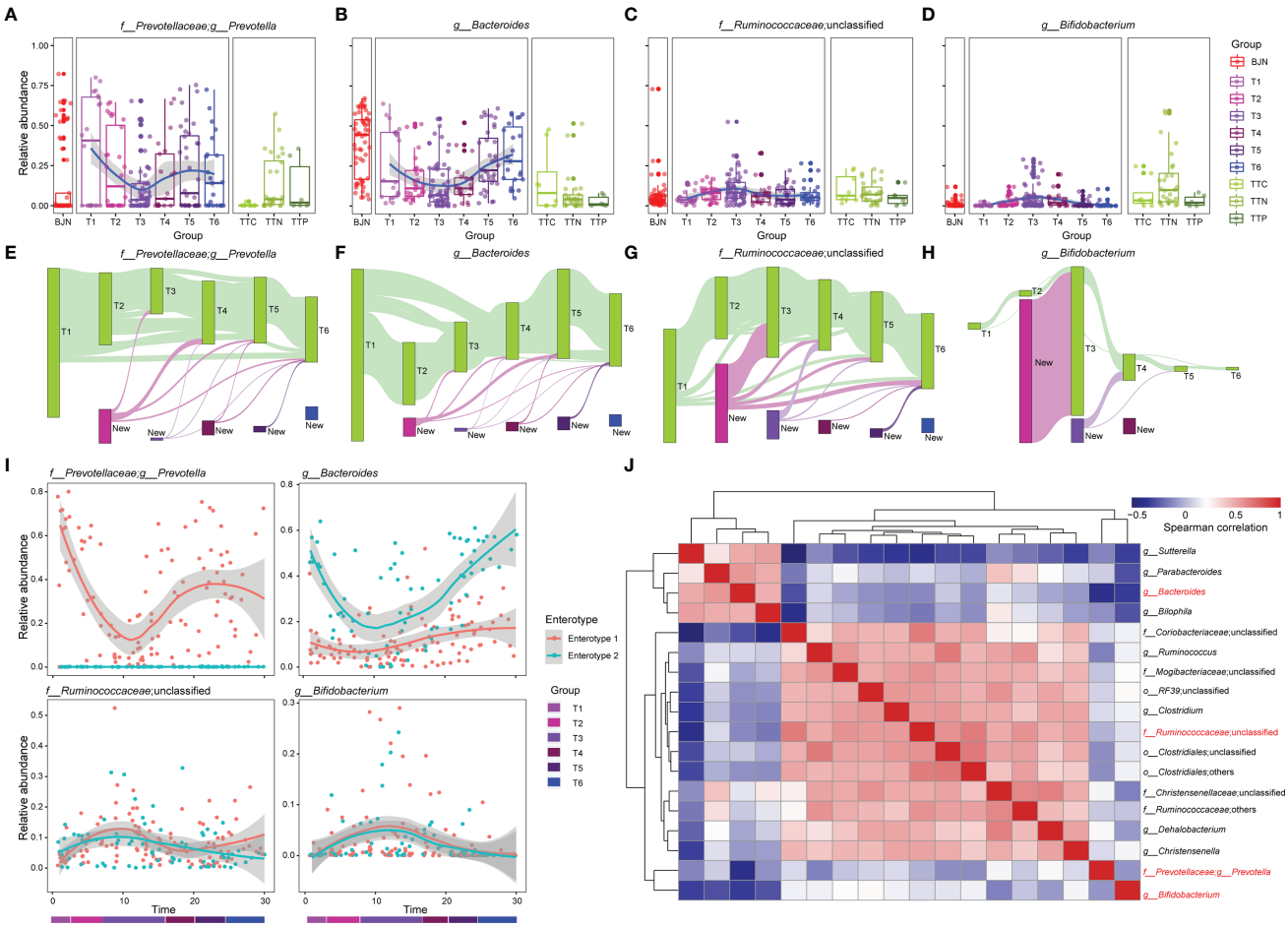

FIGURE 2 | The dynamics of four dominant genera and the bidirectional resilience of the gut microbial community were associated with enterotype. **(A–D)** Dynamics of the average relative abundances of *Prevotella*, *Bacteroides*, Ruminococcaceae_unclassified, and *Bifidobacterium* along the temporal axis. OTUs that were shared by at least 10% of fecal samples during the same phase (green bars) were tracked using Sankey plots for **(E)** *Prevotella*, **(F)** *Bacteroides*, **(G)** Ruminococcaceae_unclassified, and **(H)** *Bifidobacterium*. The heights of bars are proportional to the number of OTUs, and phases are arranged in chronological order. The newly introduced OTUs of each phase are differently colored. The lines represent the transfer of OTUs between phases and are colored by the first phase of appearance. **(I)** Dynamic changes in *Prevotella*, *Bacteroides*, Ruminococcaceae_unclassified, and *Bifidobacterium* for VT members along the temporal axis. **(J)** Co-occurrence patterns between the four dominant genera with other genera across the 287 samples, as determined by Spearman's rank correlation analysis.

Ruminococcaceae_unclassified, Lanchnospiraceae_unclassified, Bacillaceae_unclassified, and Enterobacteriaceae_unclassified CAGs showed a reversed pattern, i.e., the relative abundances were amplified first and then suppressed. To quantitatively measure the plasticity of gut microbial communities, we designed an index, namely the adaptation index, which was calculated by comparing communities of volunteer team members with that of the TTN (**Supplementary Figure S3**). The adaptation index first decreased and then increased. More importantly, the index could serve to better understand the response time of gut microbial communities to alternations of environments. When we monitored the differences of adaptation indices between two neighboring phases, we observed that the adaptation index showed a sharp decrease from T1 to T2 (1.18×10^{-3}) and a sharp increase from T4 to T5 (0.88×10^{-3}), with these differences being significantly higher than the difference between T1 and T5 (0.50×10^{-3}). This indicates a quick response time (within one month) and also a quick recovery time (within one month).

These findings suggested that the bidirectional plastic pattern of the human gut microbial communities was largely driven by the bidirectional quantitative alterations in CAGs. Moreover, the changes in the relative abundances of the genera were the underlying reasons for the bidirectional resilience of enterotypes.

Microbial Drivers at the Species Level for the Enterotype-Dependent Resilience of Human Microbial Communities

To examine differences at the species level and functional differences in the enterotype-dependent resilience of human microbial communities, we selected 62 representative fecal samples for whole-metagenomic sequencing. These samples

consisted of time series data for three members of the VT (VT3, VT6, and VT10; 47 samples), two BJNs (9 samples), and three TTNs (3 samples; **Supplementary Figure S1** and **Supplementary Table 1**). These samples can well represent most conditions of each group. For instance, VT3, VT6, and VT10, present non-symptom, abdominal distension, and a condition of an early return, respectively, in a half-year travel. The other selected individuals including BJNs and TTNs were used for comparisons with the VTs. Two BJNs were randomly selected, and three TTNs were selected from three different families. We found that the gut microbial communities in BJNs and VT members at phage T1 who belonged to enterotype 2 varied in *Bacteroides* strain profiles, including *Bacteroides dorei*, *Bacteroides ovatus*, *Bacteroides plebeius*, and *Bacteroides massiliensis*, whereas those with *Prevotella* enriched in enterotype 1 consisted of only a single strain of *Prevotella copri* (**Figure 3A**).

In contrast to the enriched genera profiled by 16S amplicon analysis, we found that the dominant genera in enterotype 3 were *Faecalibacterium*, *Eubacterium*, *Ruminococcus*, and *Bifidobacterium* (**Figure 3A**, **Supplementary Table 2**). The dominant species in enterotype 3 were *Faecalibacterium prausnitzii* and *Eubacterium rectale* (**Figure 3A**, **Supplementary Table 3**). During the long stay, we found that the relative abundances of *Bacteroides dorei*, *Bacteroides plebeius*, and *Prevotella copri* decreased first when the VT members stayed in TAT and then increased after their return. Conversely, the relative abundances of *Faecalibacterium prausnitzii* and *Eubacterium rectale* increased first and then decreased (**Figure 3A**). The transformation of enterotype was caused by changes in these species.

Next, we identified the subspecies in the metagenomic samples and found a series of species with varying subspecies during the study. Importantly, we observed that the average number of subspecies varied considerably when the VT members changed their spatial position (**Figure 3B**). For example, the average number of subspecies of *Bacteroides ovatus* and *Faecalibacterium prausnitzii* immediately decreased from 2.66 and 3.0 subspecies/sample to 1.25 and 2.0 subspecies/sample, respectively when VT members arrived at TAT and increased from 2.0 and 2.5 subspecies/sample to 2.42 and 3.0 subspecies/sample, respectively, after their return (**Figure 3B**, **Supplementary Table 4**). In contrast, *Dorea formicigenerans*, *Ruminococcus* sp. S_1_39BFAA, *Coprococcus comes*, *Dorea longicatena*, and *Streptococcus salivarius* showed an opposite trend (**Figure 3B**, **Supplementary Table 4**). These results suggested that the bidirectional resilience of gut microbial communities was associated with species composition, particularly for the dominant species and their subspecies.

Functional Plasticity in the Gut Microbial Communities

Based on the aforementioned findings, we hypothesized that the bidirectional resilience of the gut microbial community may be associated with dynamic functional changes. To test this hypothesis, we first annotated the predicted genes using the CAZyme database and then divided fecal samples of BJNs and VT members into three groups- BJN-T1 (fecal samples collected in Beijing before departure), T2–T4 (fecal samples collected in TAT), and T5–T6 (fecal samples collected after returning to Beijing). By comparing inverse Simpson indices, we found that the diversity of enzymes for utilizing carbohydrates was significantly different between samples in TAT and samples collected in Beijing ($p < 0.05$, Wilcoxon test, **Figure 4A**). Similarly, by principal component analysis (PCA) of CAZyme profiles generated from microbiome samples, we found that the functional composition of the gut microbial community—which shifted from those similar to BJNs to those similar to TTNs and then reverted after the return—was resilient during the long stay (**Figure 4B**). Additionally, the similarities of functional compositions among these samples were also consistent with the enterotypes (PERMANOVA test based on Euclidean distances with 9,999 permutations: $P = 0.0897$ for enterotype 1 versus 2, $p < 0.0005$ for enterotype 1 versus 3, $p < 0.0005$ for enterotype 2 versus 3) and followed a bidirectional plastic pattern (**Figure 4C**).

Possible Functional Drivers of the Plasticity of the Human Microbial Communities

We observed that the abundances of glycoside hydrolases (GHs) decreased during the T2–T4 and then increased after the VT member returned to Beijing (**Figure 4D**). In contrast, glycosyltransferases (GTs) and carbohydrate esterases (CEs) increased during phases T2–T4 and then decreased after the VT members returned (**Figures 4E, F**).

We extended our analysis to distinguish groups by a supervised learning approach that integrated a linear combination of the top 19 components of CAZyme (**Figure 4G**). The combination of these 19 components of CAZyme showed considerable power to distinguish fecal samples of VT members collected in Beijing from those of VT members collected in TAT (PERMANOVA, Bray-Curtis distance, permutation = 9,999, $p < 0.001$) and to distinguish fecal samples of VT members collected in Beijing with those from TTNs, TTCs, and TTPs (PERMANOVA, Bray-Curtis distance, permutation = 9,999, $p < 0.001$). However, this combination failed to clearly distinguish T1 samples from T5–T6 samples (PERMANOVA, Bray-Curtis distance, permutation = 9,999, $p > 0.05$; **Figure 4G**).

In addition, no significant differences were observed in the compositions of GHs (**Figure 4H**) and GTs (**Figure 4I**) among three enterotypes, whereas CEs showed significant differences between enterotypes 1 and 3 (t-test, $P = 2.5 \times 10^{-5}$) and between enterotypes 2 and 3 (t-test, $P = 1.95 \times 10^{-6}$; **Figure 4J**).

Similarly, the combinations of these 19 components of CAZymes exhibited considerable power for distinguishing fecal samples of enterotype 1 from those of enterotype 3 (PERMANOVA, Bray-Curtis distance, permutation = 9,999, $P = 0.001$; **Figure 4K**) and those of enterotype 2 from those of enterotype 3 (PERMANOVA, Bray-Curtis distance, permutation = 9,999, $P = 0.001$; **Figure 4L**). These representative enterotype-dependent guilds (40) highlighted the resilience pattern.

FIGURE 3 | Linking dynamic changes in species and subspecies to the bidirectional resilience of the gut microbial community. **(A)** Dynamic changes in the taxonomic composition of gut microbial communities at the species level. The order of species was sorted by the importance of random forests for identifying the enterotype. **(B)** Dynamic changes in the number of subspecies (left panel) and the average number of subspecies (right panel) during the time series.

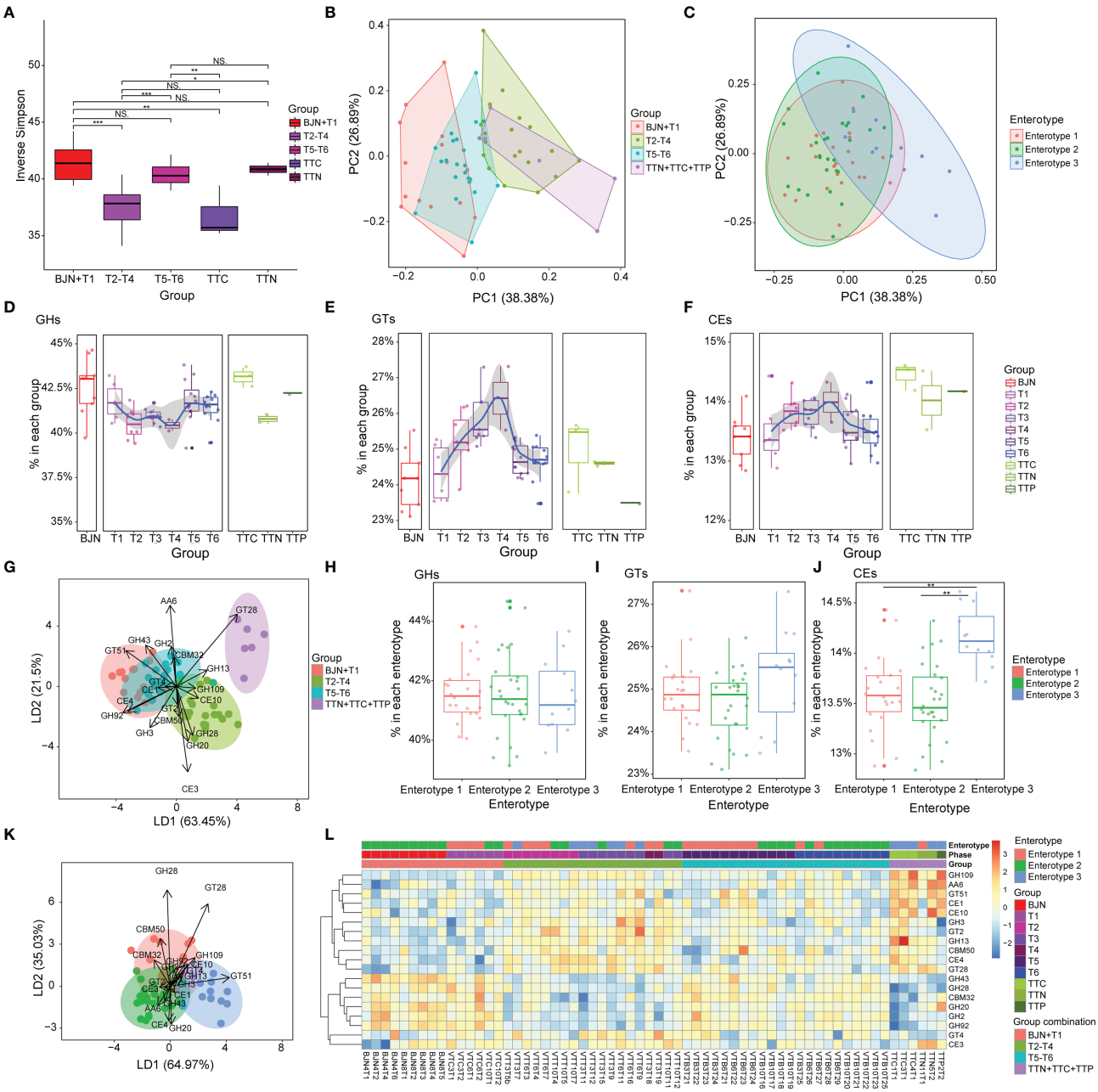

FIGURE 4 | Compositions of carbohydrate metabolism pathways in the human gut microbiome were resilient during the long stay. **(A)** Inverse Simpson index for CAZyme components for microbiome samples from the individuals selected from the cohort of Chinese VT members, TTNs, TTCs, and TTPs. Statistical significance is tested using Wilcoxon test, $^{***}P < 0.001$, $^{**}P < 0.01$, $^{*}P < 0.05$, and NS, not significant. **(B)** PCA results showing the trajectory of samples, which were colored according to the predefined groups (four groups: BJN-T1, T2–T4, T5–T6, TTN+TTC+TTP), based on the CAZyme component. **(C)** In total, 62 samples were projected to the two-dimensional plane by PCA based on their CAZyme components, and each was then color-labeled and grouped according to their respective enterotype. **(D–F)** Dynamics of the average relative abundance of GHs, GTs, and CEs across the time series. **(G)** Linear discriminant analysis was used to utilize a linear combination of CAZyme components to maximize the separation of the groups. The ellipses represent different groups, and the lengths and directions of the arrows show the normalized scales for each component scaling (for 19 components of CAZyme). **(H–J)** Differences in the average relative abundances of GHs, GTs, and CEs among the three enterotypes. **(K)** Linear discriminant analysis was used to utilize a linear combination of CAZyme components to maximize the separation of the enterotypes. The ellipses represent different groups, and the lengths and directions of the arrows show the normalized scales for each component scaling (for 19 components of CAZyme). **(L)** Heatmap showing the clustering results for CAZyme features and the discernibility of how these CAZyme features differed among groups.

Based on these dynamic patterns observed for GHs, GTs, and CEs during the long stay and for different enterotypes, we speculated that the bidirectional resilience of the microbial community may be associated with the metabolism of carbohydrates from different diets.

Accordingly, we performed the PCAs to trace the dynamics of metabolic pathways according to the different groups (**Figure 5A**) and three enterotypes (**Figure 5B**). We found that the metabolic compositions of the VT members during T1 differed slightly from that of samples in T5–T6 phase (PERMANOVA, Bray-Curtis distance, permutation = 9,999, $P = 0.4639$). In contrast, there was a significant difference between the metabolic composition of the VT members at T1 and that of samples at T2–T4 (PERMANOVA, Bray-Curtis distance, permutation = 9,999, $P = 0.0054$; **Figure 5A**). Moreover, we found that there were significant differences among the compositions of the three enterotypes (PERMANOVA, Bray-Curtis distance, permutation = 9,999, $P < 0.005$; **Figure 5B**). Among the functional pathways, we observed that unintegrated pathways of *Prevotella copri*, *Bacteroides* sp. (e.g., *Bacteroides dorei* and *Bacteroides plebeius*), and *Faecalibacterium prausnitzii* corresponded to enterotypes 1, 2, and 3, respectively (**Figure 5B**). For other known pathways, we found dynamic changes in coenzyme A biosynthesis II, thiamin formation from pyrithiamine and oxythiamine, and glucose metabolism, including glycolysis IV and pyruvate fermentation to acetate and lactate II, also exhibited a plastic pattern (**Figure 5C**). The relative abundances of these pathways increased when VT members arrived at TAT, remained stable during the stay at TAT, and decreased after return to Beijing.

Dietary Shifts Were Correlated With the Plastic Pattern of the Human Microbial Communities

The VT members exhibited dietary habits considerably different from those in Beijing during their stay in TAT. Among their diets, the increased consumption of foods such as fish, seafood, dairy products, and refined grains was significantly correlated with changes in gut microbial community structures ($p < 0.05$, **Figure 6A**). However, in contrast to VT members, the composition of gut microbial communities in TAT natives was tightly associated with the consumption of bananas, mangos, papayas, cheese, and carrot potatoes ($p < 0.05$, **Figure 6B**). These findings are consistent with previous studies demonstrating that changes in diet affect the composition of the human gut microbial communities (7, 41–43). Therefore, the diet in TAT, which was different from that in Beijing, may have led to changes in the gut microbial communities of VT members during this study.

DISCUSSION

This longitudinal study was based on high-density sampling (average of more than 20 per individual) of volunteers with multiple dietary shifts, and reported the dynamic variation of the human gut microbiome in a whole half-year travel, which was reflected by the switching and restoring of enterotypes.

The enterotypes switch and alterations in specific driven species might exert effects on human immunity. We found that

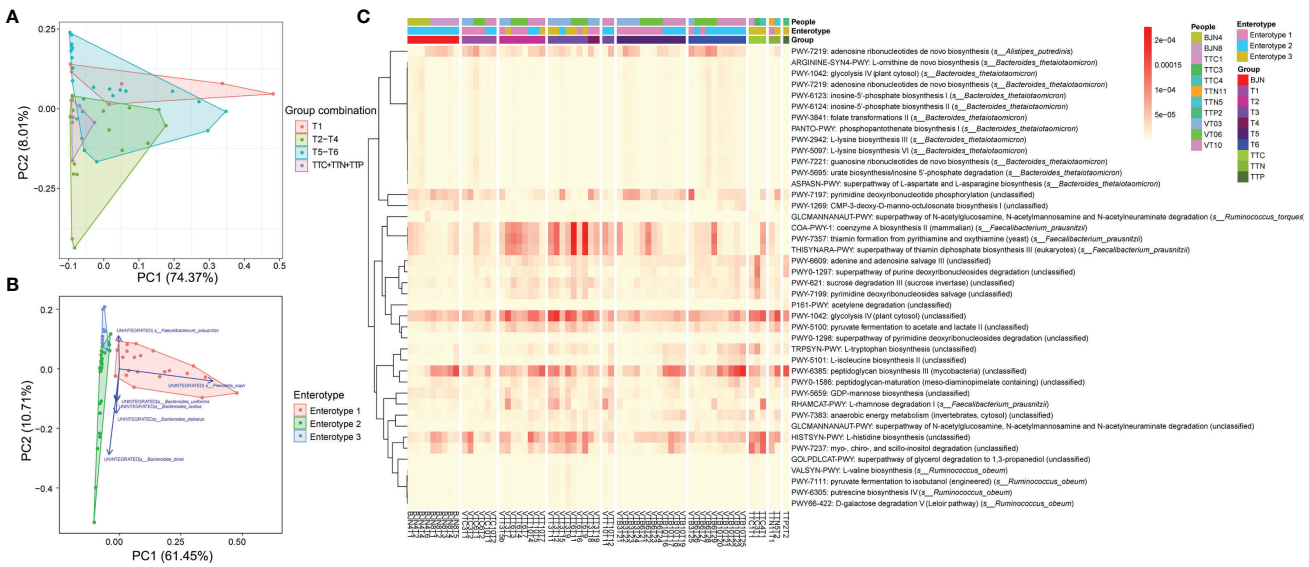

FIGURE 5 | Functional pathways contributed to the bidirectional resilience of human gut microbial communities. **(A)** PCA results showing the trajectory of samples, which were colored according to their defined groups (four groups: T1, T2– T4, T5– T6, TTN+ TTC+ TTP), based on the component of stratified functional pathways. **(B)** PCA results showing the trajectory of samples, which were colored according to the three enterotypes, based on the component of stratified functional pathways. **(C)** Heatmap showing the compositions of enriched and significant functional pathways, which contributed to the bidirectional resilience of the human gut microbial community, across all metagenomics samples.

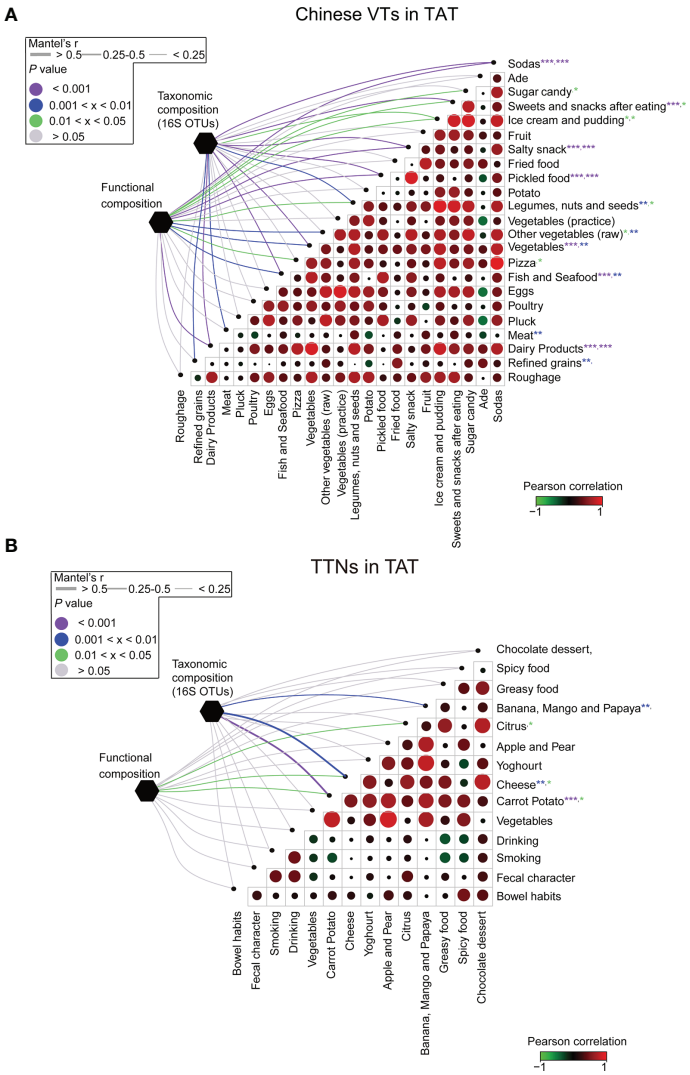

FIGURE 6 | Association between diet and the structural and functional compositions of the microbial communities for VT members and TAT natives. The associations between dietary variables and the taxonomic and functional compositions for **(A)** VT members staying in TAT and **(B)** TAT natives. Circle sizes in the matrices represent the absolute values of Pearson correlation coefficients for the two corresponding factors, whereas circle colors represent either positive or negative correlations. The edge widths represent the Mantel's *r* statistic for distance correlations, and the edge color denotes the statistical significance based on 9,999 permutations. ***$P < 0.001$, **$P < 0.01$, and *$P < 0.05$.

the resilience of taxonomical and functional compositions of the human gut microbiome was highly enterotype-specific. The identified genera and species that may drive the observed plasticity included variations in *Prevotella*, *Bacteroides*, Ruminococcaceae_unclassified, and *Bifidobacterium* at the genus level and *Bacteroides dorei*, *Bacteroides ovatus*, *Bacteroides plebeius*, *Bacteroides massiliensis*, *Prevotella copri*, *Faecalibacterium prausnitzii*, and *Eubacterium rectale* at the species level. Many of these microbial species were reported to be correlated with immunity modulation. For instance, *Bacteroides dorei* was reported to be depleted in patients with coronary artery disease (CAD), and the gavage of *B. dorei* could attenuate atherosclerotic lesion formation in atherosclerosis-prone mice, notably ameliorating endotoxemia followed by decreasing gut microbial lipopolysaccharide production, effectively suppressing pro-inflammatory immune responses (44). In addition, *B. ovatus* was reported to produce indole-3-acetic acid that promoted IL-22 production by immune cells, yielding beneficial effects on colitis (45). Moreover, *P. copri* was reported to play a crucial role in rheumatoid arthritis (RA) pathogenesis, a chronic autoimmune disease (46). *P. copri* were found expanded in patients with new-onset RA (47), and the HLA-DR-presented peptide identified from the 27-kDa protein of *P. copri* was capable of stimulating a TH1 cell response in 42% of patients with new-onset RA (48). Other species have also been linked to immune diseases, such as *B. massiliensis* related to the

severity of COVID-19 (49), and *E. rectale* related to the pathogenesis of ulcerative colitis and inflammatory bowel disease (50). Therefore, if people traveled to a place where dominated enterotypes differed from theirs, the change in environment such as diet would render it possible for people to switch their enterotype, bringing about the potential risk of immunity disorders.

From a functional perspective, the bidirectional resilience of gut microbial communities was primarily driven by a few functional groups (guilds) related to carbohydrate metabolism, e.g., GHs, GTs, and CEs, and a series of glucose metabolic pathways. We found GHs were decreased but GTs and CEs increased during the travel, and these functions were then restored after VTs returned to Beijing. Carbohydrate metabolism can modulate innate immunity (51), thus the change in the ability of carbohydrate metabolism during the travel, together with the taxonomic composition, warranted a microbial intervention to maintain health.

The taxonomic and functional changes in the gut microbiome were found mediated by dietary change. For instance, VT people had increased consumption of seafood, dairy products, and refined grains during their stay in TAT, which were significantly correlated with their microbiome variation. Accordingly, prior prediction of one's microbial resilience patterns could facilitate the preparation of travelers. Proper dietary guidance, designed according to an individual's original enterotype and the dominated enterotype in the destination, would be beneficial for the individual to maintain the enterotype stability in travel for months.

More efforts are needed to improve our understanding of the plastic patterns of the human gut microbiome after a half-year travel and their health implications. First, many confounding factors, including living conditions and disruption of the circadian rhythm, may influence the dynamics of the human gut microbiome, however, the mechanisms remained unknown. Second, the effects of genetic factors in shaping the enterotype-dependent plastic patterns of the gut microbiome should be examined. Third, the relationships between enterotype-dependent plastic patterns in the gut microbiome and the health status of the host needs further experiments and detailed clinical records. These issues should be addressed in future studies.

Collectively, this study has profiled the longitudinal dynamics of human gut microbial communities in a travel for months, and opened new avenues for probing the effects of diet and environments on human gut microbial communities, as well as the implications of human gut microbial communities on immunity and other health indicators.

DATA AVAILABILITY STATEMENT

All sequencing data (including 287 16S rRNA data and 62 metagenomic data) for fecal samples were deposited in NCBI's Sequence Read Archive database under Bioproject number PRJNA393237.

ETHICS STATEMENT

Ethical review and approval was not required for the study on human participants in accordance with the local legislation and institutional requirements. The patients/participants provided their written informed consent to participate in this study.

AUTHOR CONTRIBUTIONS

This study was designed by MC, HL, MH, JW, GT, and KN. MC, HL, MH, ZH, RW, YL, FC, JP, HP, HS, YX, LC, QZ, and FG collected samples. MC, HL, MH, RW, and PY analyzed the data. MC, HL, MH, SL, DB, SS, and KN wrote the initial draft of the manuscript. All authors revised the manuscript. This study was supervised by JW, GT, and KN. All authors contributed to the article and approved the submitted version.

FUNDING

This work was partially supported by National Natural Science Foundation of China (grant nos. 31871334, 32071465, 31671374, 31327901, 31671369, 31770775, 61521092, 91430218, 61472395, and 61432018), National Key Research and Development Program of China (grant nos. 2018YFC0910502 and 2018YFC0910405), and the GRF Research Project 9042348 (grant no. CityU11257316).

ACKNOWLEDGMENTS

We thank Yumin Song and all other members of the Embassy of the People's Republic of China in the Republic of Trinidad and Tobago for their support in sample collection for this work. We are grateful to Le Cao and Chaofang Zhong from College of Life Science and Technology, Huazhong University of Science and Technology, Wuhan, China for their help in preparing the figures. We thank Torsten Juelich from the Chinese Academy of Sciences for linguistic assistance during the preparation of this manuscript.

SUPPLEMENTARY MATERIAL

The Supplementary Material for this article can be found online at: https://www.frontiersin.org/articles/10.3389/fimmu.2022.848994/full#supplementary-material

REFERENCES

1. Qin J, Li R, Raes J, Arumugam M, Burgdorf KS, Manichanh C, et al. A Human Gut Microbial Gene Catalogue Established by Metagenomic Sequencing. *Nature* (2010) 464(7285):59–65. doi: 10.1038/nature08821
2. Glasner ME. Finding Enzymes in the Gut Metagenome. *Science* (2017) 355 (6325):577–8. doi: 10.1126/science.aam7446
3. Yatsunenko T, Rey FE, Manary MJ, Trehan I, Dominguez-Bello MG, Contreras M, et al. Human Gut Microbiome Viewed Across Age and Geography. *Nature* (2012) 486(7402):222–7. doi: 10.1038/nature11053
4. Rothschild D, Weissbrod O, Barkan E, Kurilshikov A, Korem T, Zeevi D, et al. Environment Dominates Over Host Genetics in Shaping Human Gut Microbiota. *Nature* (2018) 555(7695):210–5. doi: 10.1038/nature25973
5. Turnbaugh PJ, Hamady M, Yatsunenko T, Cantarel BL, Duncan A, Ley RE, et al. A Core Gut Microbiome in Obese and Lean Twins. *Nature* (2009) 457 (7228):480–4. doi: 10.1038/nature07540
6. Claesson MJ, Jeffery IB, Conde S, Power SE, O'Connor EM, Cusack S, et al. Gut Microbiota Composition Correlates With Diet and Health in the Elderly. *Nature* (2012) 488(7410):178–84. doi: 10.1038/nature11319
7. David LA, Maurice CF, Carmody RN, Gootenberg DB, Button JE, Wolfe BE, et al. Diet Rapidly and Reproducibly Alters the Human Gut Microbiome. *Nature* (2014) 505(7484):559–63. doi: 10.1038/nature12820
8. Wu GD, Chen J, Hoffmann C, Bittinger K, Chen YY, Keilbaugh SA, et al. Linking Long-Term Dietary Patterns With Gut Microbial Enterotypes. *Science* (2011) 334(6052):105–8. doi: 10.1126/science.1208344
9. Faith JJ, Guruge JL, Charbonneau M, Subramanian S, Seedorf H, Goodman AL, et al. The Long-Term Stability of the Human Gut Microbiota. *Science* (2013) 341(6141):1237439. doi: 10.1126/science.1237439
10. Moeller AH, Degnan PH, Pusey AE, Wilson ML, Hahn BH, Ochman H. Chimpanzees and Humans Harbor Compositionally Similar Gut Enterotypes. *Nat Commun* (2012) 3:1179. doi: 10.1038/ncomms2159
11. Sonnenburg JL, Bäckhed F. Diet-Microbiota Interactions as Moderators of Human Metabolism. *Nature* (2016) 535(7610):56–64. doi: 10.1038/nature18846
12. Vangay P, Johnson AJ, Ward TL, Al-Ghalith GA, Shields-Cutler RR, Hillmann BM, et al. US Immigration Westernizes the Human Gut Microbiome. *Cell* (2018) 175(4):962–972.e910. doi: 10.1016/j.cell.2018.10.029
13. Keohane DM, Ghosh TS, Jeffery IB, Molloy MG, O'Toole PW, Shanahan F. Microbiome and Health Implications for Ethnic Minorities After Enforced Lifestyle Changes. *Nat Med* (2020) 26(7):1089–95. doi: 10.1038/s41591-020-0963-8
14. Liu H, Han M, Li SC, Tan G, Sun S, Hu Z, et al. Resilience of Human Gut Microbial Communities for the Long Stay With Multiple Dietary Shifts. *Gut* (2019) 68(12):2254–5. doi: 10.1136/gutjnl-2018-317298
15. Magoč T, Salzberg SL. FLASH: Fast Length Adjustment of Short Reads to Improve Genome Assemblies. *Bioinformatics* (2011) 27(21):2957–63. doi: 10.1093/bioinformatics/btr507
16. Quast C, Pruesse E, Yilmaz P, Gerken J, Schweer T, Yarza P, et al. The SILVA Ribosomal RNA Gene Database Project: Improved Data Processing and Web-Based Tools. *Nucleic Acids Res* (2013) 41(D1):D590–6. doi: 10.1093/nar/gks1219
17. Schloss PD, Westcott SL, Ryabin T, Hall JR, Hartmann M, Hollister EB, et al. Introducing Mothur: Open-Source, Platform-Independent, Community-Supported Software for Describing and Comparing Microbial Communities. *Appl Environ Microbiol* (2009) 75(23):7537–41. doi: 10.1128/AEM.01541-09
18. Caporaso JG, Kuczynski J, Stombaugh J, Bittinger K, Bushman FD, Costello EK, et al. QIIME Allows Analysis of High-Throughput Community Sequencing Data. *Nat Methods* (2010) 7(5):335–6. doi: 10.1038/nmeth.f.303
19. Callahan BJ, McMurdie PJ, Rosen MJ, Han AW, Johnson AJ, Holmes SP. DADA2: High-Resolution Sample Inference From Illumina Amplicon Data. *Nat Methods* (2016) 13(7):581–3. doi: 10.1038/nmeth.3869
20. Amir A, McDonald D, Navas-Molina JA, Kopylova E, Morton JT, Zech Xu Z, et al. Deblur Rapidly Resolves Single-Nucleotide Community Sequence Patterns. *mSystems* (2017) 2(2):e00191–00116. doi: 10.1128/mSystems.00191-16
21. Caporaso JG, Bittinger K, Bushman FD, DeSantis TZ, Andersen GL, Knight R. PyNAST: A Flexible Tool for Aligning Sequences to a Template Alignment. *Bioinformatics* (2010) 26(2):266–7. doi: 10.1093/bioinformatics/btp636
22. DeSantis TZ, Hugenholtz P, Larsen N, Rojas M, Brodie EL, Keller K, et al. Greengenes, a Chimera-Checked 16S rRNA Gene Database and Workbench Compatible With ARB. *Appl Environ Microbiol* (2006) 72(7):5069–72. doi: 10.1128/AEM.03006-05
23. Lozupone C, Knight R. UniFrac: A New Phylogenetic Method for Comparing Microbial Communities. *Appl Environ Microbiol* (2005) 71(12):8228–35. doi: 10.1128/AEM.71.12.8228-8235.2005
24. Benjamini Y, Krieger AM, Yekutieli D. Adaptive Linear Step-Up Procedures That Control the False Discovery Rate. *Biometrika* (2006) 93(3):491–507. doi: 10.1093/biomet/93.3.491
25. Cline MS, Smoot M, Cerami E, Kuchinsky A, Landys N, Workman C, et al. Integration of Biological Networks and Gene Expression Data Using Cytoscape. *Nat Protoc* (2007) 2(10):2366–82. doi: 10.1038/nprot.2007.324
26. Arumugam M, Raes J, Pelletier E, Le Paslier D, Yamada T, Mende DR, et al. Enterotypes of the Human Gut Microbiome. *Nature* (2011) 473(7346):174–80. doi: 10.1038/nature09944
27. Li J, Zhao F, Wang Y, Chen J, Tao J, Tian G, et al. Gut Microbiota Dysbiosis Contributes to the Development of Hypertension. *Microbiome* (2017) 5(1):14. doi: 10.1186/s40168-016-0222-x
28. Lim MY, Rho M, Song Y-M, Lee K, Sung J, Ko G. Stability of Gut Enterotypes in Korean Monozygotic Twins and Their Association With Biomarkers and Diet. *Sci Rep* (2014) 4:7348. doi: 10.1038/srep07348
29. Langille MG, Zaneveld J, Caporaso JG, McDonald D, Knights D, Reyes JA, et al. Predictive Functional Profiling of Microbial Communities Using 16S rRNA Marker Gene Sequences. *Nat Biotechnol* (2013) 31(9):814–21. doi: 10.1038/nbt.2676
30. Kang C, Zhang Y, Zhu X, Liu K, Wang X, Chen M, et al. Healthy Subjects Differentially Respond to Dietary Capsaicin Correlating With Specific Gut Enterotypes. *J Clin Endocrinol Metab* (2016) 101(12):4681–9. doi: 10.1210/jc.2016-2786
31. Sunagawa S, Coelho LP, Chaffron S, Kultima JR, Labadie K, Salazar G, et al. Ocean Plankton. Structure and Function of the Global Ocean Microbiome. *Science* (2015) 348(6237):1261359. doi: 10.1126/science.1261359
32. Li D, Luo R, Liu CM, Leung CM, Ting HF, Sadakane K, et al. MEGAHIT V1.0: A Fast and Scalable Metagenome Assembler Driven by Advanced Methodologies and Community Practices. *Methods* (2016) 102:3–11. doi: 10.1016/j.ymeth.2016.02.020
33. Hyatt D, Chen GL, Locascio PF, Land ML, Larimer FW, Hauser LJ. Prodigal: Prokaryotic Gene Recognition and Translation Initiation Site Identification. *BMC Bioinf* (2010) 11:119. doi: 10.1186/1471-2105-11-119
34. Li W, Godzik A. Cd-Hit: A Fast Program for Clustering and Comparing Large Sets of Protein or Nucleotide Sequences. *Bioinformatics* (2006) 22(13):1658–9. doi: 10.1093/bioinformatics/btl158
35. Lombard V, Golaconda Ramulu H, Drula E, Coutinho PM, Henrissat B. The Carbohydrate-Active Enzymes Database (CAZy) in 2013. *Nucleic Acids Res* (2014) 42(Database issue):D490–5. doi: 10.1093/nar/gkt1178
36. Truong DT, Franzosa EA, Tickle TL, Scholz M, Weingart G, Pasolli E, et al. MetaPhlAn2 for Enhanced Metagenomic Taxonomic Profiling. *Nat Methods* (2015) 12(10):902–3. doi: 10.1038/nmeth.3589
37. Abubucker S, Segata N, Goll J, Schubert AM, Izard J, Cantarel BL, et al. Metabolic Reconstruction for Metagenomic Data and its Application to the Human Microbiome. *PloS Comput Biol* (2012) 8(6):e1002358. doi: 10.1371/journal.pcbi.1002358
38. Suzek BE, Wang Y, Huang H, McGarvey PB, Wu CH, UniProt C. UniRef Clusters: A Comprehensive and Scalable Alternative for Improving Sequence Similarity Searches. *Bioinformatics* (2015) 31(6):926–32. doi: 10.1093/bioinformatics/btu739
39. Caspi R, Foerster H, Fulcher CA, Kaipa P, Krummenacker M, Latendresse M, et al. The MetaCyc Database of Metabolic Pathways and Enzymes and the BioCyc Collection of Pathway/Genome Databases. *Nucleic Acids Res* (2008) 36 (Database issue):D623–631. doi: 10.1093/nar/gkm900
40. Zhao L, Zhang F, Ding X, Wu G, Lam YY, Wang X, et al. Gut Bacteria Selectively Promoted by Dietary Fibers Alleviate Type 2 Diabetes. *Science* (2018) 359(6380):1151–6. doi: 10.1126/science.aao5774
41. De Filippo C, Cavalieri D, Di Paola M, Ramazzotti M, Poullet JB, Massart S, et al. Impact of Diet in Shaping Gut Microbiota Revealed by a Comparative Study in Children From Europe and Rural Africa. *Proc Natl Acad Sci USA* (2010) 107(33):14691–6. doi: 10.1073/pnas.1005963107

42. Tremaroli V, Bäckhed F. Functional Interactions Between the Gut Microbiota and Host Metabolism. *Nature* (2012) 489(7415):242–9. doi: 10.1038/nature11552
43. David LA, Materna AC, Friedman J, Campos-Baptista MI, Blackburn MC, Perrotta A, et al. Host Lifestyle Affects Human Microbiota on Daily Timescales. *Genome Biol* (2014) 15(7):R89. doi: 10.1186/gb-2014-15-7-r89
44. Yoshida N, Emoto T, Yamashita T, Watanabe H, Hayashi T, Tabata T, et al. Bacteroides Vulgatus and Bacteroides Dorei Reduce Gut Microbial Lipopolysaccharide Production and Inhibit Atherosclerosis. *Circulation* (2018) 138(22):2486–98. doi: 10.1161/CIRCULATIONAHA.118.033714
45. Ihekweazu FD, Engevik MA, Ruan W, Shi Z, Fultz R, Engevik KA, et al. Bacteroides Ovatus Promotes IL-22 Production and Reduces Trinitrobenzene Sulfonic Acid-Driven Colonic Inflammation. *Am J Pathol* (2021) 191(4):704–19. doi: 10.1016/j.ajpath.2021.01.009
46. Zaiss MM, Joyce Wu HJ, Mauro D, Schett G, Ciccia F. The Gut-Joint Axis in Rheumatoid Arthritis. *Nat Rev Rheumatol* (2021) 17(4):224–37. doi: 10.1038/s41584-021-00585-3
47. Scher JU, Sczesnak A, Longman RS, Segata N, Ubeda C, Bielski C, et al. Expansion of Intestinal Prevotella Copri Correlates With Enhanced Susceptibility to Arthritis. *Elife* (2013) 2:e01202. doi: 10.7554/eLife.01202
48. Pianta A, Arvikar S, Strle K, Drouin EE, Wang Q, Costello CE, et al. Evidence of the Immune Relevance of Prevotella Copri, a Gut Microbe, in Patients With Rheumatoid Arthritis. *Arthritis Rheumatol* (2017) 69(5):964–75. doi: 10.1002/art.40003
49. Baradaran Ghavami S, Pourhamzeh M, Farmani M, Raftar SKA, Shahrokh S, Shpichka A, et al. Cross-Talk Between Immune System and Microbiota in COVID-19. *Expert Rev Gastroenterol Hepatol* (2021) 15(11):1281–94. doi: 10.1080/17474124.2021.1991311
50. Zhang SL, Wang SN, Miao CY. Influence of Microbiota on Intestinal Immune System in Ulcerative Colitis and Its Intervention. *Front Immunol* (2017) 8:1674. doi: 10.3389/fimmu.2017.01674
51. Zhao H, Raines LN, Huang SC. Carbohydrate and Amino Acid Metabolism as Hallmarks for Innate Immune Cell Activation and Function. *Cells* (2020) 9(3):562. doi: 10.3390/cells9030562

Conflict of Interest: The authors declare that the research was conducted in the absence of any commercial or financial relationships that could be construed as a potential conflict of interest.

Publisher's Note: All claims expressed in this article are solely those of the authors and do not necessarily represent those of their affiliated organizations, or those of the publisher, the editors and the reviewers. Any product that may be evaluated in this article, or claim that may be made by its manufacturer, is not guaranteed or endorsed by the publisher.

frontiers in Immunology

ORIGINAL RESEARCH
published: 28 February 2022
doi: 10.3389/fimmu.2022.812996

Altered Fecal Metabolomics and Potential Biomarkers of Psoriatic Arthritis Differing From Rheumatoid Arthritis

Nan Wang[1†], Linjiao Yang[2†], Lili Shang[1], Zhaojun Liang[1], Yanlin Wang[1], Min Feng[1], Shuting Yu[2], Xiaoying Li[2], Chong Gao[3], Zhenyu Li[2] and Jing Luo[1*]*

[1] Division of Rheumatology, Department of Medicine, The Second Hospital of Shanxi Medical University, Taiyuan, China, [2] Modern Research Center for Traditional Chinese Medicine of Shanxi University, Taiyuan, China, [3] Department of Pathology, Brigham and Women's Hospital, Harvard Medical School, Boston, MA, United States

OPEN ACCESS

Edited by:
Qinglong Wu,
Baylor College of Medicine,
United States

Reviewed by:
Jinxin Liu,
Nanjing Agricultural University, China
Siqian Li,
Shenzhen University, China

***Correspondence:**
Zhenyu Li
lizhenyu@sxu.edu.cn
Jing Luo
ljty966@hotmail.com

[†]These authors have contributed equally to this work and share first authorship

Specialty section:
This article was submitted to Autoimmune and Autoinflammatory Disorders, a section of the journal Frontiers in Immunology

Received: 11 November 2021
Accepted: 31 January 2022
Published: 28 February 2022

Citation:
Wang N, Yang L, Shang L, Liang Z, Wang Y, Feng M, Yu S, Li X, Gao C, Li Z and Luo J (2022) Altered Fecal Metabolomics and Potential Biomarkers of Psoriatic Arthritis Differing From Rheumatoid Arthritis. Front. Immunol. 13:812996. doi: 10.3389/fimmu.2022.812996

Psoriatic arthritis (PsA) is a chronic inflammatory joint disease, and the diagnosis is quite difficult due to the unavailability of reliable clinical markers. This study aimed to investigate the fecal metabolites in PsA by comparison with rheumatoid arthritis (RA), and to identify potential diagnostic biomarkers for PsA. The metabolic profiles of the fecal samples from 27 PsA and 29 RA patients and also 36 healthy controls (HCs) were performed on ultra-high-performance liquid chromatography coupled with hybrid triple quadrupole time-of-flight mass spectrometry (UHPLC-Q-TOF-MS). And differentially altered metabolites were screened and assessed using multivariate analysis for exploring the potential biomarkers of PsA. The results showed that 154 fecal metabolites were significantly altered in PsA patients when compared with HCs, and 45 metabolites were different when compared with RA patients. A total of 14 common differential metabolites could be defined as candidate biomarkers. Furthermore, a support vector machines (SVM) model was performed to distinguish PsA from RA patients and HCs, and 5 fecal metabolites, namely, α/β-turmerone, glycerol 1-hexadecanoate, dihydrosphingosine, pantothenic acid and glutamine, were determined as biomarkers for PsA. Through the metabolic pathways analysis, we found that the abnormality of amino acid metabolism, bile acid metabolism and lipid metabolism might contribute to the occurrence and development of PsA. In summary, our research provided ideas for the early diagnosis and treatment of PsA by identifying fecal biomarkers and analyzing metabolic pathways.

Keywords: feces, metabolomics, biomarker, psoriatic arthritis, UHPLC-Q-TOF-MS

INTRODUCTION

Psoriatic arthritis (PsA) is a chronic autoimmune disease characterized by joint inflammation and skin psoriasis (1). Its effects on men and women are almost the same, with peak onset ages of 40 and 50 years, respectively (1, 2). It is a heterogeneous disease that affects multiple organ systems, namely, peripheral joints, axial joints, attachment points, skin, and nails (3, 4), which tend to be associated

with obesity, metabolic syndrome, uveitis, atherosclerosis, chronic liver disease, cardiovascular disease and mental disorders (4–7). PsA is known to be affected by many aspects, namely, genetic, immune, and environmental factors, which play key roles in the development of PsA (1, 8). At present, the pathogenesis of PsA is not fully clear and its early diagnosis, and its treatment is still challenging.

Clinically, PsA is difficult to distinguish from other inflammatory joint diseases, especially rheumatoid arthritis (RA) in the early stages of onset, because their clinical presentation and manifestations have many similarities (9–12). PsA and RA are both characterized by joint pain and swelling, and have the same organ systems affected, namely, the skin, joints, eyes, vascular system, and even the immune system (12). The diagnosis of RA is mainly based on clinical symptoms and seropositivity of specific antibodies such as rheumatoid factor (RF) and anti-cyclic citrullinated peptide antibodies (anti-CCPs), while for PsA, only clinical and imaging features are helpful for the diagnosis of the disease (13). Although most patients with PsA can be differentiated from patients with RA by specific non-articular clinical features being present, and also the infrequent seropositivity for RF and anti-CCPs (13, 14). However, in clinical practice, the differential diagnosis between PsA and RA can be challenging, especially if there is a peripheral phenotype and RF or anti-CCPs are negative in about 15–20% of cases (14, 15). Therefore, new tools are needed to discover biomarkers that can be used to reliably diagnose PsA.

With the rise of new technologies for the analysis of genome, transcription, protein, metabolomics, and others, new approaches have been provided for the study of pathogenesis (16). The intestinal microbiome may affect distant sites except the intestine through immunomodulation, such as the joints (17). Recent studies have shown that metabolites in the gut play a fundamental role in the evolutionary relationship between symbiotic microorganisms and their hosts (16, 18). Metabolite profiles provide functional readings of microbial activity and can be used as intermediate phenotypes to mediate interactions between human and microorganism (19). Although studies have found that the intestinal flora has a certain influence on the occurrence and development of PsA, such as a significant increase of the Firmicutes and Actinobacteria phyla in patients with psoriatic (20), there is little evidence on the connection between the gut microbiota and psoriatic arthritis, especially their metabolites.

Metabolomics can provide information of high-throughput quantification of metabolites. It is extensively used in the research of intestinal microbiota to explore the variation of gut microbiota derived metabolites, which are closely related to the physiological and pathological processes of the host (21, 22). Nowadays, metabolomics has been widely used to discover biomarkers and key pathways related to many diseases and explain the pathological mechanisms, due to the high throughput, high sensitivity, wide coverage, and relatively low cost (21, 23, 24). Previous metabolomic studies have detected potential biomarkers of some autoimmune diseases through plasma (25), serum (26), urine (27), and synovial fluid samples (28). Previous studies have also compared the serum metabolic profiles of patients with PsA and other autoimmune diseases by a global metabolomic approach using gas chromatography time-of-flight mass spectrometry or proton nuclear magnetic resonance (14, 29). Many research groups have also focused on analyzing possible differential biomarkers between PsA and RA in synovium and serum (14, 15). However, studies on the fecal metabolism profile of PsA patients are relatively rare.

In this study, a total of 91 human fecal samples were enrolled, namely, 36 HCs, 27 PsA and 29 RA. An untargeted fecal metabolomic approach based on UHPLC-Q-TOF-MS was used to identify the differential metabolites. First, the differential metabolites between PsA and HCs, and also PsA and RA were determined. Moreover, disordered metabolic pathways in PsA patients were predicted according to differential metabolites. Finally, potential biomarkers were screened for distinguishing PsA from HCs and RA, and the biomarkers in this study showed satisfactory performance in identifying PsA.

MATERIALS AND METHODS

Chemicals and Reagents

Analytical grade methanol and methyl tert-butyl ether (MTBE) were obtained from the Tianjin Damao chemical reagent factory. Ultrapure water was prepared using a Milli-Q water purification system (Millipore, USA). Acetonitrile (ACN), isopropanol (IPA), formic acid and ammonium acetate (LC-MS grade) were from Thermo (USA).

Patients and Sample Collection

Between January 2019 and January 2021, 27 PsA patients, 29 RA patients (disease control) and 36 healthy controls (HCs) with matched age and gender were enrolled from the Second Hospital of Shanxi Medical University. All patients were in accord with the American College of Rheumatology (ACR) classification criteria for PsA and RA, and without the history of other autoimmune diseases. HCs also had no history of autoimmune diseases. All participants did not use probiotic diet and antibiotics in the past month, so the additional effects of gut microorganisms on intestinal metabolites were avoided. Fresh stool samples were collected from each subject within the first to two days of the hospitalization of the patient, frozen immediately, and stored at −80°C until use.

Clinical Data Collection

Clinical data of all participants had been collected during routine laboratory assessments, namely, blood routine examination, biochemical indicators, erythrocyte sedimentation rate (ESR), C-reactive protein (CRP), rheumatoid factor (RF), anti-cyclic citrullinated peptide (anti-CCP), cytokine levels, peripheral lymphocytes and $CD4^+$ T cell subset data. Blood routine examination, namely, white blood cell (WBC), hemoglobin (HGB), platelets (PLT), lymphocytes (LYM), monocytes (MON), and neutrophiles (NEU), were evaluated using the Sysmex XN-9000 automated hematology analyzer. Biochemical indicators, namely, alanine amiotransferase (ALT), aspartate

aminotransferase (AST), alkaline phosphatase (ALP), glucose (GLU), urea, and creatinine (Cr), were measured using the Beckman Coulter AU680 biochemical analyzer. The levels of CRP were evaluated using the Beckman Coulter IMMAGE800 automatic protein analyzer. The quantitative detection of RF was evaluated by an enzyme-linked immunosorbent assay (ELISA), and anti-CCP was detected by an automatic chemiluminescence analyzer (KEASER 6600). Peripheral lymphocytes and $CD4^+$ T cell subset were analyzed by monoclonal antibodies on a BD-FACS-CANTO II flow cytometer (Becton Dickinson, USA). The serum concentrations of IL-2, IL-4, IL-6, IL-10, IL-17, TNF-α, and IFN-γ were detected using magnetic bead-based multiplex assays (Human Th1/Th2/Th17 subpopulation test kit: Jiangxi Cellgene Biotech Co., Ltd.) following the manufacturer's instructions.

Sample Preparation

Polar extracts: The fecal samples were subjected to sequential solvent extraction by water and methanol according to the previous study (30). Briefly, 20 mg of lyophilized feces were weighed, and dissolved in 1 ml of ice-cold water, then vortexed and extracted by ultrasonicating in an ice bath for 20 min. The extracts were centrifuged, and the supernatant was immediately transferred. The feces were further extracted with 1 ml of ice-cold methanol for 20 min. The extracts were centrifuged, and the supernatant was immediately transferred. Then 500 µl of each supernatant was combined, and 1 ml of ice-cold methanol was added, vortexed to precipitate protein and centrifuged at 13,000 rpm for 15 min. The supernatant was evaporated to dryness using the speed vacuum concentrator. The residue was redissolved in 100 µl of methanol-water (80:20, v/v) and centrifuged at 13,000 rpm for 15 min to obtain the supernatant for metabolomic analysis.

Non-polar extracts: The fecal residue was further extracted with 1 ml of ice-cold MTBE, and then 500 µl of the supernatant was dried under a nitrogen stream. The residue was redissolved in 100 µl of isopropanol–water (70:30, v/v) and centrifuged at 13,000 rpm for 15 min, then the supernatant were transferred the for lipidomic analysis.

To ensure the stability and repeatability of the experiments, 10 µl each supernatant was pooled together as a quality control (QC) sample for both the polar and non-polar extracts, respectively.

LC–MS Analysis

Briefly, the metabolic profiles of the fecal samples were performed on a UHPLC (ExionLCTM AD) coupled with Triple TOF 5600+ mass spectrometer (American, AB Sciex). Chromatographic separation was acquired on a Waters Acquity UPLC HSS T3 (1.8 µm, 2.1 × 100 mm). The column temperature was set at 40°C and the injected volume was 5 µl. Date acquisition was performed in full scan mode both in the positive and negative ion modes, and also coupled with information-dependent acquisition (IDA) trigger product ion scan modes. The parameters of the MS acquisition of electron spray ionization (ESI) source were listed as follows: ion spray voltage, 4,500 V in the negative ion mode and 5,500 V in the positive mode; nebulizer gas of 55 psi; heater gas of 55 psi; curtain gas of 30 psi; decluttering potential of 60 V (positive) and −60V (negative); collision energy of 35 eV (positive) and −35 eV (negative); turbo spray temperature of 550°C; the full scan range of 100–1,500 m/z and the ion scan range of 50–1,250 m/z with high sensitivity.

Polar extracts analysis: The mobile phase was consisted of 0.1% formic acid aqueous solution (A) and ACN (B) with the optimized gradient elution program as follows: 0–2 min, 2% B; 2–3.5 min, 15% B; 3.5–5 min, 15% B; 5–18 min, 60% B; 18–27 min, 60% B; 27–29 min, 95% B; 29–36 min, 95% B; 36–36.5 min, 2% B; 36.5–39 min, 2% B. The flow rate was set at 0.3 ml/min.

Non-polar extracts analysis: The mobile phase A was ACN/H_2O (6:4) with 0.1% formic acid and the mobile phase B was IPA/ACN (9:1) mixed with 10 mM ammonium acetate. The gradient elution program was optimized as follows: 0–3 min, 32% B; 3–6 min, 45% B; 6–8 min, 52% B; 8–12 min, 58% B; 12–14 min, 66% B; 14–20 min, 70% B; 20–25 min, 75% B; 25–28 min, 99% B; 28–31 min, 99% B; 31–31.5 min, 32% B; 31.5–34 min, 32% B. The flow rate was set at 0.25 ml/min.

Determination of Differential Metabolites by Multivariate Analysis

The raw data was imported to XCMS (version 3.6.3) for automatic data prepossessing, namely, peak picking and retention time correction. Then the resulting data matrix were imported into SIMCA 14.0 software (Umetrics, Sweden) for multivariate data analysis, namely, principal component analysis (PCA), partial least square discriminant analysis (PLS-DA), and orthogonal partial least square discriminant analysis (OPLS-DA). The variable importance in the projection (VIP) values from OPLS-DA models, fold change (FC), *t*-test (GraphPad prism 8.0) and false discovery rate (FDR, R-Studio software, version 3.6.3) correction were performed to screen the differential metabolites. The metabolites with VIP >1, FC >1.2 or FC <0.8, p <0.05 and FDR <0.05 were considered to be the differential metabolites, which were identified by OSI/SMMS software (Dalian ChemData Solution Information Technology Co., Ltd., PR China) and other online databases, namely, Human Metabolome Database (http://www.hmdb.ca/), Lipidmaps (https://lipidmaps.org/) and LipidBlast (https://fiehnlab.ucdavis.edu/projects/lipidblast). The differential metabolites were further presented in a heatmap with hierarchical cluster analysis (HCA) using MetaboAnalyst 5.0.

Statistical Analysis

Statistical analysis of clinical data and differential metabolites was performed using the SPSS 22.0, Graphpad Prism 8.0 and MetaboAnalyst 5.0. Categorical and quantitative variables were described as frequencies, percentage, mean ± standard deviation or median (Q25, Q75). Data of demographic and clinical features were compared between groups by the non-parametric Mann–Whitney *U* test or Independent Sample *t*-test, as appropriate. Correlation analysis was performed using the Pearson correlation test. Receiver operating characteristic (ROC) curve analysis was used to evaluate the diagnostic performance of potential biomarkers. The support vector machines (SVM) classification

model and ROC analysis for multiple biomarkers were performed by Biomarker analysis module in MetaboAnalyst 5.0.

RESULTS

Demographical and Clinical Characteristics of PsA Patients

All 27 PsA patients (12 men and 15 women) were Han Chinese population (100%). Their mean age was 46.56 ± 15.04 years old. The median disease duration of PsA was 41 months (range 1–180 months). The median age at onset of PsA was 43.22 years (range 11–64 years). In 81.5% of patients with PsA, the onset began with skin manifestations, followed by joint inflammation. Among the 27 patients with PsA, 18 cases showed peripheral arthritis, 1 case showed axial arthritis, and 8 cases showed mixed peripheral spine. In terms of skin manifestations, 3 cases of PsA had no skin damage, and the remaining 24 cases had psoriatic rashes of varying degrees; In addition, 3 patients with PsA had nail lesions. All patients of PsA were newly diagnosed, with no current treatment with disease-modifying antirheumatic drugs (DMARDs) and corticosteroid for joint symptoms.

The demographics and clinical characteristics of PsA and RA patients are tabulated in **Table 1** (Additional clinical data were listed in **Supplementary Tables S1**, **S2**). There were no significant differences in age (p = 0.1589) and BMI (p = 0.6114) between the PsA and RA group by two-tailed unpaired Student's t-test, and also PsA group and HC group (age p = 0.4750).

Metabolic Profiling of UHPLC-Q-TOF-MS

The polar and non-polar extracts of all the fecal samples (HC, PsA, and RA groups) were analyzed by UHPLC-Q-TOF-MS. After data processing, namely, peak picking, retention time correction, and missing value filling, 12,457 and 7,622 metabolic features were detected in the positive and negative ion modes for the polar extracts, and 11,749 and 9,513 metabolic features were detected in the positive and negative ion modes for the non-polar extracts. The typical total ion chromatograms of the polar and non-polar extracts of the fecal samples are shown in **Supplementary Figure S1**.

UHPLC-Q-TOF-MS Method Validation

Polar extracts: In order to evaluate the data quality of the metabolic profiles, a PCA model was constructed, and the repeatability of metabolic profiling was evaluated using QC samples. For the positive ion mode (**Supplementary Figure S2A**), all QC samples were tightly clustered together in the center of the PCA score plot, and fell within the 2 SD's region and 95% confidence interval, which indicated that the analytical methods were reliable and acceptable (**Supplementary Figure S2C**). For the negative ion mode, the PCA model also showed good reliability of metabolomic platform in this study (**Supplementary Figures S2B, D**).

Non-polar extracts: In the positive and negative ion modes (**Supplementary Figure S3**), 14 QC samples were clustered closely in the PCA model and all fell within the 2 SD's region and 95% confidence interval, which also indicated that the analytical platform provided excellent reliability required for a large-scale metabolomic study.

Multivariate Statistical Analysis

Polar extracts: As shown in the PCA score plot of the positive ion mode (**Supplementary Figure S2A**), the PsA and RA groups showed obvious separation from HC group, whereas PsA group and RA group were overlapped. Then 3D PLS-DA was applied to further maximize their difference, in which both PsA and RA groups were separated from the HC group, and PsA and RA groups could be further separated (**Figure 1A**). In the negative ion mode, the PsA, RA, and HC groups were overlapped in the unsupervised PCA model (**Supplementary Figure S2B**), and the

TABLE 1 | Demographics and clinical characteristics of PsA and RA patients and health control[a].

	PsA patients (n = 27)	RA patients (n = 29)	HC (n = 36)
Female: male	15:12	17:12	19:17
Age and years (mean ± SD)	46.56 ± 15.04	51.4 ± 9.84	49.08 ± 12.98
BMI (kg/m^2, mean ± SD)	23.41 ± 4.20	23.93 ± 3.12	
DISEASE ACTIVITY PARAMETERS			
Age at onset (mean years, range)	43.22 (11–64)	45.62 (24–65)	
Disease duration (mean month, range)	41 (1–180)	70 (1–300)	
ESR (median mm/h, range)	21 (1–120)	46.5 (5–120)	7.5 (1–20)
CRP (median mg/, range)	7.23 (1–177)	13.35 (1–197)	
DAS28 (mean ± SD)	4.09 ± 1.31	5.25 ± 1.46	
% active (DAS28 >3.2)	20 (74.07%)	26 (89.66%)	
% remission (DAS28<2.6)	6 (22.22%)	1 (3.44%)	
SJC (mean ± SD)	3.74 ± 6.04	7.0 ± 7.44	
TJC (mean ± SD)	6.52 ± 6.73	10.17 ± 8.12	
PASI (mean ± SD)	1.54 ± 1.37	–	
AUTOANTIBODY STATUS			
RF positive, n (%)	2 (7.4%)	20 (69.0%)	
Anti- CCP positive, n (%)	1 (3.7%)	22 (75.9%)	

[a]*ESR, erythrocyte sedimentation rate; CRP, C-reactive protein; RF, rheumatoid factor; Anti-CCP, anti-cyclic citrullinated peptide; SJC, swollen joint count; TJC, tender joint count; PASI, Psoriasis Area and Severity Index.*

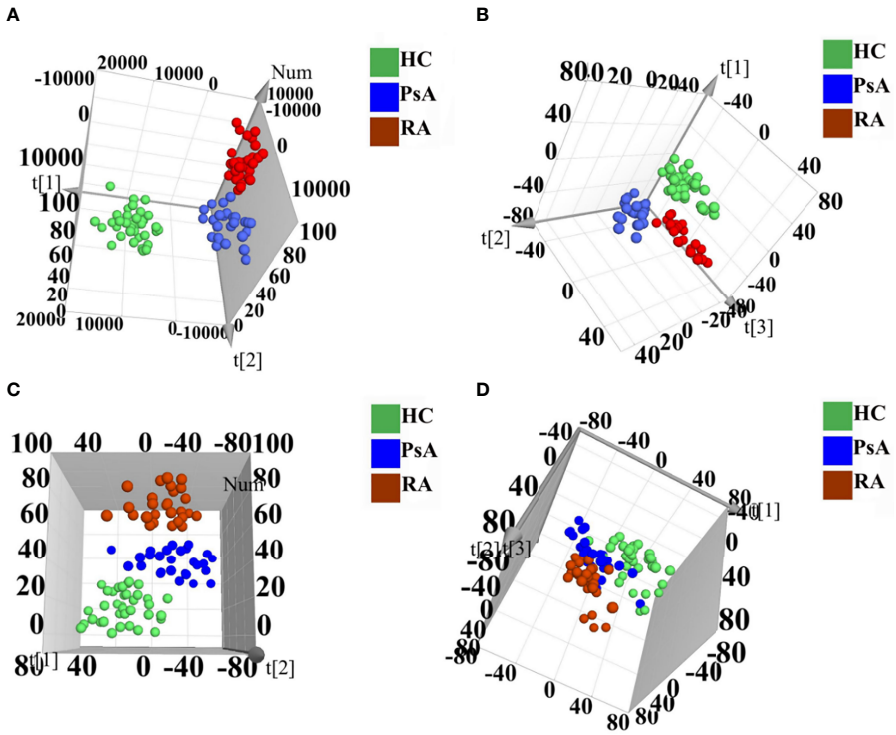

FIGURE 1 | 3D PLS-DA score scatter plots of polar extracts in positive ion mode **(A)** and negative ion mode **(B)**. 3D PLS-DA score scatter plots of non-polar extracts in positive ion mode **(C)** and negative ion mode **(D)**. HC group (green circle), PsA group (blue circle), and RA group (red circle).

supervised 3D PLS-DA model could distinguish them with good separations (**Figure 1B**).

Non-polar extracts: For the PCA model, the PsA, RA, and HC groups were overlapped both in the negative and positive ion modes (**Supplementary Figures S3A, B**). While the 3D PLS-DA models could totally distinguish them in the positive ion mode, and partially distinguish them in the negative ion mode (**Figures 1C, D**).

Differential Metabolites Between HC Group and PsA Group

Polar extracts: The OPLS-DA model was further constructed to determine the differential fecal metabolites between PsA and HC groups (**Figure 2**). The model parameters showed the goodness of fit and prediction ability of the OPLS-DA model both in the positive and negative ion mode (**Table 2**). Based on the criteria of VIP-values (VIP >1), *p*-value (p <0.05), FDR (FDR <0.05) and fold change (FC >1.2 or FC <0.8), a total of 93 differential metabolites were determined between the PsA and HC groups. Among them, 14 fecal metabolites were increased, and 79 fecal metabolites were decreased in the PsA group (**Supplementary Table S3**).

Non-polar extracts: The OPLS-DA model between PsA group and HC group was also constructed for the non-polar extracts with good model parameters (**Supplementary Figure S4** and **Table 2**). Based on the same criteria as described above, 61 differential metabolites were screened out. Among them, 13 fecal metabolites were increased, and 48 metabolites were decreased in the PsA patients when compared with the HCs (**Supplementary Table S3**).

Comparison Between RA Group and PsA Group

Polar extracts: Further, the OPLS-DA model was constructed between RA group and PsA group, and model parameters also indicated the goodness of fit and prediction ability of the model for the positive ion mode (**Supplementary Figure S5** and **Table 2**). With the same criteria, 25 fecal metabolites were found higher in PsA patients, and 7 fecal metabolites were higher in RA patients (**Supplementary Table S4**). However, the model was invalid for the negative ion mode, thus no further analysis was performed (**Supplementary Figure S5**).

Non-polar extracts: Both the OPLS-DA modes in the positive and negative ion modes were valid (**Supplementary Figure S6** and **Table 2**). Thus, a total of 13 metabolites were found to express differently in PsA group compared to RA group (**Supplementary Table S4**). Among them, 8 fecal metabolites were higher in PsA patients, and 5 fecal metabolites were higher in RA patients.

The Heatmap Analysis of RA, PsA and HC Groups

A heatmap was generated to provide an intuitive visualization of the content variation of the differential metabolites among 3 groups (**Figure 3** and **Supplementary Table S5**). The result was

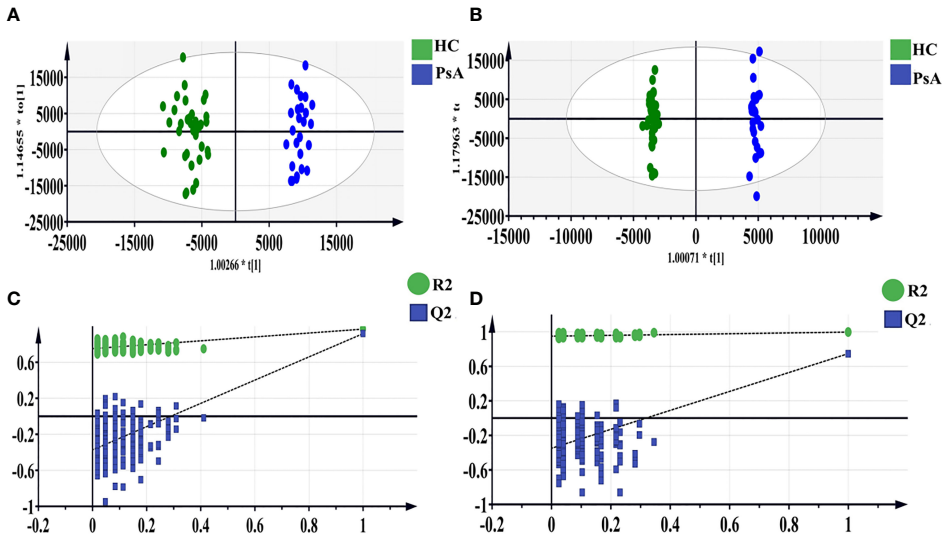

FIGURE 2 | OPLS-DA score scatter plots of polar extracts between HC group and PsA group in positive **(A)** and negative ion mode **(B)**. The result of permutation test in positive ion mode **(C)** and negative ion mode **(D)**. The R^2 and Q^2 values were R^2X (cum) = 0.317, R^2Y (cum) = 0.968, Q^2 (cum) = 0.918 in positive mode. The R^2 and Q^2 values were R^2X (cum) = 0.362, R^2Y (cum) = 0.997, Q^2 (cum) = 0.748 in negative mode. The intercept of Q^2 of positive and negative ion modes on the y-axis was <0, indicating a valid model.

TABLE 2 | The parameters of OPLS-DA model.

		R^2Y	Q^2	*p*-value
HC vs PsA	polar (ESI+)	0.968	0.918	1.50E–28
	polar (ESI–)	0.997	0.748	2.18E–11
	non-polar (ESI+)	0.962	0.525	1.19E–06
	non-polar (ESI–)	0.995	0.592	1.38E–05
RA vs PsA	polar (ESI+)	0.93	0.533	1.13E–06
	polar (ESI–)	0.969	0.169	5.25E–01
	non-polar (ESI+)	0.919	0.293	7.15E–03
	non-polar (ESI–)	0.995	0.387	2.51E–02

consistent with the multivariate analysis, and the HC group was obviously separated from the other groups, as most of the differential metabolites showed the highest contents in the HC group (**Figure 3**). In addition, the difference between the PsA and RA groups were also evident.

Potential Biomarkers for PsA

A total of 154 differential metabolites were screened out between PsA and HC groups, and 45 differential metabolites were found to express differently between PsA and RA groups. There were 14 common metabolites among these differential metabolites, which were defined as candidate biomarkers (**Figure 4**), namely, dihydrosphingosine, hexadecasphinganine, α/β-turmerone, ϵ-caprolactam, serine, glutamine, 4-cholesten-3-one, pantothenic acid, methylimidazoleacetic acid, vaccenic acid, deoxycholic acid, 4α-formyl-4-methylzymosterol, glycerol 1-hexadecanoate, and 1-linoleoyl-rac-glycerol. The potential discriminant biomarkers for PsA diagnosis were evaluated by ROC curve analysis to evaluate their diagnostic efficacy preliminarily (**Figure 5A** and **Supplementary Table S6**).

The areas under the ROC curve (AUCs) of 4α-formyl-4-methylzymosterol (M45), methylimidazoleacetic acid (M66), pantothenic acid (M88), 4-cholesten-3-one (M99), glycerol 1-hexadecanoate (M133), ϵ-caprolactam (M150), α/β-turmerone (M154) were 0.734, 0.704, 0.737, 0.715, 0.755, 0.996, and 0.959, respectively, for discrimination of PsA versus non-PsA (namely, HC and RA). To improve the diagnostic performance of PsA, we constructed a classifier established by Support vector machines (SVM) model in MetaboAnalyst. Since ϵ-caprolactam is an exogenous compound and cannot be synthesized in the body, it cannot be used as a biomarker and was excluded from the model. Thus, we included the 13 common differential metabolites into the SVM model. Based on the SVM classification method, the importance of the variables was ranked according to the sample weighting coefficient of the SVM analysis (**Figure 5B**). The top 2, 3, 5, 10, and 13 important features were respectively selected to build the classification/regression model, and ROC analysis on the joint model were performed (**Figure 5C**). It was found that when the top 5 metabolites in importance, namely, glycerol 1-

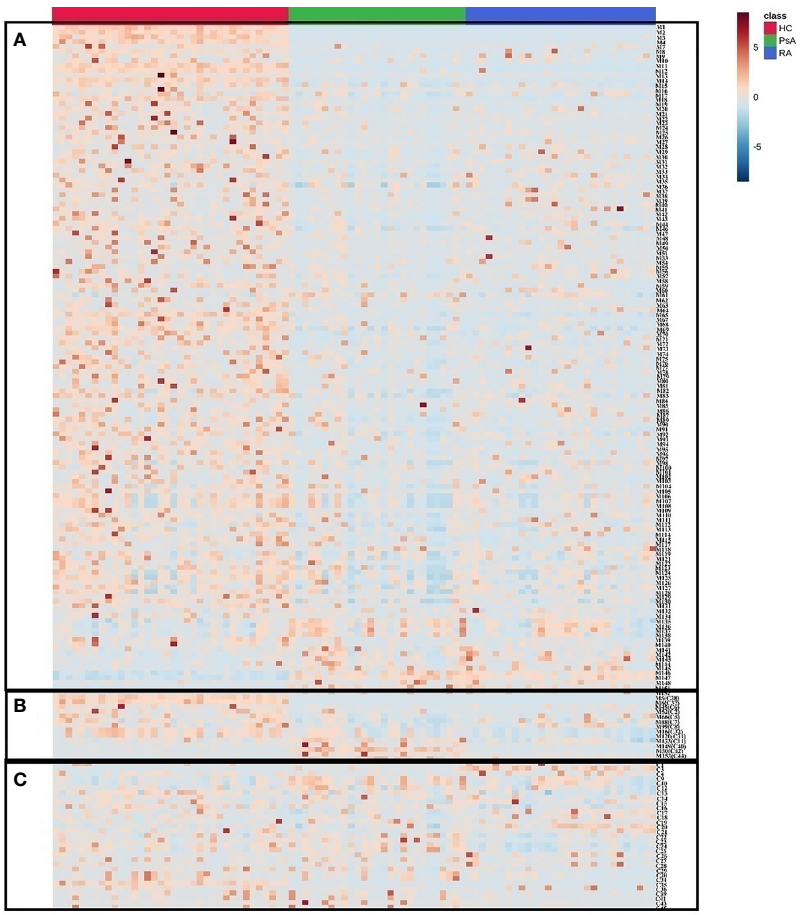

FIGURE 3 | The heatmap of differential metabolites in HC, PsA and RA groups. Red color indicates high level of metabolites and blue color indicates low level of metabolites. **(A)** Metabolites distinguishing HC from PsA groups; **(B)** Metabolites distinguishing PsA from all other groups; **(C)** Metabolites distinguishing PsA from RA groups.

hexadecanoate, dihydrosphingosine, pantothenic acid and glutamine, were combined for ROC analysis, the AUC reached 0.971, which had high sensitivity and specificity (**Figure 5D**). Therefore, these five metabolites have been identified as potential biomarkers that distinguish PsA patients from non-PsA.

Differential Metabolic Pathway Analysis

To further explore the pathway that was possibly related with PsA, 154 different metabolites between the HCs and PsA, and 45 different metabolites between PsA and RA, respectively, were used to perform metabolic pathway analysis (**Figure 6**). As shown in **Figure 6A**, most disease-associated metabolites were decreased in PsA when compared with HCs, such as amino acid, bile acid, fatty acid, involving a variety of metabolic pathways such as amino acid metabolism, bile acid metabolism and fatty acid synthesis. When compared with RA (**Figure 6B**), the metabolic processes associated with inflammatory rheumatic diseases were altered in PsA even when clinical features were similar. The difference metabolites between PsA and RA were involved metabolic pathways, namely, sphingolipid metabolism, secondary bile acid biosynthesis, biosynthesis of unsaturated fatty acids and biosynthesis of amino acids. In addition, it was interesting that significant enrichment of ϵ-caprolactam in PsA patients, whether it is compared with HC or RA, implied the weakening of the degradation pathway of ϵ-caprolactam in PsA.

Correlations of Metabolites With Clinical Phenotype

Compared with HCs, the ESR and neutrophils (NEU) in PsA increased (p <0.05). We investigated the correlations between the differentially altered metabolites and immunological parameters in patients with PsA. As indicated in **Table 3**, geranylgeraniol, lysophosphatidylethanolamine and hexadecasphinganine positively correlated with ESR and CRP. We also observed positive correlations between organic acid (namely, homovanillic acid, trans-cinnamic acid and 2-hydroxy cinnamic acid) and white blood cells (WBCs).

It was proved that T cells are heavily involved in PsA. Studies have shown that the immune system, in particular lymphocytes, has an important influence on the pathogenesis of PsA (1, 2).

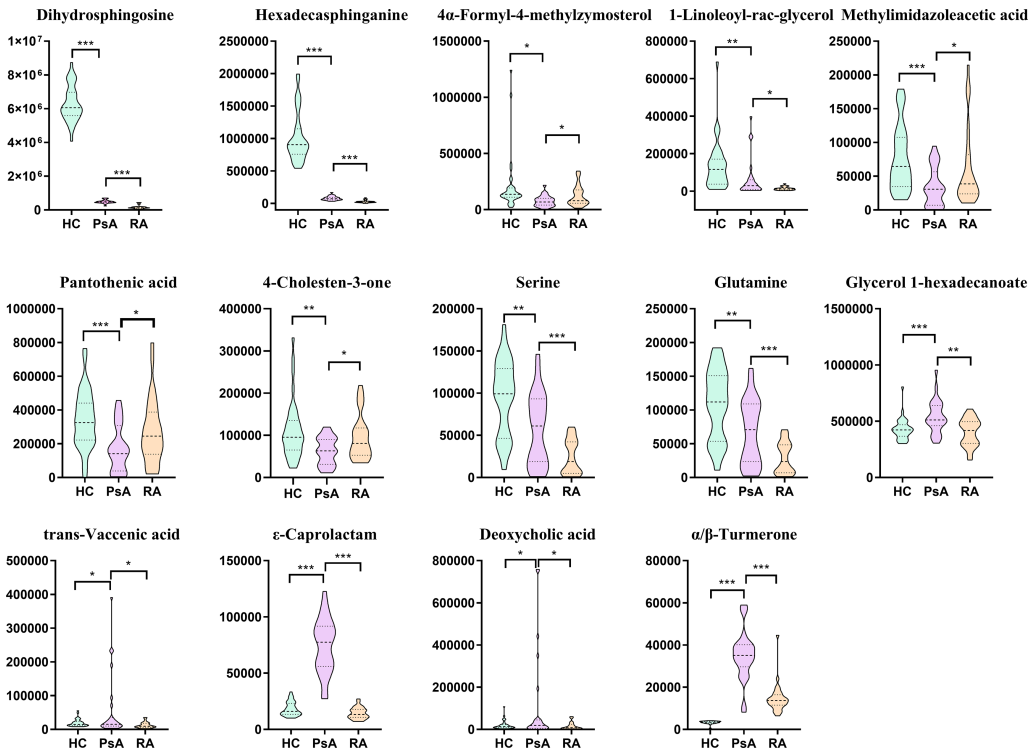

FIGURE 4 | Box plots of biomarker candidates. *, **, *** denoted p <0.05, p <0.01, and p <0.001 in the PsA and other two groups comparison, respectively.

The correlation between the differential metabolites (PsA vs HC) and immune cell subsets was analyzed in 27 PsA patients (**Figure 7A**). Our results showed that increased glycerol 1-hexadecanoate were positively correlated with the absolute numbers of Th2 and Treg, while many decreased metabolites (such as geranylgeraniol, homovanillic acid, glycerol 1-hexadecanoate, lysophosphatidylethanolamine, malic acid and docosahexaenoic acid) were negatively correlated with the absolute numbers of B cells, Treg and T cell effector subsets Th1, Th2, and Th17. In addition, some lipids (namely, hexadecasphinganine, docosahexaenoic acid, heneicosanoic acid, and hexadecan-1-ol) exhibited negative association with Treg, and lower levels of homovanillic acid and lysophosphatidylethanolamine accompanied with increased Th2 (**Figure 7A**). The imbalance between Tregs and T cell effector subsets Th1, Th2, and Th17 might result in chronic inflammation of gut, skin or joints.

Furthermore, correlation between differential metabolites and cytokines were also calculated using Pearson correlation (**Figure 7B**). The results indicated that fecal metabolites differentially depleted in PsA showed higher correlation with cytokines of IL-6, IL-10, IL-17 and IFN-γ. For example, lysophosphatidylethanolamine in PsA was positively linked to IL-10 and IFN-γ ($p < 0.01$).

Even when symptoms of joint involvement are similar between PsA and RA, their cytokines and the metabolic processes associated with inflammatory rheumatic diseases are different. Compared with RA, the cytokines (namely, IL-2, IL-4, IL-10, IL-17, IFN-γ, and TNF-α) in PsA were significantly lower (**Supplementary Table S2**). To further understand whether characteristic metabolites of PsA contribute to disease severity, we tested for their correlations with cytokines using Pearson correlation (**Figure 7C**). We observed that the fecal metabolites differentially abundant in PsA, such as palmitic acid, abscisic acid, cholesteryl laurate, glutamine and serine, exhibited positive association with IL-2, IL-4, IL-10, IL-17, IFN-γ, and TNF-α. For example, increased abscisic acid in PsA was positively linked to IL-2 and IL-4 ($p < 0.01$).

Due to the small sample size of the PsA group, many correlations were not strong enough, the data still suggested a potential link between the fecal metabolites and clinical features of disease.

DISCUSSION

PsA is a chronic autoimmune disease, and its clinical features are variable and may be similar to other rheumatic diseases. It is difficult to diagnose and treat this disease early due to the lack of specificity markers. In the recent years, there has been an increasing interest to the alteration of gut microbiota in the PsA research, which has been proved to have important significance in the pathogenesis of diseases (1, 7, 20, 31). This study is the first published report on fecal metabolome of PsA to

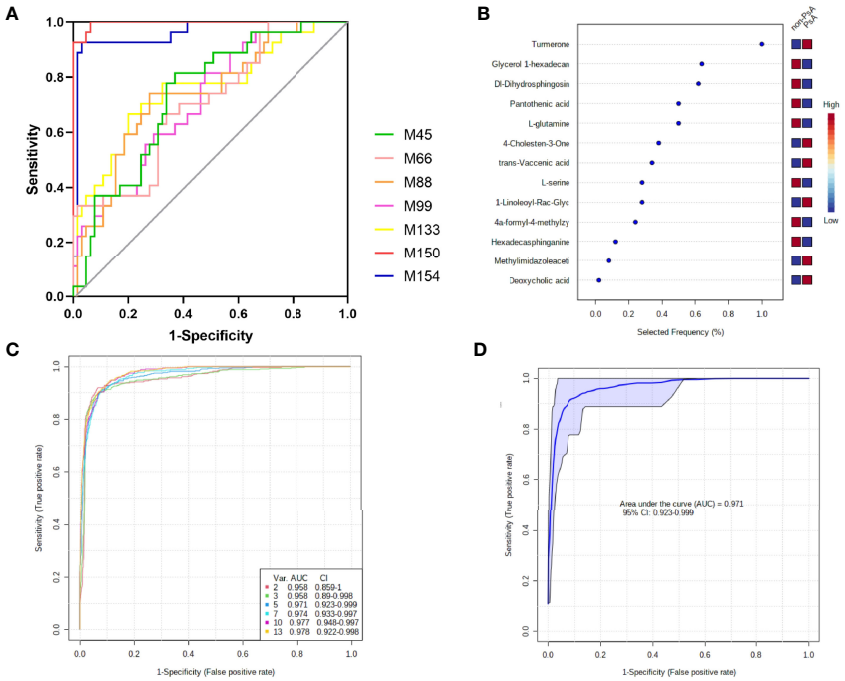

FIGURE 5 | Diagnostic performance of the biomarker model for PsA diagnosis. **(A)** ROC curve analysis of 7 fecal metabolites with AUC >0.7; **(B)** The selected frequency of 13 significant features in SVM model; **(C)** SVM classifier performance for classifying PsA versus non-PsA metabolites; **(D)** ROC curve for 5 fecal microbial markers.

explore the potential diagnostic markers. The metabolic profiles of fecal samples might allow differentiation of PsA patients from RA patients and HCs.

A total of 154 fecal metabolites were significantly altered in PsA patients compared with the healthy controls. Interestingly, there were 45 fecal metabolites also different between PsA and RA patients. Furthermore, 14 common metabolites among these differential metabolites could be defined as candidate biomarkers. It was noteworthy that some disease-associated metabolites were altered in PsA when both compared with HCs and RA, such as amino acid, bile acid, fatty acid, vitamins and so on, involving a variety of metabolic pathways, namely, amino acid metabolism, bile acid metabolism and lipid metabolism.

Amino Acid Metabolism

In the present study, several amino acids were altered in PsA patients compared with the HCs and RA. The levels of fecal kynurenic acid and indole-3-lactic acid were reduced in PsA patients, which are catabolites of tryptophan through the kynurenine pathway. In addition, the content of serine, glutamic acid, glutamine, and oxyproline in PsA decreased, and the content of degradation products of phenylalanine metabolism, such as 2-hydroxy cinnamic acid and 3-(3-hydroxyphenyl) propanoic acid, also decreased. The reduced glutamine was consistent with previous results found in serum of PsA (29). Differences in protein synthesis rate, immune cell consumption of glutamine and transglutaminase levels may be the reasons for the variation of glutamine levels in PsA patients (29). Other work has reported that altered amino acid concentrations may affect changes in energy metabolism (32, 33). Therefore, the data reported in this study indicated that the energy metabolism in PsA was significantly inhibited.

Bile Acid Metabolism

The fecal primary and secondary bile acids, namely, cholic acid, nutriacholic acid, glycocholate, deoxycholic acid and 7-ketodeoxycholic acid, were depleted in PsA when compared with HCs, whereas deoxycholic acid was lower in RA. It is well known that bile acids, such as cholic acid and deoxycholic acid, are signal molecules produced by the decomposition of cholesterol through the interaction between the host and the intestinal flora, which activate bile acid activated receptors (BARs) to regulate liver lipid and glucose metabolic homeostasis and energy metabolism (34–37). Furthermore, in intestinal macrophages, G protein-coupled bile acid receptor 1 (GPBAR1) and Farnesoid-X-receptor (FXR) are highly expressed, which also occurs in innate immunity such as dendritic cells and natural killer cells (16, 35). Additionally, secondary bile acids, namely, lithocholic acid and deoxycholic acid, have been reported to protect the intestinal barrier (38, 39). Taken together, the data reported in our study indicated that alteration of bile acid homeostasis may be related to the occurrence and development of PsA.

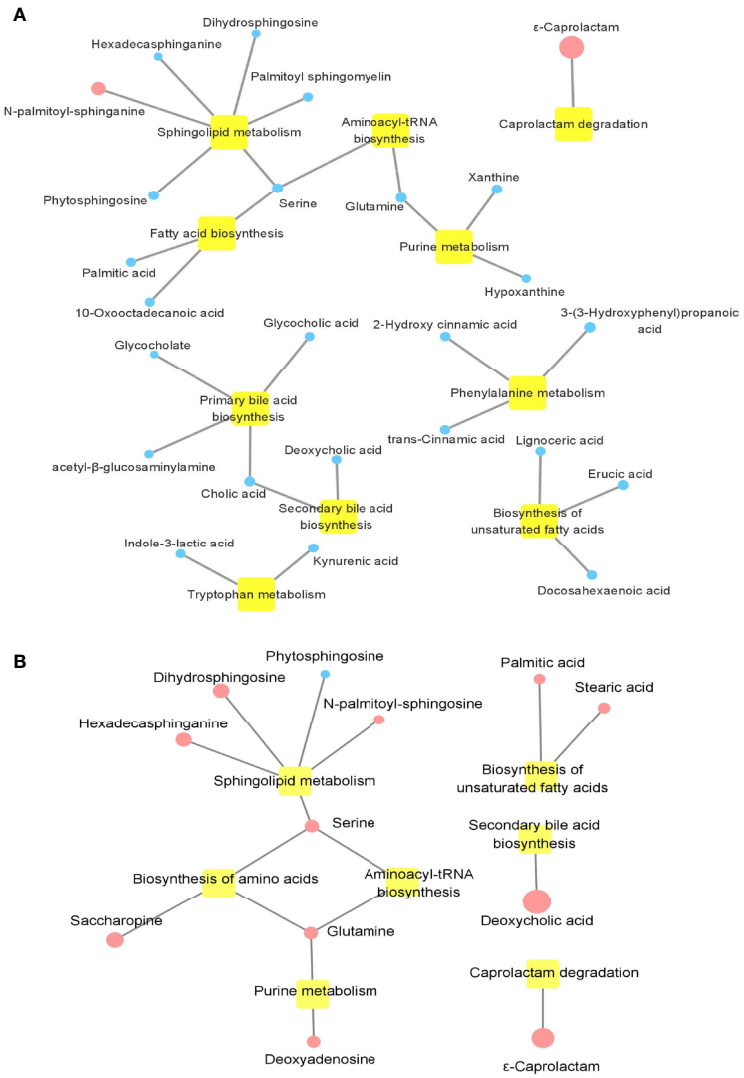

FIGURE 6 | Enrichment map of metabolic pathways involved in differential metabolites. **(A)** Metabolic pathways involved in differential metabolites between PsA and HC. **(B)** Metabolic pathways involved in differential metabolites between PsA and RA. Yellow nodes represent metabolic pathways involved. Circular node represents the change in metabolite, where blue indicates a decrease in PsA, and red indicates an increase in PsA; the size of the circle indicates the fold change of metabolites in PsA compared with HC or RA.

TABLE 3 | Pearson's correlation analysis between differentially altered metabolites and immunological parameters.

Immunological parameters	Metabolites	R	*p*- value
ESR	geranylgeraniol	0.436*	0.023
	lysophosphatidylethanolamine	0.400*	0.038
	hexadecasphinganine	0.424*	0.028
CRP	geranylgeraniol	0.531**	0.008
	lysophosphatidylethanolamine	0.423*	0.039
	hexadecasphinganine	0.557**	0.005
WBC	homovanillic acid	0.410*	0.034
	trans-cinnamic acid	0.470*	0.013
	2-hydroxy cinnamic acid	0.529**	0.005
	4-ethylphenol	0.486*	0.01
NEU	homovanillic acid	0.492**	0.009
	2-hydroxy cinnamic acid	0.561**	0.002
	4-ethylphenol	0.505**	0.007

*, ** *denoted* $p < 0.05$, $p < 0.01$ *in differentially altered metabolites in PsA and immunological parameters comparison, respectively.*

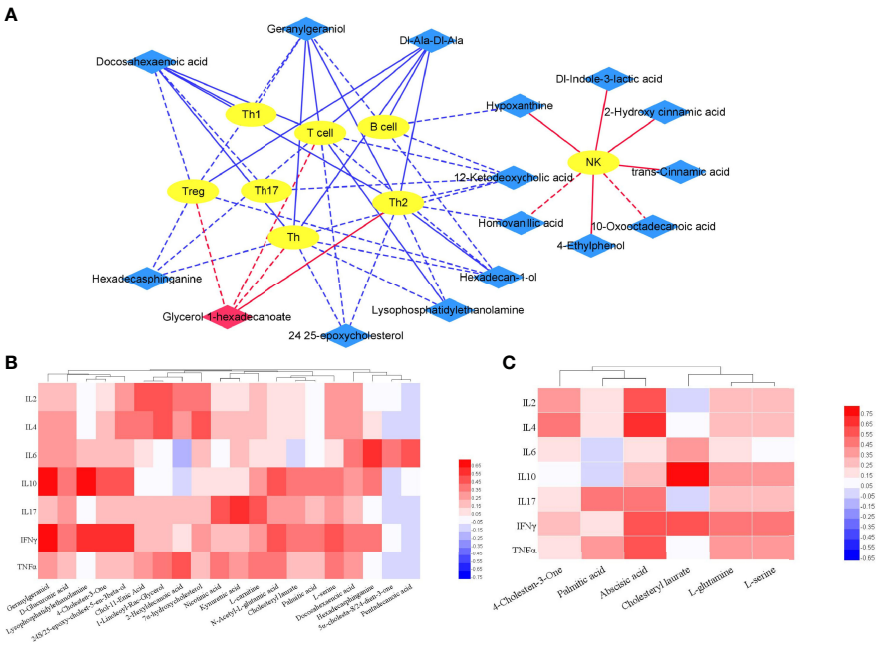

FIGURE 7 | Correlation of differential metabolites and clinical features. **(A)** Integrative network of associations reflecting the interactions of differential metabolites (PsA vs HC) and lymphocyte subpopulation *via* Cytoscape (3.8.2). Network revealed both significant (p <0.01) and suggestive associations (0.01< p <0.05) between differentially abundant metabolites and lymphocyte subpopulation in PsA. Yellow oval nodes represent immune cells, red and blue diamond nodes represent the increase and decrease of metabolites in PsA, respectively. Lines connecting nodes indicate positive (red) or negative (blue) correlations. The full lines and dotted lines indicate significant correlation and suggestive correlation respectively. **(B)** Correlation of differential metabolites (PsA vs HC) and cytokines in PsA; **(C)** Correlation of differential metabolites (PsA vs RA) and Cytokines in PsA.

Lipid Metabolism

In addition to changes of amino acid and bile acid metabolism, the alteration of lipid metabolism was also highlighted in our study. Interestingly, the PsA group was characterized by altered polyunsaturated fatty acid (PUFAs) compared with non-PsA. In particular, a decrease of docosahexaenoic acid in PsA was observed. The impaired balance of PUFAs contributes to the development of some autoimmune diseases, for example, n–6/n–3 PUFAs have a major impact on the homeostasis of the immune system (40–42). Previous studies have proposed that serum PUFAs levels in patients with rheumatic diseases were usually lower (42, 43). ω-3 Fatty acids have potential immunomodulatory and anti-inflammatory effects, which could inhibit inflammation by reducing the expression of cell surface molecules and adhesion molecules, inhibiting inflammatory factors, and affecting immune cell function (44, 45). Furthermore, studies have reported that in mouse models, dietary ω-3 fatty acids had been successfully used to reduce the severity of arthritis and atopic dermatitis by promoting the differentiation of $CD4^+$ T cells into Tregs (41, 46, 47).

We noticed that many metabolites (N-palmitoyl-sphinganine, phytosphingosine, dihydrosphingosine and serine) in sphingolipid metabolism pathway were altered in PsA. Sphingolipids, produced by both the host and specific bacteria, participate in specific signaling pathways of physiologic cellular functions by acting as signaling molecules or regulating the function of downstream signal molecules (16, 48). In the intestine, host sphingolipids have been thought to act directly or indirectly as inflammatory mediators (49). Sphingolipids have recently been identified as the most variable metabolite in the stool of patients with inflammatory bowel disease (IBD) (50), which was reported to be consistent with patients with PsA (51–53). Studies have shown that sphingolipid levels can regulate host immunity, and sphingolipid deficiency strains can trigger intestinal inflammation, which accompanied with an increase of IL-6 and monocyte chemoattractant protein-1 (MCP-1) in the colon (50).

In conclusion, these observations hinted that there was a potential connection between altered lipid metabolism and the pathology of PsA, which involved with sphingolipid metabolism and fatty acid metabolism at the pathway level.

Vitamins

In addition to the metabolic changes reported above, we also found a decrease in nicotinic acid (VB3) and pantothenic acid (VB5), both of which belong to the B vitamins. These vitamins were both produced and secreted by intestinal microbes and exhibited anti-inflammatory and antioxidant activities (33, 54). Nicotinic acid is the precursor of nicotinamide adenine dinucleotide (NAD), which plays an important role in various biological processes, namely, cell metabolism, inflammatory response, aging regulation, and cell death (16). VB3 directly activates G Protein-Coupled Receptor 109A (GPCR109A), which is one of the receptor for short chain fatty acid (SCFA).

In a preclinical model of colon inflammation, the activation of GPCR109A appeared to be related with the abundance of Treg in the intestinal lamina propria and the production of IL-10 (55). Moreover, VB3 reduced the secretion of inflammatory cytokines such as IL-6, TNF-α and MCP-1 when treated with lipopolysaccharide (LPS) in human monocytes (54). Pantothenic acid (VB5) is the precursor of the coenzyme A (CoA), and also an activator of fatty acid metabolism and oxidation reaction mediated by the tricarboxylic acid cycle, which is related to inflammatory homeostasis (16). In addition to the decrease in B vitamins found in PsA feces, a change in α-tocopherol (vitamin E) was also found. Vitamin E is one of the important antioxidants in the human, which can inhibit the peroxidation of lipids in cell membranes and circulate lipoproteins. It has also been reported to play an important role in the prevention and adjuvant treatment of certain chronic diseases (56).

Interestingly, we observed that ϵ-caprolactam and α/β-turmerone were uniquely increased in PsA patients. An increase of ϵ-caprolactam indicated the accumulation of xenobiotics and attenuated pathways for caprolactam degradation (ko00930) in the body. ϵ-Caprolactam is used as the raw material of nylon to produce a great deal of interior products, such as synthetic leather, synthetic fiber, plastifier and resin (57). The ubiquitous xenobiotic substances can be maintained and accumulated in the intestine due to continuous exposure to urban environment (58, 59), which might create the appropriate conditions for microbial communities in host to functionally adapt to the degradation of xenobiotic substances, including caprolactam (59–61). It was reported that oral exposure to titanium dioxide nanoparticles led to the increase of fecal caprolactam (62). In addition, deceased plasma caprolactam was also observed in the pregnant women with methylenetetrahydrofolate reductase (MTHFR) polymorphisms (63). A recent upper respiratory microbiome study found that compared with asthma patients, the abundance of caprolactam degradation pathway was significantly higher in the non-asthmatic group (61). In another recent work, the authors also found an increase in caprolactam degradation pathways in the gut microbiome of centenarians and semi-supercentenarians (59). Thus, the unique aggregation of caprolactam, which can irritate respiratory tract, eye, skin and mucous membrane (64), implied that it may have a certain effect on the occurrence of PsA, however, the exact mechanism need to be further clarified.

As regards turmerone, it is a class of polyphenolic compounds abundant in plant-based diets, obtained from turmeric (65). They are categorized as α-turmerone, ar-turmerone, and β-turmerone, and exhibit immunomodulatory effects (66). Research has shown that ar-turmerone can increase the expression level of differentiation clusters (CD40, CD80, CD83, and CD86), and subsequently induced the phenotypic and functional maturation of dendritic cells (DC). Further, the treatment with ar-turmerone can reduce the activity of acid phosphatase (ACP) in DC and promote the production of interleukin (IL-12) and TNF-α (65, 67). The human intestinal flora can metabolize polyphenols to form active substances with different functions, and polyphenols can also be transformed to affect their bioavailability (68). Therefore, the analysis of metabolic pathways is crucial for understanding these processes. However, the mechanism of how turmerone is transformed and metabolized in the intestine after entering the body to act on immune cells is still unclear. In our study, significant increase of α/β-turmerone in PsA indicated that the intestinal flora of PsA patients might lack bacteria that can metabolize polyphenols. All in all, our results indicated that the gut microbiome of PsA might be less equipped for the degradation of xenobiotics.

Actually, the fecal metabolites included the compounds from the host, microbiota and food residues, thus, not all the fecal compounds could reflect the biochemical status of the gut microbiota under the disease condition. In our study, tryptophan related metabolites, secondary bile acids, vitamins, dietary polyphenols and the degradation of xenobiotic substances were related with gut microbiota (16, 69), and thus, these metabolites implied the function of intestinal bacteria. However, the amino acids, unsaturated fatty acids and sphingomyelin were both produced by intestinal microbes and host (16), and the change of these metabolites might come from the metabolic status of the gut microbe or host.

In conclusion, we observed dysregulation of metabolic pathways in fecal samples from patients with PsA, which can be used for PsA diagnosis in a non-invasive manner. However, some limitations must be recognized in our research. First, the sample size of this study was relatively small, which may lead to missing of some differential metabolites and further limiting the generalization of the results. In the future, it is necessary to study a larger patient cohort to confirm these findings. Second, it is unclear how the intestinal microbiota affects blood characteristics due to the lack of blood samples. Further research integrating the metabolic characteristics of feces and blood is of great significance for further understanding the microbial functions in PsA. Finally, this study only conducted non-targeted metabolomics on fecal samples of PsA, and the selected candidate biomarkers lack accurate quantitative verification. Therefore, samples from multicenter cohort should be used to verify the discriminant power of biomarker panel.

In summary, this is the first metabolomic study applied to the feces of PsA and RA patients. We discovered that fecal metabolites were significantly different between these patients and HCs, and also between PsA and RA. The results might bring about the identification of new candidate biomarkers or targets for PsA diagnosis or treatment. In addition, our data emphasized that even if the clinical features were similar, the metabolic processes associated with inflammatory rheumatism differed greatly between PsA and RA. Further functional studies are necessary to explore the impact of these metabolic changes on the underlying pathogenesis mechanisms of PsA.

DATA AVAILABILITY STATEMENT

The original contributions presented in the study are publicly available. This data can be found here: http://www.ebi.ac.uk/metabolights/MTBLS4206.

ETHICS STATEMENT

This study was approved by the ethics committee of the Second Hospital of Shanxi Medical University (2019YX266). The patients/participants provided their written informed consent to participate in this study.

AUTHOR CONTRIBUTIONS

JL and ZL conceived and designed the study. NW, LY, SY, and XL performed the experiments and analyzed the data. LS, ZL, YW, and MF contributed to the sample collection and storage. NW and LS were responsible for clinical data collection. NW and LY wrote the manuscript. CG, ZL, and JL reviewed and edited the manuscript. All authors listed have made a substantial, direct, and intellectual contribution to the work and approved it for publication.

FUNDING

This work was supported by the Key Research and Development Project (Guide) of Shanxi Province (201803D421067), the Nature Fund Projects of Shanxi Science and Technology Department (201901D111377), the Scientific Research Project of Health commission of Shanxi Province (2019044), the Research Project Supported by Shanxi Scholarship Council of China (2020-191) and the Science and Technology Innovation Project of Shanxi Province (2020SYS08).

SUPPLEMENTARY MATERIAL

The Supplementary Material for this article can be found online at: https://www.frontiersin.org/articles/10.3389/fimmu.2022.812996/full#supplementary-material

REFERENCES

1. Chimenti MS, Perricone C, Novelli L, Caso F, Costa L, Bogdanos D, et al. Interaction Between Microbiome and Host Genetics in Psoriatic Arthritis. *Autoimmun Rev* (2018) 17(3):276–83. doi: 10.1016/j.autrev.2018.01.002
2. Ocampo DV, Gladman D. Psoriatic Arthritis. *F1000Res* (2019) 8:1665. doi: 10.12688/f1000research.19144.1
3. Raychaudhuri SP, Wilken R, Sukhov AC, Raychaudhuri SK, Maverakis E. Management of Psoriatic Arthritis: Early Diagnosis, Monitoring of Disease Severity and Cutting Edge Therapies. *J Autoimmun* (2017) 76:21–37. doi: 10.1016/j.jaut.2016.10.009
4. Sukhov A, Adamopoulos IE, Maverakis E. Interactions of the Immune System With Skin and Bone Tissue in Psoriatic Arthritis: A Comprehensive Review. *Clin Rev Allergy Immunol* (2016) 51(1):87–99. doi: 10.1007/s12016-016-8529-8
5. ElSherbiny DA, Elsayed AMA, El-Azizi NO, Ghalwash RA. Clinical and Laboratory Characteristics of Psoriatic Arthritis in a Cohort of Egyptian Patients. *Egypt Rheumatol* (2021) 43(3):229–34. doi: 10.1016/j.ejr.2021.03.003
6. Raychaudhuri SK, Maverakis E, Raychaudhuri SP. Diagnosis and Classification of Psoriasis. *Autoimmun Rev* (2014) 13(4):490–5. doi: 10.1016/j.autrev.2014.01.008
7. Myers B, Brownstone N, Reddy V, Chan S, Thibodeaux Q, Truong A, et al. The Gut Microbiome in Psoriasis and Psoriatic Arthritis. *Best Pract Res Clin Rheumatol* (2019) 33(6):101494. doi: 10.1016/j.berh.2020.101494
8. Danielsen K, Olsen AO, Wilsgaard T, Furberg AS. Is the Prevalence of Psoriasis Increasing? A 30-Year Follow-Up of a Population-Based Cohort. *Br J Dermatol* (2013) 168(6):1303–10. doi: 10.1111/bjd.12230
9. Zabotti A, Salvin S, Quartuccio L, De Vita S. Differentiation Between Early Rheumatoid and Early Psoriatic Arthritis by the Ultrasonographic Study of the Synovio-Entheseal Complex of the Small Joints of the Hands. *Clin Exp Rheumatol* (2016) 34(3):459–65. doi: 10.1136/rmdopen-2018-000656
10. Verheul MK, Fearon U, Trouw LA, Veale DJ. Biomarkers for Rheumatoid and Psoriatic Arthritis. *Clin Immunol* (2015) 161(1):2–10. doi: 10.1016/j.clim.2015.04.005
11. Merola JF, Espinoza LR, Fleischmann R. Distinguishing Rheumatoid Arthritis From Psoriatic Arthritis. *RMD Open* (2018) 4:e000656. doi: 10.1136/rmdopen-2018-000656
12. Veale DJ, Fearon U. What Makes Psoriatic and Rheumatoid Arthritis So Different? *RMD Open* (2015) 1:e000025. doi: 10.1136/rmdopen-2014-000025
13. Veale DJ, Fearon U. The Pathogenesis of Psoriatic Arthritis. *Lancet* (2018) 391 (10136):2273–84. doi: 10.1016/S0140-6736(18)30830-4
14. Souto-Carneiro M, Tóth L, Behnisch R, Urbach K, Klika KD, Carvalho RA, et al. Differences in the Serum Metabolome and Lipidome Identify Potential Biomarkers for Seronegative Rheumatoid Arthritis Versus Psoriatic Arthritis. *Ann Rheum Dis* (2020) 79(4):499–506. doi: 10.1136/annrheumdis-2019-216374
15. Alivernini S, Bruno D, Tolusso B, Bui L, Petricca L, Gigante MR, et al. Differential Synovial Tissue Biomarkers Among Psoriatic Arthritis and Rheumatoid Factor/Anti-Citrulline Antibody-Negative Rheumatoid Arthritis. *Arthritis Res Ther* (2019) 21(1):116. doi: 10.1186/s13075-019-1898-7
16. Caffaratti C, Plazy C, Mery G, Tidjani AR, Fiorini F, Thiroux S, et al. What We Know So Far About the Metabolite-Mediated Microbiota-Intestinal Immunity Dialogue and How to Hear the Sound of This Crosstalk. *Metabolites* (2021) 11 (6):406. doi: 10.3390/metabo11060406
17. Eppinga H, Konstantinov SR, Peppelenbosch MP, Thio HB. The Microbiome and Psoriatic Arthritis. *Curr Rheumatol Rep* (2014) 16(3):NO.407. doi: 10.1007/s11926-013-0407-2
18. Dorrestein PC, Mazmanian SK, Knight R. Finding the Missing Links Among Metabolites, Microbes, and the Host. *Immunity* (2014) 40(6):824–32. doi: 10.1016/j.immuni.2014.05.015
19. Zierer J, Jackson MA, Kastenmüller G, Mangino M, Long T, Telenti A, et al. The Fecal Metabolome as a Functional Readout of the Gut Microbiome. *Nat Genet* (2018) 50(6):790–5. doi: 10.1038/s41588-018-0135-7
20. Shapiro J, Cohen NA, Shalev V, Uzan A, Koren O, Maharshak N. Psoriatic Patients Have a Distinct Structural and Functional Fecal Microbiota Compared With Controls. *J Dermatol* (2019) 46(7):595–603. doi: 10.1111/1346-8138.14933
21. Nicholson JK, Lindon JC, Holmes E. 'Metabonomics': Understanding the Metabolic Responses of Living Systems to Pathophysiological Stimuli via Multivariate Statistical Analysis of Biological NMR Spectroscopic Data. *Xenobiotica* (1999) 29(11):1181–9. doi: 10.1080/004982599238047
22. Campanaro F, Batticciotto A, Zaffaroni A, Cappelli A, Donadini MP, Squizzato A. JAK Inhibitors and Psoriatic Arthritis: A Systematic Review and Meta-Analysis. *Autoimmun Rev* (2021) 20(10):102902. doi: 10.1016/j.autrev.2021.102902
23. Liu X, Zheng P, Zhao X, Zhang Y, Hu C, Li J, et al. Discovery and Validation of Plasma Biomarkers for Major Depressive Disorder Classification Based on Liquid Chromatography-Mass Spectrometry. *J Proteome Res* (2015) 14 (5):2322–30. doi: 10.1021/acs.jproteome.5b00144
24. Wang Q, Su B, Dong L, Jiang T, Tan Y, Lu X, et al. Liquid Chromatography-Mass Spectrometry-Based Nontargeted Metabolomics Predicts Prognosis of Hepatocellular Carcinoma After Curative Resection. *J Proteome Res* (2020) 19 (8):3533–41. doi: 10.1021/acs.jproteome.0c00344
25. Fernandez-Ochoa A, Borras-Linares I, Quirantes-Pine R, Alarcon-Riquelme ME, Beretta L, Segura-Carretero A, et al. Discovering New Metabolite Alterations in Primary Sjogren's Syndrome in Urinary and Plasma Samples Using an HPLC-ESI-QTOF-MS Methodology. *J Pharm BioMed Anal* (2020) 179:112999. doi: 10.1016/j.jpba.2019.112999
26. Zhang Q, Li X, Yin X, Wang H, Fu C, Wang H, et al. Metabolomic Profiling Reveals Serum L-Pyroglutamic Acid as a Potential Diagnostic Biomarker for

Systemic Lupus Erythematosus. *Rheumatol (Oxf)* (2021) 60(2):598–606. doi: 10.1093/rheumatology/keaa126
27. Tsoukalas D, Fragoulakis V, Papakonstantinou E, Antonaki M, Vozikis A, Tsatsakis A, et al. Prediction of Autoimmune Diseases by Targeted Metabolomic Assay of Urinary Organic Acids. *Metabolites* (2020) 10 (12):502. doi: 10.3390/metabo10120502
28. Carlson AK, Rawle RA, Wallace CW, Adams E, Greenwood MC, Bothner B, et al. Global Metabolomic Profiling of Human Synovial Fluid for Rheumatoid Arthritis Biomarkers. *Clin Exp Rheumatol* (2019) 37(3):393–9.
29. Armstrong AW, Wu J, Johnson MA, Grapov D, Azizi B, Dhillon J, et al. Metabolomics in Psoriatic Disease: Pilot Study Reveals Metabolite Differences in Psoriasis and Psoriatic Arthritis. *F1000Res* (2014) 3:248. doi: 10.12688/f1000research.4709.1
30. Yu M, Jia H, Zhou C, Yang Y, Zhao Y, Yang M, et al. Variations in Gut Microbiota and Fecal Metabolic Phenotype Associated With Depression by 16S rRNA Gene Sequencing and LC/MS-Based Metabolomics. *J Pharm BioMed Anal* (2017) 138:231–9. doi: 10.1016/j.jpba.2017.02.008
31. Olejniczak-Staruch I, Ciazynska M, Sobolewska-Sztychny D, Narbutt J, Skibinska M, Lesiak A. Alterations of the Skin and Gut Microbiome in Psoriasis and Psoriatic Arthritis. *Int J Mol Sci* (2021) 22(8):3998. doi: 10.3390/ijms22083998
32. Trupp M, Jonsson P, Ohrfelt A, Zetterberg H, Obudulu O, Malm L, et al. Metabolite and Peptide Levels in Plasma and CSF Differentiating Healthy Controls From Patients With Newly Diagnosed Parkinson's Disease. *J Parkinsons Dis* (2014) 4(3):549–60. doi: 10.3233/JPD-140389
33. Vascellari S, Palmas V, Melis M, Pisanu S, Cusano R, Uva P, et al. Gut Microbiota and Metabolome Alterations Associated With Parkinson's Disease. *mSystems* (2020) 5(5):e00561-20. doi: 10.1128/mSystems.00561-20
34. Chiang JYL, Ferrell JM. Bile Acid Metabolism in Liver Pathobiology. *Gene Expr* (2018) 18(2):71–87. doi: 10.3727/105221618X15156018385515
35. Fiorucci S, Biagioli M, Zampella A, Distrutti E. Bile Acids Activated Receptors Regulate Innate Immunity. *Front Immunol* (2018) 9:1853. doi: 10.3389/fimmu.2018.01853
36. Jia W, Xie G, Jia W. Bile Acid-Microbiota Crosstalk in Gastrointestinal Inflammation and Carcinogenesis. *Nat Rev Gastroenterol Hepatol* (2018) 15 (2):111–28. doi: 10.1038/nrgastro.2017.119
37. Zhan K, Zheng H, Li J, Wu H, Qin S, Luo L, et al. Gut Microbiota-Bile Acid Crosstalk in Diarrhea-Irritable Bowel Syndrome. *BioMed Res Int* (2020) 2020:3828249. doi: 10.1155/2020/3828249
38. Liu Q, Li B, Li Y, Wei Y, Huang B, Liang J, et al. Altered Faecal Microbiome and Metabolome in IgG4-Related Sclerosing Cholangitis and Primary Sclerosing Cholangitis. *Gut* (2021) 0:1–11. doi: 10.1136/gutjnl-2020-323565
39. Sinha SR, Haileselassie Y, Nguyen LP, Tropini C, Wang M, Becker LS, et al. Dysbiosis-Induced Secondary Bile Acid Deficiency Promotes Intestinal Inflammation. *Cell Host Microbe* (2020) 27(4):659–70.e5. doi: 10.1016/j.chom.2020.01.021
40. Calder PC, Grimble RF. Polyunsaturated Fatty Acids, Inflammation and Immunity. *Eur J Clin Nutr* (2002) 56 Suppl 3:S14–9. doi: 10.1038/sj.ejcn.1601478
41. Gutiérrez S, Svahn SL, Johansson ME. Effects of Omega-3 Fatty Acids on Immune Cells. *Int J Mol Sci* (2019) 20(20):5028. doi: 10.3390/ijms20205028
42. Radzikowska U, Rinaldi AO, Celebi Sozener Z, Karaguzel D, Wojcik M, Cypryk K, et al. The Influence of Dietary Fatty Acids on Immune Responses. *Nutrients* (2019) 11(12):2990. doi: 10.3390/nu11122990
43. Dai X, Chen Y, Zeng F, Sun L, Chen C, Su Y. Association Between N-3 Polyunsaturated Fatty Acids in Erythrocytes and Metabolic Syndrome in Chinese Men and Women. *Eur J Nutr* (2016) 55(3):981–9. doi: 10.1007/s00394-015-0912-3
44. Calder PC. Marine Omega-3 Fatty Acids and Inflammatory Processes: Effects, Mechanisms and Clinical Relevance. *Biochim Biophys Acta* (2015) 1851 (4):469–84. doi: 10.1016/j.bbalip.2014.08.010
45. Calder PC. Omega-3 Fatty Acids and Inflammatory Processes: From Molecules to Man. *Biochem Soc Trans* (2017) 45(5):1105–15. doi: 10.1042/BST20160474
46. Han SC, Koo DH, Kang NJ, Yoon WJ, Kang GJ, Kang HK, et al. Docosahexaenoic Acid Alleviates Atopic Dermatitis by Generating Tregs and IL-10/TGF-β-Modified Macrophages *via* a TGF-β-Dependent Mechanism. *J Invest Dermatol* (2015) 135(6):1556–64. doi: 10.1038/jid.2014.488
47. Kim JY, Lim K, Kim KH, Kim JH, Choi JS, Shim SC. N-3 Polyunsaturated Fatty Acids Restore Th17 and Treg Balance in Collagen Antibody-Induced Arthritis. *PloS One* (2018) 13(3):e0194331. doi: 10.1371/journal.pone.0194331
48. Hannun YA, Obeid LM. Sphingolipids and Their Metabolism in Physiology and Disease. *Nat Rev Mol Cell Biol* (2018) 19(3):175–91. doi: 10.1038/nrm.2017.107
49. Maceyka M, Spiegel S. Sphingolipid Metabolites in Inflammatory Disease. *Nature* (2014) 510(7503):58–67. doi: 10.1038/nature13475
50. Brown EM, Ke X, Hitchcock D, Jeanfavre S, Avila-Pacheco J, Nakata T, et al. Bacteroides-Derived Sphingolipids Are Critical for Maintaining Intestinal Homeostasis and Symbiosis. *Cell Host Microbe* (2019) 25(5):668–80. doi: 10.1016/j.chom.2019.04.002
51. Gottlieb A, Merola JF. Psoriatic Arthritis for Dermatologists. *J Dermatolog Treat* (2020) 31(7):662–79. doi: 10.1080/09546634.2019.1605142
52. Yang CR, Ker A, Kao PE, Wei JC. Risk of Inflammatory Bowel Disease in Patients With Psoriasis, Psoriatic Arthritis and Ankylosing Spondylitis Initiating Interleukin 17 Inhibitors. *Arthritis Rheumatol* (2022) 74(2):244–52. doi: 10.1002/art.41923
53. Scher JU, Ubeda C, Artacho A, Attur M, Isaac S, Reddy SM, et al. Decreased Bacterial Diversity Characterizes the Altered Gut Microbiota in Patients With Psoriatic Arthritis, Resembling Dysbiosis in Inflammatory Bowel Disease. *Arthritis Rheumatol* (2015) 67(1):128–39. doi: 10.1002/art.38892
54. Peterson CT, Rodionov DA, Osterman AL, Peterson SN. B Vitamins and Their Role in Immune Regulation and Cancer. *Nutrients* (2020) 12(11):3380. doi: 10.3390/nu12113380
55. Singh N, Gurav A, Sivaprakasam S, Brady E, Padia R, Shi H, et al. Activation of Gpr109a, Receptor for Niacin and the Commensal Metabolite Butyrate, Suppresses Colonic Inflammation and Carcinogenesis. *Immunity* (2014) 40 (1):128–39. doi: 10.1016/j.immuni.2013.12.007
56. Stacchiotti V, Rezzi S, Eggersdorfer M, Galli F. Metabolic and Functional Interplay Between Gut Microbiota and Fat-Soluble Vitamins. *Crit Rev Food Sci Nutr* (2021) 61(19):3211–32. doi: 110.1080/10408398.2020.1793728
57. Massolo L, Rehwagen M, Porta A, Ronco A, Herbarth O, Mueller A. Indoor-Outdoor Distribution and Risk Assessment of Volatile Organic Compounds in the Atmosphere of Industrial and Urban Areas. *Environ Toxicol* (2010) 25 (4):339–49. doi: 10.1002/tox.20504
58. Wright SL, Kelly FJ. Plastic and Human Health: A Micro Issue? *Environ Sci Technol* (2017) 51(12):6634–47. doi: 10.1021/acs.est.7b00423
59. Rampelli S, Soverini M, D'Amico F, Barone M, Tavella T, Monti D, et al. Shotgun Metagenomics of Gut Microbiota in Humans With Up to Extreme Longevity and the Increasing Role of Xenobiotic Degradation. *mSystems* (2020) 5(2):e00124-20. doi: 10.1128/mSystems.00124-20
60. Rampelli S, Schnorr SL, Consolandi C, Turroni S, Severgnini M, Peano C, et al. Metagenome Sequencing of the Hadza Hunter-Gatherer Gut Microbiota. *Curr Biol* (2015) 25(13):1682–93. doi: 10.1016/j.cub.2015.04.055
61. Lee JJ, Kim SH, Lee MJ, Kim BK, Song WJ, Park HW, et al. Different Upper Airway Microbiome and Their Functional Genes Associated With Asthma in Young Adults and Elderly Individuals. *Allergy* (2019) 74(4):709–19. doi: 10.1111/all.13608
62. Chen Z, Han S, Zhou D, Zhou S, Jia G. Effects of Oral Exposure to Titanium Dioxide Nanoparticles on Gut Microbiota and Gut-Associated Metabolism *In Vivo*. *Nanoscale* (2019) 11(46):22398–412. doi: 10.1039/c9nr07580a
63. Recber T, Orgul G, Aydın E, Tanacan A, Nemutlu E, Kır S, et al. Metabolic Infrastructure of Pregnant Women With Methylenetetrahydrofolate Reductase Polymorphisms: A Metabolomic Analysis. *BioMed Chromatogr* (2020) 34(8):e4842. doi: 10.1002/bmc.4842
64. Wu YH, Wu ML, Lin CC, Chu WL, Yang CC, Lin RT, et al. Determination of Caprolactam and 6-Aminocaproic Acid in Human Urine Using Hydrophilic Interaction Liquid Chromatography-Tandem Mass Spectrometry. *J Chromatogr B Analyt Technol BioMed Life Sci* (2012) 15:885–886:61–5. doi: 10.1016/j.jchromb.2011.12.014
65. Nair A, Amalraj A, Jacob J, Kunnumakkara AB, Gopi S. Non-Curcuminoids From Turmeric and Their Potential in Cancer Therapy and Anticancer Drug Delivery Formulations. *Biomolecules* (2019) 9(1):13. doi: 10.3390/biom9010013
66. Obulesu M. Chapter One - Health Benefits of Turmeric: Emphasis on Anticancer Activity. In: M Obulesu, editor. *Turmeric and Curcumin for Neurodegenerative Diseases*. Tirupati, India: Academic Press (2021). p. 3–18.
67. Tan Y, Meng Y, Zhang H, Sun C, Wang Q, Yang X, et al. Maturation and Upregulation of Functions of Murine Dendritic Cells (DCs) Under the

Influence of Purified Aromatic-Turmerone (AR). *Hum Vaccin Immunother* (2012) 8(10):1416–24. doi: 10.4161/hv.21526
68. Catalkaya G, Venema K, Lucini L, Rocchetti G, Delmas D, Daglia M, et al. Interaction of Dietary Polyphenols and Gut Microbiota: Microbial Metabolism of Polyphenols, Influence on the Gut Microbiota and Implications on Host Health. *Food Front* (2020) 1(2):109–33. doi: 10.1002/fft2.25
69. Krautkramer KA, Fan J, Bäckhed F. Gut Microbial Metabolites as Multi-Kingdom Intermediates. *Nat Rev Microbiol* (2021) 19(2):77–94. doi: 10.1038/s41579-020-0438-4

Conflict of Interest: The authors declare that the research was conducted in the absence of any commercial or financial relationships that could be construed as a potential conflict of interest.

Publisher's Note: All claims expressed in this article are solely those of the authors and do not necessarily represent those of their affiliated organizations, or those of the publisher, the editors and the reviewers. Any product that may be evaluated in this article, or claim that may be made by its manufacturer, is not guaranteed or endorsed by the publisher.

frontiers in Immunology

ORIGINAL RESEARCH
published: 16 March 2022
doi: 10.3389/fimmu.2022.861790

Immune Cell Landscaping Reveals Distinct Immune Signatures of Inflammatory Bowel Disease

Xiaowu Bai[1,2†], *Weixin Liu*[3†], *Hongxia Chen*[1,2], *Tao Zuo*[1,2*] *and Xiaojian Wu*[1,2*]

[1] *Department of Colorectal Surgery, The Sixth Affiliated Hospital, Sun Yat-sen University, Guangzhou, China,* [2] *Guangdong Institute of Gastroenterology, Guangdong Provincial Key Laboratory of Colorectal and Pelvic Floor Diseases, Supported by National Key Clinical Discipline, The Sixth Affiliated Hospital, Sun Yat-sen University, Guangzhou, China,* [3] *Department of Medicine and Therapeutics, Li Ka Shing Institute of Health Sciences, Chinese University of Hong Kong, Hong Kong, Hong Kong SAR, China*

OPEN ACCESS

Edited by:
Zhangran Chen,
Xiamen University, China

Reviewed by:
Weilin Li,
Beth Israel Deaconess Medical Center and Harvard Medical School, United States
Fengyu Jia,
960th Hospital of the PLA, China
Hye Won Lee,
Yonsei University, South Korea

***Correspondence:**
Xiaojian Wu
wuxjian@mail.sysu.edu.cn
Tao Zuo
zuot@mail.sysu.edu.cn

[†]*These authors have contributed equally to this work*

Specialty section:
This article was submitted to Autoimmune and Autoinflammatory Disorders, a section of the journal Frontiers in Immunology

Received: *25 January 2022*
Accepted: *21 February 2022*
Published: *16 March 2022*

Citation:
Bai X, Liu W, Chen H, Zuo T and Wu X (2022) Immune Cell Landscaping Reveals Distinct Immune Signatures of Inflammatory Bowel Disease. Front. Immunol. 13:861790. doi: 10.3389/fimmu.2022.861790

Determining how the profile of immune cells varies with their disease subtypes and across lesion locations is critical for understanding the pathogenesis in inflammatory bowel disease (IBD), including Crohn's disease (CD) and ulcerative colitis (UC). To that end, we herein combined the IBD TaMMA framework and the CIBERSORT pipeline to deconvolute the large amount of RNA-seq data from patients with IBD (both CD and UC were included) and healthy human controls across 28 cohorts (a total of 3,852 samples) while accommodating data heterogeneity across cohorts, to define the immune cell landscape of IBD. Our study uncovered that both absolute quantities of innate and adaptive immune cell populations were elevated in most intestinal regions of IBD patients, yet disease-specific (CD versus UC) and intestinal location (ileum, colon, and rectum)-specific features. In the ileum, the increase in innate immune cells was more pronounced in CD than UC. In contrast, innate and adaptive immune cells were elevated more drastically in the UC than CD in the rectum. Such revelation of immune signatures across the highly variable IBD phenotypes (in both disease subtypes and intestinal regions) underpins differential immune-pathophysiological mechanisms in IBD pathogenesis and therefore serves as a resource for the development of future targeted studies.

Keywords: IBD, inflammatory bowel disease, immune cell, landscape, adaptive immunity, innate immunity

INTRODUCTION

The incidence of inflammatory bowel disease (IBD) is rising in the twenty-first century (1). The exact etiology of IBD remains unclear. It is primarily thought to arise from an aggravated immune response towards the gut microbiota in genetically susceptible individuals (2). Initial activation of innate immunity provokes non-specific responses, and then, the continued stimulation of inflammation will activate adaptive immunity, which could lead to sustained chronic

Abbreviations: IBD, inflammatory bowel disease; CD, Crohn's disease; UC, ulcerative colitis; GEPs, gene expression profiles; CIBERSORT, Cell-type Identification By Estimating Relative Subsets Of RNA Transcripts; TaMMA, transcriptome and metatranscriptome meta-analysis.

inflammation. Available evidence suggests that both dysregulated innate and adaptive immune pathways contribute to the aberrant intestinal inflammatory response in patients with IBD. Subtypes of IBD include ulcerative colitis (UC), which contiguously affects the colon, and Crohn's disease (CD), which can present anywhere in the gastrointestinal tract. Different macroscopic patterns of inflammation may result from different patterns of immune response between CD and UC (3).

In the past decades, a large number of omics studies were deployed to understand the pathogenesis of IBD, particularly *via* the RNA-sequencing (RNA-seq) technology to pinpoint genes and cell compartments contributing to the disease course and phenotypes. However, due to the individual nature and small/modest sample sizes in each RNA-seq study (some studies only centered on a specific cell fraction), it hinders the power to find population-robust genes and cell types that are generic culprit to the pathogenesis and progression of IBD. Therefore, integrating the current existing RNA-seq datasets from publicly available studies, while minimizing batch effect with proper data harmonization, would largely facilitate this goal. Recently, multiple frameworks and pipelines were developed to integrate IBD datasets and to aid in cross-dataset RNA-seq analysis, including the IBD Transcriptome and Metatranscriptome Meta-Analysis (TaMMA) framework (4). The IBD TaMMA framework comprehensively collated the publicly available IBD RNA-seq (both Transcriptome and Metatranscriptome) datasets from IBD-derived and control samples across different tissues (4). In addition, CIBERSORT (Cell-type Identification By Estimating Relative Subsets Of RNA Transcripts) was recently developed to characterize immune cell compositions (including B cells, T cells, and innate immune cell subsets) in complex tissues by computing gene expression profiles (GEPs), which has a strong agreement with flow cytometry assessment of immune subsets in bulk tissues (5, 6). CIBERSORT was widely utilized in different complex tissues to analyze immune signatures (7, 8).

Here, we combined the IBD TaMMA framework and CIBERSORT to deconvolute the large amount of RNA-seq data from patients with IBD (both CD and UC—two IBD subtypes—were included) and healthy human controls across 28 cohorts (a total of 3,852 samples), to define the immune cell landscape of IBD. We identified and enumerated the composition of 22 immune cell types, which could be statistically more robust than individual studies alone. Our study uncovers both disease-specific (CD versus UC) and lesion location-specific immune cell features in IBD. Such large-scale analysis of immune signatures of IBD provides a comprehensive understanding of differential immune responses in IBD, therefore guiding precision immunotherapies for IBD in the future.

METHODS

RNA-Sequencing Data Acquisition

The Inflammatory Bowel Disease Transcriptome and Metatranscriptome Meta-Analysis (IBD TaMMA) framework contains publicly available gene expression files from 28 datasets of 26 independent studies before March 6, 2021 (4). All GEO/SRA numbers are given in **Figure 1**. GEPs of the 3,852 samples were batch corrected and merged to produce a mixture file by IBD TaMMA. We downloaded GEPs through OSFHOME (https://osf.io/yrxa7/).

Identification of Immune Cells and Their Estimated Fractions

GEPs were prepared and formatted into one input file (also known as mixture file) according to the instructions in the manual on the website (http://cibersort.stanford.edu/tutorial.php). LM22 gene signature was downloaded through CIBERSORT website (https://cibersortx.stanford.edu/download.

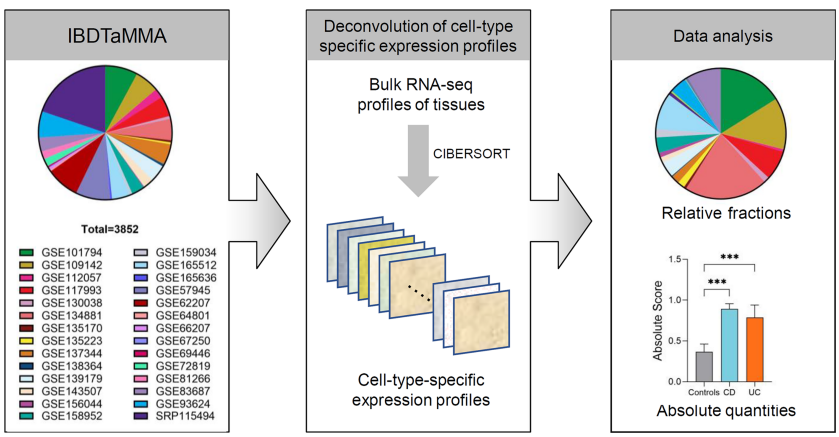

FIGURE 1 | The analytic framework of immune cells profiling in patients with IBD and healthy individuals. Schematic depicting shows that CIBERSORT is applied to a multiple-cohort (n=28) gene expression profiles from bulk tissue transcriptomic data (a total of 3,852 subjects), comprising both patients with IBD and healthy individuals. Once immune cell fractions are determined, comparisons among different disease subtypes (CD and UC versus healthy individuals) across intestinal locations (ileum, colon, and rectum) are calculated with statistics. ***$p < 0.001$.

php). R version 4.1.1 was required to run CIBERSORT R script v1.04 (https://rdrr.io/github/zy26/SSMD/src/R/CIBERSORT_modified.R). The number of statistical permutations was set to 100 and quantile normalization was disabled. The absolute and relative modes of CIBERSORT were used to analyze data, respectively. The relative output was set so that the sum of all estimated immune-cell-type fractions for each sample equaled 1. Immune cell absolute estimates were calculated using their corresponding relative fractions. In CIBERSORT, the absolute mode converts estimated relative cellular fractions into a score that reflects the sample's absolute proportion of each cell type. The median expression level of all genes in the signature matrix (LM22) divided by the median expression level of all genes in the sample yields the absolute immune score. Total innate immune cells score was calculated as a sum of NK cells (resting and activated), monocytes, macrophages (M0, M1, and M2), dendritic cells (resting and activated), mast cells (resting and activated), eosinophils, and neutrophils. Total B cells were calculated as a sum of naive B cells, memory B cells, and plasma cells. Total T cells were calculated as a sum of CD8+ T cells, naive CD4+ T cells, memory resting CD4+ T cells, memory-activated CD4+ T cells, follicular helper T cells, regulatory T (Treg) cells, and gamma delta (γδ) T cells.

Statistical Analysis

Data are presented as mean ± standard error of the mean (SEM). Differences among the three groups were compared using Kruskal–Wallis non-parametric test, and multiple comparisons testing was performed by Dunn's multiple comparisons test. All differences were considered statistically significant if $p < 0.05$. GraphPad Prism 8.0 and open-source R software (version 4.1.1) were used to perform statistical analysis.

Data Availability

The immune profile datasets generated by CIBERSORT for each sample during the current study are available from the corresponding author on reasonable request.

RESULTS

Overview of the Analytic Framework

A total of 28 source RNA-seq datasets from 26 independent studies were included from IBD TaMMA (consisting of 3,852 subjects, including 1,848 ileum, 448 colon, 480 rectum, and others). By CIBERSORT analysis, the relative fractions and absolute quantities of 22 immune cell types were calculated from all samples. We then characterized the immune cell landscape and signatures in patients with IBD (across disease subtypes and intestinal lesion locations) compared to that in healthy individuals (**Figure 1**).

Landscape of Relative Fractions of Immune Cell Populations in IBD

First, we compared the relative fractions of 22 immune cell types in different disease subtypes (CD and UC versus controls) and across different intestinal locations (ileum, colon, or rectum) (**Figure 2A**). Overall, the proportion of adaptive immune cells was decreased across the three intestinal locations (ileum, colon, and rectum) of CD and UC as compared to those of healthy controls, while the proportion of innate immune cells was correspondingly increased (**Figure 2A**). This alteration indicated the imbalance of immune system across different intestinal locations in CD and UC. The cumulative abundance (relative abundance) of innate immune cells (ileum, colon, and rectum combined) was significantly higher in both CD and UC, compared with that in healthy controls (both $p < 0.001$, **Figure 2B**). In contrast, the cumulative abundance (relative abundance) of adaptive immune cells was decreased in both CD and UC, compared with healthy controls (both $p < 0.001$, **Figure 2B**). Then, we particularly investigated the proportion of the adaptive immune cell subtypes, namely, B and T cells, in patients with IBD versus healthy controls. The relative fractions of the B- and T-cell populations were both decreased in CD and UC, compared with those in healthy controls (all $p < 0.001$, **Figure 2C**). These data together suggest a decrease in the relative fraction of adaptive immune cells (including B and T cells) concomitant with an increase in the relative fraction of innate immune cells in both CD and UC, compared to healthy individuals.

Elevated Absolute Quantities of Innate and Adaptive Immune Cell Populations in IBD Patients

To gain a fine-scale insight into the alterations in the immune cell populations in IBD versus healthy controls, we additionally analyzed the absolute quantities of 22 immune cell types, as measured by CIBERSORT in absolute score for each immune cell population. We found that the absolute quantities of B cells, T cells, and innate immune cells were all significantly increased in UC (ileum, colon, and rectum combined) compared to healthy controls ($p < 0.05$, $p < 0.001$, and $p < 0.001$, respectively, **Figure 3A**), while only the absolute quantities of T cells and innate immune cells (ileum, colon, and rectum combined) were observed to be significantly increased in CD compared to healthy controls (both $p < 0.001$, **Figure 3A**). Moreover, the absolute quantity of T cells (ileum, colon, and rectum combined) was significantly higher in UC than CD ($p < 0.05$, **Figure 3A**). These data suggest that IBD has disease-specific immune features between CD and UC.

Next, we specifically assessed the absolute quantity variations in B cells, T cells, and innate immune cells across different intestinal lesion locations (ileum, colon, and rectum) in patients with CD or UC as compared to healthy controls.

The quantity of B cells was significantly increased in the rectum but decreased in the ileum of patients with UC, compared to healthy controls and patients with CD (all $p < 0.01$, **Figure 3B**). In comparison, the quantity of T cells was significantly increased in the ileum of CD than that of healthy controls and UC ($p < 0.001$ and 0.05, respectively, **Figure 3C**). Moreover, the quantity of T cells was significantly increased in the rectum of both CD and UC than that in healthy controls ($p <$

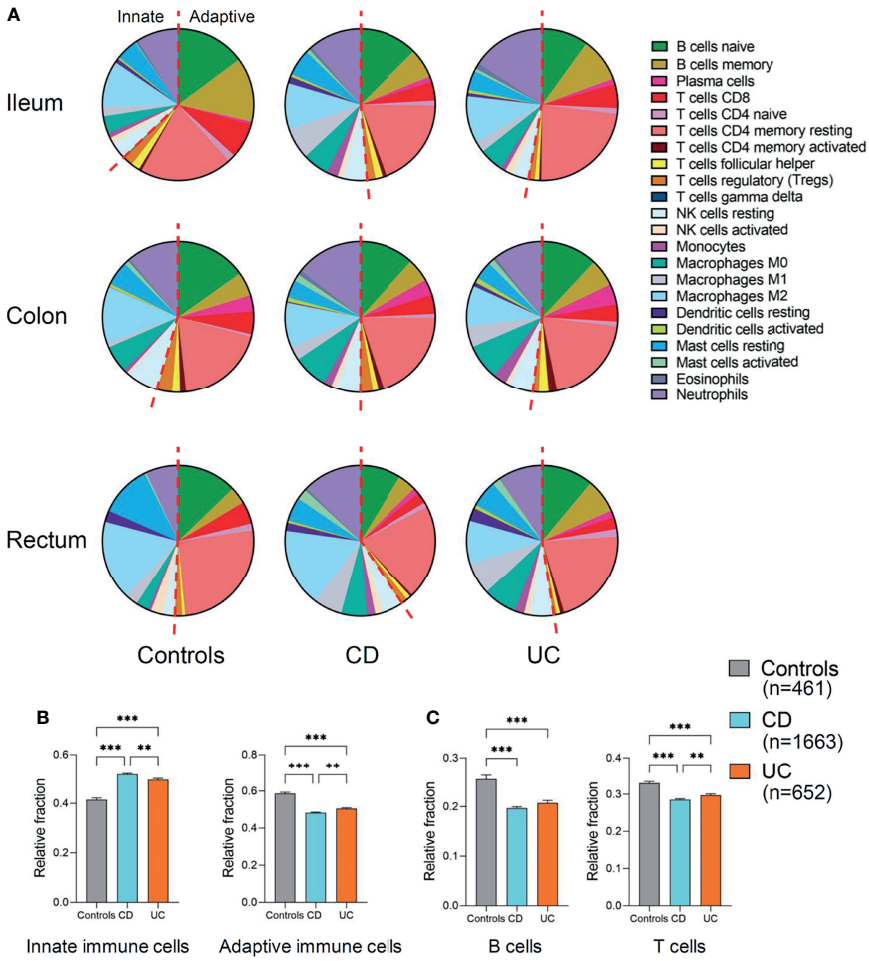

FIGURE 2 | Relative fraction of immune cells profiling in patients with IBD and healthy individuals. **(A)** Relative fractions of immune cells profiling across three intestinal locations (ileum, colon, and rectum). The left of red dashed line represents innate immune cells and the right of the dashed line represents adaptive immune cells. **(B)** Comparisons of the total innate immune cells and adaptive immune cells (ileum, colon, and rectum combined) among three disease subtypes. **(C)** Comparisons of the total B and T cells (ileum, colon, and rectum combined) among three disease subtypes. Statistical significance was determined by Kruskal–Wallis non-parametric test and Dunn's multiple comparisons test. $^{**}p < 0.01$, $^{***}p < 0.001$.

0.05 and 0.001, respectively, **Figure 3C**), while it was significantly higher in the UC rectum than that in the CD rectum ($p < 0.001$, **Figure 3C**).

We subsequently compared the quantity of innate immune cells across different intestinal lesion locations between CD, UC, and healthy controls. We found that the quantities of innate immune cells were all significantly increased in the ileum, colon, and rectum of both CD and UC patients, as compared to healthy controls (all $p < 0.001$, **Figure 3D**). The quantity of innate immune cells was significantly higher in the ileum of CD than that of UC ($p < 0.001$, **Figure 3D**), while this change was contrary to that observed in the rectum ($p < 0.001$, **Figure 3D**), hinting at intestinal location-specific alterations in the immune cell profile between CD and UC. Altogether, these data suggest that innate immune cells, B cells, and T cells are all elevated in most intestinal regions of CD and UC, yet they vary in a disease subtype and intestinal location-dependent manner.

Immune Cell Profile Alterations in the Ileum of IBD Patients

Given that the immune cell landscape exhibits location-specific features along the intestine axis (ileum, colon, and rectum), we then individually interrogated the alteration in each immune cell populations of the ileum (**Figure 4**), colon (**Figure 5**), and rectum (**Figure 6**), respectively, in IBD patients versus healthy controls.

First, we compared the immune cell profile of the ileum in CD, UC, and healthy controls (**Figure 4**). Although the absolute quantity of B cells in the ileum of UC was significantly decreased compared with healthy controls and CD (as shown in **Figure 3B**), different compartments of B cells (naive B cells, memory B cells, and plasma cells) showed discrepant alterations across the three groups (**Figure 4A**). The quantity of naive B cells was significantly decreased in UC compared with healthy controls and CD ($p < 0.01$ and 0.001, respectively, **Figure 4A**).

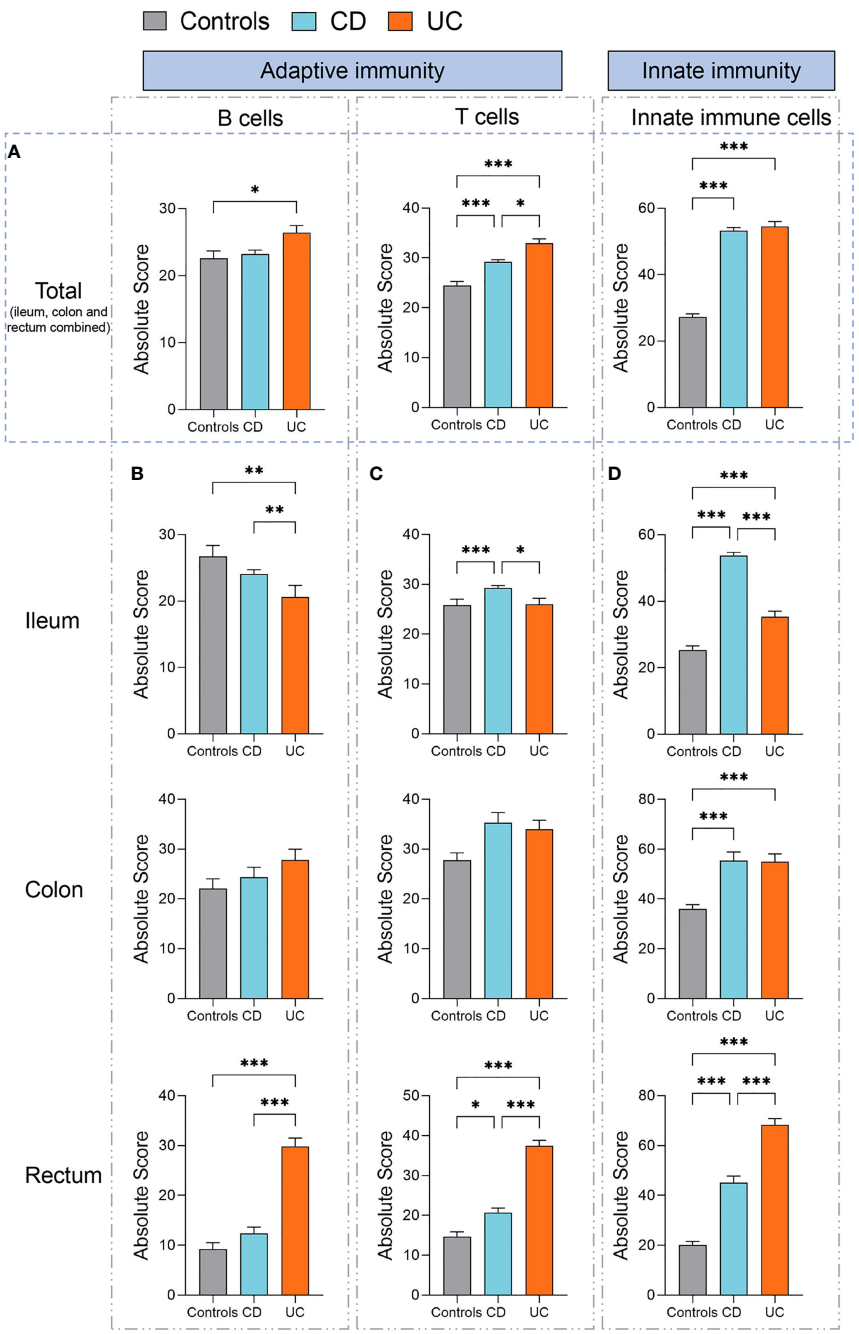

FIGURE 3 | Absolute quantity of immune cells profiling in patients with IBD and healthy individuals. **(A)** Comparisons of the total B cells, T cells, and innate immune cells (ileum, colon, and rectum combined) among three disease subtypes (healthy controls, n=461; CD, n=1663; UC, n=652). **(B)** Comparisons of the total B cells among three disease subtypes in the ileum, colon, and rectum respectively. **(C)** Comparisons of the total T cells among three disease subtypes in the ileum, colon, and rectum respectively. **(D)** Comparisons of the total innate immune cells among three disease subtypes in the ileum, colon, and rectum, respectively. Statistical significance was determined by Kruskal–Wallis non-parametric test and Dunn's multiple comparisons test. *$p < 0.05$, **$p < 0.01$, ***$p < 0.001$.

The quantity of memory B cells was significantly decreased in both CD and UC, compared with healthy controls ($p < 0.001$ and 0.05, respectively, **Figure 4A**). In contrast, the quantity of plasma cells, as main antibody-secreting B cells, was increased significantly in both CD and UC, compared to healthy controls (both $p < 0.001$, **Figure 4A**). The development trajectory of B cells originates from naive B cells, which later differentiate into plasma cells and memory B cells upon antigen recognition (9–12). These data indicate that more naive and memory B cells may transform to effector B cells in the ileum during IBD.

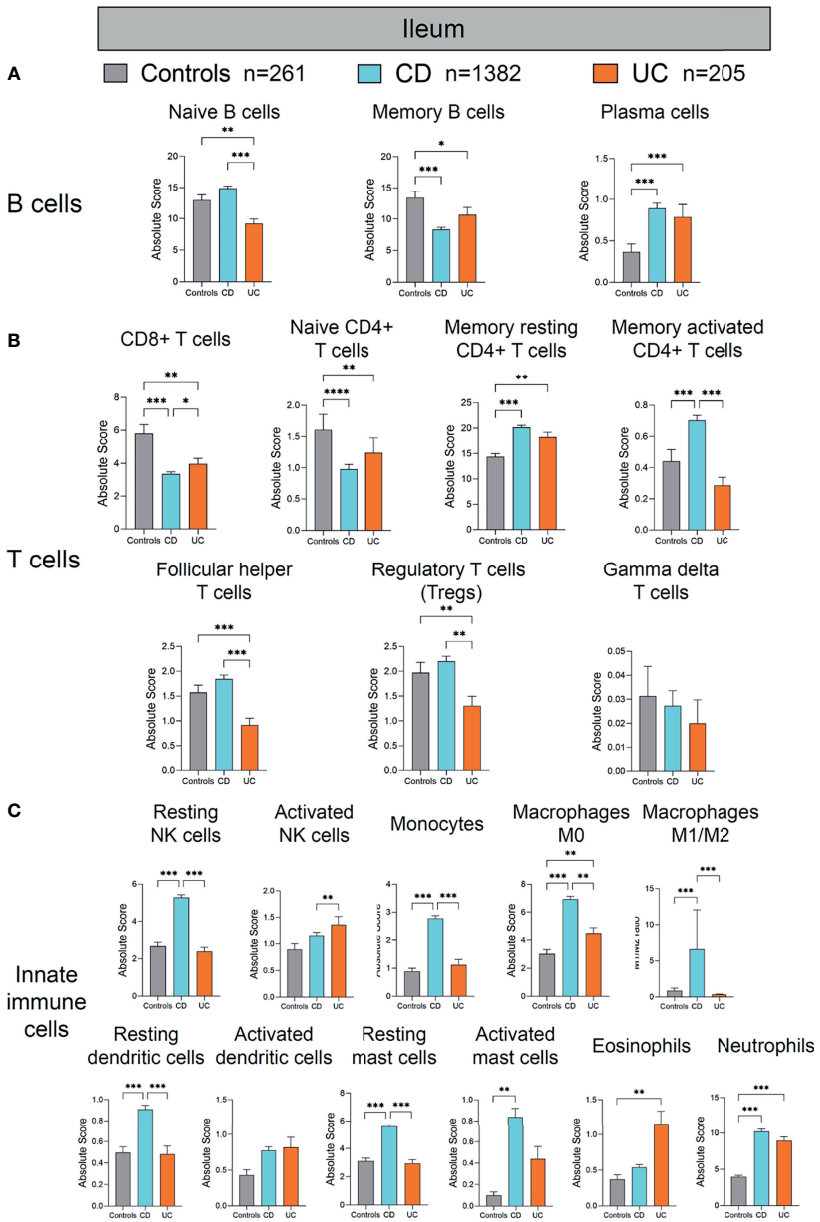

FIGURE 4 | Absolute quantity of immune cells profiling in the ileum of patients with IBD and healthy individuals. **(A)** Comparisons of the B-cell subpopulations among three disease subtypes in the ileum. **(B)** Comparisons of the T-cell subpopulations among three disease subtypes in the ileum. **(C)** Comparisons of the innate immune cell subpopulations among three disease subtypes in the ileum. Statistical significance was determined by Kruskal–Wallis non-parametric test and Dunn's multiple comparisons test. *$p < 0.05$; **$p < 0.01$, ***$p < 0.001$.

Next, we compared different T-cell populations [CD8+ T cells, naive CD4+ T cells, memory resting CD4+ T cells, memory activated CD4+ T cells, follicular helper T cells, Treg cells, gamma delta (γδ) T cells] in the ileum of CD and UC compared to healthy controls (**Figure 4B**). The quantity of CD8+ T cells was decreased significantly in CD and UC, compared with healthy controls (both $p < 0.01$, **Figure 4B**). The quantity of naive CD4+ T cells was significantly decreased, whereas that of memory resting CD4+ T cells was significantly increased in CD and UC, compared with healthy controls (all $p < 0.01$, **Figure 4B**). The quantity of memory-activated CD4+ T cells was increased significantly in CD, compared with healthy controls and UC (both $p < 0.001$, **Figure 4B**). The quantities of follicular helper T cells and Treg cells were both decreased significantly in UC, compared with healthy controls and CD (all $p < 0.01$, **Figure 4B**). Among these T-cell subpopulations, Treg cells are a specialized population acting to suppress immune response. The decrease in Tregs population in the ileum of UC patients versus healthy subjects indicates a lack of anti-inflammation mechanism in the ileum of UC, a disease mainly arising from colon and rectum inflammation (colon and rectum

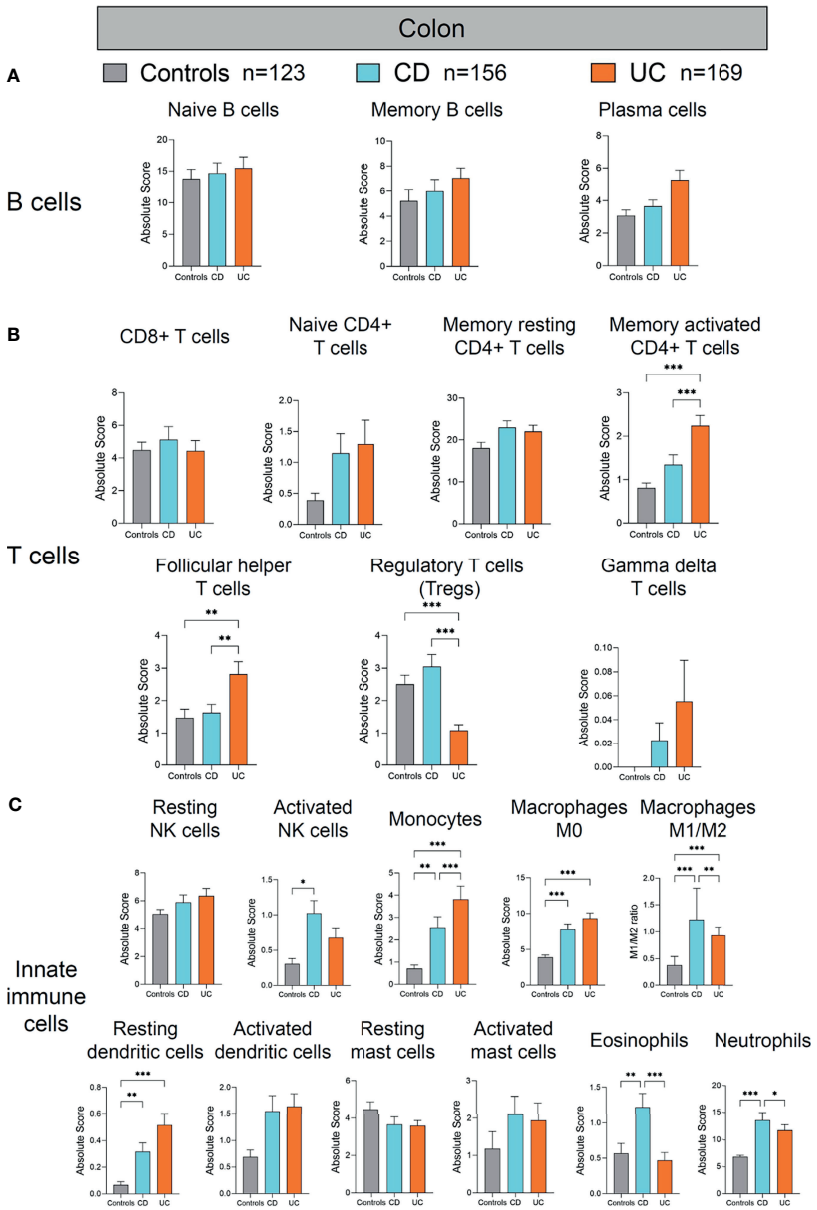

FIGURE 5 | Absolute quantity of immune cells profiling in the colon of patients with IBD and healthy individuals. **(A)** Comparisons of the B-cell subpopulations among three disease subtypes in the colon. **(B)** Comparisons of the T-cell subpopulations among three disease subtypes in the colon. **(C)** Comparisons of the innate immune cell subpopulations among three disease subtypes in the colon. Statistical significance was determined by Kruskal–Wallis non-parametric test and Dunn's multiple comparisons test. *$p < 0.05$; **$p < 0.01$, ***$p < 0.001$.

are the major inflicted intestinal region in UC). These data imply that the immune dysfunction may extend from distal intestine to proximal intestine. Overall, the largely heterogeneous alteration patterns in different ileal T-cell subpopulations between CD and UC compared to healthy controls are suggestive of a complicated, disease-specific T-cell dysfunction underlying disease pathogenesis, which warrants in-depth investigations.

We then investigated alterations in innate immune cells in the ileum of CD and UC patients versus healthy controls (**Figure 4C**). Among innate immune cells, resting NK cells, monocytes, macrophages M0, M1/M2 ratio, resting dendritic cells, and resting mast cells were all significantly increased in CD, compared with healthy controls and UC (all $p < 0.01$, **Figure 4C**). The quantity of activated mast cells was significantly increased in CD, compared with healthy controls ($p < 0.01$, **Figure 4C**). The quantity of neutrophils was increased significantly in CD and UC, compared with healthy controls (both $p < 0.001$, **Figure 4C**). The quantities of macrophages M0 and eosinophils were both increased significantly in UC, compared with healthy controls (both $p < 0.01$, **Figure 4C**). The quantity of activated NK cells was increased significantly in UC,

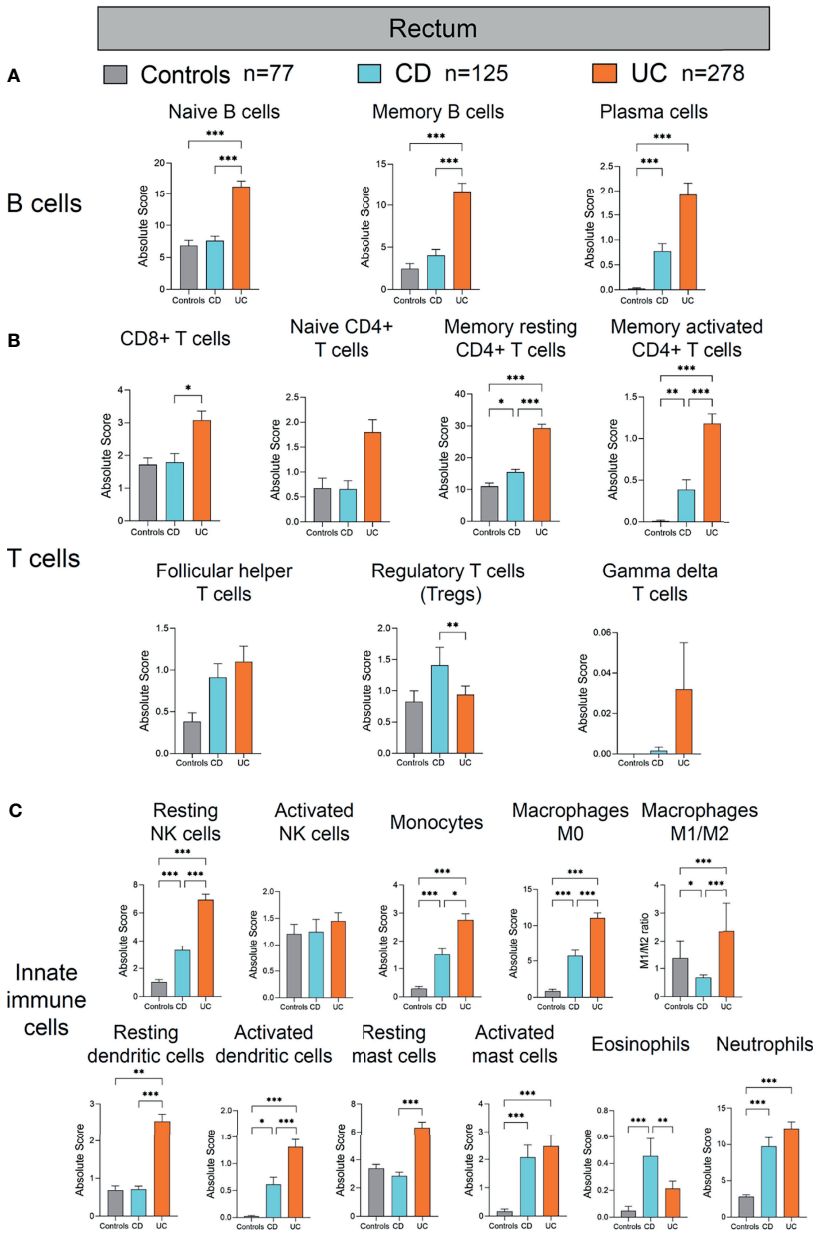

FIGURE 6 | Absolute quantity of immune cells profiling in the rectum of patients with IBD and healthy individuals. **(A)** Comparisons of the B-cell subpopulations among three disease subtypes in the rectum. **(B)** Comparisons of the T-cell subpopulations among three disease subtypes in the rectum. **(C)** Comparisons of the innate immune cell subpopulations among three disease subtypes in the rectum. Statistical significance was determined by Kruskal–Wallis non-parametric test and Dunn's multiple comparisons test. *$p < 0.05$, **$p < 0.01$, ***$p < 0.001$.

compared with CD ($p < 0.01$, **Figure 4C**). These results together indicate that hyperactivation of ileal innate immune cells was more pronounced in CD than UC.

Immune Cell Profile Alterations in the Colon of IBD Patients

Next, we analyzed the alterations of immune cells in the colon of patients with CD and UC compared to healthy controls (**Figure 5**). Among the studied subjects (CD, UC, and healthy controls), UC patients showed the most significant alterations in the colonic adaptive immune cell populations (including T- and B-cell subpopulations) (**Figures 5A, B**). Among the adaptive immune cells, colonic memory-activated CD4+ T cells and follicular helper T cells were significantly increased, whereas Treg cells were significantly decreased in UC, compared with healthy controls and CD (all $p < 0.01$, **Figure 5B**). Among the innate immune cells, activated NK cells were increased in the colon of CD, compared to healthy controls ($p < 0.05$, **Figure 5C**).

Meanwhile, monocytes, macrophages M0, M1/M2 ratio, and resting dendritic cells were also increased significantly in the colon of CD and UC, compared to healthy controls (all $p < 0.01$, **Figure 5C**). Eosinophils and neutrophils were increased in the colon of CD, compared with healthy controls and UC (all $p < 0.05$, **Figure 5C**). Overall, compared to the immune cell profile alterations in the ileum in IBD versus healthy controls, the alterations in colonic immune cell profile were rather modest in IBD versus healthy controls.

Immune Cell Profile Alterations in the Rectum of IBD Patients

Lastly, we analyzed the alterations of immune cells in the colon of patients with CD and UC compared to healthy controls (**Figure 6**). Among the B-cell subpopulations, the naive and memory B-cell populations were both increased significantly in the rectum of UC, compared with healthy controls and CD (all $p < 0.001$, **Figure 6A**). Incidentally, the plasma cell population was increased significantly in the rectum of both CD and UC, compared with healthy controls (both $p < 0.001$, **Figure 6A**). These data together suggest a concordant expansion of B-cell subpopulations in the rectum of IBD patients, different from the mere expansion of the plasma B-cell subpopulation in the ileum of IBD patients (**Figure 4A**). Among the T-cell subpopulations, the memory resting CD4+ T cell and memory-activated CD4+ T cell populations were both increased significantly in the rectum of CD and UC, compared with healthy controls (all $p < 0.05$, **Figure 6B**). Moreover, CD8+ T cells and memory resting CD4+ T cells and memory activated CD4+ T cells were all increased significantly in the rectum of UC, compared with CD ($p < 0.05$ and $p < 0.001$, $p < 0.001$, respectively, **Figure 6B**). In contrast, Tregs were decreased significantly in the UC, compared with CD ($p < 0.01$, **Figure 6B**). Taken together, these results indicate that adaptive immune cell populations in the rectum were elevated in both CD and UC, yet more drastically in UC than CD.

With regard to innate immune cells, resting NK cells, monocytes, macrophages M0, activated dendritic cells, activated mast cells, and neutrophils were all increased significantly in the rectum of CD and UC, compared with healthy controls (all $p < 0.05$, **Figure 6C**). Resting dendritic cells and macrophages M1/M2 ratio were both significantly increased in the rectum of UC, compared with healthy controls and CD (all $p < 0.01$, **Figure 6C**). In comparison, eosinophils were increased significantly in the rectum of CD, compared with healthy controls and UC ($p < 0.001$ and 0.01, respectively, **Figure 6C**). These data suggest that different innate immune cell populations were upregulated in CD and UC, potentially playing critical roles in the disease phenotype and disease course. In addition, resting NK cells, monocytes, activated dendritic cells, and resting mast cells were all increased in the rectum of UC, compared with CD (all $p < 0.05$, **Figure 6C**). However, macrophages M1/M2 ratio were decreased in the rectum of CD, compared with healthy controls ($p < 0.05$, **Figure 6C**). Overall, similar to the alteration pattern in adaptive immune cells in the rectum of IBD patients versus healthy controls, elevated innate immune cells in the rectum were observed in both CD and UC, which was more pronounced in UC than CD.

DISCUSSION

IBD is postulated to result from immune dysregulation to environmental and microbial triggers in genetically susceptible individuals. However, the exact alterations in the immune landscape across the intestinal axis (particularly different intestinal segments) have been unclear in IBD, neither were the differences between CD and UC. Improved understanding of immune cell landscapes in intestinal tissues may shed light on new therapeutic targets in IBD that can be tailored to disease type (CD versus UC), location (ileum, colon, or rectum lesions), and even individual patients.

Here, we conducted to date the largest sample sized, across-cohort study profiling the enteric immune cells composition (in both relative fraction and absolute quantity) of patients with IBD in comparison to healthy individuals. The adaptive immune responses have previously been believed to play a dominant role in the pathogenesis of IBD. However, due to recent advances in immunology and genetics, the innate immune responses are posited to be equally as important (if not more than that of adaptive immune responses) in inducing gut inflammation in IBD patients (13). Our findings confirmed this conception that both innate and adaptive immune cell populations were elevated in most intestinal regions of IBD patients. However, the elevation of innate immune cells seems higher than that of adaptive immune cells, resulting in that the relative fractions of adaptive immune cells (both B and T cells) decreased in the patients with IBD than healthy controls. Moreover, we identified both disease- and lesion location-specific immune signatures in IBD. For example, in the ileum, the increase in innate immune cells was more pronounced in CD than UC. In contrast, innate and adaptive immune cells were elevated more drastically in the UC than CD in the rectum. The rationale for our speculation is that it is somewhat related to illness characteristics and partially related to organ structure and function in various regions. For example, UC affects mainly the colon, but CD can affect any part of the GI tract, from the mouth to the anus, but is typically limited to the small intestine, particularly the terminal ileum. The main purpose of the small intestinal is to digest and absorb food, whereas the colon's main purpose is to hold stool.

Moreover, previous studies reported that B cells were enriched in IBD (3, 14–16). Our discovery of IBD-associated B cells adds to and expands on this understanding. Plasma cells expanded both in the ileum and rectum of CD and UC, while expansion of memory B cells existed only in the rectum of UC and naive B cells increased in the rectum of UC and decreased in the ileum of UC. This suggests that, basically, B cells were hyperactivated in IBD, but we should distinguish phenotypes of their subsets carefully and explore its underlying mechanism in the future.

As regards to CD4+ T cells, resting memory CD4+ T cells increased both in the rectum and ileum of CD and UC, while activated memory CD4+ T cells increased in the rectum of both CD and UC, in the ileum of CD, and in the colon of UC, respectively, when compared to healthy controls. In addition, follicular helper T cells were increased in the ileum of CD and in the colon of UC conversely. These data suggest the disparate immune cell alterations between CD and UC across intestinal regions (17), which can be

due to CD and UC both belonging to IBD but showing different behaviors. UC is limited to the colon. By contrast, CD can involve inflammation at any point of the GI tract from the mouth to the anus but is usually limited to the small intestinal, especially the terminal ileum.

The innate immune response represents our first line of defense against pathogens. It is non-specific and does not offer long-term immunity (memory), unlike the adaptive response (18–23). Innate immune cells, such as dendritic cells (DCs) and macrophages, can initiate rapid and effective inflammatory responses against microbial invasion. Our analysis suggest that many innate immune subsets were hyperactivated in tissues of CD and UC. For example, activated DCs were increased in the rectum of CD and UC, and resting DCs increased in the ileum of CD, in the rectum of UC, and in the colon of both CD and UC. Macrophage polarization occurs when macrophages respond to cues from their surroundings by adopting distinct functional programs. M1 and M2 are the two most prominent groups. Proinflammatory activity is performed by M1 macrophages. The M2, on the other hand, refers to macrophages that participate in constructive processes like wound healing and tissue repair, and those that produce anti-inflammatory cytokines like IL-10 to turn off damaging immune system activation. Our results demonstrated that the macrophage M1/M2 ratio was increased in the ileum of CD, in the rectum of UC, and in the colon of both CD and UC, which was consistent with previous studies (24, 25).

Understanding the distinct immune signatures across lesion locations in IBD is very helpful to design specific treatment strategies, especially when using biologics. For example, in ileal Crohn's disease, the therapeutic benefits of cytokine blocking are confined to a minority of individuals. The reason for this is that a subset of patients had a distinct cellular module in inflamed tissues that included IgG plasma cells, inflammatory mononuclear phagocytes, activated T cells, and stromal cells, and its presence was linked to failure to achieve long-term corticosteroid-free remission after anti-TNF therapy (26). In the future, as a result of the rapid development and different specific functions of biologics, the majority of them should be used appropriately based on the immunological signatures of individual patients. Hence, our results provide the foundation of the development of precise biological therapies in IBD.

There are several limitations to our study, which necessitate a cautious interpretation of our findings. There is the issue of missing information regarding the severity of disease, which prevents us from distinguishing the characteristic of immune cells between inactive and active lesions. In addition, common treatments for IBD include biologics can affect the immune signatures of the intestinal in IBD. In addition, our model analyzed signatures of almost all subsets of immune cells but could not analyze specific subset deeply. Lastly, additional functional research is needed to determine whether our findings contribute to the disease development and severity.

In conclusion, we demonstrated that using CIBERSORT to deconvolve whole-tissue gene expression data yields refined information on the immune cell landscape of IBD. We showed that both innate and adaptive immunity hyperactivated in most intestinal regions of patients with IBD, yet disease-specific (CD versus UC) and intestinal location (ileum, colon, and rectum)-specific features. Such revelation of immune signatures across the highly variable IBD phenotypes (in both disease subtypes and intestinal regions) underpins differential immune-pathophysiological mechanisms in IBD pathogenesis and therefore serves as a resource for development of future targeted studies.

DATA AVAILABILITY STATEMENT

The datasets presented in this study can be found in online repositories. The names of the repository/repositories and accession number(s) can be found in the article/supplementary material.

AUTHOR CONTRIBUTIONS

XB was involved in study design, performed bioinformatics analysis, and drafted the manuscript. WL performed bioinformatics analysis. HC commented on the study. TZ and XW designed and supervised the study and revised the manuscript. All authors contributed to the article and approved the submitted version.

FUNDING

This project was supported by research funds from National Natural Science Foundation of China (32100134 and 82172323).

REFERENCES

1. Ng SC, Shi HY, Hamidi N, Underwood FE, Tang W, Benchimol EI, et al. Worldwide Incidence and Prevalence of Inflammatory Bowel Disease in the 21st Century: A Systematic Review of Population-Based Studies. *Lancet* (2017) 390(10114):2769–78. doi: 10.1016/S0140-6736(17)32448-0
2. Abraham C, Cho JH. Inflammatory Bowel Disease. *N Engl J Med* (2009) 361 (21):2066–78. doi: 10.1056/NEJMra0804647
3. Mitsialis V, Wall S, Liu P, Ordovas-Montanes J, Parmet T, Vukovic M, et al. Single-Cell Analyses of Colon and Blood Reveal Distinct Immune Cell Signatures of Ulcerative Colitis and Crohn's Disease. *Gastroenterology* (2020) 159(2):591–608.e10. doi: 10.1053/j.gastro.2020.04.074
4. Massimino L, Lamparelli LA, Houshyar Y, D'Alessio S, Peyrin-Biroulet L, Vetrano S, et al. The Inflammatory Bowel Disease Transcriptome and Metatranscriptome Meta-Analysis (IBD TaMMA) Framework. *Nat Comput Sci* (2021) 1(8):511–5. doi: 10.1038/s43588-021-00114-y
5. Newman AM, Liu CL, Green MR, Gentles AJ, Feng W, Xu Y, et al. Robust Enumeration of Cell Subsets From Tissue Expression Profiles. *Nat Methods* (2015) 12(5):453–7. doi: 10.1038/nmeth.3337
6. Newman AM, Steen CB, Liu CL, Gentles AJ, Chaudhuri AA, Scherer F, et al. Determining Cell Type Abundance and Expression From Bulk Tissues With Digital Cytometry. *Nat Biotechnol* (2019) 37(7):773–82. doi: 10.1038/s41587-019-0114-2
7. Thorsson V, Gibbs DL, Brown SD, Wolf D, Bortone DS, Ou Yang TH, et al. The Immune Landscape of Cancer. *Immunity* (2018) 48(4):812–30.e14. doi: 10.1016/j.immuni.2018.03.023
8. Luca BA, Steen CB, Matusiak M, Azizi A, Varma S, Zhu C, et al. Atlas of Clinically Distinct Cell States and Ecosystems Across Human Solid Tumors. *Cell* (2021) 184(21):5482–96.e28. doi: 10.1016/j.cell.2021.09.014

9. Inoue T, Moran I, Shinnakasu R, Phan TG, Kurosaki T. Generation of Memory B Cells and Their Reactivation. *Immunol Rev* (2018) 283(1):138–49. doi: 10.1111/imr.12640
10. Dogan I, Bertocci B, Vilmont V, Delbos F, Megret J, Storck S, et al. Multiple Layers of B Cell Memory With Different Effector Functions. *Nat Immunol* (2009) 10(12):1292–9. doi: 10.1038/ni.1814
11. Pape KA, Taylor JJ, Maul RW, Gearhart PJ, Jenkins MK. Different B Cell Populations Mediate Early and Late Memory During an Endogenous Immune Response. *Science* (2011) 331(6021):1203–7. doi: 10.1126/science.1201730
12. Kometani K, Nakagawa R, Shinnakasu R, Kaji T, Rybouchkin A, Moriyama S, et al. Repression of the Transcription Factor Bach2 Contributes to Predisposition of IgG1 Memory B Cells Toward Plasma Cell Differentiation. *Immunity* (2013) 39(1):136–47. doi: 10.1016/j.immuni.2013.06.011
13. Geremia A, Biancheri P, Allan P, Corazza GR, Di Sabatino A. Innate and Adaptive Immunity in Inflammatory Bowel Disease. *Autoimmun Rev* (2014) 13(1):3–10. doi: 10.1016/j.autrev.2013.06.004
14. Huang B, Chen Z, Geng L, Wang J, Liang H, Cao Y, et al. Mucosal Profiling of Pediatric-Onset Colitis and IBD Reveals Common Pathogenics and Therapeutic Pathways. *Cell* (2019) 179(5):1160–76.e24. doi: 10.1016/j.cell.2019.10.027
15. Preisker S, Brethack AK, Bokemeyer A, Bettenworth D, Sina C, Derer S. Crohn's Disease Patients in Remission Display an Enhanced Intestinal IgM(+) B Cell Count in Concert With a Strong Activation of the Intestinal Complement System. *Cells* (2019) 8(1):78. doi: 10.3390/cells8010078
16. Noronha AM, Liang Y, Hetzel JT, Hasturk H, Kantarci A, Stucchi A, et al. Hyperactivated B Cells in Human Inflammatory Bowel Disease. *J Leukoc Biol* (2009) 86(4):1007–16. doi: 10.1189/jlb.0309203
17. Bishu S, El Zaatari M, Hayashi A, Hou G, Bowers N, Kinnucan J, et al. CD4+ Tissue-Resident Memory T Cells Expand and Are a Major Source of Mucosal Tumour Necrosis Factor Alpha in Active Crohn's Disease. *J Crohns Colitis* (2019) 13(7):905–15. doi: 10.1093/ecco-jcc/jjz010
18. Raab Y, Gerdin B, Ahlstedt S, Hallgren R. Neutrophil Mucosal Involvement is Accompanied by Enhanced Local Production of Interleukin-8 in Ulcerative Colitis. *Gut* (1993) 34(9):1203–6. doi: 10.1136/gut.34.9.1203
19. Bressenot A, Salleron J, Bastien C, Danese S, Boulagnon-Rombi C, Peyrin-Biroulet L. Comparing Histological Activity Indexes in UC. *Gut* (2015) 64 (9):1412–8. doi: 10.1136/gutjnl-2014-307477
20. Yusung S, McGovern D, Lin L, Hommes D, Lagishetty V, Braun J. NK Cells Are Biologic and Biochemical Targets of 6-Mercaptopurine in Crohn's Disease Patients. *Clin Immunol* (2017) 175:82–90. doi: 10.1016/j.clim.2016.12.004
21. Jacobs I, Ceulemans M, Wauters L, Breynaert C, Vermeire S, Verstockt B, et al. Role of Eosinophils in Intestinal Inflammation and Fibrosis in Inflammatory Bowel Disease: An Overlooked Villain? *Front Immunol* (2021) 12:754413. doi: 10.3389/fimmu.2021.754413
22. Boeckxstaens G. Mast Cells and Inflammatory Bowel Disease. *Curr Opin Pharmacol* (2015) 25:45–9. doi: 10.1016/j.coph.2015.11.005
23. Hart AL, Al-Hassi HO, Rigby RJ, Bell SJ, Emmanuel AV, Knight SC, et al. Characteristics of Intestinal Dendritic Cells in Inflammatory Bowel Diseases. *Gastroenterology* (2005) 129(1):50–65. doi: 10.1053/j.gastro.2005.05.013
24. Zhou X, Li W, Wang S, Zhang P, Wang Q, Xiao J, et al. YAP Aggravates Inflammatory Bowel Disease by Regulating M1/M2 Macrophage Polarization and Gut Microbial Homeostasis. *Cell Rep* (2019) 27(4):1176–89.e5. doi: 10.1016/j.celrep.2019.03.028
25. Lissner D, Schumann M, Batra A, Kredel LI, Kuhl AA, Erben U, et al. Monocyte and M1 Macrophage-Induced Barrier Defect Contributes to Chronic Intestinal Inflammation in IBD. *Inflamm Bowel Dis* (2015) 21 (6):1297–305. doi: 10.1097/MIB.0000000000000384
26. Martin JC, Chang C, Boschetti G, Ungaro R, Giri M, Grout JA, et al. Single-Cell Analysis of Crohn's Disease Lesions Identifies a Pathogenic Cellular Module Associated With Resistance to Anti-TNF Therapy. *Cell* (2019) 178 (6):1493–508.e20. doi: 10.1016/j.cell.2019.08.008

Conflict of Interest: The authors declare that the research was conducted in the absence of any commercial or financial relationships that could be construed as a potential conflict of interest.

Publisher's Note: All claims expressed in this article are solely those of the authors and do not necessarily represent those of their affiliated organizations, or those of the publisher, the editors and the reviewers. Any product that may be evaluated in this article, or claim that may be made by its manufacturer, is not guaranteed or endorsed by the publisher.

frontiers in Immunology

MINI REVIEW
published: 24 March 2022
doi: 10.3389/fimmu.2022.838884

MicroRNA-Mediated Epigenetic Regulation of Rheumatoid Arthritis Susceptibility and Pathogenesis

Cen Chang[1,2†], Lingxia Xu[1,2†], Runrun Zhang[3], Yehua Jin[1,2], Ping Jiang[1,2], Kai Wei[1,2], Linshuai Xu[1,2], Yiming Shi[1,2], Jianan Zhao[1,2], Momiao Xiong[4], Shicheng Guo[5,6] and Dongyi He[1,2,7*]*

[1] Guanghua Clinical Medical College, Shanghai University of Traditional Chinese Medicine, Shanghai, China, [2] Department of Rheumatology, Guanghua Hospital Affiliated to Shanghai University of Traditional Chinese Medicine, Shanghai, China, [3] The Second Affiliated Hospital of Shandong University of Traditional Chinese Medicine, Jinan, China, [4] Department of Biostatistics and Data Science, School of Public Health, University of Texas Health Science Center, Houston, TX, United States, [5] Center for Precision Medicine Research, Marshfield Clinic Research Institute, Marshfield, WI, United States, [6] Department of Medical Genetics, School of Medicine and Public Health, University of Wisconsin-Madison, Madison, WI, United States, [7] Arthritis Institute of Integrated Traditional and Western Medicine, Shanghai Chinese Medicine Research Institute, Shanghai, China

OPEN ACCESS

Edited by:
Zhangran Chen,
Xiamen University, China

Reviewed by:
Zhigang Lu,
Nanjing University of Chinese Medicine, China
Shu Li,
Central South University, China

***Correspondence:**
Shicheng Guo
shicheng.guo@wisc.edu
Dongyi He
hedongyi1967@shutcm.edu.cn

†These authors have contributed equally to this work

Specialty section:
This article was submitted to Autoimmune and Autoinflammatory Disorders, a section of the journal Frontiers in Immunology

Received: *18 December 2021*
Accepted: *02 March 2022*
Published: *24 March 2022*

Citation:
Chang C, Xu L, Zhang R, Jin Y, Jiang P, Wei K, Xu L, Shi Y, Zhao J, Xiong M, Guo S and He D (2022) MicroRNA-Mediated Epigenetic Regulation of Rheumatoid Arthritis Susceptibility and Pathogenesis. Front. Immunol. 13:838884. doi: 10.3389/fimmu.2022.838884

MicroRNAs (miRNAs) play crucial roles in regulating the transcriptome and development of rheumatoid arthritis (RA). Currently, a comprehensive map illustrating how miRNAs regulate transcripts, pathways, immune system differentiation, and their interactions with terminal cells such as fibroblast-like synoviocytes (FLS), immune-cells, osteoblasts, and osteoclasts are still laking. In this review, we summarize the roles of miRNAs in the susceptibility, pathogenesis, diagnosis, therapeutic intervention, and prognosis of RA. Numerous miRNAs are abnormally expressed in cells involved in RA and regulate target genes and pathways, including NF-κB, Fas-FasL, JAK-STAT, and mTOR pathways. We outline how functional genetic variants of *miR-499* and *miR-146a* partly explain susceptibility to RA. By regulating gene expression, miRNAs affect T cell differentiation into diverse cell types, including Th17 and Treg cells, thus constituting promising gene therapy targets to modulate the immune system in RA. We summarize the diagnostic and prognostic potential of blood-circulating and cell-free miRNAs, highlighting the opportunity to combine these miRNAs with antibodies to cyclic citrullinated peptide (ACCP) to allow accurate diagnosis and prognosis, particularly for seronegative patients. Furthermore, we review the evidence implicating miRNAs as promising biomarkers of efficiency and response of, and resistance to, disease-modifying anti-rheumatic drugs and immunotherapy. Finally, we discuss the autotherapeutic effect of miRNA intervention as a step toward the development of miRNA-based anti-RA drugs. Collectively, the current evidence supports miRNAs as interesting targets to better understand the pathogenetic mechanisms of RA and design more efficient therapeutic interventions.

Keywords: rheumatoid arthritis, microRNA, susceptibility, pathogenesis, epigenetics

INTRODUCTION

Rheumatoid arthritis (RA) is an autoimmune disease characterized by chronic joint inflammation and structural damage, accompanied by extra-articular manifestations such as rheumatoid nodules, interstitial pneumonia, vasculitis, and systemic complications. RA is typically progressive and insidious, with an incidence rate of 0.5–1% in Europe and North America (1). However, the precise mechanisms underlying the pathogenesis, disease activity, and severity of RA as well as the causes of different response to treatment are not fully understood. In view of current therapy strategies and treatment frames, early accurate diagnosis, effective and personalized treatment, and precision medicine have become increasingly urgent for patients with RA. A comprehensive understanding of RA is required from the perspectives of both genetics (2) [human leukocyte antigen (HLA) and non-HLA variants] and epigenetics [DNA methylation (3–5), microRNA (6), long non-coding RNA (7, 8), and histone modifications (9)].

MicroRNAs (miRNAs) are small endogenous non-coding RNAs with a length of around 22 nucleotides, and are involved in the post-transcriptional regulation of gene expression. In recent years, accumulating studies have demonstrated that miRNAs play a key role in various cancers (10–14) and autoimmune diseases, including RA, systemic lupus erythematosus (15, 16), Sjögren's syndrome (17), and systemic sclerosis (18). In this review, we systematically summarize recent advances in understanding the role of miRNAs in RA. Emphasize the important role of miRNA in RA susceptibility, pathogenesis, and efficacy evaluation. Provide evidence supporting precision medicine research in RA.

GENETIC VARIATIONS IN miRNAs EXPLAINS SUSCEPTIBILITY OF RA

Genome-wide association studies have identified >100 genetic factors for RA. However, these genetic variants only explain < 40% of the overall heritability of RA, and thus most of the heritability has not been explained, suggesting the need for more studies using different approaches and populations to identify the missing causes. Association studies of miRNA loci can reveal RA-associated functional or causal variants within different populations, such as Chinese (19, 20), Egyptian (21–23), Polish (24), Mexican (25), and Iranian (26) subjects. Gene expression and genetic polymorphisms of *miR-146a* and *miR-499* showed diagnostic potential for RA (23). Consistently, the polymorphism rs3027898 in *IRAK1*, the target gene of *miR-146a*, is linked to RA in the Greek population (27). In contrast, *miR-146a* rs2431697 is associated with RA susceptibility in Chinese population (28). The rs3746444 (20q11.22, A>G) polymorphism of *miR-499*, which is encoded by the intron of *MYH7B*, is significantly linked to RA risk, disease activity, and methotrexate (MTX) toxicity. Interestingly, the AA genotype shows higher disease activity and MTX toxicity than the AG/GG genotypes (29). The AA and AG genotypes in the miRNA binding site rs3135500 of *NOD2* are significantly associated with the risk of RA, with rs3135500 (A allele) showing a significant relationship with increased erythrocyte sedimentation rates (ESR) and C-reactive protein (CRP) concentrations (30). However, some studies showed inconsistent results in Polish (24), Mexican (25), and Chinese (19, 20, 31, 32) populations, suggesting that genetic polymorphisms of miR-146a and miR-499 are not significantly associated with RA susceptibility. For example, *miR-499* rs3746444 A/G are not significantly associated with RA in Mexican people (25). *miR-146a* rs2910164 (20, 32) and *miR-499* rs3746444 (20, 31) do not significantly correlate with RA in Chinese people. However, in addition to race, factors of individual heterogeneity and sample size should also be considered while evaluating inconsistent results. Moreover, the sample size of the above studies was not large. We recently demonstrated that meta-analysis could identify more significant single-nucleotide polymorphisms in a large sample size, and found that the interaction between HLA alleles and miRNA single-nucleotide polymorphisms (such as rs5997893 in *miR-3928* and rs4947332 in *HLA-DRB1*) should be considered to explain susceptibility (33). In summary, genetic variations in miRNAs can help to explain the susceptibility to RA.

REGULATORY ROLES OF miRNAs IN CELLS AND THEIR SECRETIONS INVOLVED IN RA PATHOGENESIS

Fibroblast-like synoviocytes (FLS) and immune cells are the main cell types involved in the pathogenesis of RA. These cells can secrete exosomes and other substances to affect the occurrence and development of RA. Current researches have mainly focused on understanding miRNA-mediated transcriptional regulation of *FAF1* (34), *TNF-α* (35), *STAT1* (36), *STAT3* (37), and *mTOR* (38, 39). miRNAs regulate inflammation, immune response, proliferation, and differentiation. Meanwhile, miRNA influence the micro-environment within synovial joints by targeting target genes and their related pathways, including Fas-FasL (34) and the NF-κB (40, 41) pathways. In this section, we summarize the regulatory roles of miRNAs in the main RA-associated cell entities, focusing on FLS, immune cells, and exosomes to highlight the importance of miRNAs in the pathogenesis of RA.

Effects of miRNAs on FLS in RA

FLS in RA (RA-FLS) are key regulators of inflammation and bone destruction in RA. The aberrantly expression of miRNAs in RA-FLS play an important role in the pathogenesis of RA. For example, *miR-625* is down-regulated in RA-FLS, which negatively impacts the expression of *CTSC*, *KLF8*, and *EBF3*. In contrast, *miR-551b* is up-regulated in RA-FLS, inhibiting the expression of *ITGBL1* (42).

Dysregulation of miRNAs in RA-FLS affects biological functions such as cell proliferation, invasion, migration and apoptosis. Up-regulation of *miR-145* affects all biological

functions of RA-FLS by targeting *SEMA3A* (43). The expression of *miR-29c-3p* and *miR-132-3p* are decreased while *miR-31-5p* was increased in RA- FLS, and their dysregulation are associated with proliferation, invasion and migration of RA-FLS. Down-regulated *miR-29c-3p* promoted proliferation, invasion and migration of RA-FLS through up-regulation of *COLA1* expression. Interestingly, up-regulated *miR-31-5p* and down-regulated *miR-132-3p* inhibited the proliferation, invasion and migration of RA-FLS by negatively regulating *WASF3* and *RB1*, respectively, suggested that *miR-31-5p* and *miR-132-3p* are protective factors in RA (44). Down-regulation of *miR-199a-3p* (45), *miR-449* (46), *miR-431-5p* (47), and up-regulation of *miR-483-3p* (48) can promote the proliferation and suppressed apoptosis by targeting *RB1*, *HDAC1*, *XIAP*, *IGF-1*, respectively. *miR-124a* is down-regulated and targets *CDK2 and MCP-1* which only enhanced the proliferation of RA-FLS (49).

Dysregulation of miRNAs in RA-FLS can also affects the level of inflammation. Down-regulation of *miR-126* (35), *miR-23* (50) and up-regulation of *miR-143* (43) can increase the release of inflammatory factors such as TNF-α, IL-1β, IL-6 through up-regulation of *IL-23R*, *CXCL12* and down-regulation of *IGFBP5* and thus affect the course of RA. What's more, some miRNAs not only affects the level of inflammation, but also associated with biological functions of RA-FLS. For example, down-regulation of *miR-137* (51) and *miR-23a-5p* (52) targeting LSD and TLR4 promotes proliferation, invasion, migration and inhibits apoptosis of RA-FLS and inhibits the release of inflammatory factors IL-1β and IL-6. Down-regulation of *miR-29a* (37) and *miR-27a-3p* (53) are associated with proliferation, apoptosis, and promoting secretion of TNF-α, IL-1, IL-6 and IL-8. Then, down-regulation of *miR-22* (54), *miR-124* (55) and *miR-34a-5p* (56) can enhanced proliferation of RA-FLS and the level of IL-6.

Additionally, the biological functions of RA-FLS and the level of inflammation are correlated with matrix metalloproteinases (MMPs) (57). Down-regulation of *miR-203* (41, 42) and *miR-147b-3p* (58) increased the expression of *MMP-1*, *MMP3* and *MMP9*, respectively, which in turn enhanced the expression of some inflammatory factors, such as IL-6 and TNF-α. Down-regulation of *miR-27a* (59) can contribute to *MMPs gene* expression by targeting the IL-17 pathways, thereby affecting the proliferation and invasion of RA-FLS. Conversely, up-regulated *miR-155* could be a protective factor by inhibiting proliferation and invasion while attenuating the expression of *MMP3* and *IKBKE* (60, 61).

In addition, dysregulation of miRNAs in RA-FLS affects joint bone erosion through the release of inflammatory cytokines, chemokines and MMPs, which may be an option for RA treatment (62, 63). For example, up-regulated *miR-145-5p* (40) and down-regulated *miR-17-5p* (64) affect bone and cartilage destruction through the release of IL-1β, IL-6, IL-8, *MMP-1*, *MMP-3* and *MMP-9*. *In vitro*, overexpression of *miR-221-3p* inhibits osteoblast differentiation (65). Instead, *miR-218* overexpression promotes osteogenic differentiation of RA-FLS by suppressing the Roundabout-1/Dickkopf-1 axis (66). *miR-20a* (67) and *miR-21* (68) are targets of the TLR4/p38 and JAK/STAT3 signaling pathways respectively, affecting the proliferation and osteogenic differentiation of RA-FLS.

In summary, studies of miRNAs in RA-FLS have improved the understanding of the pathogenesis of RA. miRNAs are widely involved in the functions of FLS, and therefore are promising targets for drug development (**Figure 1**).

Effects of miRNAs on Immune Cells in RA

miRNAs have recently emerged as key regulators of the immune system, being involved in lymphocyte selection and proliferation, in T(reg) cells differentiation. In peripheral blood mononuclear cells (PBMCs), decreased expression of *miR-671* and *miR-7* may correlate with the expression of *CDR1* and *mTOR* (38). And *miR-29b* enhances the anti-apoptotic effect by inhibiting the high-mobility group box-containing protein 1 (HBP1) (69).

In T cells sub-population derived from PBMCs, *miR-99b-5p* down-regulates *mTOR* and *RASSF4*, thereby inhibiting T cell apoptosis and promoting T cell proliferation and inflammatory response (39). Besides, *miR-146a, miR-26, miR-let-7a, miR-146b, miR-150, miR-155* are increased and *miR-363, miR-498* are decreased in the $CD4^+$ T cell sub-type in PBMCs, Among *these m*iRNAs, *miR-146a* may affect the apoptosis of T cell and RA progression by targeting *IL-17* and Fas associated factor 1 (*FAF1*) (34, 70). Interestingly, *miR-233* is highly expressed only in naive CD4+ lymphocytes but not in T(h)-17 cells, suggesting the importance to investigate the impact of miRNA on the pathogenesis of RA at the single-cell level (71).

There are numerous of miRNAs are also associated with other T cells sub-types, such as Treg cells and Th17 cells. The balance of Th17/Treg cells plays a crucial role in RA. IL-17 released by Th17 up-regulates the expression of *RANKL* on synovial fibroblasts stimulating the production of inflammatory cytokines such as TNF-α, IL-1, and IL-6 (72). Decreased levels of *miR-20a* (73) and *miR-21* (74, 75) exacerbate the RA process by stimulating the *NLRP3* inflammasome pathway and increasing *STAT3* expression, respectively, while decreasing *STAT5* expression, all of which are associated with the imbalance of Th17/Treg cells. Although *miR-210*-mediated negative regulation of *HIF-1* also affects the dynamic equilibrium of Th17/Treg cells. Regrettably, the levels of *miR-210* between RA and healthy controls have no significant difference (76). Interestingly, the expression of *miR-146a* is decreased in Treg cells during high RA activity, leading to a proinflammatory phenotype in these cells caused by concomitant up-regulation of its target *STAT1* (36). For instance, *miR-21* and *miR-155* are related to the memory phenotype, and *miR-92a* relative to the naïve phenotype (77).

Besides, in macrophages, binding of *miR-6089* and *lncRNA-HIX003209* enhances the expression of *TLR4* and exacerbates inflammation *via* the TLR4/NF-κB pathway (78). Up-regulation of *miR-33* induces the expression of *NLRP3* and 73 (79). Overall, miRNAs cooperate with other non-coding RNAs to alter the DNA methylation and/or expression of their targets, thus regulating innate and adaptive immune cells differentiation and apoptosis, ultimately influencing the inflammatory and autoimmune response in RA (**Table 1**).

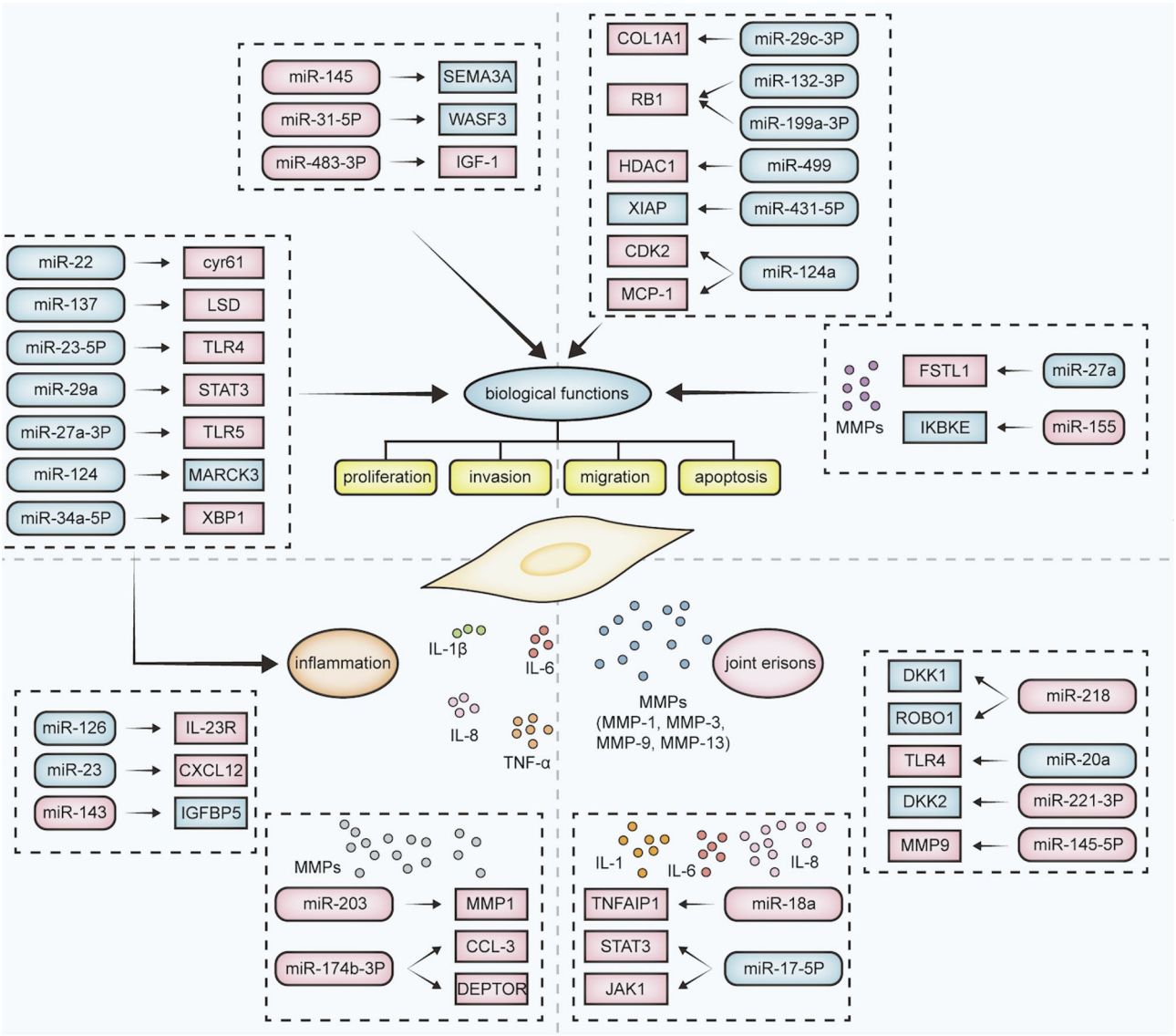

FIGURE 1 | Effects of dysregulation of the miRNA-mRNA network on RA-FLS. The dysregulation of miRNAs and their target mRNAs in RA-FLS affects the biological function (such as proliferation, invasion, migration, and apoptosis), inflammatory levels, and joint bone destruction. Inflammatory levels are mainly related to the release of inflammatory factors such as IL-8, IL-6, and joint bone destruction is mainly related to the release of MMPs. Dysregulation of different miRNA-mRNA combinations affects different processes in RA-FLS. Rounded rectangles represent miRNAs; rectangles represent target mRNAs; pink represents upregulation; blue represents downregulation.

Effects of miRNAs on Cell Secretions in RA

Exosomes are secreted from cells and contain signal molecules such as miRNA, protein, and DNA, which have biological functions. Exosomal miRNA derived from bone marrow-derived mesenchymal stem cells has been shown to be closely related to the occurrence and development of RA. Among these exosomes, MSCs-drived *miR-124a* over-expression exosomes inhibit the proliferation and migration and promote the apoptosis of RA-FLS (80). Over-expression of *miR-23b* (83) and *miR-34a* (81) can inhibit the differentiation of Th17 cells, by reducing IL-17 secretion and targeting the cyclin I/ATM/ATR/p53 signaling pathway, respectively. Up-regulated of *miR-21* (82) which targets *TET1*, reduce RA inflammation. Macrophage-derived exosomes *miR-506-3p* (84) and *miR-103a* (85) regulate the progression of RA by inhibiting the RANKL/NFATc1 signaling pathway and activating the JAK/STAT3 signaling pathway. *miR-132* secreted by aryl hydrocarbon receptor activation Th17 in extracellular vesicles acts as a pro-inflammatory mediator to reduce the production of *COX2*, to increase the production of osteoclast (86). In addition, cell-derived small extracellular vesicles of *miR-574-5p* induces

TABLE 1 | Effects of microRNAs on immune cells in rheumatoid arthritis.

miRNA	miRNA trends	Targets	Targets trends	Location	Functions	Reference
miR-671	↓	CDR1	↑	PBMC	/	(40)
miR-7	↓	mTOR	↑			
miR-29b	↑	HBP1	↑			(73)
miR-99b-5p	↑	mTOR RASSF4	↑	T cell	inhibiting T cell apoptosis, promoting T cell proliferation, inflammatory response	(41)
miR-146a	↑	FAF1	↑		inhibiting apoptosis of T cell and RA progression	(35)
		IL-17	↑			(74)
miR-26	↑	/	/		/	(35, 74)
miR-let-7a	↑					
miR-146b	↑					
miR-150	↑					
miR-155	↑					
miR-363	↓					
miR-498	↓					
miR-233	↑					(75)
miR-20a	↓	NLRP3	↑	Treg/Th17	the imbalance of Th17/Treg cells	(77)
miR-21	↓	STAT3	↑			(78, 79)
		STAT5	↓			
miR-210	↓	HIF-1	↑			(80)
miR-146a	↓	STAT1	↑	Treg cells	/	(38)
miR-6089	↓	TLR4	↑	macrophages	exacerbates inflammation *via* the TLR4/NF-κB pathway	(81)
miR-33	↑	NLRP3 caspase-1	↑		/	(82)

osteoclast differentiation by targeting *TLR 7/8* (87), whereas *miR-150-5p* exosomes alleviates RA-FLS proliferation and angiogenesis and reduces RA joint destruction by targeting *MMP14* and *VEGF* (88). Based on these results, miRNAs play an important role in the pathogenesis of RA and may represent promising outcome biomarkers and novel drug targets to decrease disease severity.

BLOOD AND SERUM-CIRCULATING miRNAs PROVIDE NOVEL OPPORTUNITIES FOR PRECISION MEDICINE OF RA

miRNAs as Potential Biomarkers for Early Prevention and Precision Diagnosis

Emerging evidence indicates the potential of blood-circulating miRNAs associated with RA as biomarkers for early prevention. The levels of *miR-371b*, *miR-483*, and *miR-642b* are significantly up-regulated, whereas *miR-25* and *miR-378d* are down-regulated in PBMCs in individuals who eventually develop RA from early undifferentiated arthritis (89). Additionally, *miR-22* (90), *miR-361-5p* (91), and *miR-223-3p* (91) are significantly up-regulated in high-risk or CCP-positive populations. All these miRNAs may therefore be useful biomarkers for the early diagnosis of RA. Expression of *miR-103a-3p* is significantly increased in autoantibody-positive, symptomatic first-degree relatives and patients with RA, suggesting it as a potential biomarker for predicting imminent disease in individuals at risk for developing RA (92). Additionally, higher level of *miR-99b-5p* is found in the plasma of patients with early RA who progress to bone erosion after 12 months, indicating that *miR-99b-5* can be monitored for bone erosion surveillance in RA patients (93).

In addition to playing a role in the early prevention of RA, the expression of some miRNAs can aid in improving the accuracy of RA diagnosis (94). The expression of *miR-146a* and *miR-155* are significantly increased in RA PBMCs and whole blood (95). The levels of *miR-24* and *miR-125a* are significantly higher in the serum of patients with RA regardless of the CCP status (96). Interestingly, analysis of *miR-24-3p*, *miR-26a-5p*, and *miR-125a-5p* levels in combination are a better diagnostic tool for RA, even though these miRNAs are not related to disease activity (97). Furthermore, *miR-122-3p*, *miR-3925-3p*, *miR-342-3p*, and *miR-4764-5p* show differential expression not only between healthy individuals and RA patients, but also between patients with RA and patients with osteoarthritis, systemic lupus erythematosus, or Graves, which show great potential as biomarkers to distinguish RA patients from HC or other diseases (98). The serum levels of *miR-146a* (99, 100), *miR-22-3p* (101), *miR-5571-3p* (102), and *miR-135b-5p* (102) are significantly higher in RA patients than in healthy controls and osteoarthritis patients. Other differentially expressed miRNAs in patients with RA serum include *miR-4634*, *miR-181d*, *miR-3926*, *miR-9-5p*, *miR-219-2-3p6*, *miR-221*, *miR-222*, *miR-532*, *miR-106a*, and *miR-98* highlighting their potential as RA-specific diagnostic markers (98, 103). Nevertheless, the above miRNAs should be selected as biomarkers with caution. Their sensitivity and specificity need to be taken into consideration because they were only compared with patients with osteoarthritis (OA) or healthy control, and rarely analyzed with patients with other inflammatory autoimmune diseases, such as ankylosing spondylitis. In addition, it should be determined if the miRNA as diagnostic markers are expressed

differently in patients before the onset of clinical symptoms. The above studies were conducted after patients were confirmed with RA diagnosis. Thus, more robust sample studies are needed to validate these markers in early RA.

miRNAs as Potential Biomarkers for Disease Activity and Treatment Response

The expression of *miR-451* in T cells is significantly increased, which is positively correlated with the levels of disease activity score 28 (DAS-28), ESR, and serum IL-6 in RA (77). The level of *miR-146a* is positively correlated with the level of ESR and DAS-28 (99), whereas *miR-5571-3p* (102) correlates with the level of ESR and CRP, and *miR-135b-5p* only correlate with CRP (102). These miRNAs may therefore be suitable markers of disease activity in patients with RA. Increased serum *miR-194-5p* level is associated with disease recurrence (104). Concentration of circulating *miR-23b*, which positively correlates with ESR, CRP, and DAS-28, is significantly up-regulated after appropriate treatment, indicating that *miR-23b* is a dual marker for disease activity and prognosis (105). Similarly, *miR-96-5p, miR-134-5p, miR-140-3p, miR-627-5p, miR-224, miR-760, miR-483-5p, miR-378, and miR-375* are not only diagnostic markers for RA, but also mirror disease activity (106, 107). However, these studies are still descriptive. Therefore, the underlying pathophysiology needs to be validated using other techniques.

Common and widely used anti-rheumatic drugs include cDMARDs (MTX, sulfasalazine, and hydroxychloroquine), bDMARDs (TNF-α inhibitors, rituximab, and tocilizumab), tsDMARDs (tofacitinib, barretinib, and filgotinib). Several studies have explored the relationship between serum miRNA levels and drug response. Evidence shows that high serum levels of miR-10 in patients with RA is correlated with good response to MTX (108). After 3 months of adalimumab/MTX combined treatment, the level of *miR-27a-3p* significantly decreased and clinical symptoms significantly improved (109). The reduced serum level of *miR-5196* is positively correlated with the delta DAS28 after anti-TNF-α therapy (110). The level of *miR-146a* is increased in RA patients who respond well to anti-TNF therapy and, interestingly, can be considered as predictors of the response to anti-TNFα therapy together with CRP (24, 111, 112). In contrast, the serum levels of *miR-23* and *miR-223* are increased in patients with RA who respond well to anti-TNF-α/DMARD combination therapy, but correlate negatively with the response to anti-TNF drugs (111). High serum level of *miR-125b* is an indicator for good clinical response to rituximab therapy (113). Notably, *miR-432-5p* is significantly down-regulated in RA patients who are responsive to tofacitinib therapy but up-regulated in patients showing RA relapse (104). In RA, treatment with rituximab increases the levels of *miR-16-5p* and *miR-23a-3p* in the peripheral blood (114). The expression of *miR-550b-2-5p*, *miR-4797-5p*, *miR-6509-5p*, *miR-378g*, *miR-4720-5p*, *miR-374b-5p*, and *miR-185-3p* are different between individuals who show good *vs* poor responses to treatment with tripterygium glycosides (115, 116). Finally, the expression of *miR-124a* in FLS is increased following geniposide treatment; however, the relevance of this finding has not been assessed in clinical response studies (117).

In addition to DMARD treatment, alternative and complementary medicine preparations and mesenchymal stem cell treatments are also used in clinical practice. The auto-therapeutic effect of miRNAs has been demonstrated in mouse models of RA-FLS and autoimmune arthritis. For example, *miR-449a* mimics also inhibit the proliferation, migration, and IL-6 production of RA-FLS by regulating *HMGB1* and *YY1* expression (118). In the rat model with collagen-induced arthritis, *miR-708-5p* mimic improved pathological changes by inhibiting inflammatory cell infiltration, synovial hyperplasia, and cartilage destruction (119). An *miR-126* agonist inhibits the expression of IL-23R, TNF-α, and IFN-γ in FLS (35). Furthermore, *miR-26b-5p*, *miR-487b-3p*, and *miR-495-3p* are significantly up-regulated in responders to adipose-derived mesenchymal stem cell treatment (120).

In summary, the changes of circulation miRNA in RA provide a promising opportunity for standard treatment, as well as indicate disease activity and predict RA outcomes.

miRNAs RESEARCH IN RA: REMAINING CHALLENGES AND FUTURE OPPORTUNITIES

In conclusion, miRNAs play multiple roles in the development of RA, from susceptibility to pathogenesis. Blood and serum-circulating miRNAs have been explored as important biomarkers for early diagnosis, prognosis, and drug response prediction. Furthermore, miRNAs have been proposed for autotherapeutic approaches and as novel drug targets for the treatment of RA. Genetic variants in specific miRNAs can increase or decrease the risk and disease activity of RA in various racial. Meanwhile they are associated with methotrexate toxicity and responses to other treatments. Moreover, changes in miRNAs in various cells are related to the pathogenesis of RA, such as the proliferation and differentiation of immune cells, proliferation and apoptosis of synovial cells, and synovial inflammation and cartilage destruction. Research has remarkably progressed towards the development of miRNAs as biomarkers in the diagnosis, prognosis, disease activity, and response to therapeutic drugs with RA, providing a direction for early diagnosis and accurate treatment of RA, to achieve better treatment efficiency and precision medicine. Numerous miRNAs have been shown to act as therapeutic targets in RA-FLS and collagen-induced arthritis rat models. Furthermore, miRNAs show potential for identifying the subtypes of RA. For example, the levels of *miR-7* and *miR-214-5p* are significantly increased in the serum of patients with RA associated-interstitial lung disease (121), and *miR-9-5p* targets the REST/miR-132 pathway to protect Schwann cells from inflammatory damage in RA-induced peripheral neuropathy (122). Although we have reached exciting milestones in the research on the multiple roles of miRNA in RA, further studies should be performed to

translate this knowledge for clinical applications and resolve the current inconsistent results among different studies employing different methods or populations. For example, studies of *miR-99*, *miR-143*, and *miR-197* as landmark miRNAs for predicting the response to anti-TNF-α therapy have failed to yield consistent results (123). Finally, future development of miRNA-based baseline RA polygenetic risk score models, particularly in conjunction with HLA, is needed. miRNA-based early diagnosis, prognosis, and drug response prediction models can be applied in the clinic. With the identification of additional miRNAs-based drug targets in clinical research, miRNA-based autotherapeutic treatments may show more promising results.

AUTHOR CONTRIBUTIONS

SG and DH conceived the content. CC and LXX wrote the manuscript. RZ, YJ, PJ, KW, and MX edited the manuscript. YS, JZ and LSX checked the manuscript information. LXX wrote the manuscript and LSX checked the manuscript information.

FUNDING

This work was funded by the National Natural Science Funds of China (82074234 and 82004166); Shanghai Chinese Medicine Development Office, National Administration of Traditional Chinese Medicine, Regional Chinese Medicine (Specialist) Diagnosis and Treatment Center Construction Project-Rheumatology; State Administration of Traditional Chinese Medicine, National TCM Evidence-Based Medicine Research and Construction Project, Basic TCM Evidence-Based Capacity Development Program; Shanghai Municipal Health Commission, East China Region based Chinese and Western Medicine Joint Disease Specialist Alliance.

REFERENCES

1. Ibanez-Cabellos JS, Seco-Cervera M, Osca-Verdegal R, Pallardo FV, Garcia-Gimenez JL, et al. Epigenetic Regulation in the Pathogenesis of Sjogren Syndrome and Rheumatoid Arthritis. *Front Genet* (2019) 10:1104. doi: 10.3389/fgene.2019.01104
2. Okada Y, Wu D, Trynka G, Raj T, Terao C, Ikari K, et al. Genetics of Rheumatoid Arthritis Contributes to Biology and Drug Discovery. *Nature* (2014) 506(7488):376–81. doi: 10.1038/nature12873
3. Guo S, Zhu Q, Jiang T, Wang R, Shen Y, Zhu X, et al. Genome-Wide DNA Methylation Patterns in CD4+ T Cells From Chinese Han Patients With Rheumatoid Arthritis. *Mod Rheumatol* (2017) 27(3):441–7. doi: 10.1080/14397595.2016.1218595
4. Chen S, Pu W, Guo S, Jin L, He D, Wang J. Genome-Wide DNA Methylation Profiles Reveal Common Epigenetic Patterns of Interferon-Related Genes in Multiple Autoimmune Diseases. *Front Genet* (2019) 10:223. doi: 10.3389/fgene.2019.00223
5. Guo S, Xu L, Chang C, Zhang R, Jin Y, He D. Epigenetic Regulation Mediated by Methylation in the Pathogenesis and Precision Medicine of Rheumatoid Arthritis. *Preprints* (2020) 11:811. doi: 10.3389/fgene.2020.00811
6. Furer V, Greenberg JD, Attur M, Abramson SB, Pillinger MH. The Role of microRNA in Rheumatoid Arthritis and Other Autoimmune Diseases. *Clin Immunol* (2010) 136(1):1–15. doi: 10.1016/j.clim.2010.02.005
7. Guo S, Liu J, Jiang T, Lee D, Wang R, Zhou X, et al. (5r)-5-Hydroxytriptolide (LLDT-8) Induces Substantial Epigenetic Mediated Immune Response Network Changes in Fibroblast-Like Synoviocytes From Rheumatoid Arthritis Patients. *Sci Rep* (2019) 9(1):11155. doi: 10.1038/s41598-019-47411-1
8. Bi X, Guo XH, Mo BY, Wang ML, Luo XQ, Chen YX, et al. LncRNA PICSAR Promotes Cell Proliferation, Migration and Invasion of Fibroblast-Like Synoviocytes by Sponging miRNA-4701-5p in Rheumatoid Arthritis. *EBioMedicine* (2019) 50:408–20. doi: 10.1016/j.ebiom.2019.11.024
9. Angiolilli C, Kabala PA, Grabiec AM, Van Baarsen IM, Ferguson BS, Garcia S, et al. Histone Deacetylase 3 Regulates the Inflammatory Gene Expression Programme of Rheumatoid Arthritis Fibroblast-Like Synoviocytes. *Ann Rheum Dis* (2017) 76(1):277–85. doi: 10.1136/annrheumdis-2015-209064
10. Ding H, Gao G, Zhang L, Shen G, Sun W, Gu Z, et al. The Protective Effects of Curculigoside A on Adjuvant-Induced Arthritis by Inhibiting NF-Small Ka, CyrillicB/NLRP3 Activation in Rats. *Int Immunopharmacol* (2016) 30:43–9. doi: 10.1016/j.intimp.2015.11.026
11. Fan L, Chen L, Ni X, Guo S, Zhou Y, Wang C, et al. Genetic Variant of miR-4293 Rs12220909 Is Associated With Susceptibility to Non-Small Cell Lung Cancer in a Chinese Han Population. *PloS One* (2017) 12(4):e0175666. doi: 10.1371/journal.pone.0175666
12. He Y, Cui Y, Wang W, Gu J, Guo S, Ma K, et al. Hypomethylation of the hsa-miR-191 Locus Causes High Expression of Hsa-Mir-191 and Promotes the Epithelial-to-Mesenchymal Transition in Hepatocellular Carcinoma. *Neoplasia* (2011) 13(9):841–53. doi: 10.1593/neo.11698
13. Lin S, Pan L, Guo S, Wu J, Jin L, Wang JC, et al. Prognostic Role of microRNA-181a/B in Hematological Malignancies: A Meta-Analysis. *PloS One* (2013) 8(3):e59532. doi: 10.1371/journal.pone.0059532
14. Zhang P, Wang J, Lu T, Wang X, Zheng Y, Guo S, et al. miR-449b Rs10061133 and miR-4293 Rs12220909 Polymorphisms Are Associated With Decreased Esophageal Squamous Cell Carcinoma in a Chinese Population. *Tumour Biol* (2015) 36(11):8789–95. doi: 10.1007/s13277-015-3422-2
15. Xie L, Xu J. Role of MiR-98 and Its Underlying Mechanisms in Systemic Lupus Erythematosus. *J Rheumatol* (2018) 45(10):1397–405. doi: 10.3899/jrheum.171290
16. Senousy MA, Helmy HS, Fathy N, Shaker OG, Ayeldeen GM. Association of MTMR3 Rs12537 at miR-181a Binding Site With Rheumatoid Arthritis and Systemic Lupus Erythematosus Risk in Egyptian Patients. *Sci Rep* (2019) 9(1):12299. doi: 10.1038/s41598-019-48770-5
17. Jang SI, Tandon M, Teos L, Zheng C, Warner BM, Alevizos I. Dual Function of miR-1248 Links Interferon Induction and Calcium Signaling Defects in Sjogren's Syndrome. *EBioMedicine* (2019) 48:526–38. doi: 10.1016/j.ebiom.2019.09.010
18. Iwamoto N, Vettori S, Maurer B, Brock M, Pachera E, Jungel A, et al. Downregulation of miR-193b in Systemic Sclerosis Regulates the Proliferative Vasculopathy by Urokinase-Type Plasminogen Activator Expression. *Ann Rheum Dis* (2016) 75(1):303–10. doi: 10.1136/annrheumdis-2014-205326
19. Yang B, Chen J, Li Y, Zhang J, Li D, Huang Z, et al. Association of Polymorphisms in pre-miRNA With Inflammatory Biomarkers in Rheumatoid Arthritis in the Chinese Han Population. *Hum Immunol* (2012) 73(1):101–6. doi: 10.1016/j.humimm.2011.10.005
20. Yang B, Zhang JL, Shi YY, Li DD, Chen J, Huang ZC, et al. Association Study of Single Nucleotide Polymorphisms in Pre-miRNA and Rheumatoid Arthritis in a Han Chinese Population. *Mol Biol Rep* (2011) 38(8):4913–9. doi: 10.1007/s11033-010-0633-x
21. El-Shal AS, Aly NM, Galil SM, Moustafa MA, Kandel WA. Association of microRNAs Genes Polymorphisms With Rheumatoid Arthritis in Egyptian Female Patients. *Joint Bone Spine* (2013) 80(6):626–31. doi: 10.1016/j.jbspin.2013.03.005

22. Shaker OG, El Boghdady NA, El Sayed AE. Association of MiRNA-146a, MiRNA-499, IRAK1 and PADI4 Polymorphisms With Rheumatoid Arthritis in Egyptian Population. *Cell Physiol Biochem* (2018) 46(6):2239–49. doi: 10.1159/000489592
23. Ayeldeen G, Nassar Y, Ahmed H, Shaker O, Gheita T. Possible Use of miRNAs-146a and -499 Expression and Their Polymorphisms as Diagnostic Markers for Rheumatoid Arthritis. *Mol Cell Biochem* (2018) 449(1-2):145–56. doi: 10.1007/s11010-018-3351-7
24. Bogunia-Kubik K, Wysoczańska B, Piątek D, Iwaszko M, Ciechomska M, Świerkot J. Significance of Polymorphism and Expression of miR-146a and NFkB1 Genetic Variants in Patients With Rheumatoid Arthritis. *Arch Immunol Ther Exp (Warsz)* (2016) 64(Suppl 1):131–6. doi: 10.1007/s00005-016-0443-5
25. Aleman-Avila I, Jimenez-Morales M, Beltran-Ramirez O, Barbosa-Cobos RE, Jimenez-Morales S, Sanchez-Munoz F, et al. Functional Polymorphisms in Pre-Mir146a and Pre-Mir499 Are Associated With Systemic Lupus Erythematosus But Not With Rheumatoid Arthritis or Graves' Disease in Mexican Patients. *Oncotarget* (2017) 8(54):91876–86. doi: 10.18632/oncotarget.19621
26. Hashemi M, Eskandari-Nasab E, Zakeri Z, Atabaki M, Bahari G, Jahantigh M, et al. Association of Pre-miRNA-146a Rs2910164 and premiRNA-499 Rs3746444 Polymorphisms and Susceptibility to Rheumatoid Arthritis. *Mol Med Rep* (2013) 7(1):287–91. doi: 10.3892/mmr.2012.1176
27. Chatzikyriakidou A, Voulgari PV, Georgiou I, Drosos AA. A Polymorphism in the 3'-UTR of Interleukin-1 Receptor-Associated Kinase (IRAK1), a Target Gene of miR-146a, Is Associated With Rheumatoid Arthritis Susceptibility. *Joint Bone Spine* (2010) 77(5):411–3. doi: 10.1016/j.jbspin.2010.05.013
28. Zhang LL, Wu XX, Wang XF, Di DS, Huang Q, Liu RS, et al. Genetic Variant in microRNA-146a Gene Is Associated With Risk of Rheumatoid Arthritis. *Ann Med* (2021) 53(1):824–9. doi: 10.1080/07853890.2021.1933163
29. Toraih EA, Ismail NM, Toraih AA, Hussein MH, Fawzy MS. Precursor miR-499a Variant But Not miR-196a2 Is Associated With Rheumatoid Arthritis Susceptibility in an Egyptian Population. *Mol Diagn Ther* (2016) 20(3):279–95. doi: 10.1007/s40291-016-0194-3
30. Ehtesham N, Alani B, Mortazavi D, Azhdari S, Kenarangi T, Esmaeilzadeh E, et al. Association of Rs3135500 and Rs3135499 Polymorphisms in the MicroRNA-Binding Site of Nucleotide-Binding Oligomerization Domain 2 (NOD2) Gene With Susceptibility to Rheumatoid Arthritis. *Iran J Allergy Asthma Immunol* (2021) 20(2):178–87. doi: 10.18502/ijaai.v20i2.6051
31. Yang XK, Li P, Zhang C, Leng RX, Li S, Liu J, et al. Association Between IRAK1 Rs3027898 and miRNA-499 Rs3746444 Polymorphisms and Rheumatoid Arthritis: A Case Control Study and Meta-Analysis. *Z Rheumatol* (2017) 76(7):622–9. doi: 10.1007/s00393-016-0169-0
32. Zhou X, Zhu J, Zhang H, Zhou G, Huang Y, Liu R. Is the microRNA-146a (Rs2910164) Polymorphism Associated With Rheumatoid Arthritis? Association of microRNA-146a (Rs2910164) Polymorphism and Rheumatoid Arthritis Could Depend on Gender. *Joint Bone Spine* (2015) 82(3):166–71. doi: 10.1016/j.jbspin.2014.12.009
33. Guo S, Jin Y, Zhou J, Zhu Q, Jiang T, Bian Y, et al. MicroRNA Variants and HLA-miRNA Interactions Are Novel Rheumatoid Arthritis Susceptibility Factors. *Front Genet* (2099) 2021:12. doi: 10.3389/fgene.2021.747274
34. Li J, Wan Y, Guo Q, Zou L, Zhang J, Fang Y, et al. Altered microRNA Expression Profile With miR-146a Upregulation in CD4+ T Cells From Patients With Rheumatoid Arthritis. *Arthritis Res Ther* (2010) 12(3):R81. doi: 10.1186/ar3006
35. Gao J, Kong R, Zhou X, Ji L, Zhang J, Zhao D. MiRNA-126 Expression Inhibits IL-23R Mediated TNF-Alpha or IFN-Gamma Production in Fibroblast-Like Synoviocytes in a Mice Model of Collagen-Induced Rheumatoid Arthritis. *Apoptosis* (2018) 23(11-12):607–15. doi: 10.1007/s10495-018-1474-7
36. Zhou Q, Haupt S, Kreuzer JT, Hammitzsch A, Proft F, Neumann C, et al. Decreased Expression of miR-146a and miR-155 Contributes to an Abnormal Treg Phenotype in Patients With Rheumatoid Arthritis. *Ann Rheum Dis* (2015) 74(6):1265–74. doi: 10.1136/annrheumdis-2013-204377
37. Liu J, Fei D, Xing J, Du J, et al. MicroRNA-29a Inhibits Proliferation and Induces Apoptosis in Rheumatoid Arthritis Fibroblast-Like Synoviocytes by Repressing STAT3. *BioMed Pharmacother* (2017) 96:173–81. doi: 10.1016/j.biopha.2017.09.120
38. Tang X, Wang J, Xia X, Tian J, Rui K, Xu H, et al. Elevated Expression of ciRS-7 in Peripheral Blood Mononuclear Cells From Rheumatoid Arthritis Patients. *Diagn Pathol* (2019) 14(1):11. doi: 10.1186/s13000-019-0783-7
39. Zhu X, Wu L, Mo X, Xia W, Guo Y, Wang M, et al. Identification of PBMC-Expressed miRNAs for Rheumatoid Arthritis. *Epigenetics* (2020) 15(4):386–97. doi: 10.1080/15592294.2019.1676613
40. Wang X, Tang K, Wang Y, Chen Y, Yang M, Gu C, et al. Elevated Microrna1455p Increases Matrix Metalloproteinase9 by Activating the Nuclear factorkappaB Pathway in Rheumatoid Arthritis. *Mol Med Rep* (2019) 20(3):2703–11. doi: 10.3892/mmr.2019.10499
41. Stanczyk J, Ospelt C, Karouzakis E, Filer A, Raza K, Kolling C, et al. Altered Expression of microRNA-203 in Rheumatoid Arthritis Synovial Fibroblasts and its Role in Fibroblast Activation. *Arthritis Rheum* (2011) 63(2):373–81. doi: 10.1002/art.30115
42. de la Rica L, Urquiza JM, Gomez-Cabrero D, Islam AB, Lopez-Bigas N, Tegner J, et al. Identification of Novel Markers in Rheumatoid Arthritis Through Integrated Analysis of DNA Methylation and microRNA Expression. *J Autoimmun* (2013) 41:6–16. doi: 10.1016/j.jaut.2012.12.005
43. Hong BK, You S, Yoo SA, Park D, Hwang D, Cho CS, et al. MicroRNA-143 and -145 Modulate the Phenotype of Synovial Fibroblasts in Rheumatoid Arthritis. *Exp Mol Med* (2017) 49(8):e363. doi: 10.1038/emm.2017.108
44. Tseng CC, Wu LY, Tsai WC, Ou TC, Wu CC, Sung WY, et al. Differential Expression Profiles of the Transcriptome and miRNA Interactome in Synovial Fibroblasts of Rheumatoid Arthritis Revealed by Next Generation Sequencing. *Diagn (Basel)* (2019) 9(3). doi: 10.3390/diagnostics9030098
45. Wangyang Y, Yi L, Wang T, Feng Y, Liu G, Li D, et al. MiR-199a-3p Inhibits Proliferation and Induces Apoptosis in Rheumatoid Arthritis Fibroblast-Like Synoviocytes *via* Suppressing Retinoblastoma 1. *Biosci Rep* (2018) 38 (6). doi: 10.1042/BSR20180982
46. Guo J, Cao X, Zhao W, Zhu H, Ma X, Hao C, et al. MicroRNA-449 Targets Histone Deacetylase 1 to Regulate the Proliferation, Invasion, and Apoptosis of Synovial Fibroblasts in Rheumatoid Arthritis. *Ann Palliat Med* (2021) 10 (7):7960–9. doi: 10.21037/apm-21-1383
47. Wang Y, Zhang K, Yuan X, Xu N, Zhao S, Hou L, et al. miR-431-5p Regulates Cell Proliferation and Apoptosis in Fibroblast-Like Synoviocytes in Rheumatoid Arthritis by Targeting XIAP. *Arthritis Res Ther* (2020) 22 (1):231. doi: 10.1186/s13075-020-02328-3
48. Wang Y, Hou L, Yuan X, Xu N, Zhao S, Yang L, et al. miR-483-3p Promotes Cell Proliferation and Suppresses Apoptosis in Rheumatoid Arthritis Fibroblast-Like Synoviocytes by Targeting IGF-1. *BioMed Pharmacother* (2020) 130:110519. doi: 10.1016/j.biopha.2020.110519
49. Nakamachi Y, Kawano S, Takenokuchi M, Nishimura K, Sakai Y, Chin T, et al. MicroRNA-124a Is a Key Regulator of Proliferation and Monocyte Chemoattractant Protein 1 Secretion in Fibroblast-Like Synoviocytes From Patients With Rheumatoid Arthritis. *Arthritis Rheum* (2009) 60(5):1294–304. doi: 10.1002/art.24475
50. Gao B, Sun G, Wang Y, Geng Y, Zhou L, Chen X, et al. microRNA-23 Inhibits Inflammation to Alleviate Rheumatoid Arthritis *via* Regulating CXCL12. *Exp Ther Med* (2021) 21(5):459. doi: 10.3892/etm.2021.9890
51. Sun W, Zhang Y, Wang G. MicroRNA-137-Mediated Inhibition of Lysine-Specific Demethylase-1 Prevents Against Rheumatoid Arthritis in an Association With the REST/mTOR Axis. *Mol Pain* (2021) 17:17448069211041847. doi: 10.1177/17448069211041847
52. Bao X, Ma L, He C. MicroRNA-23a-5p Regulates Cell Proliferation, Migration and Inflammation of TNF-α-Stimulated Human Fibroblast-Like MH7A Synoviocytes by Targeting TLR4 in Rheumatoid Arthritis. *Exp Ther Med* (2021) 21(5):479. doi: 10.3892/etm.2021.9910
53. Chen L, Lu Q, Chen J, Feng R, Yang C. Upregulating miR-27a-3p Inhibits Cell Proliferation and Inflammation of Rheumatoid Arthritis Synovial Fibroblasts Through Targeting Toll-Like Receptor 5. *Exp Ther Med* (2021) 22(5):1227. doi: 10.3892/etm.2021.10661
54. Lin J, Huo R, Xiao L, Zhu X, Xie J, Sun S, et al. A Novel P53/microRNA-22/Cyr61 Axis in Synovial Cells Regulates Inflammation in Rheumatoid Arthritis. *Arthritis Rheumatol* (2014) 66(1):49–59. doi: 10.1002/art.38142
55. Meng Q, Pan B, Sheng P. Histone Deacetylase 1 Is Increased in Rheumatoid Arthritis Synovium and Promotes Synovial Cell Hyperplasia and Synovial Inflammation in the Collagen-Induced Arthritis Mouse Model *via* the

microRNA-124-Dependent MARCKS-JAK/STAT Axis. *Clin Exp Rheumatol* (2021) 39(5):970–81.
56. Song AF, Kang L, Wang YF, Wang M. MiR-34a-5p Inhibits Fibroblast–Like Synoviocytes Proliferation *via* XBP1. *Eur Rev Med Pharmacol Sci* (2020) 24 (22):11675–82. doi: 10.26355/eurrev_202011_23812
57. Tolboom TC, Pieterman E, van der Laan WH, Toes RE, Huidekoper AL, Nelissen RG, et al. Invasive Properties of Fibroblast-Like Synoviocytes: Correlation With Growth Characteristics and Expression of MMP-1, MMP-3, and MMP-10. *Ann Rheum Dis* (2002) 61(11):975–80. doi: 10.1136/ard.61.11.975
58. Jiang C, Wu X, Li X, Li M, Zhang W, Tao P, et al. Loss of microRNA-147 Function Alleviates Synovial Inflammation Through ZNF148 in Rheumatoid and Experimental Arthritis. *Eur J Immunol* (2021) 51 (8):2062–73. doi: 10.1002/eji.202048850
59. Shi DL, Shi GR, Xie J, Du XZ, Yang H. MicroRNA-27a Inhibits Cell Migration and Invasion of Fibroblast-Like Synoviocytes by Targeting Follistatin-Like Protein 1 in Rheumatoid Arthritis. *Mol Cells* (2016) 39 (8):611–8. doi: 10.14348/molcells.2016.0103
60. Stanczyk J, Pedrioli DM, Brentano F, Sanchez-Pernaute O, Kolling C, Gay RE, et al. Altered Expression of MicroRNA in Synovial Fibroblasts and Synovial Tissue in Rheumatoid Arthritis. *Arthritis Rheum* (2008) 58 (4):1001–9. doi: 10.1002/art.23386
61. Long L, Yu P, Liu Y, Wang S, Li R, Shi J, et al. Upregulated microRNA-155 Expression in Peripheral Blood Mononuclear Cells and Fibroblast-Like Synoviocytes in Rheumatoid Arthritis. *Clin Dev Immunol* (2013) 2013p:296139. doi: 10.1155/2013/296139
62. Okamoto K, Nakashima T, Shinohara M, Negishi-Koga T, Komatsu N, Terashima A, et al. Osteoimmunology: The Conceptual Framework Unifying the Immune and Skeletal Systems. *Physiol Rev* (2017) 97 (4):1295–349. doi: 10.1152/physrev.00036.2016
63. Rana AK, Li Y, Dang Q, Yang F, et al. Monocytes in Rheumatoid Arthritis: Circulating Precursors of Macrophages and Osteoclasts and, Their Heterogeneity and Plasticity Role in RA Pathogenesis. *Int Immunopharmacol* (2018) 65:348–59. doi: 10.1016/j.intimp.2018.10.016
64. Najm A, Masson FM, Preuss P, Georges S, Ory B, Quillard T, et al. MicroRNA-17-5p Reduces Inflammation and Bone Erosions in Mice With Collagen-Induced Arthritis and Directly Targets the JAK/STAT Pathway in Rheumatoid Arthritis Fibroblast-Like Synoviocytes. *Arthritis Rheumatol* (2020) 72(12):2030–9. doi: 10.1002/art.41441
65. Maeda Y, Farina NH, Matzelle MM, Fanning PJ, Lian JB, Gravallese EM. Synovium-Derived MicroRNAs Regulate Bone Pathways in Rheumatoid Arthritis. *J Bone Miner Res* (2017) 32(3):461–72. doi: 10.1002/jbmr.3005
66. Iwamoto N, Fukui S, Takatani A, Shimizu T, Umeda M, Nishino A, et al. Osteogenic Differentiation of Fibroblast-Like Synovial Cells in Rheumatoid Arthritis Is Induced by microRNA-218 Through a ROBO/Slit Pathway. *Arthritis Res Ther* (2018) 20(1):189. doi: 10.1186/s13075-018-1703-z
67. Kong XH, Shi SF, Hu HJ, Wang JX. MicroRNA-20a Suppresses RANKL-Modulated Osteoclastogenesis and Prevents Bone Erosion in Mice With Rheumatoid Arthritis Through the TLR4/p38 Pathway. *J Biol Regul Homeost Agents* (2021) 35(3):921–31. doi: 10.23812/20-604-a
68. Li HW, Zeng HS. Regulation of JAK/STAT Signal Pathway by miR-21 in the Pathogenesis of Juvenile Idiopathic Arthritis. *World J Pediatr* (2020) 16 (5):502–13. doi: 10.1007/s12519-019-00268-w
69. Ren B, Liu J, Wu K, Zhang J, Lv Y, Wang S, et al. TNF-Alpha-Elicited miR-29b Potentiates Resistance to Apoptosis in Peripheral Blood Monocytes From Patients With Rheumatoid Arthritis. *Apoptosis* (2019) 24(11-12):892–904. doi: 10.1007/s10495-019-01567-3
70. Niimoto T, Nakasa T, Ishikawa M, Okuhara A, Izumi B, Deie M, et al. MicroRNA-146a Expresses in Interleukin-17 Producing T Cells in Rheumatoid Arthritis Patients. *BMC Musculoskelet Disord* (2010) 11:209. doi: 10.1186/1471-2474-11-209
71. Fulci V, Scappucci G, Sebastiani GD, Giannitti C, Franceschini D, Meloni F, et al. miR-223 Is Overexpressed in T-Lymphocytes of Patients Affected by Rheumatoid Arthritis. *Hum Immunol* (2010) 71(2):206–11. doi: 10.1016/j.humimm.2009.11.008
72. van Hamburg JP, Tas SW. Molecular Mechanisms Underpinning T Helper 17 Cell Heterogeneity and Functions in Rheumatoid Arthritis. *J Autoimmun* (2018) 87:69–81. doi: 10.1016/j.jaut.2017.12.006
73. Jin S, Sun S, Ling H, Ma J, Zhang X, Xie Z, et al. Protectin DX Restores Treg/T(h)17 Cell Balance in Rheumatoid Arthritis by Inhibiting NLRP3 Inflammasome *via* miR-20a. *Cell Death Dis* (2021) 12(3):280. doi: 10.1038/s41419-021-03562-6
74. Dong L, Wang X, Tan J, Li H, Qian W, Chen J, et al. Decreased Expression of microRNA-21 Correlates With the Imbalance of Th17 and Treg Cells in Patients With Rheumatoid Arthritis. *J Cell Mol Med* (2014) 18(11):2213–24. doi: 10.1111/jcmm.12353
75. Guggino G, Orlando V, Saieva L, Ruscitti P, Cipriani P, La Manna MP, et al. Downregulation of Mirna17-92 Cluster Marks Vgamma9Vdelta2 T Cells From Patients With Rheumatoid Arthritis. *Arthritis Res Ther* (2018) 20 (1):236. doi: 10.1186/s13075-018-1740-7
76. Huang Q, Chen SS, Li J, Tao SS, Wang M, Leng RX, et al. miR-210 Expression in PBMCs From Patients With Systemic Lupus Erythematosus and Rheumatoid Arthritis. *Ir J Med Sci* (2018) 187(1):243–9. doi: 10.1007/s11845-017-1634-8
77. Smigielska-Czepiel K, van den Berg A, Jellema P, van der Lei RJ, Bijzet J, Kluiver J, et al. Comprehensive Analysis of miRNA Expression in T-Cell Subsets of Rheumatoid Arthritis Patients Reveals Defined Signatures of Naive and Memory Tregs. *Genes Immun* (2014) 15(2):115–25. doi: 10.1038/gene.2013.69
78. Yan S, Wang P, Wang J, Yang J, Lu H, Jin C, et al. Long Non-Coding RNA HIX003209 Promotes Inflammation by Sponging miR-6089 *via* TLR4/NF-kappaB Signaling Pathway in Rheumatoid Arthritis. *Front Immunol* (2019) 10:2218. doi: 10.3389/fimmu.2019.02218
79. Xie Q, Wei M, Zhang B, Kang X, Liu D, Zheng W, et al. MicroRNA33 Regulates the NLRP3 Inflammasome Signaling Pathway in Macrophages. *Mol Med Rep* (2018) 17(2):3318–27. doi: 10.3892/mmr.2017.8224
80. Meng HY, Chen LQ, Chen LH. The Inhibition by Human MSCs-Derived miRNA-124a Overexpression Exosomes in the Proliferation and Migration of Rheumatoid Arthritis-Related Fibroblast-Like Synoviocyte Cell. *BMC Musculoskelet Disord* (2020) 21(1):150. doi: 10.1186/s12891-020-3159-y
81. Wu H, Zhou X, Wang X, Cheng W, Hu X, Wang Y, et al. miR-34a in Extracellular Vesicles From Bone Marrow Mesenchymal Stem Cells Reduces Rheumatoid Arthritis Inflammation *via* the Cyclin I/ATM/ATR/p53 Axis. *J Cell Mol Med* (2021) 25(4):1896–910. doi: 10.1111/jcmm.15857
82. Li GQ, Fang YX, Liu Y, Meng FR, Wu X, Zhang CW, et al. MicroRNA-21 From Bone Marrow Mesenchymal Stem Cell-Derived Extracellular Vesicles Targets TET1 to Suppress KLF4 and Alleviate Rheumatoid Arthritis. *Ther Adv Chronic Dis* (2021) 12:20406223211007369. doi: 10.1177/20406223211007369
83. Hu R, Lv W, Zhang S, Liu Y, Sun B, Meng Y, et al. Combining miR-23b Exposure With Mesenchymal Stem Cell Transplantation Enhances Therapeutic Effects on EAE. *Immunol Lett* (2021) 229:18–26. doi: 10.1016/j.imlet.2020.11.007
84. Dinesh P, Kalaiselvan S, Sujitha S, Rasool M. miR-506-3p Alleviates Uncontrolled Osteoclastogenesis *via* Repression of RANKL/NFATc1 Signaling Pathway. *J Cell Physiol* (2020) 235(12):9497–509. doi: 10.1002/jcp.29757
85. Chen M, Li MH, Zhang N, Sun WW, Wang H, Wang YA, et al. Pro-Angiogenic Effect of Exosomal microRNA-103a in Mice With Rheumatoid Arthritis *via* the Downregulation of Hepatocyte Nuclear Factor 4 Alpha and Activation of the JAK/STAT3 Signaling Pathway. *J Biol Regul Homeost Agents* (2021) 35(2):629–40. doi: 10.23812/20-537-a
86. Donate PB, Alves de Lima K, Peres RS, Almeida F, Fukada SY, Silva TA, et al. Cigarette Smoke Induces miR-132 in Th17 Cells That Enhance Osteoclastogenesis in Inflammatory Arthritis. *Proc Natl Acad Sci USA* (2021) 118(1). doi: 10.1073/pnas.2017120118
87. Hegewald AB, Breitwieser K, Ottinger SM, Mobarrez F, Korotkova M, Rethi B, et al. Extracellular miR-574-5p Induces Osteoclast Differentiation *via* TLR 7/8 in Rheumatoid Arthritis. *Front Immunol* (2020) 11:585282. doi: 10.3389/fimmu.2020.585282
88. Chen Z, Wang H, Xia Y, Yan F, Lu Y. Therapeutic Potential of Mesenchymal Cell-Derived miRNA-150-5p-Expressing Exosomes in Rheumatoid Arthritis Mediated by the Modulation of MMP14 and VEGF. *J Immunol* (2018) 201 (8):2472–82. doi: 10.4049/jimmunol.1800304
89. Kurowska W, Kuca-Warnawin E, Radzikowska A, Jakubaszek M, Maślińska M, Kwiatkowska B, et al. Monocyte-Related Biomarkers of Rheumatoid

Arthritis Development in Undifferentiated Arthritis Patients - A Pilot Study. *Reumatologia* (2018) 56(1):10–6. doi: 10.5114/reum.2018.74742

90. Ouboussad L, Hunt L, Hensor EMA, Nam JL, Barnes NA, Emery P, et al. Profiling microRNAs in Individuals at Risk of Progression to Rheumatoid Arthritis. *Arthritis Res Ther* (2017) 19(1):288. doi: 10.1186/s13075-017-1492-9
91. Romo-García MF, Bastian Y, Zapata-Zuñiga M, Macías-Segura N, Castillo-Ortiz JD, Lara-Ramírez EE, et al. Identification of Putative miRNA Biomarkers in Early Rheumatoid Arthritis by Genome-Wide Microarray Profiling: A Pilot Study. *Gene* (2019) 720:144081. doi: 10.1016/j.gene.2019.144081
92. Anaparti V, Smolik I, Meng X, Spicer V, Mookherjee N, El-Gabalawy H, et al. Whole Blood microRNA Expression Pattern Differentiates Patients With Rheumatoid Arthritis, Their Seropositive First-Degree Relatives, and Healthy Unrelated Control Subjects. *Arthritis Res Ther* (2017) 19(1):249. doi: 10.1186/s13075-017-1459-x
93. Yue J, Lau TCK, Griffith JF, Xu J, Xiao F, Shi L, et al. Circulating miR-99b-5p as a Novel Predictor of Erosion Progression on High-Resolution Peripheral Quantitative Computed Tomography in Early Rheumatoid Arthritis: A Prospective Cohort Study. *Int J Rheum Dis* (2019) 22(9):1724–33. doi: 10.1111/1756-185X.13644
94. Evangelatos G, Fragoulis GE, Koulouri V, Lambrou GI. MicroRNAs in Rheumatoid Arthritis: From Pathogenesis to Clinical Impact. *Autoimmun Rev* (2019) 18(11):102391. doi: 10.1016/j.autrev.2019.102391
95. Mookherjee N, El-Gabalawy HS. High Degree of Correlation Between Whole Blood and PBMC Expression Levels of miR-155 and miR-146a in Healthy Controls and Rheumatoid Arthritis Patients. *J Immunol Methods* (2013) 400-401:106–10. doi: 10.1016/j.jim.2013.10.001
96. Murata K, Furu M, Yoshitomi H, Ishikawa M, Shibuya H, Hashimoto M, et al. Comprehensive microRNA Analysis Identifies miR-24 and miR-125a-5p as Plasma Biomarkers for Rheumatoid Arthritis. *PloS One* (2013) 8(7):e69118. doi: 10.1371/journal.pone.0069118
97. Ormseth MJ, Solus JF, Vickers KC, Oeser AM, Raggi P, Stein CM, et al. Utility of Select Plasma MicroRNA for Disease and Cardiovascular Risk Assessment in Patients With Rheumatoid Arthritis. *J Rheumatol* (2015) 42(10):1746–51. doi: 10.3899/jrheum.150232
98. Wang W, Zhang Y, Zhu B, Duan T, Xu Q, Wang R, et al. Plasma microRNA Expression Profiles in Chinese Patients With Rheumatoid Arthritis. *Oncotarget* (2015) 6(40):42557–68. doi: 10.18632/oncotarget.6449
99. Abou-Zeid A, Saad M, Soliman E. MicroRNA 146a Expression in Rheumatoid Arthritis: Association With Tumor Necrosis Factor-Alpha and Disease Activity. *Genet Test Mol Biomarkers* (2011) 15(11):807–12. doi: 10.1089/gtmb.2011.0026
100. Ciechomska M, Wojtas B, Bonek K, Roszkowski L, Gluszko P, Benes V, et al. Comprehensive microRNA and Transcriptomic Profiling of Rheumatoid Arthritis Monocytes: Role of microRNA-146b in Proinflammatory Progression. *Rheumatol (Oxford)* (2021). doi: 10.1093/rheumatology/keab407
101. Ormseth MJ, Solus JF, Sheng Q, Ye F, Song H, Wu Q, et al. The Endogenous Plasma Small RNAome of Rheumatoid Arthritis. *ACR Open Rheumatol* (2020) 2(2):97–105. doi: 10.1002/acr2.11098
102. Liu C, Pan A, Chen X, Tu J, Xia X, Sun L, et al. MiR-5571-3p and miR-135b-5p, Derived From Analyses of microRNA Profile Sequencing, Correlate With Increased Disease Risk and Activity of Rheumatoid Arthritis. *Clin Rheumatol* (2019) 38(6):1753–65. doi: 10.1007/s10067-018-04417-w
103. Khalifa O, Pers YM, Ferreira R, Senechal A, Jorgensen C, Apparailly F, et al. X-Linked miRNAs Associated With Gender Differences in Rheumatoid Arthritis. *Int J Mol Sci* (2016) 17(11). doi: 10.3390/ijms17111852
104. Fernández-Ruiz JC, Ramos-Remus C, Sánchez-Corona J, Castillo-Ortiz JD, Castañeda-Sánchez JJ, Bastian Y, et al. Analysis of miRNA Expression in Patients With Rheumatoid Arthritis During Remission and Relapse After a 5-Year Trial of Tofacitinib Treatment. *Int Immunopharmacol* (2018) 63:35–42. doi: 10.1016/j.intimp.2018.07.028
105. Liu X, Ni S, Li C, Xu N, Chen W, Wu M, et al. Circulating microRNA-23b as a New Biomarker for Rheumatoid Arthritis. *Gene* (2019) 712:143911. doi: 10.1016/j.gene.2019.06.001
106. Ormseth MJ, Solus JF, Sheng Q, Ye F, Wu Q, Guo Y, et al. Development and Validation of a MicroRNA Panel to Differentiate Between Patients With Rheumatoid Arthritis or Systemic Lupus Erythematosus and Controls. *J Rheumatol* (2020) 47(2):188–96. doi: 10.3899/jrheum.181029
107. Abdelaleem OO, Fouad NA, Shaker OG, Ahmed TI, Abdelghaffar NK, Eid HM, et al. Serum miR-224, miR-760, miR-483-5p, miR-378 and miR-375 as Potential Novel Biomarkers in Rheumatoid Arthritis. *Int J Clin Pract* (2021) p:e14651. doi: 10.1111/ijcp.14651
108. Hong H, Yang H, Xia Y. Circulating miR-10a as Predictor of Therapy Response in Rheumatoid Arthritis Patients Treated With Methotrexate. *Curr Pharm Biotechnol* (2018) 19(1):79–86. doi: 10.2174/1389201019666180417155140
109. Sode J, Krintel SB, Carlsen AL, Hetland ML, Johansen JS, Hørslev-Petersen K, et al. Plasma MicroRNA Profiles in Patients With Early Rheumatoid Arthritis Responding to Adalimumab Plus Methotrexate *vs* Methotrexate Alone: A Placebo-Controlled Clinical Trial. *J Rheumatol* (2018) 45(1):53–61. doi: 10.3899/jrheum.170266
110. Ciechomska M, Bonek K, Merdas M, Zarecki P, Swierkot J, Gluszko P, et al. Changes in MiRNA-5196 Expression as a Potential Biomarker of Anti-TNF-Alpha Therapy in Rheumatoid Arthritis and Ankylosing Spondylitis Patients. *Arch Immunol Ther Exp (Warsz)* (2018) 66(5):389–97. doi: 10.1007/s00005-018-0513-y
111. Castro-Villegas C, Perez-Sanchez C, Escudero A, Filipescu I, Verdu M, Ruiz-Limon P, et al. Circulating miRNAs as Potential Biomarkers of Therapy Effectiveness in Rheumatoid Arthritis Patients Treated With Anti-TNFalpha. *Arthritis Res Ther* (2015) 17:49. doi: 10.1186/s13075-015-0555-z
112. Liu Y, Han Y, Qu H, Fang J, Ye M, Yin W, et al. Correlation of microRNA Expression Profile With Clinical Response to Tumor Necrosis Factor Inhibitor in Treating Rheumatoid Arthritis Patients: A Prospective Cohort Study. *J Clin Lab Anal* (2019) 33(7):e22953. doi: 10.1002/jcla.22953
113. Duroux-Richard I, Pers YM, Fabre S, Ammari M, Baeten D, Cartron G, et al. Circulating miRNA-125b Is a Potential Biomarker Predicting Response to Rituximab in Rheumatoid Arthritis. *Mediators Inflamm 2014* (2014) p:342524. doi: 10.1155/2014/342524
114. Perez-Sanchez C, Cecchi I, Barbarroja N, Patino-Trives AM, Luque-Tevar M, Perez-Sanchez L, et al. Early Restoration of Immune and Vascular Phenotypes in Systemic Lupus Erythematosus and Rheumatoid Arthritis Patients After B Cell Depletion. *J Cell Mol Med* (2019) 23(9):6308–18. doi: 10.1111/jcmm.14517
115. Zhang Y, Wang H, Mao X, Guo Q, Li W, Wang X, et al. A Novel Circulating miRNA-Based Model Predicts the Response to Tripterysium Glycosides Tablets: Moving Toward Model-Based Precision Medicine in Rheumatoid Arthritis. *Front Pharmacol* (2018) 9:378. doi: 10.3389/fphar.2018.00378
116. Wang XY, Wang HL, Mao X, Li GY, Guo QY, Li WJ, et al. [Identification of Biomarkers to Response of Tripterygium Glycosides Tablets Acting on Rheumatoid Arthritis by Integrating Transcriptional Data Mining and Biomolecular Network Analysis]. *Zhongguo Zhong Yao Za Zhi* (2019) 44(16):3415–22. doi: 10.19540/j.cnki.cjcmm.20181031.001
117. Wang Y, Dai L, Wu H, Zhang ZR, Wang WY, Fu J, et al. Novel Anti-Inflammatory Target of Geniposide: Inhibiting Itgbeta1/Ras-Erk1/2 Signal Pathway *via* the miRNA-124a in Rheumatoid Arthritis Synovial Fibroblasts. *Int Immunopharmacol* (2018) 65:284–94. doi: 10.1016/j.intimp.2018.09.049
118. Cai Y, Jiang C, Zhu J, Xu K, Ren X, Xu L, et al. miR-449a Inhibits Cell Proliferation, Migration, and Inflammation by Regulating High-Mobility Group Box Protein 1 and Forms a Mutual Inhibition Loop With Yin Yang 1 in Rheumatoid Arthritis Fibroblast-Like Synoviocytes. *Arthritis Res Ther* (2019) 21(1):134. doi: 10.1186/s13075-019-1920-0
119. Wu J, Fan W, Ma L, Geng X. miR-708-5p Promotes Fibroblast-Like Synoviocytes' Cell Apoptosis and Ameliorates Rheumatoid Arthritis by the Inhibition of Wnt3a/beta-Catenin Pathway. *Drug Des Devel Ther* (2018) 12:3439–47. doi: 10.2147/DDDT.S177128
120. Mallinson DJ, Dunbar DR, Ridha S, Sutton ER, De la Rosa O, Dalemans W, et al. Identification of Potential Plasma microRNA Stratification Biomarkers for Response to Allogeneic Adipose-Derived Mesenchymal Stem Cells in Rheumatoid Arthritis. *Stem Cells Transl Med* (2017) 6(4):1202–6. doi: 10.1002/sctm.16-0356
121. Oka S, Furukawa H, Shimada K, Hashimoto A, Komiya A, Fukui N, et al. Plasma miRNA Expression Profiles in Rheumatoid Arthritis Associated Interstitial Lung Disease. *BMC Musculoskelet Disord* (2017) 18(1):21. doi: 10.1186/s12891-017-1389-4

122. Li Z, Li Y, Li Q, Zhang Z, Jiang L, Li X, et al. Role of miR-9-5p in Preventing Peripheral Neuropathy in Patients With Rheumatoid Arthritis by Targeting REST/miR-132 Pathway. *In Vitro Cell Dev Biol Anim* (2019) 55(1):52–61. doi: 10.1007/s11626-018-0310-2
123. Cuppen BV, Rossato M, Fritsch-Stork RD, Concepcion AN, Schenk Y, Bijlsma JW, et al. Can Baseline Serum microRNAs Predict Response to TNF-Alpha Inhibitors in Rheumatoid Arthritis? *Arthritis Res Ther* (2016) 18:189. doi: 10.1186/s13075-016-1085-z

Conflict of Interest: The authors declare that the research was conducted in the absence of any commercial or financial relationships that could be construed as a potential conflict of interest.

Publisher's Note: All claims expressed in this article are solely those of the authors and do not necessarily represent those of their affiliated organizations, or those of the publisher, the editors and the reviewers. Any product that may be evaluated in this article, or claim that may be made by its manufacturer, is not guaranteed or endorsed by the publisher.

frontiers in Immunology

ORIGINAL RESEARCH
published: 28 March 2022
doi: 10.3389/fimmu.2022.876963

A Novel Gene CDC27 Causes SLE and Is Associated With the Disease Activity

Shunlai Shang[1,2†], Yena Zhou[1†], Keng Chen[3†], Lang Chen[4], Ping Li[2], Diangeng Li[5], Shaoyuan Cui[2], Mei-Jun Zhang[6*], Xiangmei Chen[1,2*] and Qinggang Li[2*]*

[1] School of Medicine, Nankai University, Tianjin, China, [2] Department of Nephrology, The First Medical Center, Chinese PLA General Hospital, Medical School of Chinese PLA, Chinese PLA Institute of Nephrology, State Key Laboratory of Kidney Diseases, National Clinical Research Center for Kidney Diseases, Beijing, China, [3] Clinical Medical School, Guangdong Pharmaceutical University, Guangzhou, China, [4] Medical Technology & Bioinformatics Department, Beijing Mygenostics co., LTD, Beijing, China, [5] Department of Academic Research, Beijing-Chaoyang Hospital, Capital Medical University, Beijing, China, [6] Bioinformation Department, Geneis (Beijing) Co., Ltd., Beijing, China

OPEN ACCESS

Edited by:
Ming Zhao,
Central South University, China

Reviewed by:
Jurong Yang,
The Third Affiliated Hospital of Chongqing Medical University, China
Ningshao Xia,
Xiamen University, China

***Correspondence:**
Shaoyuan Cui
cshaoyuan@hotmail.com
Mei-Jun Zhang
zhangmj@geneis.cn
Xiangmei Chen
xmchen301@126.com
Qinggang Li
qgbj301@126.com

[†]These authors share first authorship

Specialty section:
This article was submitted to Autoimmune and Autoinflammatory Disorders, a section of the journal Frontiers in Immunology

Received: *16 February 2022*
Accepted: *03 March 2022*
Published: *28 March 2022*

Citation:
Shang S, Zhou Y, Chen K, Chen L, Li P, Li D, Cui S, Zhang M-J, Chen X and Li Q (2022) A Novel Gene CDC27 Causes SLE and Is Associated With the Disease Activity. Front. Immunol. 13:876963. doi: 10.3389/fimmu.2022.876963

Background: As genetic genetic factors are important in SLE, so screening causative genes is of great significance for the prediction and early prevention in people who may develop SLE. At present, it is very difficult to screen causative genes through pedigrees. The analytical method described herein can be used to screen causative genes for SLE and other complex diseases through pedigrees.

Methods: For the first time, 24 lupus pedigrees were analyzed by combining whole exon sequencing and a variety of biological information tools including common-specific analysis, pVAAST (pedigree variant annotation, analysis and search tool), Exomiser (Combining phenotype and PPI associated analysis), and FARVAT (family based gene burden), and the causative genes of these families with lupus identified. Selected causative genes in peripheral-blood mononuclear cells (PBMCs) were evaluated by quantitative polymerase chain reaction (qPCR).

Results: Cell division cycle 27 (CDC27) was screened out by common-specific analysis and Exomiser causative gene screening. FARVAT analysis on these families detected only CDC27 at the extremely significant level (false discovery rate <0.05) by three family-based burden analyses (BURDEN, CALPHA, and SKATO). QPCR was performed to detect for CDC27 in the PBMCs of the SLE family patients, sporadic lupus patients, and healthy people. Compared with the healthy control group, CDC27 expression was low in lupus patients (familial and sporadic patients) (P<0.05) and correlated with lupus activity indicators: negatively with C-reactive protein (CRP) (P<0.05) and erythrocyte sedimentation rate (P<0.05) and positively with complement C3 and C4 (P<0.05). The CDC27 expression was upregulated in PBMCs from SLE patients with reduced lupus activity after immunotherapy (P<0.05). Based on Receiver operating characteristic (ROC) curve analysis, the sensitivity and specificity of CDC27 in diagnosing SLE were 82.30% and 94.40%.

Conclusion: The CDC27 gene, as found through WES combined with multiple analytical method may be a causative gene of lupus. CDC27 may serve as a marker for the diagnosis of SLE and is closely related to the lupus activity. We hope that the analytical method in this study will be used to screen causative genes for other diseases through small pedigrees, especially among non-close relatives.

Keywords: lupus family, multiple bioinformatics analysis, CDC27, whole exone sequencing, marker

1 BACKGROUND

Systemic lupus erythematosus (SLE) is a chronic systemic inflammatory disease that can affect many organs, such as the kidneys, lungs, and skin (1, 2). Prediction and early prevention are of great significance for people who are likely to develop SLE (1). Although the etiology of SLE remains unclear, genetic factors are thought to be important for its occurrence (3). More than 5% of cases of lupus are familial, and the agreement rate between identical twins is 40% (4). Moreover, onset of lupus shows a familial aggregation, and the heritability rate is estimated to be 44-66% (5–7). The risk of SLE increases significantly in individuals with first-degree relatives with SLE (3). SLE has obvious genetic clustering and genetic predisposition, which strongly suggests the important role of genetic factors in its pathogenesis (7, 8).

Compared with traditional research methods for single-gene diseases, whole-exome sequencing (WES) has the advantages of being less time-consuming and having high throughput, low sample requirements, high sensitivity, and low cost (9). WES improves the efficiency of causative gene discovery at lowcost (10), which is important for the diagnosis, treatment, and prevention of many diseases (11–15).

In this study many lupus families (24 families) were for the first time evaluated by combining WES with multiple analytical methods, and possible causative genes of SLE were identified, enriching our knowledge on the causative mechanism of SLE. This study identified cell division cycle 27 (CDC27) as a possible causative gene for SLE. Quantitative polymerase chain reaction (qPCR) showed that compared with healthy individuals, the expression trend of CDC27 in patients with sporadic lupus was the same as that in familial patients, indicating that CDC27 might serve as a marker for the diagnosis of SLE. CDC27 is a component of the anaphase-promoting complex (APC), is an E3 ubiquitin ligase that catalyzes ubiquitin-mediated proteasomal degradation of type B cell cycle proteins and stimulates the cell cycle transition from the middle stage to the later stage (16, 17). Abnormal CDC27 expression is associated with autoimmune diseases (18) and cancer (19), and it can help significantly in predicting breast cancer recurrence (20). No study to date has reported familial aggregation of CDC27 in specific diseases, nor has the direct relationship between abnormal CDC27 expression and the pathogenesis of SLE been investigated. We hope that this study will improve the utility of CDC27 in the diagnosis of SLE.

Abbreviations: dsDNA, Anti-double-stranded DNA; C3, Complement protein C3; C4, Complement protein C4; SLE, Systemic lupus erythematosus; SLEDAI, Systemic Lupus Erythematosus Disease Activity Index.

2 EXPERIMENTAL MATERIALS AND METHODS

2.1 Family Ascertainment

The subjects involved in this study met the research classification criteria of the 2012 Systemic Lupus Collaborating Clinics for SLE. On the one hand, familial lupus patients were included. Familial SLE was defined as SLE confirmed in at least two relatives. The family members of the lupus patients were all nonconsanguineous members, and the healthy members of the family were studied as the familial control group. Patients with sporadic lupus were also included. The above patients were all admitted to the People's Liberation Army General Hospital between December 2016 and December 2020. The healthy control group for sporadic patients were volunteers from the same hospital with normal physical examination at the same time. Voluntary, written, fully informed consent was obtained from all participants.

2.2 DNA Extraction, Library Preparation, and Whole-Exome Sequencing

2.2.1 DNA Extraction

Peripheral-blood samples were collected from participating subjects, and genomic DNA was obtained using the TIANamp genomic DNA kit (Catalog no. DP304; TIANGEN) according to the manufacturer's protocol.

2.2.2 Exon Library Preparation

The genomic DNA template was used for library preparation (small fragments) according to the method and procedure of SureSelectXT Target Enrichment System (G7530-90000), and followed by hybridization and capture.

2.2.3 Sequencing

For qualified libraries, paired-end sequencing (PE150) was performed on the HiSeq sequencing platform to obtain 150-bp sequence reads. Exon data of each sample (25-30 Gbp) were sequenced at a depth of 200X.

2.3 Bioinformatic Analysis

The families with lupus were divided according to whether male family members had the disease, into class 1 (families with both male and female members having the disease) and class 2

(families with female members having the disease, but without it being clear whether male members would develop have the disease in the future). The bioinformatic analysis scheme of this study is shown in **Figure 1**.

2.3.1 Data Quality Control

Sequencing data were quality-controlled with adapter and aligned to human reference genome build hg19 (ftp://hgdownload.soe.ucsc.edu/goldenPath/hg19/) with Burrows–Wheeler Aligner (bwa) software version 0.7.12-r1039. The aligned reads were sorted and indexed using SAMtools version 1.2.1, and the Genome Analysis Toolkit (GATK, version 3.8) was used to realign reads to the genome and eliminate PCR duplicates. The GATK4.0 best practice haplotype caller pipeline was used for SNP and indel calling. All SNPs were annotated using ANNOVAR and related database download at Feb. 20.2020 Several genomic databases, including 1,000 Genomes (1000G), ExAC (Exome Aggregation Consortium), Exome Sequencing Project (ESP), gnomAD (both WES and WGS databases) (v2.1.1), and CG46, were used to assess the variant frequency in the population. MCAP(v1.3), SIFT, Polyphen2-HDIV, Polyphen2-HVAR, MutationTaster, MutationAssessor, and Clinvar (version 20200316) were used to annotate the effect of missense variants. GERPs were used to evaluate the conservation of the variant locus.

2.3.2 Data Analysis

Considering the importance of sexfor onset (21–27), lupus families were divided into two types: class 1 and class 2. Preliminary screening of causative genes and related loci was performed using three methods based on variant loci (common-specific analysis; Pedigree Variant Annotation, Analysis, and Search Tool (pVAAST) multiline linkage and correlation analysis; Exomiser causative gene screening). As a method in pedigree studies, gene-based FARVAT was also used to perform gene burden analysis, which directly considers some genes with weak single-locus effect values and low single-locus mutation frequencies, in order to supplement the above three methods. The candidate genes screened by the above methods were annotated in the DisGenet database.

2.3.2.1 Pedigree Screening for Common-Specific Analysis in Affected Members

We screened the families with multiple affected individuals as well as healthy family members and there is procedure of common-specific analysis in **Figure 2** (28).

2.3.2.2 pVAAST Multiline Linkage and Correlation Analysis

pVAAST combines two different statistical methods used for identifying disease-causing gene mutations (29). This combination approach outperforms individual familial analytical methods by increasing the power or speed with which mutations are identified and reducing complications through study design and analysis. pVAAST is robust with regard to incomplete penetrance and locus heterogeneity and is applicable to a variety of genetic traits. pVAAST performs well in research on a single gene or a highly permeable phenotype in a single lineage or in research on a highly polygenic and common phenotype involving hundreds of lineages.

2.3.2.3 Human Phenotype Ontology tTerm Conversion and Exomiser CausativeGene Screening in Diseased Samples

Exomiser uses random-walk analysis of protein interaction networks, clinical correlation and cross-species phenotype comparison, and various other computational filters (for variable frequency, pathogenicity prediction, and lineage analysis) to prioritize exon sequences (30). Exomiser can detect potential disease-causing variants in one exon or a whole genome. It mines causative genes and variant loci based on mutation frequency, pathogenicity, mutation quality, genetic pattern, and HPO phenotype data. Based on the Exomiser screening results, the genes with an Exomiser score, Phenotype score, and Variant score all of 0 were filtered out and combined with the annotation results

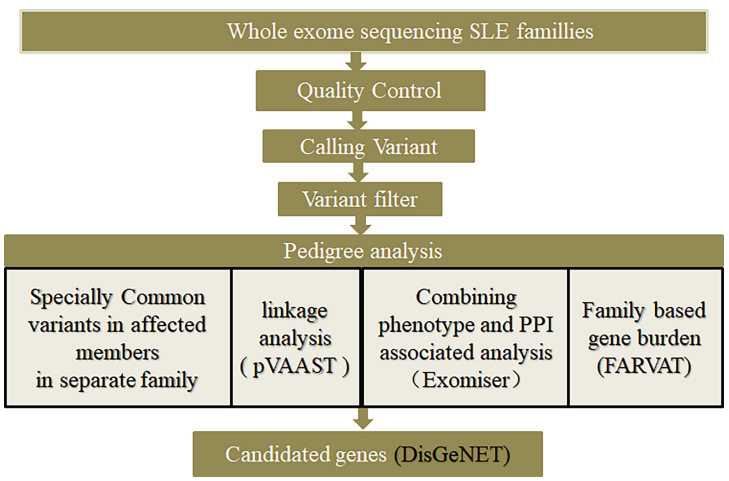

FIGURE 1 | Diagram of bioinformatic analysis.

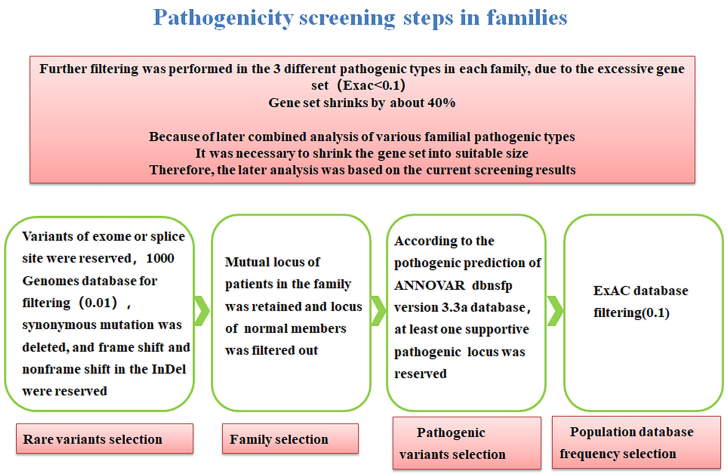

FIGURE 2 | Procedure of common-specific analysis.

of the variant loci by Exomiser. Nonpathogenic loci were filtered out (definition of causative locus: any one of CADD, POLYPHEN, MUTATIONTASTER, and SIFT identified it as pathogenic, or it had not been annotated).

2.3.2.4 FARVAT: Family Based Correlation Analysis

FARVAT, a family-based rare variant association test, can be used to study extended families (31). The software combines the burden test and the variant component test and employs three types of parameters to perform the correlation test. When all the loci in a certain region are pathogenic, the BURDEN parameters perform the best; when some of the loci in a certain region are causative, the CALPHA parameters perform the best; SKATO combines the statistical strategies of the former two to achieve very robust performance. FARVAT uses only SNPs for analysis. If a sample contains only one parent and the other parent is missing, then this sample is excluded from analysis. Note: The software can obtain the *p* values of three parameters, and any one parameter with $P<0.05$ is a candidate.

2.3.2.5 Annotation of Candidate Genes in the DisGenet Database

DisGeNET (Janet Piñero, Núria Queralt-Rosinach, Àlex Bravo, Jordi Deu-Pons, Anna Bauer-Mehren, Martin Baron, Ferran Sanz, Laura I. Furlong, DisGeNET: a discovery platform for the dynamical exploration of human diseases and their genes *Database*, Volume 2015, 2015, bav028,https://doi.org/10.1093/database/bav028) integrates expert-curated databases with text-mined data, covers information on Mendelian and complex diseases, and includes data from animal disease models. It is a good choice for complex disease research, and it contains many important lupus studies based on the supporting evidenceto prioritize gene-and lupus associations.

2.4 RNA Extraction and PCR

RNA extraction: Fasting ethylenediaminetetraacetic acid (EDTA)-anticoagulated peripheral blood (2 mL) was collected from SLE patients and controls and was tested within 3 h. Ficoll separating solution was used to extract peripheral-blood mononuclear cells (PBMCs), lysis buffer was added to the extracted human PBMCs, the solution was placed at room temperature for 5 min, and 0.2 mL chloroform was added (2). Complementary DNA (cDNA) synthesis: The mixture was prepared in RNase-free microfuge tubes using a cDNA reverse transcription kit (Shanghai Yisheng Biotechnology Co., Ltd.), and the reverse transcription reaction system was prepared (20 μL) (3). PCR: According to the qPCR SYBR Green reagent kit, 2× real-time quantitative PCR amplification premixed solution, upstream and downstream primers, template DNA, and sterile ultrapure water were added. The reaction was performed in a fluorescence quantitative PCR machine (Thermo Scientific). The fluorescence quantitative PCR primer sequences are listed in **Supplementary Table 1**. According to the Ct value of the samples, the relative quantitative method was used to analyze the results of RT-PCR, and $2^{-\Delta Ct}$ was calculated (32).

3 STATISTICAL ANALYSIS

SPSS 17.0 software was used to analyze the data. Measurement data with a normal distribution are expressed as the mean ± standard deviation (x ± S). The t test was used for intergroup comparison, and the paired t test was used for intragroup comparison. Measurement data with a nonnormal distribution are represented by the median (interquartile range), and the rank test was used for their intergroup and intragroup comparisons. Correlations between two variables were calculated using linear correlation analysis. Receiver operating characteristic (ROC) curve analysis was done to evaluate the sensitivity and specificity of CDC27 expression in PBMCs for SLE diagnosis. $P<0.05$ was considered statistically significant.

4 RESULTS

4.1 Included Lupus Families

There were 9 families in class 1, and 15 families in class 2 (**Figure 3**). CDC27 was involved in 10 families (see the family10-20 in **Figure 3** for details). Gray refers to people with uncertain lupus disease; open refers to healthy controls; filled refers to lupus patients in **Figure 3**.

4.2 Selected Candidate Genes

The two types of families, class 1 and class 2, were analyzed by three methods (common-specific analysis, pVAAST multiline linkage and correlation analysis, and Exomiser). The screening results are shown in **Supplementary Table 2**.

4.3 FARVAT Results

In addition to the above three analytical methods, FARVAT was used to analyze all the families. The results showed that only CDC27 was detected at the extremely significant level (P<0.05) in three burden analyses (BURDEN, CALPHA, and SKATO), as shown in **Table 1**.

4.4 Annotation of Candidate Genes in the DisGenet Database

The candidate genes obtained from common-specific analysis, pVAAST multiline linkage and correlation analysis, FARVAT, and Exomiser pathogenic gene screening were annotated in the DisGenet database. Some genes in the database are reportedly related to lupus, as shown in **Supplementary Tables 3-6**.

4.5 Relationship Between the CDC27 Expression in PBMCs and Clinical Manifestations in SLE Patients

There were no significant differences in sex, age, or body mass index between the two groups (sporadic lupus and healthy control group), nor between the familial lupus patients and the familial control group. QPCR was performed to detect for CDC27 in the PBMCs of the SLE familial patients, sporadic lupus patients, and healthy people. In the lupus family study of 15 patients with lupus and 14 healthy controls, CDC27 expression was lower in the patients than in the healthy controls, as depicted in **Figure 4A**. In the sporadic lupus analysis involving 92 patients and 48 healthy controls, CDC27 expression was also lower in the patients than in the healthy controls, as shown in **Figure 4B**.

The clinical manifestations and laboratory tests of 107 SLE patients including 92 sporadic and 15 familial patients were collected in detail, and the SLE disease activity index (SLEDAI) was calculated (33). Clinical manifestations and laboratory indicators, such as erythrocyte sedimentation rate, C-reactive protein (CRP), complement C3, complement C4, antinuclear antibodies, double-stranded DNA, proteinuria, and hematuria, were examined to analyze the relationship between these indicators and the CDC27 expression in SLE patient PBMCs. The results showed that the CDC27 expression in PBMCs correlated negatively with CRP (r=-0.919, P<0.01), erythrocyte sedimentation rate (r=–0.804, P<0.001), C3 (r=0.927, P<0.001) and C4 (r=0.962, P<0.001), but not with the remaining indicators. Details are provided in **Figure 5**.

4.6 Relationship Between the CDC27 Expression in PBMCs of SLE Patients and Immunosuppressive Therapy

Among the 100 sporadic SLE patients enrolled, 18 exhibited decreased disease activity after immunosuppressive therapy (P<0.05), and samples before and after the activity changes were collected for CDC27 detection in PBMCs. CDC27 expression was upregulated after treatment, a difference that was statistically significant (P < 0.05), as shown in **Table 2**.

4.7 Evaluation of the Diagnostic Value of CDC27 Expression in PBMCs for the SLE Patients

The CDC27 expression in PBMCs from107 SLE patients and 48 controls was analyzed by ROC analysis. The area under the ROC curve (AUC) was 0.880 (95% CI: 0. 814 <0. 946; P ~0. 001), the sensitivity was 82.30%, the specificity was 94.40% and the Youden index was 0.767. The positive predictive value is 90.09% and the negative predictive value is 89.47%.Details are shown in **Figure 6**.

5 DISCUSSION

To date, a variety of genetic abnormalities have been found to be closely related to the occurrence and progression of SLE (34). However, there are few studies on causative genes obtained through pedigrees (35), especially on nonconsanguineous pedigrees through sequencing techniques.

In pedigree studies, WES is not limited to small pedigrees, multiple generations of inherited pedigrees, or core pedigrees with polygenic complex diseases, and it can create conditions to find causative genes (36). In this study, for the first time, many Chinese familial SLE patients (a total of 24 families) were sequenced using WES, and common-specific analysis, pVAAST multiple-line linkage and correlation analysis, FARVAT, and Exomiser were used to screen the causative genes of lupus families in order to screen for SLE causative genes through a pedigree study, especially SLE pedigrees of nonclose relatives. Common-specific analysis, pVAAST multiline linkage and correlation analysis, and Exomiser were used to screen genes and their corresponding loci. Common-specific analysis is a widely used strategy for patients with familial diseases. As the pathogenic loci of the corresponding disease may be enriched in the family, pVAAST was used. Exomiser considers the correlation between the phenotypes and genes found in humans and animal models and combines protein–protein interactions and other information, giving it an advantagefor locus the screening. When a certain gene is screened out by multiple methods, the reliability and scientific support for its causative role is high. FARVAT can be used for multiple pedigrees; it analyzes gene burden using the gene as a

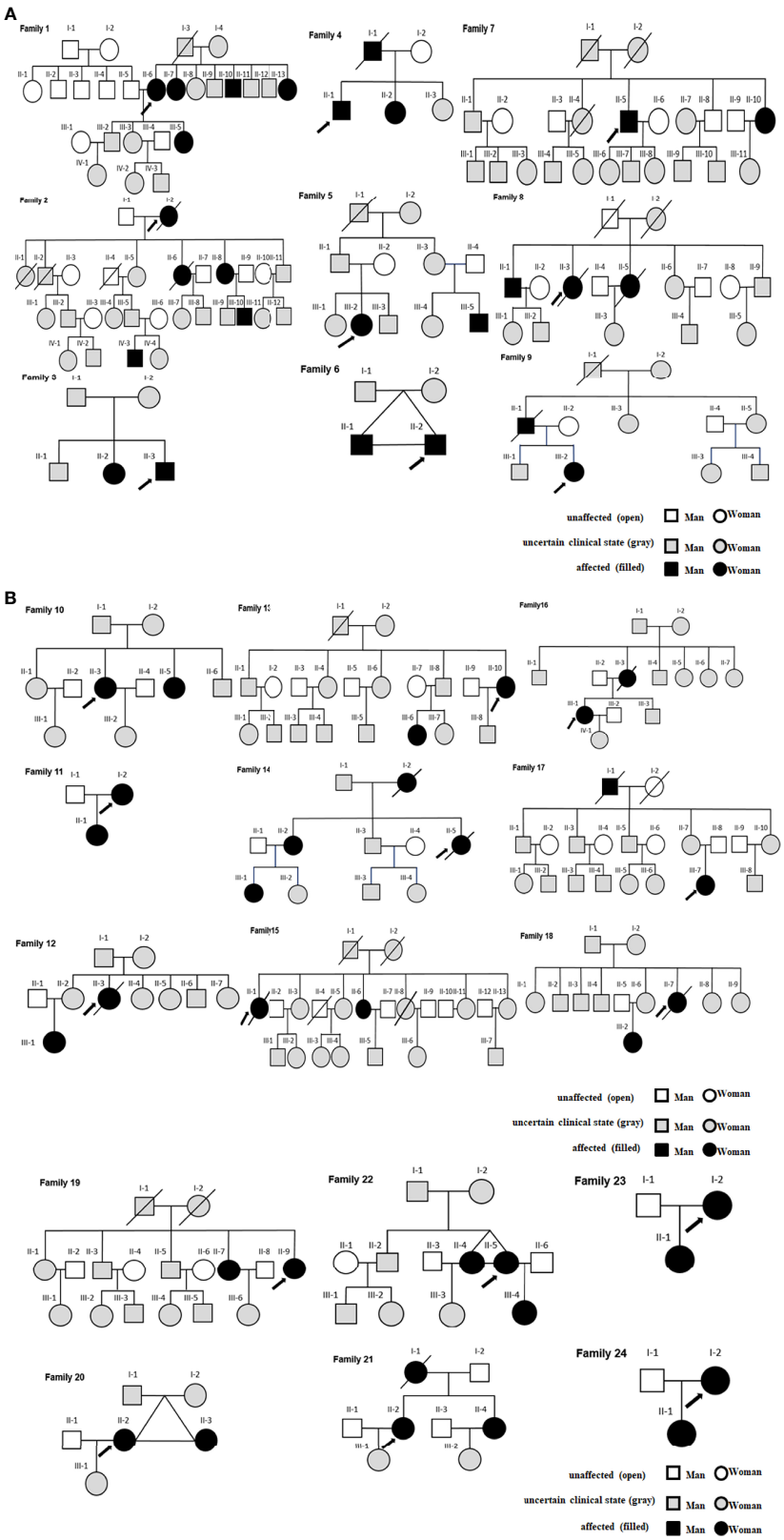

FIGURE 3 | **(A)** Class 1-SLE families. **(B)** Class 2-SLE families.

TABLE 1 | Results of family-based analysis using three types of burden (BURDEN, CALPHA, SKATO).

CHR	GENE	NSAMP	NVARIANT	MAC	NIMP	START	END	P-CALPHA	P-BURDEN	P-SKATO
17	CDC27	74	138	1969	8168	45198086	45266730	0.011191	0.007543	0.007507

NSAMP, Number of samples; "NVARIANT", variance.

unit, and directly considers some genes with weak single-locus effect values. Thus, it is a supplement to the above three methods. In this study, the four analytical methods were combined to improve the reference value for screening causative genes of SLE through pedigrees.

Genetic factors play a significant role in the occurrence and progression of many diseases, such as coronary heart disease (37, 38), diabetes (39) and diabetes insipidus (40). However, it is very difficult to screen causative genes through pedigrees, and there is no unified and standardized method. Various methods have shortcomings, i.e., some can only perform enrichment (41), some can only find regions of causative genes, it is difficult to clearly identify specific genes in studies from small pedigrees (42) some pedigrees are difficult to screen due to incomplete data (43), and many related studies have been conducted on the consanguineous pedigrees. This study also provides a method for screening other diseases through pedigrees, especially consanguineous pedigrees (**Figure 1**).

We annotated the candidate genes in the DisGenet database. Much of the information we found is related to lupus, which indicates that the candidate genes in this study are important in the pathogenesis of lupus and have a certain degree of credibility. Among the four bioinformatic analyses, CDC27 was obtained using three methods. Therefore, we focused on this gene.

The major functional isomers of CDC27 are encoded by 19 exons, and CDC27 has two tetratricopeptide repeat (TPR) domains, five TPR motifs at the N-terminal domain and nine TPR motifs in the C-terminal domain (44). The protein encoded by CDC27 is a component of APC, which had a TPR sequence of its own that is necessary for interaction with certain proteins (45). CDC27 expression is abnormal in several tumors and autoimmune diseases (19), and their pathogenesis may be related to APC/C activation. Phosphorylation of CDC27 is the key for APC/C activation, which is achieved through the action of transforming growth factor β (TGF-β) (46). The TGF-β signaling pathway plays an important role in many biological processes, including cell growth, differentiation, apoptosis, and migration, and the occurrence and progression of autoimmune diseases (47). The activation of the TGF-β pathway is involved in the pathogenesis of SLE (48). Vanarsa et al. found that expression of TGF-β1 in the urine was increased in patients with active lupus (49).

To date, there had been no direct study on the relationship between CDC27 and lupus. In the present study, peripheral blood of familial SLE patients and healthy controls was submitted to qPCR to detect CDC27, and the results showed low CDC27 expression in lupus patients. We speculate that the downregulation of CDC27 in lupus may lead to immune disorders. Because CDC27 is a downstream molecule of the TGF-β pathway, it activates APC/C (ubiquitin ligase) under the action of TGF-β through phosphorylation, thereby activating the ubiquitin-proteasome system, which may affect the cell cycle process, hinder protein degradation, and cause immune abnormalities. The mechanism of abnormal CDC27 expression in lupus still needs to be further explored.

Diagnosis of SLE is mainly based on clinical symptoms, signs, and laboratory tests. However, the clinical manifestations of SLE are complex, and the severity of the disease varies; hence, clinicians often misdiagnose SLE as other diseases. The diagnostic sensitivity of commonly used autoantibodies (such as antinuclear antibodies, double-stranded DNA, and anti-Smith antibody) against SLE is not perfectat only 20-60% (50). Thus, there is no ideal diagnostic marker for SLE. This study used ROC curve analysis to assess the diagnostic value of CDC27 and found a sensitivity of 82.30%,and specificity of 94.40%,indicating that CDC27 has high value in the diagnosis of SLE (51). In addition, the expression level of CDC27 correlated with the activity of lupus and had certain value in predicting the condition.

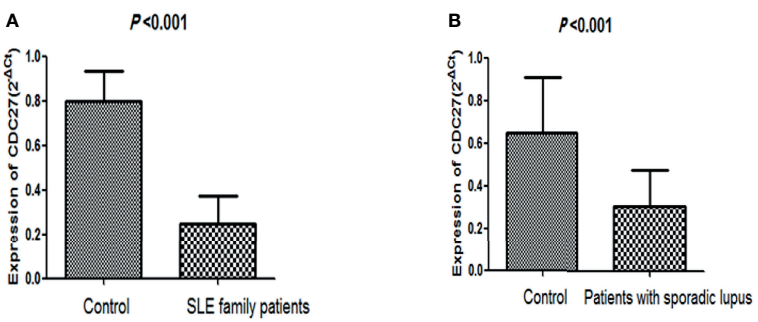

FIGURE 4 | Comparison of CDC27 expression levels between healthy controls and lupus patients. **(A)** Comparison of healthy controls and family patients with lupus; **(B)** comparison of healthy controls and sporadic lupus patients.

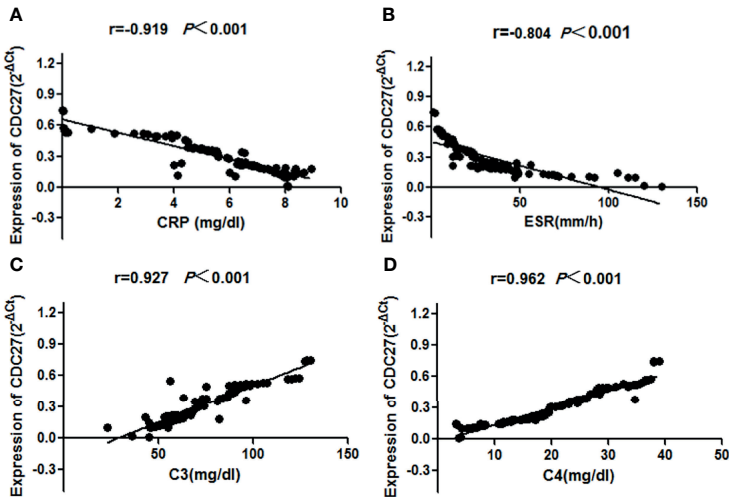

FIGURE 5 | Correlations between the SLE disease activity index and CDC27 expression were calculated using linear correlation analysis **(A)** CRP, **(B)** ESR, **(C)** C3, **(D)** C4.

TABLE 2 | The relationship between the expression of CDC27 in PBMC of SLE patients and immunosuppressive therapy.

Progect	Before immunotherapy	After immunotherapy	*P*
SLE Activity Score	10.944±2.127	4.778±1.833	*P*<0.001
CDC27 expression	0.3081±0.217	0.8966±0.981	0.023

Although we screened for abnormal expression of CDC27 in SLE patients through pedigrees, this gene's role is not limited to familial SLE. To further investigate the general role of abnormal CDC27 expression in the pathogenesis of SLE, we detected CDC27 expression in patients with sporadic SLE and compared it with that in the healthy control. As expected, CDC27 expression in sporadic SLE patients was reduced, indicating that family-based causative gene exploration is not

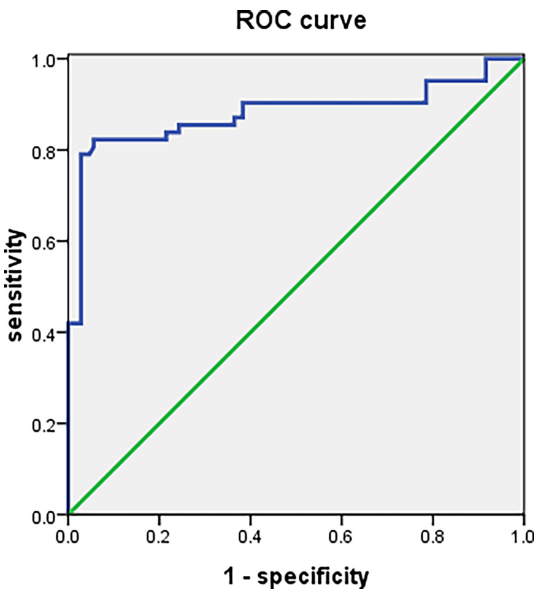

FIGURE 6 | ROC curve analysis for sporadic lupus patients and healthy controls.

be limited to familial diseases, and that decreased expression of CDC27 has significance for the diagnosis of both familial and sporadic SLE. This study has reference value for research methods that study diseases through pedigrees to find patterns and apply them to the whole population.

6 CONCLUSION

For the first time, WES combined with a variety of analytical methods showed that the CDC27 gene plays an important role in the occurrence and progression of SLE and may be a causative gene and a marker of the disease. This study performed a preliminary verification, but further verification is still needed. We hope that the analytical method described herein provide new ideas for screening causative genes of other diseases through small pedigrees.

DATA AVAILABILITY STATEMENT

The data presented in the study are deposited in the https://bigd.big.ac.cn/gsa-human/browse repository, accession number HRA002049.

ETHICS STATEMENT

The studies involving human participants were reviewed and approved by the Ethics Committee of the People's Liberation Army General Hospital, and the ethics number is S2019-095-01. The patients/participants provided their written informed consent to participate in this study.

AUTHOR CONTRIBUTIONS

SS, XC, SC, and QL designed the study. SS and YZ wrote the original draft. SS, PL, XC, LC and QL provided the patient plasma samples and the corresponding clinical data. SS and MZ validated and interpreted the data. SS, KC and DL did the statistical analyses. MZ provided the code (https://github.com/zmj168/genetics). All authors contributed to the article and approved the submitted version.

FUNDING

This study was funded by the National Natural Science Foundation of China (No. 81830019) and Beijing Natural Science Foundation(7202188).

ACKNOWLEDGMENTS

We thank AJE (https://www.aje.cn) for English language editing,

SUPPLEMENTARY MATERIAL

The Supplementary Material for this article can be found online at: https://www.frontiersin.org/articles/10.3389/fimmu.2022.876963/full#supplementary-material

REFERENCES

1. Almaani S, Meara A, Rovin BH. Update on Lupus Nephritis. *Clin J Am Soc Nephrol* (2016) 12(5):825–35. doi: 10.2215/CJN.05780616
2. Alarcón GS. Multiethnic Lupus Cohorts: What Have They Taught Us? *Reumatol Clin* (2011) 7(1):3–6. doi: 10.1016/j.reuma.2010.11.001
3. Ulff-Møller CJ, Simonsen J, Kyvik KO, Jacobsen S, Frisch M. Family History of Systemic Lupus Erythematosus and Risk of Autoimmune Disease: Nationwide Cohort Study in Denmark 1977-2013. *Rheumatol (Oxford)* (2017) 56(6):957–64. doi: 10.1093/rheumatology/kex005
4. Perdriger A, Werner-Leyval S, Rollot-Elamrani K. The Genetic Basis for Systemic Lupus Erythematosus. *Joint Bone Spine* (2003) 70(2):103–8. doi: 10.1016/s1297-319x(03)00007-1
5. Yang J, Visscher PM, Wray NR. Sporadic Cases are the Norm for Complex Disease. *Eur J Hum Genet* (2010) 18:1039–43. doi: 10.1038/ejhg.2009.177
6. Kuo CF, Grainge MJ, Valdes AM, See LC, Luo SF, Yu KH, et al. Familial Aggregation of Systemic Lupus Erythematosus and Coaggregation of Autoimmune Diseases in Affected Families. *JAMA Intern Med* (2015) 175:1518–26. doi: 10.1001/jamainternmed.2015.3528
7. Michel M, Johanet C, Meyer O, Francès C, Wittke F, Michel C, et al. Familial Lupus Erythematosus. Clinical and Immunologic Features of 125 Multiplex Families. *Medicine (Baltimore)* (2001) 80(3):153–8. doi: 10.1097/00005792-200105000-00001
8. Mohan C, Putterman C. Genetics and Pathogenesis of Systemic Lupus Erythematosus and Lupus Nephritis. *Nat Rev Nephrol* (2015) 11(6):329–41. doi: 10.1038/nrneph.2015.33
9. Fan H, Ives AR, Surget-Groba Y, Cannon CH. An Assembly and Alignment-Freemethod of Phylogeny Reconstruction From Next-Generation Sequencing Data. *BMC Genomics* (2015) 16(1):522–39. doi: 10.1186/s12864-015-1647-5
10. Ng SB, Turner EH, Robertson PD, Flygare SD, Bigham AW, Lee C, et al. Targeted Capture and Massively Parallel Sequencing of 12 Human Exomes. *Nature* (2009) 461(7261):272–6. doi: 10.1038/nature08250
11. Xu DL, Tian HL, Cai WL, Zheng J, Gao M, Zhang MX, et al. Novel 6-Bp Deletion in MEF2A Linked to Premature Coronary Artery Disease in a Large Chinese Family. *Mol Med Rep* (2016) 14(1):649–54. doi: 10.3892/mmr.2016.5297
12. Do R, Stitziel NO, Won HH, Jørgensen AB, Duga S, Merlini PA, et al. Exome Sequencing Identifies Rare LDLR and APOA5 Alleles Conferring Risk for Myocardial Infarction. *Nature* (2015) 518(7537):102–6. doi: 10.1038/nature13917
13. Xie X, Zheng YY, Adi D, Yang YN, Ma YT, Li XM, et al. Exome Sequencing in a Family Identifies RECQL5 Mutation Resulting in Early Myocardial Infarction. *Med (Baltimore)* (2016) 95(5):e2737. doi: 10.1097/MD.0000000000002737
14. Crosby J, Peloso GM, Auer PL, Crosslin DR, Stitziel NO, Lange LA, et al. Loss-of-Function Mutations in APOC3, Triglycerides, and Coronary Disease. *N Engl J Med* (2014) 371(1):22–31. doi: 10.1056/NEJMoa1307095
15. InanlooRahatloo K, Parsa AFZ, Huse K, Rasooli P, Davaran S, Platzer M, et al. Mutation in ST6GALNAC5 Identified in Family With Coronary Artery Disease. *Sci Rep* (2014) 4:3595–602. doi: 10.1038/srep03595
16. Chang LF, Zhang ZG, Yang J, McLaughlin SH, Barford D. Molecular Architecture and Mechanism of the Anaphase-Promoting Complex. *Nature* (2014) 513(7518):388–93. doi: 10.1038/nature13543

17. Pawar SA, Sarkar TR, Balamurugan K, Sharan S, Wang J, Zhang Y, et al. C/Ebpδ Targets Cyclin D1 for Proteasome-Mediated Degradation *via* Induction of CDC27/APC3 Expression. *Proc Natl Acad Sci USA* (2010) 107(20):9210–5. doi: 10.1073/pnas.0913813107
18. Qi F, Li Y, Yang X, Wu Y, Lin L, Liu X. Hsa_Circ_0044226 Knockdown Attenuates Progression of Pulmonary Fibrosis by Inhibiting CDC27. *Aging (Albany NY)* (2020) 12(14):14808–18. doi: 10.18632/aging.103543
19. Qiu L, Wu J, Pan C, Tan X, Lin J, Liu R, et al. Downregulation of CDC27 Inhibits the Proliferation of Colorectal Cancer Cells *via* the Accumulation of p21Cip1/Waf1. *Cell Death Dis* (2016) 7(1):e2074. doi: 10.1038/cddis.2015.402
20. Talvinen K, Karra H, Pitkänen R, Ahonen I, Nykänen M, Lintunen M, et al. Low Cdc27 and High Securin Expression Predict Short Survival for Breast Cancer Patients. *APMIS* (2013) 121(10):945–53. doi: 10.1111/apm.12110
21. Moulton VR. Sex Hormones in Acquired Immunity and Autoimmune Disease. *Front Immunol* (2018) 9:2279. doi: 10.3389/fimmu.2018.02279
22. Strickland FM, Hewagama A, Lu Q, Wu A, Hinderer R, Webb R, et al. Environmental Exposure, Estrogen and Two X Chromosomes are Required for Disease Development in an Epigenetic Model of Lupus. *J Autoimmun* (2012) 38(2–3):J135–43. doi: 10.1016/j.jaut.2011.11.001
23. Grimaldi CM, Cleary J, Dagtas AS, Moussai D, Diamond B. Estrogen Alters Thresholds for B Cell Apoptosis and Activation. *J Clin Invest* (2002) 109 (12):1625–33. doi: 10.1172/JCI14873
24. Buyon JP, Petri MA, Kim MY, Kalunian KC, Grossman J, Hahn BH, et al. The Effect of Combined Estrogen and Progesterone Hormone Replacement Therapy on Disease Activity in Systemic Lupus Erythematosus: A Randomized Trial. *Ann Intern Med* (2005) 142:953–62. doi: 10.7326/0003-4819-142-12_part_1-200506210-00004
25. Chang DM, Lan JL, Lin HY, Luo SF. Dehydroepiandrosterone Treatment of Women With Mild-Tomoderate Systemic Lupus Erythematosus: A Multicenter Randomized, Double-Blind, Placebocontrolled Trial. *Arthritis Rheum* (2002) 46(11):2924–7. doi: 10.1002/art.10615
26. McMurray RW, May W. Sex Hormones and Systemic Lupus Erythematosus: Review and Meta-Analysis. *Arthritis Rheum* (2003) 48(8):2100–10. doi: 10.1002/art.11105
27. Vera-Lastra O, Jara LJ, Espinoza LR. Prolactin and Autoimmunity. *Autoimmun Rev* (2002) 1(6):360–4. doi: 10.1016/s1568-9972(02)00081-2
28. Zhang SQ, Jiang T, Li M, Zhang X, Ren YQ, Wei SC, et al. Exome Sequencing Identifies MVK Mutations in Disseminated Superficial Actinic Porokeratosis. *Nat Genet* (2012) 44:1156–60. doi: 10.1038/ng.2409
29. Hu H, Roach JC, Coon H, Guthery SL, Voelkerding KV, Margraf RL, et al. A Unified Test of Linkage Analysis and Rare-Variant Association for Analysis of Pedigree Sequence Data. *Nat Biotechnol* (2014) 32(7):663–9. doi: 10.1038/nbt.2895
30. Holtgrewe M, Schubach M, Siragusa E, Zemojtel T, Buske OJ, Washington NL, et al. Next-Generation Diagnostics and Disease-Gene Discovery With the Exomiser. *Nat Protoc* (2015) 10(12):2004–15. doi: 10.1038/nprot.2015.124
31. Choi S, Lee S, Cichon S, Nöthen MM, Lange C, Park T, et al. FARVAT: A Family-Based Rare Variant Association Test. *Bioinformatics* (2014) 30 (22):3197–205. doi: 10.1093/bioinformatics/btu496
32. Tezcan G, Aksoy SA, Tunca B, Bekar A, Mutlu M, Cecener G, et al. Oleuropein Modulates Glio-Blastoma Mirna Pattern Different From Olea Europaea Leaf Extract. *Hum Exp Toxicol* (2019) 38(9):1102–10. doi: 10.1177/0960327119855123
33. Bombardier C, Gladman DD, Urowitz MB, Caron D, Chang CH. Derivation of the SLEDAI. A Disease Activity Index for Lupus Patients. The Committee on Prognosis Studies in SLE. *Arthritis Rheum* (1992) 35(6):630–40. doi: 10.1002/art.1780350606
34. Schafer PH, Ye Y, Wu L, Kosek J, Ringheim G, Yang Z, et al. Cereblon Modulator Iberdomide Induces Degradation of the Transcription Factors Ikaros and Aiolos: Immunomodulation in Healthy Volunteers and Relevance to Systemic Lupus Erythematosus. *Ann Rheum Dis* (2018) 77(10):1516–23. doi: 10.1136/annrheumdis-2017-212916
35. Almlöf JC, Nystedt S, Leonard D, Eloranta ML, Grosso G, Sjöwall C, et al. Whole-Genome Sequencing Identifies Complex Contributions to Genetic Risk by Variants in Genes Causing Monogenic Systemic Lupus Erythematosus. *Hum Genet* (2019) 138(2):141–50. doi: 10.1007/s00439-018-01966-7
36. Zhang X, Li M, Zhang XJ. Exome Sequencing and its Application. *HEREDITAS (Beijing)* (2011) 33(8):847–56. doi: 10.3724/SP.J.1005.2011.00847
37. Vinkhuyzen AA, Wray NR, Yang J, Goddard ME, Visscher PM. Estimation and Partition of Heritability in Human Populations Using Whole-Genome Analysis Methods. *Annu Rev Genet* (2013) 47:75–9. doi: 10.1146/annurev-genet-111212-133258
38. Kim C, Chang HJ, Cho I, Sung JM, Choi D, Jeong MH, et al. Impact of Family History on the Presentation and Clinical Outcomes of Coronary Heart Disease: Data From the Korea Acute Myocardial Infarction Registry. *Korean J Intern Med* (2013) 28(5):547–56. doi: 10.3904/kjim.2013.28.5.547
39. Wu RR, Myers RA, Hauser ER, Vorderstrasse A, Cho A, Ginsburg GS, et al. Impact of Genetic Testing and Family Health History Based Risk Counseling on Behavior Change and Cognitive Precursors for Type 2 Diabetes. *J Genet Couns* (2017) 26(1):133–40. doi: 10.1007/s10897-016-9988-z
40. Rutishauser J, Spiess M, Kopp P. Genetic Forms of Neurohypophyseal Diabetes Insipidus. *Best Pract Res Clin Endocrinol Metab* (2016) 30(2):249–62. doi: 10.1016/j.beem.2016.02.008
41. Wang Y, Chen S, Chen J, Xie X, Gao S, Zhang C, et al. Germline Genetic Patterns Underlying Familial Rheumatoid Arthritis, Systemic Lupus Erythematosus and Primary Sjögren's Syndrome Highlight T Cell-Initiated Autoimmunity. *Ann Rheum Dis* (2020) 79(2):268–75. doi: 10.1136/annrheumdis-2019-215533
42. Nath SK, Kelly JA, Namjou B, Lam T, Bruner GR, Scofield RH, et al. Evidence for a Susceptibility Gene, SLEV1, on Chromosome 17p13 in Families With Vitiligo-Related Systemic Lupus Erythematosus. *Am J Hum Genet* (2001) 69 (6):1401–6. doi: 10.1086/324470
43. Laird NM, Lange C. Family-Based Methods for Linkage and Association Analysis. *Adv Genet* (2008) 60:219–52. doi: 10.1016/S0065-2660(07)00410-5
44. Kazemi-Sefat GE, Keramatipour M, Talebi S, Kavousi K, Sajed R, Kazemi-Sefat NA, et al. The Importance of CDC27 in Cancer: Molecular Pathology and Clinical Aspects. *Cancer Cell Int* (2021) 21(1):160–70. doi: 10.1186/s12935-021-01860-9
45. Morgan DO. Regulation of the APC and the Exit From Mitosis. *Nat Cell Biol* (1999) 1(2):47–53. doi: 10.1038/10039
46. Zhang L, Fujita T, Wu G, Xiao X, Wan Y. Phosphorylation of the Anaphase-Promoting Complex/Cdc27 Is Involved in TGF-Beta Signaling. *J Biol Chem* (2011) 286(12):10041–50. doi: 10.1074/jbc.M110.205518
47. Shi Y, Massagué J. Mechanisms of TGF-β Signaling From Cell Membrane to the Nucleus. *Cell* (2003) 113(6):685–700. doi: 10.1016/s0092-8674(03)00432-x
48. Pang B, Zhen Y, Hu C, Ma Z, Lin S, Yi H. Myeloid-Derived Suppressor Cells Shift Th17/Treg Ratio and Promote Systemic Lupus Erythematosus Progression Through Arginase-1/Mir-322-5p/TGF-β Pathway. *Clin Sci* (2020) 134(16):2209–22. doi: 10.1042/CS20200799
49. Vanarsa K, Soomro S, Zhang T, Strachan B, Pedroza C, Nidhi M, et al. Quantitative Planar Array Screen of 1000 Proteins Uncovers Novel Urinary Protein Biomarkers of Lupus Nephritis. *Ann Rheum Dis* (2020) 79(10):1349–61. doi: 10.1136/annrheumdis-2019-216312
50. Yung S, Chan TM. Mechanisms of Kidney Injury in Lupus Nephri- Tis – the Role of Anti-Ds DNA Antibodies. *Front Immunol* (2015) 6:475. doi: 10.3389/fimmu.2015.00475
51. Li S, Zhang J, Tan X, Deng J, Li Y, Piao Y, et al. Microarray Expression Profile of Cir-Cular RNas and MRNas in Children With Systemic Lupus Erythema-Tosus. *Clin Rheumatol* (2019) 38(5):1339-. doi: 10.1007/s10067-018-4392-8

Conflict of Interest: Author LC was employed by Beijing Mygenostics co., LTD and author MZ was employed by Geneis (Beijing) Co., Ltd., Beijing, China.

The remaining authors declare that the research was conducted in the absence of any commercial or financial relationships that could be construed as a potential conflict of interest.

Publisher's Note: All claims expressed in this article are solely those of the authors and do not necessarily represent those of their affiliated organizations, or those of the publisher, the editors and the reviewers. Any product that may be evaluated in this article, or claim that may be made by its manufacturer, is not guaranteed or endorsed by the publisher.

frontiers | Frontiers in Immunology

ORIGINAL RESEARCH
published: 06 May 2022
doi: 10.3389/fimmu.2022.865425

Proteome Profiling Identifies Serum Biomarkers in Rheumatoid Arthritis

Congqi Hu[1†], Zhao Dai[2†], Jia Xu[2], Lianyu Zhao[2], Yanping Xu[3], Meilin Li[2], Jiahui Yu[2], Lu Zhang[2], Hui Deng[2], Lijuan Liu[1], Mingying Zhang[1], Jiarong Huang[4], Linping Wu[4] and Guangxing Chen[1,3*]*

[1] Department of Rheumatology, First Affiliated Hospital of Guangzhou University of Chinese Medicine, Guangzhou, China, [2] First Clinical Medical School, Guangzhou University of Chinese Medicine, Guangzhou, China, [3] Baiyun Hospital of the First Affiliated Hospital of Guangzhou University of Chinese Medicine, Guangzhou, China, [4] Center for Chemical Biology and Drug Discovery, Guangzhou Institute of Biomedicine and Health, Chinese Academy of Sciences (CAS), Guangzhou, China

OPEN ACCESS

Edited by:
Qinglong Wu,
Baylor College of Medicine,
United States

Reviewed by:
Jinxin Liu,
Nanjing Agricultural University, China
Dong Lu,
Baylor College of Medicine,
United States
Hee-Gyoo Kang,
Eulji University, South Korea

***Correspondence:**
Linping Wu
wu_linping@gibh.ac.cn
Guangxing Chen
cgx02@gzucm.edu.cn

[†]These authors have contributed equally to this work

Specialty section:
This article was submitted to Autoimmune and Autoinflammatory Disorders, a section of the journal Frontiers in Immunology

Received: 29 January 2022
Accepted: 30 March 2022
Published: 06 May 2022

Citation:
Hu C, Dai Z, Xu J, Zhao L, Xu Y, Li M, Yu J, Zhang L, Deng H, Liu L, Zhang M, Huang J, Wu L and Chen G (2022) Proteome Profiling Identifies Serum Biomarkers in Rheumatoid Arthritis. Front. Immunol. 13:865425. doi: 10.3389/fimmu.2022.865425

Rheumatoid arthritis (RA) causes serious disability and productivity loss, and there is an urgent need for appropriate biomarkers for diagnosis, treatment assessment, and prognosis evaluation. To identify serum markers of RA, we performed mass spectrometry (MS)-based proteomics, and we obtained 24 important markers in normal and RA patient samples using a random forest machine learning model and 11 protein–protein interaction (PPI) network topological analysis methods. Markers were reanalyzed using additional proteomics datasets, immune infiltration status, tissue specificity, subcellular localization, correlation analysis with disease activity-based diagnostic indications, and diagnostic receiver-operating characteristic analysis. We discovered that ORM1 in serum is significantly differentially expressed in normal and RA patient samples, which is positively correlated with disease activity, and is closely related to CD56dim natural killer cell, effector memory CD8$^+$T cell, and natural killer cell in the pathological mechanism, which can be better utilized for future research on RA. This study supplies a comprehensive strategy for discovering potential serum biomarkers of RA and provides a different perspective for comprehending the pathological mechanism of RA, identifying potential therapeutic targets, and disease management.

Keywords: rheumatoid arthritis, biomarker, proteomics, ORM1, serum

INTRODUCTION

Rheumatoid arthritis (RA) is an autoimmune disease characterized by chronic erosive arthritis, which affects 1% of the world's population and usually occurs in middle-aged and elderly women (1). The clinical manifestations are symmetrical and persistent polyarticular swelling and pain and can also involve extra-articular tissues, such as skin and mucosal lesions, cardiovascular diseases, and lung diseases, which seriously affect work and daily life (2, 3).

Current common laboratory indicators are rheumatoid factor (RF), anti-cyclic citrullinated peptide antibody (ACPA), erythrocyte sedimentation rate (ESR), and C-reactive protein (CRP) (4). However, the RF-positive rate and ACPA specificity of RA are only 60%–70% and 60%–75%, respectively, suggesting low diagnostic efficacy (5, 6). Furthermore, the RF-positive rate and ACPA specificity are difficult to distinguish between high and low disease activity. ESR or CRP can reflect the inflammatory activity of the disease but is not a characteristic diagnosis of RA (7). The situation largely limits the timely and efficient treatment and analysis of patients, Thus, the diagnosis of the disease can still be much improved. Biomarkers specifically and powerfully related to RA disease have been increasing; it can be helpful especially in patients who are seronegative for RF and ACPA.

It is known that proteins have an important role in RA pathogenesis with the formation of a new epitope; compared with other techniques such as transcription, proteomics can study the posttranscriptional modification of proteins and their interactions in cells and tissues (8). Previous proteomic studies according to quantitative analyses using clinical serum samples between RA patients and healthy controls identified a lot of differentially expressed proteins. Cheng et al. set up protein profiles of serum through high-resolution mass spectrometry using the Orbitrap Q Exactive mass spectrometer and identified 18 overexpressed proteins, among which FCN-2 was found to be elevated in RA and correlated with disease activity (9). Sora et al. using a nano-LC-MS/MS-based proteomics approach speculated that SAA might be a biomarker of AA amyloidosis in rheumatoid arthritis; gelsolin and VDBP might be potent biomarker candidates for the early diagnosis of RA (10). Lee et al. suggested that protein S100-A9 is involved in joint destruction by matrix metalloproteinases and the pro-inflammatory response, showing potential for use as a diagnostic biomarker that reflects the mechanism of inflammation in RA (10). However, these studies only aimed at identifying the protein difference between normal and RA patients, rarely combined with disease activity, and noticed differences in protein expression after drug intervention.

In this study, our comprehensive analysis of serum proteins in RA from multiple perspectives is shown (**Figure 1**). We obtained differential proteins based on serum proteomics by LC-MS/MS, and we referred to the results of other proteomics datasets. Analysis of immune infiltration, tissue and subcellular localization, and the correlation between differential proteins and RA laboratory diagnostic indicators and diagnostic receiver-operating characteristic analysis from the perspective of disease activity were performed. These results provide a worthy reference for future proteomic and multi-angle analysis studies on RA serum protein biomarkers.

METHODS AND MATERIALS

Patients

Human serum specimens were collected from the First Affiliated Hospital of Guangzhou University of Chinese Medicine (Guangzhou, China). The study was approved by the Chinese Clinical Trial Registry (ChiCTR), and the registration number is ChiCTR2100043294. This study was approved by the local research ethics committee; the approval document number of the ethics committee is NO. JY[2020]264. All subjects in this study were asked for consent. Human serum samples included 8 healthy control and 7 patients at different time points of 0 and 6 after administration. All samples were frozen and stored at −80°C in aliquots of polyethylene tubes until use.

Protein Preparation

Bicinchoninic acid (BCA) assay was used for protein quantification, taking 500 μg of protein and using High Select™ Top14 Abundant Protein Depletion Resin to remove high-abundance proteins. After adding the supernatant obtained in the previous step to dithiothreitol (DTT) at a final concentration of 10 mM, polypeptide samples were prepared using the filter-aided sample preparation (FASP) method from previous literatures (11, 12). In brief, proteins were added onto a 30-kDa cutoff filter and centrifuged at 11,000 rpm at 20°C for 15 min. 50 mM iodoacetamide (IAA) in urea buffer was used to alkylate proteins at 20°C for 15 min. After a few washes with urea and 50 mM ABC buffer, 100 ng of trypsin in 50 mM ABC buffer was used to digest proteins in a wet chamber overnight at 37°C. Peptides were extracted with 50 mM ABC buffer and acidified by trifluoroacetic acid (TFA). After the FASP protocol as described above, the peptides were desalted and concentrated using C18 stage tips. Each of these samples was measured in a 1-h gradient of LC-MS/MS.

Protein Quantification and Analysis

Tryptic peptides were separated using a 60-min total data collection for peptide separation, with the Easy-nLC 1200 system connected online to an Orbitrap Eclipse mass spectrometer equipped with FAIMS Pro (Thermo). Scans were collected in data-dependent top-speed mode with dynamic exclusion at 90 s. Raw data were analyzed using MaxQuant version 1.6.17.0 search against the Human Fasta database, with label-free quantification and match-between-run functions enabled. The identification of proteins that were differentially expressed between patients with RA and HCs was conducted based on the empirical Bayes method using the limma R package. The *p*-values were obtained by using the t-test, and the *p*-values of comparisons were adjusted for multiple comparisons to preserve an error rate of 5%. To identify the significant pair(s), we used multiple comparisons. The Benjamini–Hochberg method was used for the multiple comparisons.

Identification of Differentially Expressed Proteins

Key Protein Screening

Machine learning was combined with PPI network analysis to screen differential proteins. The random forest classifier (RFC) was used to perform feature extraction on protein sample expression data, screen out the top 30 key proteins based on classification features, and use MeanDecreaseGini to plot. 11 topological analysis methods, including Degree, Edge Percolated Component (EPC), Maximum Neighborhood Component

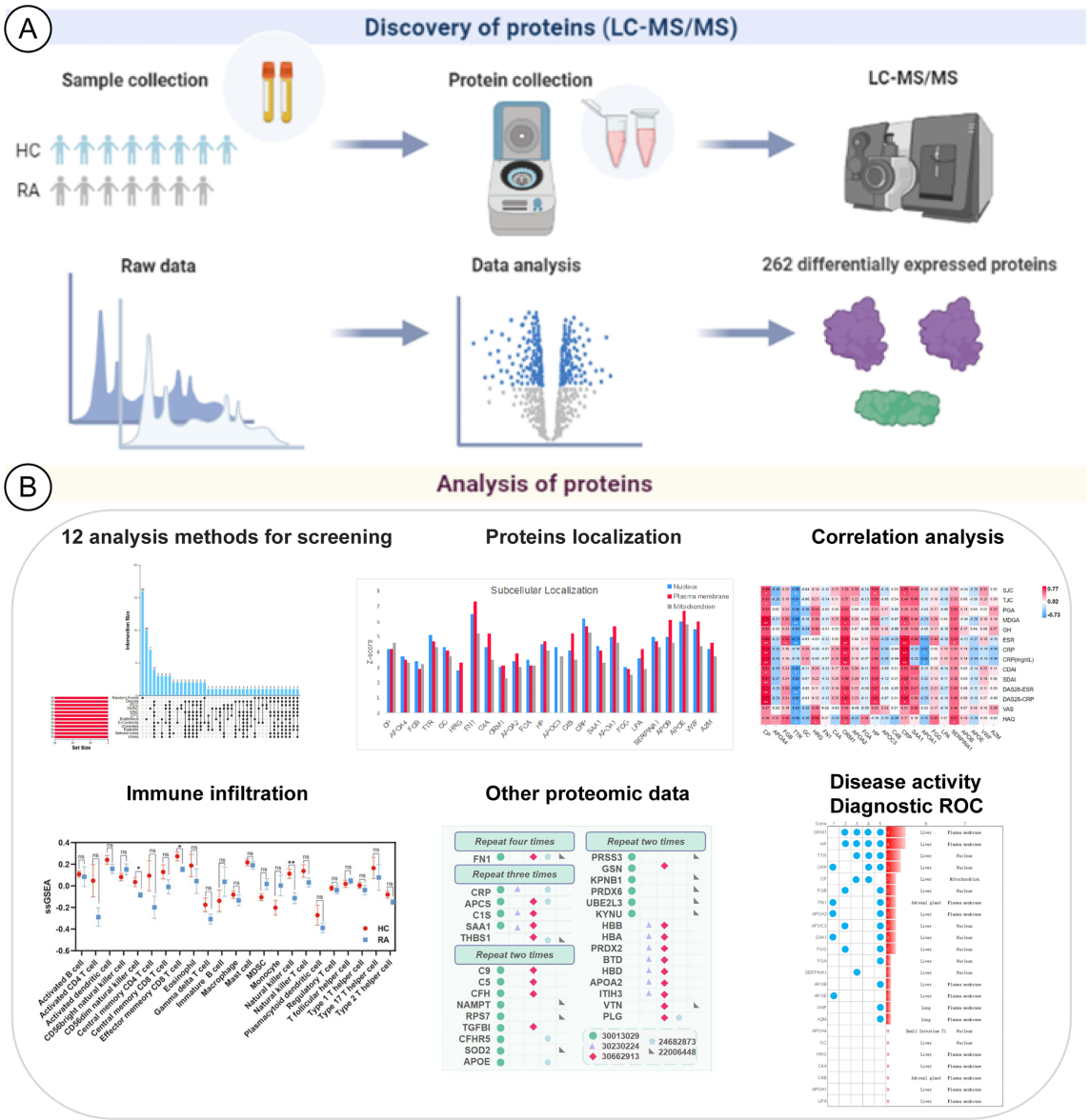

FIGURE 1 | Schematic diagram about the analysis of RA potential proteins based on LC-MS proteomics. **(A)** Identification of differentially expressed proteins. **(B)** Multiple-analysis methods to assess the importance of differentially expressed proteins.

(MNC), Density of Maximum Neighborhood Component (DMNC), Maximal Clique Centrality (MCC), and six centralities (Bottleneck, EcCentricity, Closeness, Radiality, Betweenness, and Stress) based on shortest paths were used to measure the true efficiency of nodes in the PPI network to evaluate their importance.

Enrichment Analysis

R (version 3.6.3)'s ggplot2 package and clusterProfiler package were used to analyze the enrichment analysis of 24 differential proteins, including KEGG pathway, biological process (BP), cell component (CC), and molecular function (MF).

Compilation of Other Proteomic Datasets

"rheumatoid arthritis" and "proteomics" were used as keywords, PubMed (https://pubmed.ncbi.nlm.nih.gov/) was used to search, and clinical samples with healthy people were selected as the control group. A total of 5 datasets were collected, including 155 healthy controls and 183 RA patients. The differentially expressed proteins were summarized in each dataset, and candidate proteins with the

number of repetitions greater than 2 were selected. An NCBI gene ID was assigned to each protein based on gene symbol, and we kept proteins with the NCBI gene IDs for subsequent analysis.

Multi-Angle Analysis of Differentially Expressed Proteins

Immune Infiltration

The R (version 3.6.3) ssGSEA method was used for immune cell infiltration analysis, the degree of infiltration of 28 immune cells was calculated, and $p < 0.05$ was considered statistically significant. The following 28 types of immune cells were obtained: activated B cells, activated $CD4^+$T cells, activated $CD8^+$T cells, activated dendritic cells, CD56bright natural killer cells, CD56dim natural killer cells, central memory $CD4^+$T cells, central memory $CD8^+$T cells, effector memory $CD4^+$T cells, effector memory $CD8^+$T cells, eosinophils, follicular helper T cells, gamma delta T cells, immature B cells, immature dendritic cells, macrophages, mast cells, memory B cells, monocytes, myeloid-derived suppressor cells, natural killer cells, natural killer T cells, neutrophils, plasmacytoid dendritic cells, regulatory T cells, type 1 T helper cells, type 17 T helper cells, and type 2 T helper cells. We used the Spearman correlation analysis method to compare the obtained immune cells and correlation analysis of key proteins to further discover RA disease proteins closely related to immune infiltration.

Tissue Specificity and Subcellular Localization

Tissue specificity data were obtained from GTEx (https://gtexportal.org/). GTEx is a tissue-specific database of gene expression and regulation derived from simultaneous transcriptome sequencing and genetic analysis of samples from multiple human tissues and organs.

Subcellular localization was performed through COMPARTMENTS (https://compartments.jensenlab.org/). COMPARTMENTS is a powerful website for predicting the subcellular localization of proteins, helping us to better understand candidate proteins.

Analyze Differential Proteins in Combination With Disease Activity

Diagnostic Correlation Analysis

R (version 3.6.3) was used for statistical analysis and visualization, the ggplot2 package (version 3.3.3) was used for visualization, and the statistical method used was Spearman. A heatmap was used to display the pairwise correlation (spearman correlation) of all elements between the two tables (protein expression table and diagnostic index change table). Statistical significance was marked on the heatmap.

Diagnostic ROC Analysis

We used the pROC package for diagnostic ROC analysis and used the ggplot2 package for visualization. The value of the area under the curve (AUC) is between 0.5 and 1. The closer the AUC is to 1, the better the diagnostic effect. The AUC has a low accuracy when it is 0.5–0.7, it has a certain accuracy when it is 0.7–0.9, and it has a high accuracy when it is above 0.9; key proteins were further screened based on an AUC greater than 0.7.

Statistical Analysis and Network Visualization

The statistical analysis in this study was performed by the differential enrichment test of R platforms (version3.6.3, http://www.r-project.org/). Data visualization was generated by the clusterProfiler package (version3.14.3) of R and Microsoft Office 2019.

RESULTS

Identification of Proteins by LC-MS/MS

Raw counts of proteomics data and corresponding clinical information from healthy control and RA patients were obtained from the First Affiliated Hospital of Guangzhou University of Chinese Medicine (Guangzhou, China). The differential enrichment test of R software was used to study the differential expression of proteins. Test-diff was used to perform a differential enrichment test based on protein-wise linear models and empirical Bayes statistics using limma. False discovery rates were estimated using the fdrtool package (version 1.2.17). p-value < 0.05 was defined as the threshold for the screening of differential expression. A total of 2,051 proteins and peptides were identified by LC-MS/MS. There were a total of 262 candidate proteins that are statistically significant between healthy control cases and RA patients, and a total of 93 candidate proteins during the active and inactive phases of the disease.

Identify Candidates Proteins for RA

Key Protein Screening

Analyzing 262 candidate proteins, according to the RFC machine learning method and 11 topological analysis methods (**Figure 2A**), the top 30 key proteins under each method are obtained. Proteins present in more than 8 of the 12 analytical methods were defined as key proteins for follow-up research, and 24 proteins obtained were CP, APOA4, FGB, TTR, GC, HRG, FN1, C4A, ORM1, APOA2, FGA, HP, APOC3, C4B, CRP, SAA1, APOA1, FGG, LPA, SERPINA1, APOB, APOE, VWF, and A2M.

Enrichment Analysis

To further confirm the underlying function of potential targets, we use Fisher's exact test to calculate the enrichment significance of each term in KEGG, biological process (BP), cell composition (CC), and molecular function (MF) and arrange them in ascending order of p-value. **Figure 2B** visually displays the relationship between the proteins and KEGG, BP, CC, and MF.

24 proteins overlapping the reference datasets were analyzed. The first 3 KEGG pathways with the smallest p-value were "Complement and coagulation cascades (TermID: hsa04610, p-value<0.001); Cholesterol metabolism (TermID: hsa04979, p-value<0.001); Vitamin digestion and absorption (TermID: hsa04977, p-value<0.001)." The first 3 BPs with the smallest p-value were extracellular structure organization "(TermID: GO:0043062,

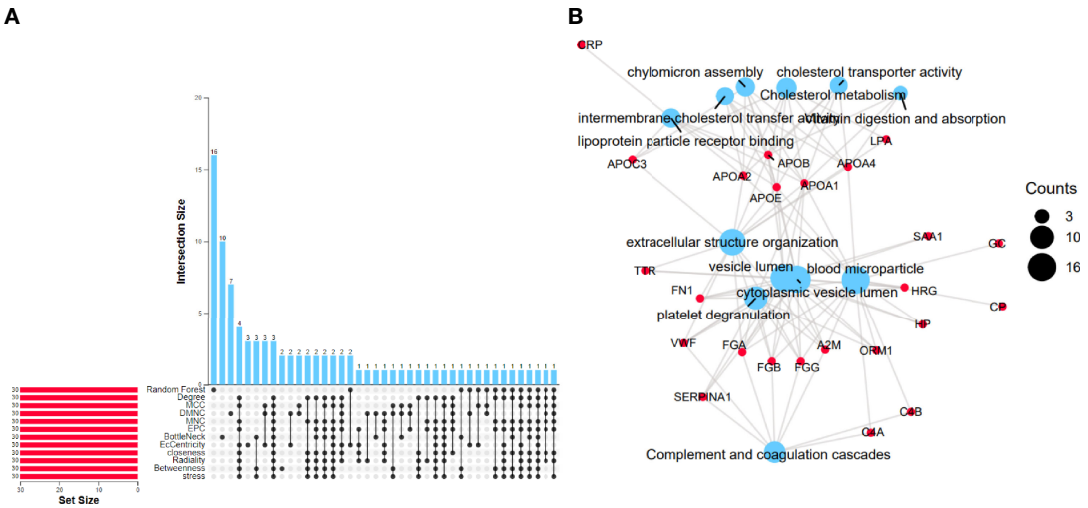

FIGURE 2 | Identification of differentially expressed proteins. **(A)** Random forest machine learning method combined with the PPI network importance analysis algorithm to screen differential proteins. **(B)** Enrichment results of 24 differential proteins. The blue size represents the number of counts corresponding to the result.

p-value<0.001); platelet degranulation (TermID: GO:0002576, *p*-value<0.001); chylomicron assembly (TermID: GO:0034378, *p*-value<0.001)." The first 3 CCs with the smallest p-value were "blood microparticle (TermID: GO:0072562, *p*-value<0.001); cytoplasmic vesicle lumen (TermID: GO:0060205, *p*-value<0.001); vesicle lumen (TermID: GO:0031983, *p*-value<0.001)." The first 3 MFs with the smallest p-value were "lipoprotein particle receptor binding (TermID: GO:0070325, *p*-value<0.001); cholesterol transporter activity (TermID: GO:0017127, *p*-value<0.001); intermembrane cholesterol transfer activity (TermID: GO:0120020, *p*-value<0.001)".

Identify Proteins from Other Proteomics Datasets

In order to systematically investigate the biomarkers related to the pathogenesis of RA, we conducted a comprehensive analysis of 5 independent RA proteomic datasets. These datasets cover 5 ultra-deep reference datasets from FLS and serum. The five in-depth reference datasets were as shown in **Table 1**. We collected

TABLE 1 | Literature summary of differential proteins.

Official Full Name	Symbol	Total articles	RA related articles	PMID	Level Change
Orosomucoid 1	**ORM1**	3,701	5	26915672	Up
Haptoglobin	**HP**	96,237	996	4029960	Up
Transthyretin	**TTR**	13,127	61	30308029	Down
C-Reactive Protein	**CRP**	108,764	6,602	33385862	Up
Ceruloplasmin	**CP**	139,242	649	26001728	Up
Fibrinogen Beta Chain	**FGB**	1,920	15	26059223	Up
Fibronectin 1	**FN1**	25,482	14	34764682	Down
Apolipoprotein A2	**APOA2**	3,263	3	12027302	Down
Apolipoprotein C3	**APOC3**	1,230	2	31966382	Down
Serum Amyloid A1	**SAA1**	986	52	17985847	Up
Fibrinogen Gamma Chain	**FGG**	2,003	11	32408093	Up
Fibrinogen Alpha Chain	**FGA**	3,606	10	22267327	Up
Serpin Family A Member 1	**SERPINA1**	909	9	34712268	Up
Apolipoprotein B	**APOB**	20,164	93	29997113	Down
Apolipoprotein E	**APOE**	33,596	53	32253242	Up
Von Willebrand Factor	**VWF**	24,468	129	25973092	Up
Alpha-2-Macroglobulin	**A2M**	5,871	113	10343526	Up
Apolipoprotein A4	**APOA4**	1,212	1	2547867	Up
GC Vitamin D Binding Protein	**GC**	158,417	727	3874814	Down
Histidine Rich Glycoprotein	**HRG**	1,662	6	29246875	Up
Complement C4A	**C4A**	1,813	44	22076784	Down
Complement C4B	**C4B**	3,242	79	22076784	Up
Apolipoprotein A1	**APOA1**	15,810	60	31694752	Down
Lipoprotein A	**LPA**	16,481	114	19369465	Up

450 DEPs from 183 RA patients and 155 healthy control cases and established a relatively comprehensive RA proteomic dataset.

The DEPs of 5 reference datasets were statistically sorted, and the number of overlaps greater than 2 was used as the screening condition; 30 proteins were obtained as potential biomarker proteins. We used the upset diagram (**Figure 3A**) to visually show the overlap of each dataset. **Figure 3B** shows the 30 overlapping proteins and their respective datasets.

To further confirm the underlying function of potential targets, we used Fisher's exact test to calculate the enrichment significance of each term in KEGG, biological process (BP), cell composition (CC), and molecular function (MF) and arrange them in ascending order of *p*-value. The bar chart in **Figures 3C, D** visually displays Log10 (*p*-adjust), and **Figure 3C, D** visually display the relationship between the proteins and KEGG, BP, CC, and MF.

The 30 proteins overlapping the reference datasets were analyzed. The first 3 KEGG pathways with the smallest *p*-value were "Complement and coagulation cascades (TermID: hsa04610, *p*-value<0.001); Staphylococcus aureus infection (TermID: hsa05150, *p*-value:0.000); ECM-receptor interaction (TermID: hsa04512, *p*-value:0.001)." The first 3 BPs with the smallest *p*-value were "acute inflammatory response (TermID: GO:0002526, *p*-value<0.001); complement activation (TermID: GO:0006956, *p*-value<0.001); regulation of protein processing (TermID: GO:0070613, *p*-value<0.001)." The first 3 CCs with the smallest p-value were "blood microparticle (TermID: GO:0072562, *p*-value<0.001); cytoplasmic vesicle lumen (TermID: GO:0060205, *p*-value<0.001); vesicle lumen (TermID: GO:0031983, *p*-value<0.001)". The first 3 MF with the smallest p-value were "lipoprotein particle binding (TermID: GO:0071813, *p*-value:0.000); protein-lipid complex binding

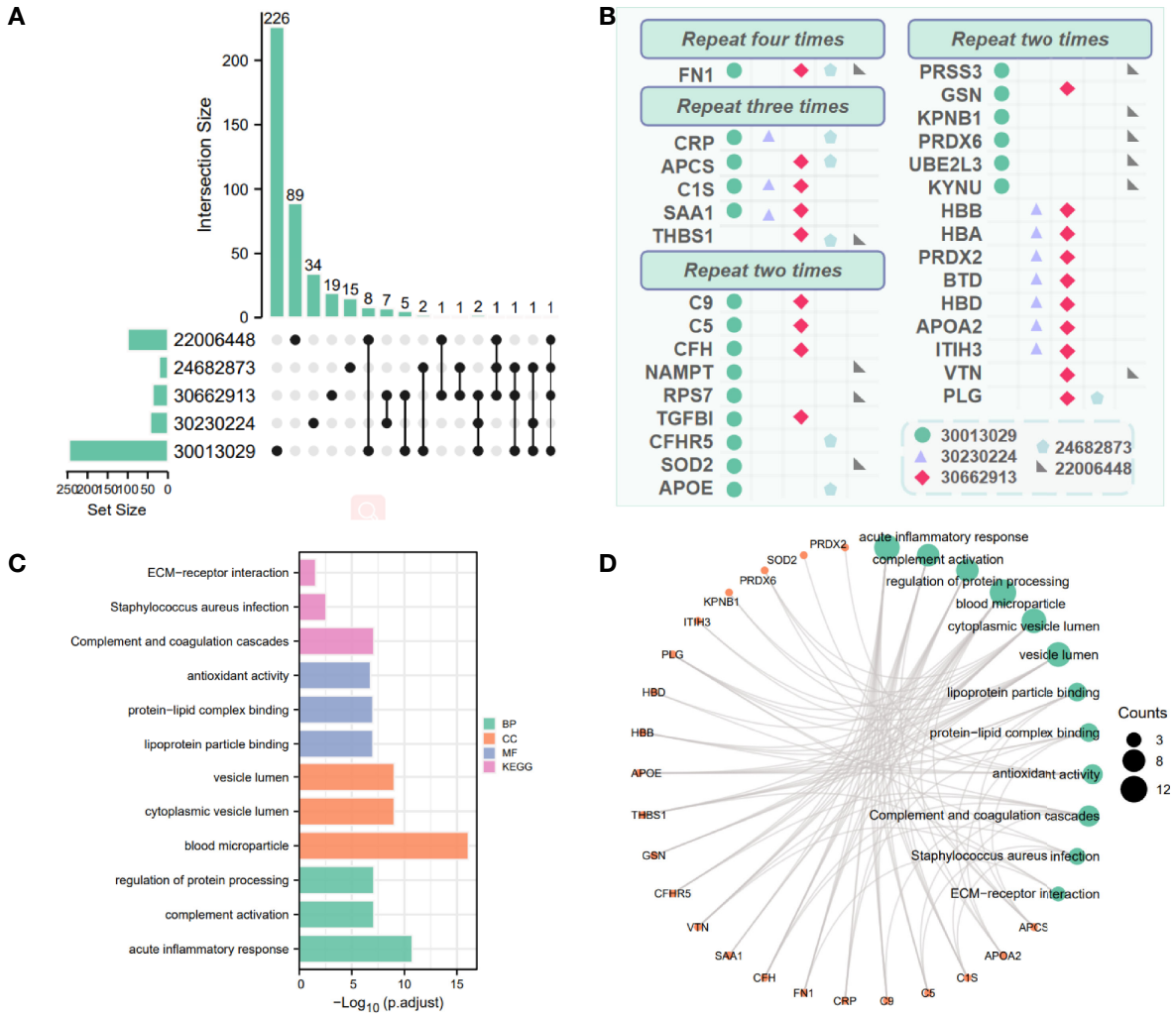

FIGURE 3 | Combine other proteomics datasets to analyze differential proteins. **(A)** Crossover situation in 5 proteomics datasets. **(B)** Visually display differential proteins co-expressed (greater than 2) in multiple proteomics datasets. Different shapes and colors represent different datasets. **(C, D)** Enrichment results of 30 differential proteins in 5 proteomics datasets. The green size represents the number of counts corresponding to the result.

(TermID: GO:0071814, *p*-value:0.000); antioxidant activity (TermID: GO:0016209, *p*-value:0.000)".

Multi-Angle Analysis of Candidate Proteins

Immune Infiltration

We found that the degree of immune cell infiltration in RA patients is generally lower than that in normal people. We analyzed 28 types of immune cells and obtained data on 23 types of immune cells, which are activated B cell, activated $CD4^+$T cell, activated dendritic cell, CD56bright natural killer cell, CD56dim natural killer cell, central memory $CD4^+$T cell, central memory $CD8^+$T cell, effector memory $CD8^+$T cell, eosinophil, gamma delta T cell, immature B cell, macrophage, mast cell, myeloid-derived suppressor cell, monocyte, natural killer cell, natural killer T cell, plasmacytoid dendritic cell, regulatory T cell, follicular helper cell, type 1 T helper cell, type 17 T helper cell, and type 2 T helper cell. As shown in **Figure 4A**, among 23 immune cells, the degree of immune infiltration of CD56dim natural killer cell, effector memory $CD8^+$T cell, and natural killer cell was significantly different between HC and RA ($p < 0.05$, $p < 0.05$, $p < 0.01$). Through Spearman correlation analysis, we found that 13 of the 24 differential genes were significantly related to the degree of immune cell infiltration, which are ORM1, HP, TTR, CRP, FGB, FN1, APOA2, APOC3, SAA1, FGG, FGA, APOB, and VWF; we believe that these 13 genes are potential biomarkers for the treatment of RA and related to immune cell infiltration, as shown in **Figure 4B**.

Tissue Specificity and Subcellular Localization

As shown in **Figure 4C**, we studied the tissue specificity of 24 key proteins and found that 21 differential proteins are abundant in the liver (VWF, A2M, CP, FGB, TTR, GC, HRG, C4A, ORM1, APOA2, FGA, HP, APOC3, CRP, SAA1, APOA1, FGG, LPA, SERPINA1, APOB, APOE), FN1 and C4B are abundant in the adrenal gland, VWF and A2M are abundant in lung tissue, and APOA4 is the most abundant in small intestine T1, and these proteins are in whole blood; skeletal muscle protein abundance was relatively low.

As shown in **Figure 4D**, we have studied the subcellular localization of 24 key proteins. Here we focus on their expression on the nucleus, plasma membrane, and mitochondrion and found that 10 proteins (APOA4, FGB, TTR, GC, FGA, APOC3, CRP, SAA1, FGG, SERPINA1) are contained in the nucleus and 13 proteins (HRG, FN1, C4A, ORM1, APOA2, HP, C4B, APOA1, LPA, APOB, APOE, VWF, A2M) are contained in plasma membranes. CP is more abundant in the mitochondrion.

Analyze Candidate Proteins from Disease Activity

Diagnostic Correlation Analysis

Table 2 shows that changes in diagnostic indicators in patient 13 correlated with disease activity before and after treatment. The judging index of disease activity is DAS28-ESR. It can be seen from **Table 2** that the DAS28-ESR of DAP patients is 5.5, and the DAS28-ESR of DIP after treatment is 2.33 (Wilcoxon test $p<0.001$). After using Spearman correlation analysis between 24 proteins and 13 diagnostic indicators (SJC, TJC, PGA, MDGA, GH, ESR, CRP, CDAI, SDAI, DAS28-ESR, DAS28-CRP, VAS, HAQ), the correlation analysis between CP and 11 diagnostic indicators except CRP and GH was statistically significant, as shown in **Figure 5**. The correlation analysis between CP and 9 diagnostic indicators (CRP, SJC, TJC, CDAI, SDAI, DAS28-ESR, DAS28-CRP, MDGA, ESR) was statistically significant. The correlation analysis between CRP and 7 diagnostic indicators (CRP, SJC, SDAI, DAS28-ESR, DAS28-CRP, MDGA, ESR) was statistically significant. The correlation analysis between ORM1 and 6 diagnostic indicators (CRP, DAS28-ESR, DAS28-CRP, MDGA, ESR, HAQ) was statistically significant. The correlation analysis between HP and 4 diagnostic indicators (SJC, SDAI, DAS28-ESR, DAS28-CRP) was statistically significant. The correlation analysis between SERPINA1 and ESR and HAQ was statistically significant. The correlation analysis between FGB and ESR was statistically significant. The correlation analysis between HRG and HAQ was statistically significant. The correlation analysis between APOA1 and CRP was statistically significant. We chose proteins that were statistically significant in the correlation analysis with more than 3 diagnostic indicators as key proteins. We believe that among the 24 proteins, the five proteins TTR, CP, CRP, ORM1, and HP are more closely related to diagnostic indicators and have the potential to become markers for the diagnosis and treatment of RA.

Diagnostic ROC analysis

In terms of predicting disease activity, CP (AUC=0.837), TTR (AUC=0.776), ORM1 (AUC=0.796), HP (AUC=0.816), SERPINA1 (AUC=0.796). They have a certain accuracy in the diagnosis and prediction of disease activity, but they are not statistically significant compared with other diagnosis results.

Analysis of Differentially Expressed Proteins

As shown in **Figure 6**, we combined other proteomics verification conditions, immune infiltration conditions, disease activity, correlation analysis, and diagnostic ROC analysis to comprehensively analyze the 24 differential proteins. The results show that ORM1 and HP were differentially expressed and diagnosed in the disease activity and inactive phases. An ROC value greater than 0.7 has good diagnostic ability for the analysis of the active and inactive stages of the disease, is significantly related to more diagnostic indicators of RA, and has a good performance in terms of immune infiltration. ORM1 and HP show good distinguishing ability in the diagnosis and treatment of RA.

DISCUSSION

Through diverse-perspective analysis, our study provides novel insights into RA-related proteomics research. Using random forest machine learning methods and analysis of 11 other topological analysis methods, our proteomics data selected 24 potential differential proteins in normal and RA patient samples. When searching the PubMed database for 24 potential proteins,

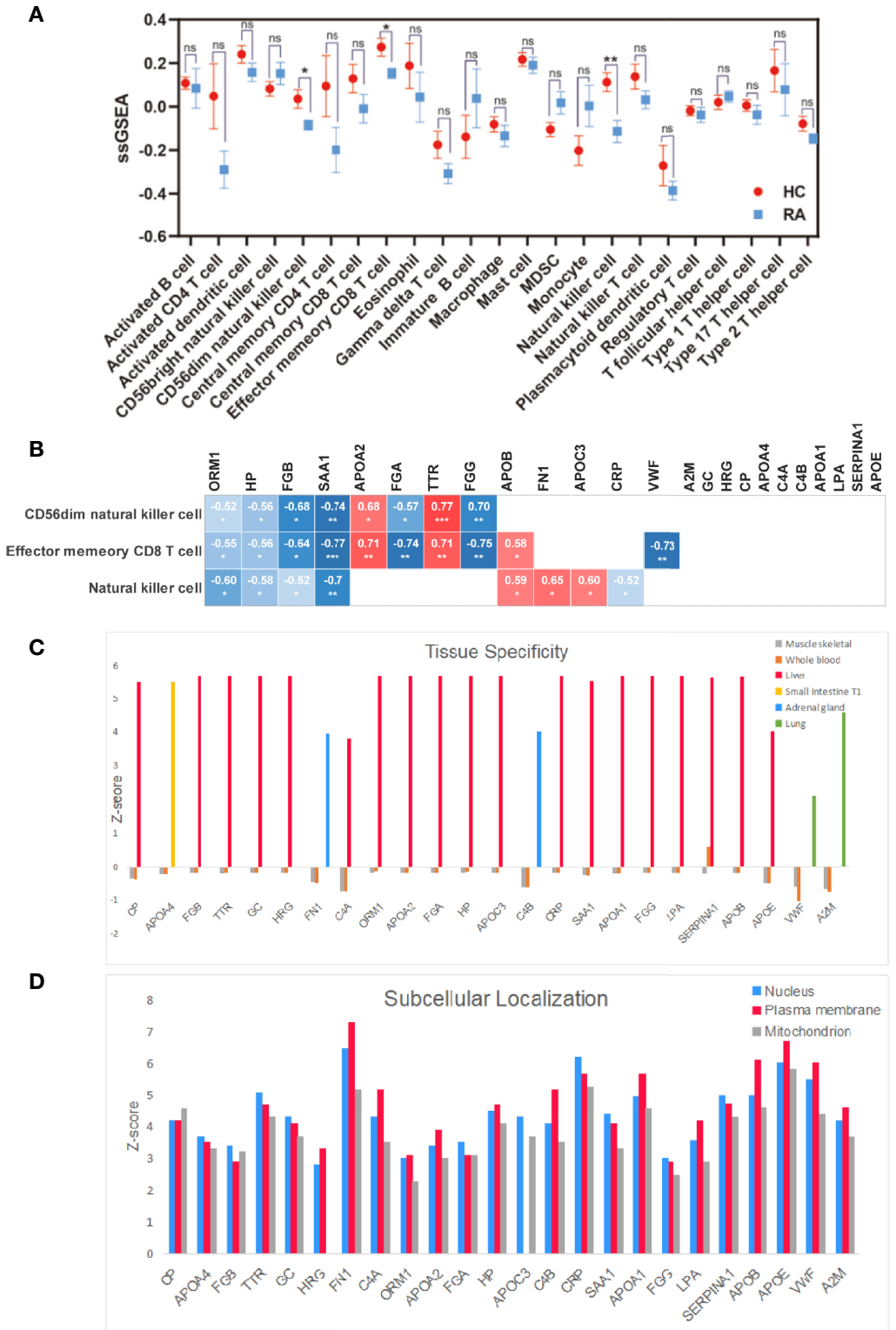

FIGURE 4 | Multi-angle analysis of 24 differentially expressed proteins. **(A)** Immune infiltration analysis protein expression in 23 immune cells in healthy controls and RA patient. **(B)** Correlation analysis of 24 proteins with statistically significant immune cells. **(C)** Tissue specificity of 24 differential proteins. **(D)** Subcellular localization of 24 differential proteins. $^{*}p < 0.05$, $^{**}p < 0.01$, $^{***}p < 0.001$. ns, no significance.

TABLE 2 | Clinical indicator information.

Characteristic	DAP	DIP	*p*	Method
n	7	7		
SJC, n (%)			0.051	Chisq.test
0	0 (0%)	3 (21.4%)		
1	0 (0%)	2 (14.3%)		
3	2 (14.3%)	0 (0%)		
4	2 (14.3%)	0 (0%)		
5	0 (0%)	2 (14.3%)		
7	1 (7.1%)	0 (0%)		
13	1 (7.1%)	0 (0%)		
28	1 (7.1%)	0 (0%)		
TJC, n (%)			0.051	Chisq.test
0	0 (0%)	5 (35.7%)		
1	0 (0%)	1 (7.1%)		
3	0 (0%)	1 (7.1%)		
5	3 (21.4%)	0 (0%)		
6	1 (7.1%)	0 (0%)		
7	1 (7.1%)	0 (0%)		
10	1 (7.1%)	0 (0%)		
28	1 (7.1%)	0 (0%)		
PGA, n (%)			0.051	Chisq.test
0.5	0 (0%)	1 (7.1%)		
1	0 (0%)	3 (21.4%)		
3	0 (0%)	2 (14.3%)		
4	0 (0%)	1 (7.1%)		
5	4 (28.6%)	0 (0%)		
6	1 (7.1%)	0 (0%)		
7	1 (7.1%)	0 (0%)		
9	1 (7.1%)	0 (0%)		
MDGA, n (%)			0.215	Chisq.test
0.5	0 (0%)	1 (7.1%)		
1	0 (0%)	2 (14.3%)		
3	1 (7.1%)	3 (21.4%)		
4	2 (14.3%)	1 (7.1%)		
5	1 (7.1%)	0 (0%)		
6	2 (14.3%)	0 (0%)		
9	1 (7.1%)	0 (0%)		
GH, n (%)			0.101	Chisq.test
5	0 (0%)	1 (7.1%)		
10	0 (0%)	3 (21.4%)		
30	0 (0%)	2 (14.3%)		
40	1 (7.1%)	1 (7.1%)		
50	3 (21.4%)	0 (0%)		
60	1 (7.1%)	0 (0%)		
70	1 (7.1%)	0 (0%)		
90	1 (7.1%)	0 (0%)		
ESR, mean ± SD	46.57 ± 15.87	25.71 ± 12.53	0.018	T test
CRP, median (IQR)	9.32 (6.47, 46.8)	3.53 (2.01, 13.59)	0.097	Wilcoxon
CDAI, median (IQR)	22 (18.5, 28.5)	7 (2.5, 9.5)	0.002	Wilcoxon
SDAI, median (IQR)	22.93 (18.97, 34.95)	7.14 (2.76, 11.36)	0.002	Wilcoxon
DAS28-ESR, median (IQR)	5.5 (5.16, 5.88)	2.33 (2.27, 3.66)	< 0.001	Wilcoxon
DAS28-CRP, mean ± SD	5.16 ± 1.41	2.4 ± 1	0.001	T test
VAS, median (IQR)	5 (4.5, 5.5)	0.5 (0.5, 1.5)	0.004	Wilcoxon
HAQ, median (IQR)	0.5 (0.32, 3.56)	0 (0, 1.13)	0.195	Wilcoxon

According to different data types, different analysis methods are selected.

at least 19 (79.17%) were found in RA-related reports (**Table 3**). Meanwhile, 5 of the 24 differential protein species, including CRP, FN1, APOA2, SAA1, and APOE, have been verified in additional proteomics datasets. Separately, CRP, a diagnostic marker of RA in clinical practice, is significantly elevated in plasma levels in response to infection, inflammatory stimuli, or other tissue damage in the acute phase. Additionally, we found that our DEP list is significantly enriched in the other two DEP lists (**Table 1**) from proteomics in a gene background of 20,462 human protein-coding genes from the NCBI database, for example, dataset iv ($p = 3.25 * 10^{-32}$, Fisher test) and dataset iii ($p = 4.56 * 10^{-31}$, Fisher test). Collectively, we showed the

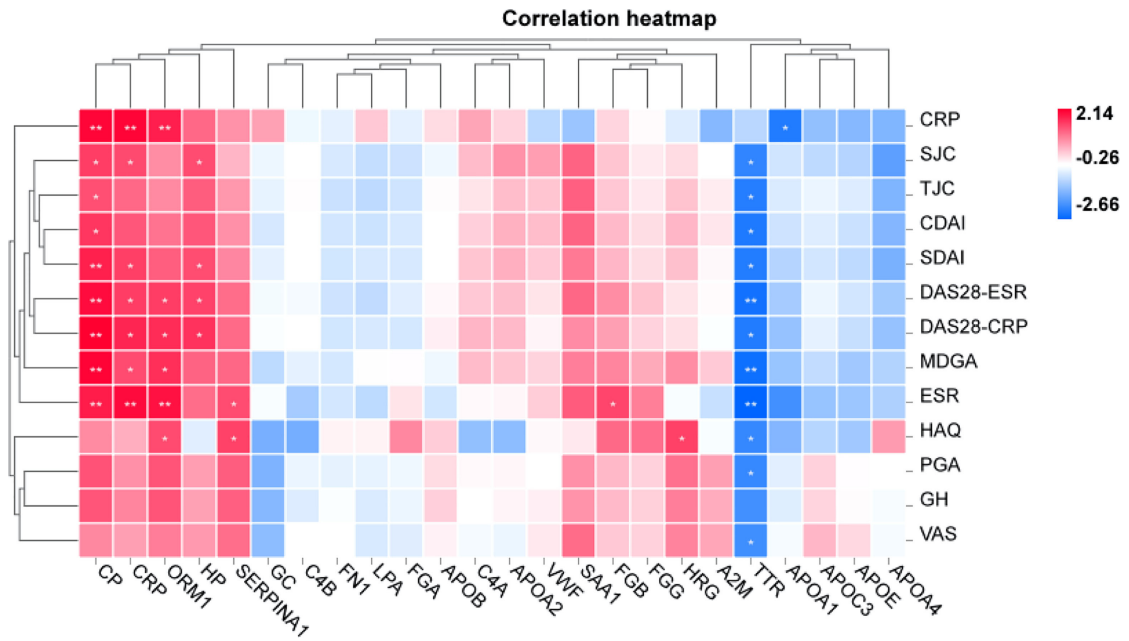

FIGURE 5 | Correlation analysis between RA laboratory diagnostic indicators and disease activity. Positive and negative signs indicate the direction of the correlation. A positive sign indicates a positive correlation (red), and a negative sign indicates a negative correlation (blue). $^{*}p < 0.05$, $^{**}p < 0.01$.

reliability and accuracy of our protein list, and it is in accordance with previous publication. We will upload this information together. The above evidence demonstrates the reliability and accuracy of our analysis.

FN1, a multidomain extracellular matrix (ECM) protein, binds to multiple compounds on the cell surface, including collagen (13), fibrin (14), growth factors (15), and cell surface integrins (16), and prominently participates in several fundamental biological processes, such as tissue repair (17), fibrosis (18), tumorigenesis (2016), cell adhesion (19), cell motility (20), and cell shape maintenance (21). Apolipoprotein A2 (APOA2) is the second most abundant protein of the high-density lipoprotein particles. The related pathway peroxisome proliferator-activated receptor (PPAR)-α regulates metabolism (22). SAA1 (serum amyloid A1) is a major acute-phase protein that is highly expressed in response to inflammation and tissue injury. Studies show that tumor necrosis factor α (TNF-α) and interleukin 1β (IL-1β) induce activation of the IL-6-STAT3 pathway to increase SAA1 expression (23). High levels of this protein are connected with chronic inflammatory diseases including rheumatoid arthritis (24), atherosclerosis (25), and Alzheimer's disease (26). Apolipoprotein E (APOE) is a multifunctional cholesterol carrier that plays a central role in lipid metabolism in the peripheral and central nervous systems. Related pathways include the mTOR signaling pathway (27) and the AMPK signaling pathway (28), which are essential for the normal catabolism of triglyceride-rich lipoprotein components. These results not only verify the accuracy of our experiment but also provide a new direction for the research of RA fundamental research. At the same time, we found that lipid metabolism is closely related to the occurrence and development of RA according to our proteomics research and other proteomics verifications. Lipid levels are dynamic and can fluctuate along with changes in inflammation or as a result of disease-modifying antirheumatic drug (DMARD) therapy, which needs further study.

In addition, our research reevaluated the importance of 24 candidate proteins in terms of immune infiltration, disease activity, experimental diagnosis correlation analysis, and diagnostic ROC analysis. After a comprehensive analysis, both HP and ORM1 exceled in this aspect.

HP has many physiological functions. It can combine with free hemoglobin to prevent oxidative damage to various organs (29) and activate local and systemic levels of innate and adaptive immune cells, as an acute-phase reactant protein; plasma concentration greatly increases during inflammation (30). HP is mainly synthesized in the liver and rarely expressed in other inflamed tissues. It is synthesized at the injured site during acute-phase reactions such as inflammation and tissue damage. There are few reports about HP in RA, and it can be determined that the level in RA synovial fluid and arthritis tissue is related to disease activity (31). Previous studies have shown that serum haptoglobin levels increase during arthritis (32). Studies have shown that locally expressed HP promotes cell migration in cartilage and therefore may play a role in the progression of arthritis (31). Studies have determined that haptoglobin is an important factor in cell migration (33). Haptoglobin knockout cells exhibit impaired migration,

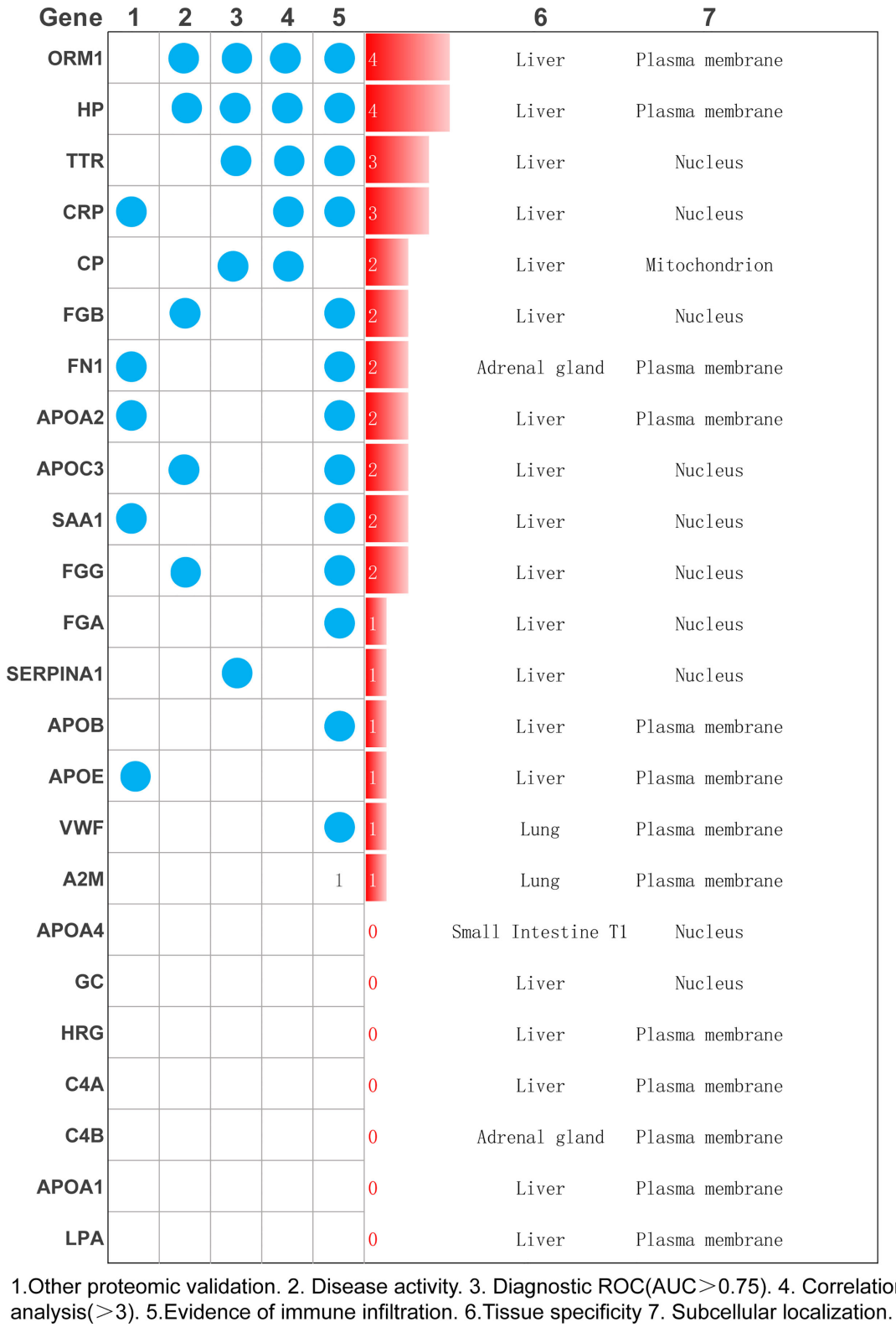

FIGURE 6 | Summarize a variety of analysis methods to select the most meaningful protein as the key protein of RA.

TABLE 3 | Summary of human proteome datasets for biomarker analysis.

Official full name	Symbol	Total articles	RA-related articles	PMID	Level change
Orosomucoid 1	**ORM1**	3,555	1	26915672	Up
Haptoglobin	**HP**	10,621	80	4029960	Up
Transthyretin	**TTR**	10,864	13	30308029	Down
C-reactive protein	**CRP**	91,372	3,271	33385862	Up
Ceruloplasmin	**CP**	9,192	55	26001728	Up
Fibrinogen beta chain	**FGB**	1,453	6	26059223	Up
Fibronectin 1	**FN1**	24,248	2	34764682	Down
Apolipoprotein A2	**APOA2**	3,112	NA	NA	Down
Apolipoprotein C3	**APOC3**	734	NA	NA	Down
Serum amyloid A1	**SAA1**	444	2	17985847	Up
Fibrinogen gamma chain	**FGG**	441	NA	NA	Up
Fibrinogen alpha chain	**FGA**	2,059	NA	NA	Up
Serpin family A member 1	**SERPINA1**	4	2	34712268	Up
Apolipoprotein B	**APOB**	15,507	36	29997113	Down
Apolipoprotein E	**APOE**	27,281	15	32253242	Up
Von Willebrand factor	**VWF**	22,539	43	25973092	Up
Alpha-2-macroglobulin	**A2M**	5,061	43	10343526	Up
Apolipoprotein A4	**APOA4**	1,046	NA	NA	Up
GC vitamin D-binding protein	**GC**	849	1	3874814	Down
Histidine-rich glycoprotein	**HRG**	876	1	29246875	Up
Complement C4A	**C4A**	1,224	3	22076784	Down
Complement C4B	**C4B**	2,889	1	22076784	Up
Apolipoprotein A1	**APOA1**	14,603	15	31694752	Down
Lipoprotein A	**LPA**	9,068	37	19369465	Up

NA, not available.

which can be restored by supplementing the cells with exogenous haptoglobin. Our research once again verified the importance of HP and confirmed that the immunomodulatory effect of HP is related to CD56dim natural killer cells, effector memory $CD8^+$T cells, and natural killer cells.

Orosomucoid 1 (ORM1) is different from HP in that it has less research. When we searched in PubMed, there were only 3,555 related articles (**Table 3**), which is more meaningful and valuable from the perspective of innovation. ORM1 is a key acute-phase plasma protein, which is related to acute inflammation. Its specific function has not yet been determined, which may involve immunosuppressive aspects. ORM1 is rich in liver tissue, secreted into the blood. Subcellular locations of ORM1 are mainly in the extracellular space; the plasma membrane is more abundant than the mitochondrion and nucleus. The immunomodulatory effect of ORM1 is related to CD56dim natural killer cells, effector memory $CD8^+$T cells, and natural killer cells. ORM has many activities including, but not limited to, acting as an acute-phase reactant and disease marker, modulating immunity, binding and carrying drugs, maintaining the barrier function of the capillary, and mediating the sphingolipid metabolism (34). In RA patients, a study of the combination of transcriptome and proteome in human urine showed that urinary ORM1 levels in RA patients had a positive correlation with the status of the disease activity (35). Although the literature in RA is limited, ORM has been shown to have anti-inflammatory protective effects in other diseases. Exogenous ORM can significantly reduce the infarct size and neurological deficit score of ischemic stroke. The specific mechanism is to inhibit the production of IL-1β, IL-6, and TNF-α, significantly reduce inflammation, improve malondialdehyde (MDA) and superoxide dismutase (SOD) balance to reduce oxidative stress, and reduce the activity of caspase-3 to inhibit apoptosis (36). Based on data obtained from the Gene Expression Omnibus (GEO) database, previous research revealed that ORM1 was highly expressed and positively correlated with the expression of inflammatory factors (MAPK1, MAPK3, IL1B, and CASP9) (37). In general, ORM1 is a protein related to disease activity and is expected to become a marker for the treatment and diagnosis of RA. Our research group will study in depth the specific mechanism of ORM1 in future research.

However, one of the disadvantages in this experiment design is that proteins are the performers of functions; it is necessary to consider combining the results of transcriptome and metabolomics for multidimensional research. Also, the serum proteome has its limitations, and the perspective of synovial proteomics is worth further studying. If possible, the systematic research on the differentially expressed proteins should be screened out, combined with animal experiments, clinical trials, etc., using molecular biology techniques to verify and enrich the rationality of high-throughput screening results.

The innovation of this study is that we refer to the results of other RA proteomic studies to make our findings more convincing. Our analysis of differential proteins, combined with disease activity, is more clinically meaningful and valuable. In general, these rich data are expected to stimulate subsequent hypothesis-driven research, deepen our understanding of the pathogenesis of RA, provide potential biomarkers, and provide new strategies to facilitate the diagnosis and treatment of this harmful disease.

DATA AVAILABILITY STATEMENT

The data presented in the study are deposited in the PRIDE and ProteomeXchange repository. ProteomeXchange accession number PXD032912.

ETHICS STATEMENT

The studies involving human participants were reviewed and approved by the First Affiliated Hospital of Guangzhou University of Chinese Medicine Ethics Committee.[2020]264. The patients/participants provided their written informed consent to participate in this study. Written informed consent was obtained from the individual(s) for the publication of any potentially identifiable images or data included in this article.

AUTHOR CONTRIBUTIONS

GC, LW, and CH conceived and designed the experiments. ZD and JX conducted the experiments and wrote the manuscript. LiZ, YX, ML, JY, LuZ, and HD provided some of the data. LL, MZ, JH, LW, and GC reviewed and revised the manuscript. CH and ZD have contributed equally to this work. All authors contributed to the article and approved the submitted version.

FUNDING

This study was funded by the Guangzhou Science Technology and Innovation Commission Technology Research Projects (No. 201904010336) and the Innovative and Strong Hospital Project of The First Affiliated Hospital of Guangzhou University of Chinese Medicine (No. 211010010705).

REFERENCES

1. Tobón GJ, Youinou P, Saraux A. The Environment, Geo-Epidemiology, and Autoimmune Disease: Rheumatoid Arthritis. *J Autoimmun* (2010) 35:10–4. doi: 10.1016/j.jaut.2009.12.009
2. Glick EN. Immunopathogenesis of Rheumatoid Arthritis. *J R Soc Med* (1980) 73:80. doi: 10.1177/014107688007300129
3. Nies J, Krabben A, Schoones JW, Huizinga T, Kloppenburg M, Mil A.H.M.V.D.H.-V. What is the Evidence for the Presence of a Therapeutic Window of Opportunity in Rheumatoid Arthritis? A Systematic Literature Review. *Ann Rheumat Dis* (2014) 73:861–70. doi: 10.1136/annrheumdis-2012-203130
4. Wells G, Li T, Maxwell L, Maclean R, Tugwell P. Responsiveness of Patient Reported Outcomes Including Fatigue, Sleep Quality, Activity Limitation, and Quality of Life Following Treatment With Abatacept for Rheumatoid Arthritis. *Ann Rheumat Dis* (2008) 67:260–5. doi: 10.1136/ard.2007.069690
5. Kroot EJJA, Jong B, Leeuwen M, Swinkels H, Hoogen F.H.J.V.D., Hof MVT, et al. The Prognostic Value of Anti-Cyclic Citrullinated Peptide Antibody in Patients With Recent-Onset Rheumatoid Arthritis. *Arthritis Rheumatol* (2000) 43:1831–5. doi: 10.1002/1529-0131(200008)43:8<1831::AID-ANR19>3.0.CO;2-6
6. Generali E, Santis M, Isailovic N, Palermo B, Selmi C. Rheumatoid Factor and Anti-Citrullinated Peptide Antibodies in the General Population: Hepatitis B and C Virus Association and 15-Year-Risk of Rheumatoid Arthritis. *Clin Exp Rheumatol* (2020) 39:38–43.
7. Pincus T, Braun J, Kavanaugh A, Smolen J. Optimisation of Assessment for Rheumatic Diseases in Clinical Trials, Observational Studies and Routine Clinical Care. *Clin Exp Rheumatol* (2014) 32:S.
8. Lourido L, Blanco FJ, Ruiz-Romero C. Defining the Proteomic Landscape of Rheumatoid Arthritis: Progress and Prospective Clinical Applications. *Expert Rev Proteomics* (2017) 14:431–44. doi: 10.1080/14789450.2017.1321481
9. Cheng Y, Chen Y, Sun X, Li Y, Li Z. Identification of Potential Serum Biomarkers for Rheumatoid Arthritis by High-Resolution Quantitative Proteomic Analysis. *Inflammation* (2014) 37:1459–67. doi: 10.1007/s10753-014-9871-8
10. Mun S, Lee J, Park A, Kim H-J, Kang H-G. Proteomics Approach for the Discovery of Rheumatoid Arthritis Biomarkers Using Mass Spectrometry. *Int J Mol Sci* (2019) 20:4368. doi: 10.3390/ijms20184368
11. Zhang X, Smits AH, Tilburg GV, Jansen P, Makowski MM, Ovaa H, et al. An Interaction Landscape of Ubiquitin Signaling. *Mol Cell* (2017) 65:941–955.e948. doi: 10.1016/j.molcel.2017.01.004
12. Zhang X, Smits AH, Tilburg GV, Ovaa H, Huber W, Vermeulen M. Proteome-Wide Identification of Ubiquitin Interactions Using UbIA-MS. *Nat Protoc* (2018) 13:530. doi: 10.1038/nprot.2017.147
13. Owens RJ, Baralle FE. Mapping the Collagen-Binding Site of Human Fibronectin by Expression in Escherichia Coli. *EMBO J* (1986) 5:2825–30. doi: 10.1002/j.1460-2075.1986.tb04575.x
14. Rostagno A, Williams MJ, Baron M, Campbell ID, Gold LI. Further Characterization of the NH2-Terminal Fibrin-Binding Site on Fibronectin. *J Biol Chem* (1995) 269:31938–45. doi: 10.1016/S0021-9258(18)31786-1
15. Zollinger AJ, Smith ML. Fibronectin, the Extracellular Glue. *Matrix Biol* (2016) 60–61:27–37. doi: 10.1016/j.matbio.2016.07.011
16. Akiyama SK, Olden K, Yamada KM. Fibronectin and Integrins in Invasion and Metastasis. *Cancer Metastasis Rev* (1995) 14:173–89. doi: 10.1007/BF00690290.
17. Midwood KS, Mao Y, Hsia HC, Valenick LV, Schwarzbauer JE. Modulation of Cell-Fibronectin Matrix Interactions During Tissue Repair. *J Investig Dermatol SYMP Proc* (2006) 11(1):73–8. doi: 10.1038/sj.jidsymp.5650005
18. Kawelke N, Vasel M, Sens C, Au VA, Dooley S. Fibronectin Protects From Excessive Liver Fibrosis by Modulating the Availability of and Responsiveness of Stellate Cells to Active TGF-β. *PLoS One* (2011) 6(11):e28181. doi:10.1371/journal.pone.0028181.
19. Ruoslahti E. Fibronectin in Cell Adhesion and Invasion. *Cancer Metastasis Rev* (1984) 3:43–51. doi: 10.1007/BF00047692.
20. Wang W-Y, Twu C-W, Liu Y-C, Lin H-H, Chen C-J. Fibronectin Promotes Nasopharyngeal Cancer Cell Motility and Proliferation. *Biomed Pharmacother* (2018) 109:1772–84. doi: doi:10.1016/j.biopha.2018.11.055.
21. Luo MZ, Jing-Bao LI, Sheng-Sheng LI, Cao JP, Meng R, Zhang W. Roles of Autocrine Soluble Fibronectin on the Maintenance of Cell Shape of Osteosarcoma MG-63 Cells. *Xi Bao Yu Fen Zi Mian Yi Xue Za Zhi = Chin J Cell Mol Immunol* (2010) 26:1210–3.
22. Kopylov AT, Papysheva O, Gribova I, Kotaysch G, Morozov SG. Molecular Pathophysiology of Diabetes Mellitus During Pregnancy With Antenatal Complications. *Sci Rep* (2020) 10:19641. doi: 10.1038/s41598-020-76689-9
23. Ohkuro M, Kim JD, Kuboi Y, Hayashi Y, Fukamizu A. Calreticulin and Integrin Alpha Dissociation Induces Anti-Inflammatory Programming in Animal Models of Inflammatory Bowel Disease. *Nat Commun* (2018) 9:1982. doi: 10.1038/s41467-018-04420-4
24. Yamada T, Okuda Y, Takasugi K, Itoh K, Igari J. Relative Serum Amyloid A (SAA) Values: The Influence of SAA1 Genotypes and Corticosteroid Treatment in Japanese Patients With Rheumatoid Arthritis. *Ann Rheumat Dis* (2001) 60:124–7. doi: 10.1136/ard.60.2.124
25. Getz GS, Reardon CA. Apoproteins E, A-I, and SAA in Macrophage Pathobiology Related to Atherogenesis. *Front Pharmacol* (2019) 10:536. doi: 10.3389/fphar.2019.00536
26. Jang WY, Lee BR, Jeong J, Sung Y, Choi M, Song P, et al. Overexpression of Serum Amyloid a 1 Induces Depressive-Like Behavior in Mice. *Brain Res* (2016) 1654:55–65. doi:10.1016/j.brainres.2016.09.003 .

27. Aslan C, Maralbashi S, Salari F, Kahroba H, Sigaroodi F. Tumor-Derived Exosomes: Implication in Angiogenesis and Antiangiogenesis Cancer Therapy. *J Cell Physiol* (2019) 234:16885–903. doi: 10.1002/jcp.28374.
28. Rühlmann C, Wlk T, Blümel T, Stahn L, Kuhla A. Long-Term Caloric Restriction in ApoE-Deficient Mice Results in Neuroprotection *via* Fgf21-Induced AMPK/mTOR Pathway. *Aging* (2016) 8:2777–89. doi: 10.18632/aging.101086
29. Dobryszycka W. Biological Functions of Haptoglobin–New Pieces to an Old Puzzle. *Eur J Clin Chem Clin Biochem J Forum Eur Clin Chem Soc* (1997) 35:647.
30. Petersen HH, Nielsen JP, Heegaard P. Application of Acute Phase Protein Measurements in Veterinary Clinical Chemistry. *Vet Res* (2004) 35:163–87. doi: 10.1051/vetres:2004002
31. Smeets MB, Fontijn J, Kavelaars A, Pasterkamp G, Kleijn D. The Acute Phase Protein Haptoglobin is Locally Expressed in Arthritic and Oncological Tissues. *Int J Exp Pathol* (2010) 84:69–74. doi: 10.1046/j.1365-2613.2003.00336.x
32. Thompson S, Kelly CA, Griffiths ID, Turner GA. Abnormally-Fucosylated Serum Haptoglobins in Patients With Inflammatory Joint Disease. *Clin Chim Acta* (1989) 184:251–8. doi: 10.1016/0009-8981(89)90058-2
33. de Kleijn DP, Smeets MB, Kemmeren PP, Lim SK, Van Middelaar BJ, Velema E, et al. Acute-Phase Protein Haptoglobin is a Cell Migration Factor Involved in Arterial Restructuring. *FASEB J* (2002) 16:1123–5. doi: 10.1096/fj.02-0019fje
34. Luo Z, Hong L, Yang S, Xia L, Su DF. Orosomucoid, an Acute Response Protein With Multiple Modulating Activities. *J Physiol Biochem* (2015) 71:329–40. doi: 10.1007/s13105-015-0389-9
35. Park YJ, Yoo SA, Hwang D, Cho CS, Kim WU. Identification of Novel Urinary Biomarkers for Assessing Disease Activity and Prognosis of Rheumatoid Arthritis. *Exp Mol Med* (2016) 48:e211. doi: 10.1038/emm.2015.120
36. Wan JJ, Wang PY, Zhang Y, Bo-Han HU, Sun Y, Dong-Ping XU, et al. Role of Acute Phase Protein ORM in A Mice Model of Ischemic Stroke. *J Cell Physiol* (2019) 234:20533–45. doi: 10.1002/jcp.28653
37. Shi M, Ma X, Yang Q, Wang W, Dang Y. miR-362-3p Targets Orosomucoid 1 to Promote Cell Proliferation, Restrain Cell Apoptosis and Thereby Mitigate Hypoxia/Reoxygenation-Induced Cardiomyocytes Injury. *Cardiovasc Toxicol* (2021) 21:387–98. doi: 10.1007/s12012-020-09631-0

Conflict of Interest: The authors declare that the research was conducted in the absence of any commercial or financial relationships that could be construed as a potential conflict of interest.

Publisher's Note: All claims expressed in this article are solely those of the authors and do not necessarily represent those of their affiliated organizations, or those of the publisher, the editors and the reviewers. Any product that may be evaluated in this article, or claim that may be made by its manufacturer, is not guaranteed or endorsed by the publisher.

frontiers | Frontiers in Immunology

ORIGINAL RESEARCH
published: 27 May 2022
doi: 10.3389/fimmu.2022.904288

Single-Cell Sequencing of Immune Cell Heterogeneity in IgG4-Related Disease

Xunyao Wu[1,2†], Yu Peng[1†], Jieqiong Li[1†], Panpan Zhang[1], Zheng Liu[1], Hui Lu[1], Linyi Peng[1], Jiaxin Zhou[1], Yunyun Fei[1], Xiaofeng Zeng[1], Yan Zhao[1] and Wen Zhang[1*]*

[1] Department of Rheumatology, Peking Union Medical College Hospital, Chinese Academy of Medical Science & Peking Union Medical College, National Clinical Research Center for Dermatologic and Immunologic Diseases, State Key Laboratory of Complex Severe and Rare Diseases, Beijing, China, [2] Clinical Biobank, Department of Medical Research Center, Peking Union Medical College Hospital, Chinese Academy of Medical Sciences and Peking Union Medical College, Beijing, China

OPEN ACCESS

Edited by:
Ming Zhao,
Central South University, China

Reviewed by:
Marco Lanzillotta,
Vita-Salute San Raffaele University, Italy
Marc Hilhorst,
Academic Medical Center, Netherlands

***Correspondence:**
Yan Zhao
zhaoyan_pumch2002@aliyun.com
Wen Zhang
zhangwen91@sina.com

[†]These authors have contributed equally to this work and share first authorship

Specialty section:
This article was submitted to Autoimmune and Autoinflammatory Disorders, a section of the journal Frontiers in Immunology

Received: *25 March 2022*
Accepted: *28 April 2022*
Published: *27 May 2022*

Citation:
Wu X, Peng Y, Li J, Zhang P, Liu Z, Lu H, Peng L, Zhou J, Fei Y, Zeng X, Zhao Y and Zhang W (2022) Single-Cell Sequencing of Immune Cell Heterogeneity in IgG4-Related Disease. Front. Immunol. 13:904288. doi: 10.3389/fimmu.2022.904288

Background: The IgG4-related disease (IgG4-RD) is an immune-mediated disorder with fibrotic manifestations. However, the transcriptional profiles of immune cell subsets at single-cell level are unknown. Herein, single-cell sequencing was used to assess the specific cell subpopulations and pathways in peripheral blood mononuclear cells (PBMCs) of IgG4-RD.

Methods: Single-cell sequencing was performed using the PBMCs from four patients with IgG4-RD and three healthy controls (HCs). Functional enrichment and cell analysis were performed through re-clustering of PBMCs to assess functional pathways and intercellular communication networks in IgG4-RD. Western blot and flow cytometry were used to verify sequencing and functional enrichment results.

Results: Four major cell types and 21 subtypes were identified. Further subclustering demonstrated that plasma B-cell proportions increased with increasing glycolysis/gluconeogenesis activity in IgG4-RD. Re-clustering of myeloid cells showed that *EGR1* and *CD36* expressions were significantly increased in $CD14^+$ monocytes of IgG4-RD, as validated by Western blot analysis. Moreover, tumor necrosis factor (TNF) production pathways were positively regulated in $CD14^+$ monocytes of IgG4-RD. *In vitro* stimulation showed that $CD14^+$ monocytes of IgG4-RD could secrete higher levels of TNF-α . Notably, the proportions of CD8 central memory T (TCM) and $TIGIT^+$ CD8 cytotoxic T (CTL) increased in patients with IgG4-RD compared with HCs. Further interaction analysis showed that B cell activation factor (BAFF) signaling pathways were enriched from myeloid cells subsets to B cells.

Conclusion: This study enhances the understanding of the cellular heterogeneity and transcriptional features involved in the pathogenesis of IgG4-RD, providing key clinical implications.

Keywords: IgG4-RD, single-cell sequencing, immune cells, B cells, myeloid cells, T cells

BACKGROUND

IgG4-related disease (IgG4-RD) is characterized by high IgG4 concentrations in serum or infiltration of $IgG4^+$ plasma cells in affected tissues (1). IgG4-RD can affect any organ, causing immune-mediated fibrotic manifestations (1, 2). Currently, glucocorticoids are considered the first-line treatment for IgG4-RD (3). However, new therapeutic strategies are needed due to the potential toxicity and side effects of long-term glucocorticoid treatment.

The pathogenesis of IgG4-RD has been thoroughly assessed in recent years. The IgG4-RD is an immune-mediated disorder with diverse autoimmune features. Moreover, anti-galectin-3 autoantibodies have been identified in some patients with IgG4-RD (4). Lanzillotta et al. showed that peripheral plasmablast and plasma B cells are increased in patients with active untreated IgG4-RD. However, they showed that glucocorticoid treatment could alleviate the effect (5, 6). Rituximab can deplete B cells, thus substantially improving symptom, further validating the pathogenicity of B cells in IgG4-RD (7, 8). Self-reactive cytotoxic CD4 T cells, T follicular helper cells, and regulatory T cells can promote fibrosis and IgG4 production by B cells in patients with IgG4-RD (9–12). However, the role of dysregulated immune cells in the pathogenesis of IgG4-RD is unclear. Furthermore, the phenotype, function, and pathogenic heterogeneity of immune cells in IgG4-RD are unknown.

Single-cell sequencing (scRNA-seq) is a novel tool that can assess the heterogeneity of different immune subpopulations. Moreover, the transcriptome analysis at a single-cell or a cell-type level can be used to assess the expression of key genes and intracellular signaling pathways involved in the disease progression. Herein, scRNA-seq analysis of PBMCs from patients with IgG4-RD was used to assess specific cell subpopulations and pathways involved in IgG4 and chronic inflammation.

MATERIALS AND METHODS

Recruitment and Ethics

This study included patients diagnosed with IgG4-RD based on the 2019 American College of Rheumatology/European League Against Rheumatism (ACR/EULAR) Classification Criteria for IgG4-RD (13) and healthy controls (HCs) at Peking Union Medical College Hospital (PUMCH). All the enrolled patients were treatment-naïve and they have not received any treatment before. This study was approved by the ethics committee of PUMCH (approval number: JS-3389), and informed consent was obtained from each patient. The detailed information on the procedure is provided in **Supplementary Table 1**.

Single-Cell Suspension Preparation and Single-Cell Sequencing

PBMCs were obtained *via* Ficoll gradients (Human Lymphocyte Separation Medium, Dakewe, China), then centrifuged at 1,800 rpm and room temperature for 20 min. The cells were washed using 1× phosphate buffered saline (PBS) containing 0.5% fetal bovine serum (FBS) and then resuspended in 1× PBS containing 0.5% FBS. An Automated Cell Counter (Bio-Rad, TC20) was used to determine cell count and viability. Briefly, complementary DNA (cDNA) was synthesized from the cells and amplified using the v2 single-cell reagent kit (10X Genomics) following the manufacturer's instructions. The sequencing library was constructed using simplified cDNA and then sequenced on Illumina (NovaSeq, Novogene).

Raw Data Processing and Combination

The cellranger v2.1.0 pipeline was used to generate and align the raw gene expression matrix of each sample to the hg19 genome and transcriptome. The samples were combined using the Seurat package (v.3.0.0) based on the integration methods described at https://satijalab.org/seurat/v3.0/integration.html (14).

Single-Cell RNA-Seq Data Processing

Single-cell RNA-seq data processing was conducted using R software (v.3.5.3) *via* the Seurat package (v.3.0.0). The following cells were filtered out: (1) cells with >10% transcripts mapping to the mitochondrial genes; (2) cells with fewer than 500 total unique transcripts; and (3) cells with a unique gene count of more than 3,500 genes. NormalizeData function was used to normalize the data. FindVariableFeatures function was used to calculate 2,000 features with high cell-to-cell variation. The RunPCA function was used to reduce the dimensionality of the datasets at default parameters on linear-transformation scaled data generated by the ScaleData function. FindNeighbors and FindClusters functions were used to perform nonlinear dimensional reduction *via* the RunUMAP function (dims = 1:30, resolution = 0.3). The details of the Seurat analyses performed in this work can be found in the website tutorial (https://satijalab.org/seurat/v3.0/pbmc3k_tutorial.html). Cell identity was annotated using the markers shown in **Figures 1B, C**. The uniform manifold approximation and projection (UMAP) were used for visualization.

Subclustering of B Cells, Myeloid Cells, and T Cells

Subclustering analysis was conducted using B cells, myeloid cells (monocytes and dendritic cells), and T cells from PBMCs. The genes were scaled to unit variance after integration. Scaling, principal component analysis (PCA), and clustering were conducted as described above. Doublet clusters were removed under the following criteria: (1) B subclusters with the mean expression of CD3D, CD14, or PPBP > 0.1; (2) myeloid subclusters with the mean expression of CD3D, CD79A, or PPBP > 0.1; and (3) T subclusters with the mean expression of CD79A, CD14, or PPBP > 0.1.

Identification of Differentially Expressed Genes

The differentially expressed genes (DEGs) were identified *via* FindMarkers function in Seurat using the parameters "test.use = wilcox" by default. The false discovery rate (FDR) was estimated using the Benjamini–Hochberg method. DEGs were filtered using a minimum $\log_2$ (fold change) of 0 and a maximum adjusted p-value of 0.05 and then ranked based on the average log2 (fold change) and FDR.

Gene Function Enrichment Analysis

Gene Set Enrichment Analysis (GSEA) (version 3.0) was used to analyze the enriched signaling pathways of plasma B and Mem-unsw B-cell subtypes. Signaling pathways with a threshold of p-value < 0.05 were considered significantly enriched (15). For myeloid or T/Natural killer (NK) cells cells, enrichment analysis for the functions of the DEGs was conducted using the clusterProfiler (v3.12.0) package. Moreover, gene sets were based on Gene Ontology (GO) terms (16).

Cell and Cell Interaction

CellChat was used to comprehensively assess the global communications among cells and quantitatively analyze intercellular communication networks (17). Briefly, the official workflow was followed, and the normalized data were loaded into *CellChat*. *CellChat* objects were created, and *CellchatDB.human* was used to set the secreted signaling pathways as the database.

Purification of Monocytes and *In Vitro* Stimulation

Peripheral blood from patients and HCs were collected in ethylene diamine tetraacetic acid tubes. The blood was then diluted with 1× PBS at a ratio of 1:1, put on the Ficoll density gradient (Dakewe, China) and then centrifuged at 1,800 rpm and 24°C for 20 min. The peripheral blood mononuclear cells (PBMCs) were collected at the interface layer, washed with PBS (300*g* for 10 min, 4°C), and then counted using cellmeter Auto T4 (Nexcelom Bioscience, USA). CD14 microbeads (Miltenyi Biotec, USA) were used to purify $CD14^+$ monocytes following the manufacturer's instructions. The purified $CD14^+$ monocytes were counted through cellmeter Auto T4 (Nexcelom Bioscience, USA) and were resuspended in dulbecco's modified eagle medium (DMEM) (Gibco, USA) containing 10% FBS (Gibco, USA) then seeded into 24-well plates (5×10^5 per well) with recombinant interferon-γ (IFN-γ) (PeproTech, USA) at 37°C for 6 h. The supernatants were then collected for further analysis.

TNF-α Detection

A human tumor necrosis factor–α (TNF-α) pre-coated ELISA kit (Dakewe, China) was used to detect TNF-α in supernatants following the manufacturer's instructions. Briefly, diluted cytokine standards (100 μl), undiluted samples (100 μl), and biotinylated antibody (50 μl) were added to 96-well plates and incubated at room temperature for 3 h. The plates were washed thrice using wash buffer, and then, streptavidin–horseradish peroxidase (HRP) working solution was added to each well and incubated at room temperature for 20 min. The plates were washed again thrice, then 100 μl of Tetramethylbenzidine (TMB) was added to each well and incubated at room temperature for 20 min away from light. A stopping solution was also added. Thermo Scientific Multiskan FC (Thermo Fisher Scientific, USA) was used to measure absorbance at 450 nm.

WESTERN BLOTTING

Purified $CD14^+$ monocytes were lysed with RIPA buffer (High, Solarbio Life Sciences, China) on ice for 30 min and then centrifuged at 12,000*g* for 10 min. A BCA protein assay kit (Thermo Scientific, USA) was used to detect protein concentration. Protein samples [5 μg per lane for CD36 and 10 μg per lane for early growth response-1 (EGR1)] were separated *via* sodium dodecylsulphate (SDS)–polyacrylamide gel electrophoresis and electrophoretically transferred to Immobilon™-P polyvinylidene difluoride membranes (MilliporeSigma, Germany). The membranes were blocked with QuickBlock™ Blocking Buffer (Beyotime, China) at room temperature for 1 h and then incubated with primary antibodies [EGR1 Rabbit mAb (Cell Signaling Technology, USA, 1:1,000), CD36 Rabbit mAb (Cell Signaling Technology, USA, 1:1,000), and β-Actin Mouse mAb (EASYBIO, China, 1:5,000)] at 4°C overnight. The membranes were washed and incubated with secondary antibody [HRP-conjugated (EASYBIO, China, 1:5,000)]. Chemiluminescent HRP Substrate (Millipore Sigma, Germany) were detected using immunoreactive bands. Images were obtained through Tanon 3000M. The relative expression of EGR1 and CD36 were analyzed using ImageJ software (US National Institutes of Health, Bethesda, MA, USA).

Data Availability

The raw sequence data were deposited in the Genome Sequence Archive of the Beijing Institute of Genomics (BIG) Data Center, BIG, Chinese Academy of Sciences (accession code, HRA001555) and are publicly accessible at http://bigd.big.ac.cn/gsa-human. Other supporting raw data are available from the corresponding author upon reasonable request.

RESULTS

An Overview of PBMC Composition in Patients with IgG4-RD

The scRNA-seq was used to analyze peripheral blood samples of three healthy individuals and four patients with IgG4-RD (**Supplementary Table 1**). A total of 47,219 cells were retained for subsequent analysis after filtering doublets and poor-quality cells (dead or dying cells). Un-supervised clustering followed by a two-dimensional UMAP identified 21 distinct subsets (**Figure 1A**). Four major populations, including T cells, NK cells, B cells, myeloid cells, were identified on the basis of canonical markers (*CD3D*, *CD8A*, *NKG7*, *CD79A*, *CD14*, *FCGR3A*, *FCER1A*, *MZB1*, and *PPBP*) (**Figure 1B**). Overall, patients with IgG4-RD had decreased B cells and increased CD14 monocytes and plasma B proportions (**Figure 1C**). Additional cluster-defining genes of each cluster are shown in **Figure 1D**.

Transcriptional and Pathway Analysis of B-Cell Subsets in IgG4-RD

Subclustering of three major populations (B cells, myeloid cells, and T/NK cells) was further conducted. IgG4-RD is characterized by increased IgG4-secreting B cells. This is the first study to report B-cell subpopulations in patients with IgG4-RD. B cells were subclustered into five major populations based on *CD79A*, *IGHD*, *CD27*, *MZB1*, *GPR183*, *IGHM*, *SOX4*, *IGHG3*, and *IGHM*: naïve B (cluster 1, $IGHD^+CD27^-$), Mem-unsw B (cluster 2, memory-

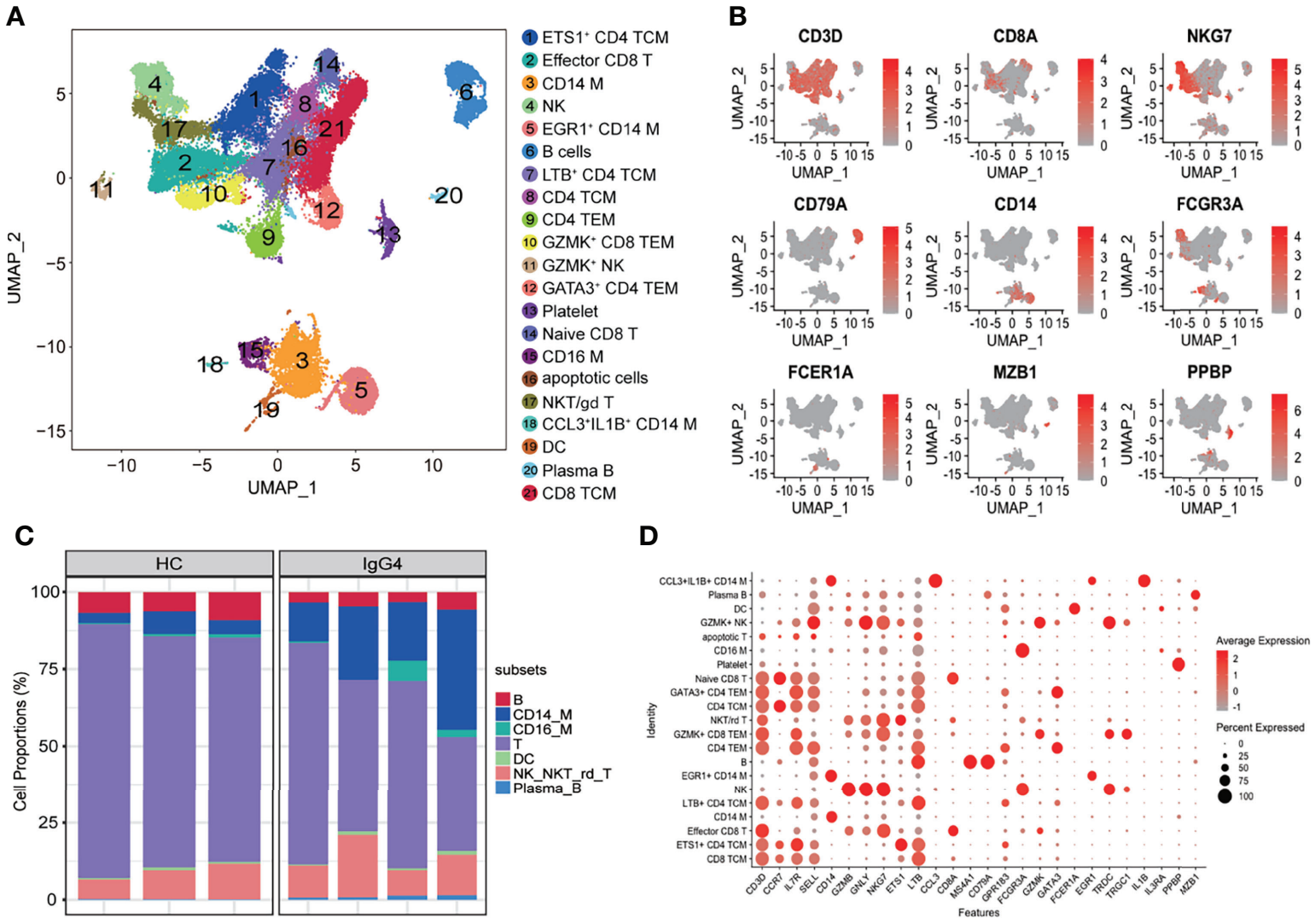

FIGURE 1 | Overview of the clustering and annotation of the sc-RNA sequencing data for IgG4-RD. **(A)** UMAP representation of 47,219 single cells from HCs (n = 3) and IgG4-RD (n = 4), showing the formation of 21 clusters. **(B)** Canonical cell markers used to label major cell types represented in the UMAP plot. The legend is labeled in log scale. **(C)** Bar plot showing cluster abundance of major cell types across all samples. **(D)** Bubble heatmap showing the selected markers annotating specific cell types. The size of the dot indicates the fraction of expressing cells, colored according to z-score–normalized expression levels.

unswitched B cells, *IGHD*$^+$*CD27*$^+$*GPR183*$^+$), Mem-sw B (cluster 3, memory-switched B cells, *IGHD*$^+$*CD27*$^+$ *GPR183*$^+$), plasma B (cluster 4, *MZB1*$^+$*IGHG3*$^+$*IGHG4*$^+$), and SOX4$^+$ naïve B (cluster 5, *IGHD*$^+$*CD27*$^-$*SOX4*$^+$) (**Figures 2A, B**). Patients with IgG4-RD had increased plasma B levels (**Figures 2C, D**). The molecular differences of various B-cell subsets between HCs and patients with IgG4-RD were assessed using volcano plots (**Figure 2E**, **Supplementary Figure 1A**). There was only one differential gene, *IGHG3*, in SOX4$^+$ naïve B-cell subsets between HCs and patients with IgG4-RD (**Supplementary Figures 1A, B**). Functional difference was assessed using GSEA. The top enriched GSEA items for the Mem_unsw B cells included "PI3K-Akt signaling pathway", "Th1 and Th2 cell differentiation," and "Th17 cell differentiation", indicating the enhanced proliferation and ability to activate T-cell responses in patients with IgG4-RD (**Figure 2F**). The top enriched GSEA items for plasma B cells in patients with IgG4-RD included "glycolysis/gluconeogenesis", "IL-17 signaling pathway", "protein export", and "protein processing in endoplasmic reticulum", indicating that abnormal metabolism can promote antibody processing and secretion (**Figure 2F**).

Pro-Inflammatory Gene Patterns of Myeloid Cells in IgG4-RD

Subclustering showed that myeloid cells are monocytes (mono) and dendritic cells (DCs). The monocytes were re-classified into seven subsets based on *CD14*, *FCGR3A*, *EGR1*, *IGHG4*, *ISG15*, *IFI6*, *IFI44*, and *CCL15*: CD14 Mono (*CD14*), CD14$^+$CD16$^+$ Mono (*CD14* and *FCGR3A*), EGR1^{hi} CD14 Mono (*EGR1* and *CD14*), CD16 Mono (*FCGR3A*), IFN-act CD14 Mono (*CD14*, *ISG15*, *IFI6*, and *IFI44*), CCL5$^+$ CD14 Mono (*CCL5* and *CD14*), and IGHG4^{hi} CD14 Mono (*IGHG4* and *CD14*) (**Figures 3A–C**). The DC and CD14 Mono proportions were lower in myeloid cells of patients with IgG4-RD (**Figures 3C, D**). Similarly, the molecular differences of various myeloid subsets between HCs and patients with IgG4-RD were assessed using volcano plots (**Figure 3E**). The expressions of *EGR1* and *CD36* were significantly higher in CD14 Mono, CD14$^+$CD16$^+$ Mono, EGR1^{hi} CD14 Mono, and IFN-act CD14 Mono than in other subsets (**Figure 4A**). Western blot of purified CD14$^+$ monocytes from HCs and patients with IgG4-RD showed that EGR1 and CD36 expressions were significantly increased in proteins of IgG4-RD–derived CD14$^+$ classical monocytes (**Figures 4B, C**).

GO pathway analysis of DEGs between different myeloid subsets showed that TNF was uniformly and significantly upregulated in CD14$^+$ Mono, IFN-act CD14$^+$ Mono, and CD16$^+$ Mono of patients with IgG4-RD (**Figure 4D**). *In vitro* stimulation analysis indicated that CD14$^+$ monocytes of IgG4-RD secreted higher levels of TNF-α (**Figure 4E**). In addition, DEGs in EGR1^{hi} CD14 Mono and CD14$^+$CD16$^+$ Mono from patients with IgG4-RD were positively enriched in neutrophil activation and neutrophil degranulation-related pathways (**Figure 4D**).

Transcriptional Features of NK/T-Cell Subsets in Patients With IgG4-RD

Subclustering of NK/T cells obtained 12 subsets based on the canonical NK/T-cell markers: two subtypes of NK cells, six subtypes of CD4$^+$ T cells, and four subtypes of CD8$^+$ T cells (**Supplementary Figure 2**). Further subclustering of NK cells identified four NK/NKT-cell clusters: PTGDS$^+$ NK (*PTGDS* and *NKG7*), NKT (*NKG7* and *CD3D*), GZMK$^+$IGFBP4$^+$ NK (*GZMK*, *IGFBP4*, and *NKG7*), and TIGIT$^+$ NKT (*TIGIT*, *NKG7*, and *CD3D*) (**Supplementary Figures 3A, B**). The proportions of each NK/NKT subsets were similar between HCs and patients with IgG4-RD (**Supplementary Figure 3C**). Moreover, GO analysis indicated that natural killer cell-mediated cytotoxicity and immunity were decreased in NK or NKT cells of patients with IgG4-RD (**Supplementary Figure 3D**).

Subclustering of CD8$^+$ T cells obtained seven subtypes: CD8 CTL (cytotoxic lymphocytes, *CD8A*, and *GZMB)*, CD8 TCM (central memory T, *CD8A*, *CCR7*, and *GRP183*), *GZMK*$^+$ Effector CD8 T (*CD8A* and *GZMK*), naïve CD8 T (*CD8A* and *CCR7)*, *NCR3*$^+$ CD8 effector memory T (TEM, *NCR3*, *CD8A*, and *GPR183*), *TIGIT*$^+$ CD8 CTL (*TIGIT*, *CD8A*, and *GZMB*), and *TIGIT*$^+$ CD8 TCM (*TIGIT*, *CD8A*, *CCR7*, and *GPR183*) (**Figures 5A–C**). Notably, CD8 TCM and TIGIT$^+$ CD8 CTL proportions were increased in patients with IgG4-RD compared with HCs (**Figures 5C, D**). The DEGs of various CD8$^+$ T subsets were assessed, and then, GO analysis was conducted based on the DEGs (**Figure 5E**). The CD8 CTL, CD8 TCM, and *GZMK*$^+$ effector CD8 T-cell subsets of patients with IgG4-RD were associated with significantly enhanced responses to IFN-γ, antigen processing and presentation, and lymphocyte differentiation (**Figure 5F**). Cell killing and leukocyte-mediated cytotoxicity were significantly positively regulated in CD8 CTL of patients with IgG4-RD (**Figure 5F**). Similarly, the levels of cytotoxicity-related markers, including *GZMA*, *PFN1*, *GZMB*, and *GZMH*, were significantly higher in CD8 CTL of patients with IgG4-RD than in HCs (**Figure 5G**). Moreover, B-cell and neutrophil activation was enhanced in *NCR3*$^+$ CD8 TEM and *TIGIT*$^+$ CD8 TCM of patients with IgG4-RD, respectively (**Figure 5F**).

CD4$^+$ T cells were further subclustered into nine subtypes: CD4 CTL (*GZMB*), CD4 TCM (*CCR7* and *GPR183*), CD4 TEM (*IL7R* and *GPR183*), GZMK$^+$ CD4 CTL (*GZMK* and *GZMB*), *HLA-DRB1*$^+$ CD4 TEM (*HLA-DRB1*, *IL7R*, and *GPR183)*, IFN-act CD4 TCM (*ISG15*, *IFI6*, *IFI44*, *CCR7*, and *GPR183*), naïve CD4 T (*CCR7*), *TIGIT*$^+$ CD4 TCM (*TIGIT*, *CCR7*, and *GPR183*), and Treg (*FOXP3*) (**Figure 6A–C**). The abundance of CD4$^+$ T subtypes was similar between HCs and patients with IgG4-RD (**Figure 6C**). The functional differences between various CD4 T subtypes were evaluated *via* GO analysis. Cellular response to IL-12 and B-cell activation were increased in Tregs of patients with IgG4-RD (**Figure 6D**). Moreover, CD4 CTL and *GZMK*$^+$ CD4 CTL from patients with IgG4-RD were more likely to respond to IFN-γ and IL-1 (**Figure 6D**).

Global Analysis of Immune Cell Communications in Patients With IgG4-RD

The cellular interactions between immune cells play critical roles in cell activation, eventually leading to disease symptoms in patients with IgG4-RD. Herein, *CellChat* was used to investigate the putative interactions between immune cells in patients with IgG4-RD.

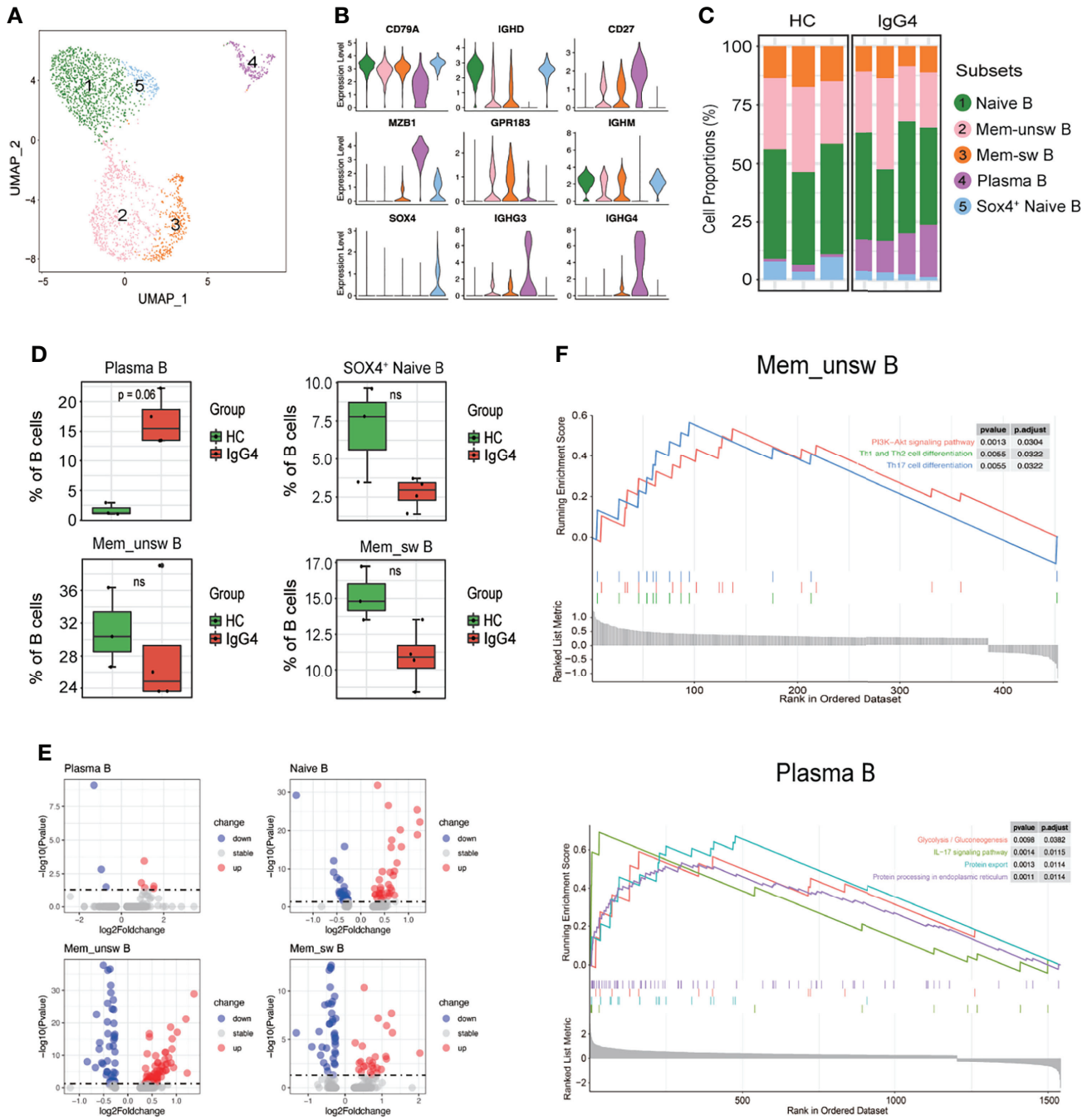

FIGURE 2 | The heterogeneity and transcriptional features of B-cell subsets in IgG4-RD. **(A)** UMAP representation of 2,449 B cells, showing the formation of five clusters. **(B)** Violin plots showing expression distribution of canonical cell markers. **(C)** Bar plot showing cluster abundance of each B-cell type across all samples. **(D)** Percentages of four types of B-cell between HCs and patients with IgG4-RD. The *y*-axis shows the average percentage of B-cell subtypes in total B cells. Error bars are shown in mean ± SEM. Student *t*-test was used for the analysis, and $P < 0.05$ is considered as a significant difference, ns stands for nonsignificant. **(E)** Volcano plot showing the DEGs of B-cell subtypes between HCs and patients with IgG4-RD. **(F)** GSEA results showing the significantly enriched pathways in Memory-unswitched (Mem-unsw) B cells and Plasma B cells of patients with IgG4-RD.

Interaction events were used to calculate the interaction times for each immune cell type. Interaction between myeloid cells and B cells was higher than in T cells subset (**Figure 7A**). *CellChat* was also used to identify significant pathways among the immune cells group. However, this study focused on the CXCL, TNF, B-cell–activating factor (BAFF), and CD40 pathways (**Figure 7B**). BAFF signaling pathways were enriched in myeloid cell subsets to B cells (**Figure 7B**). CD40 signaling

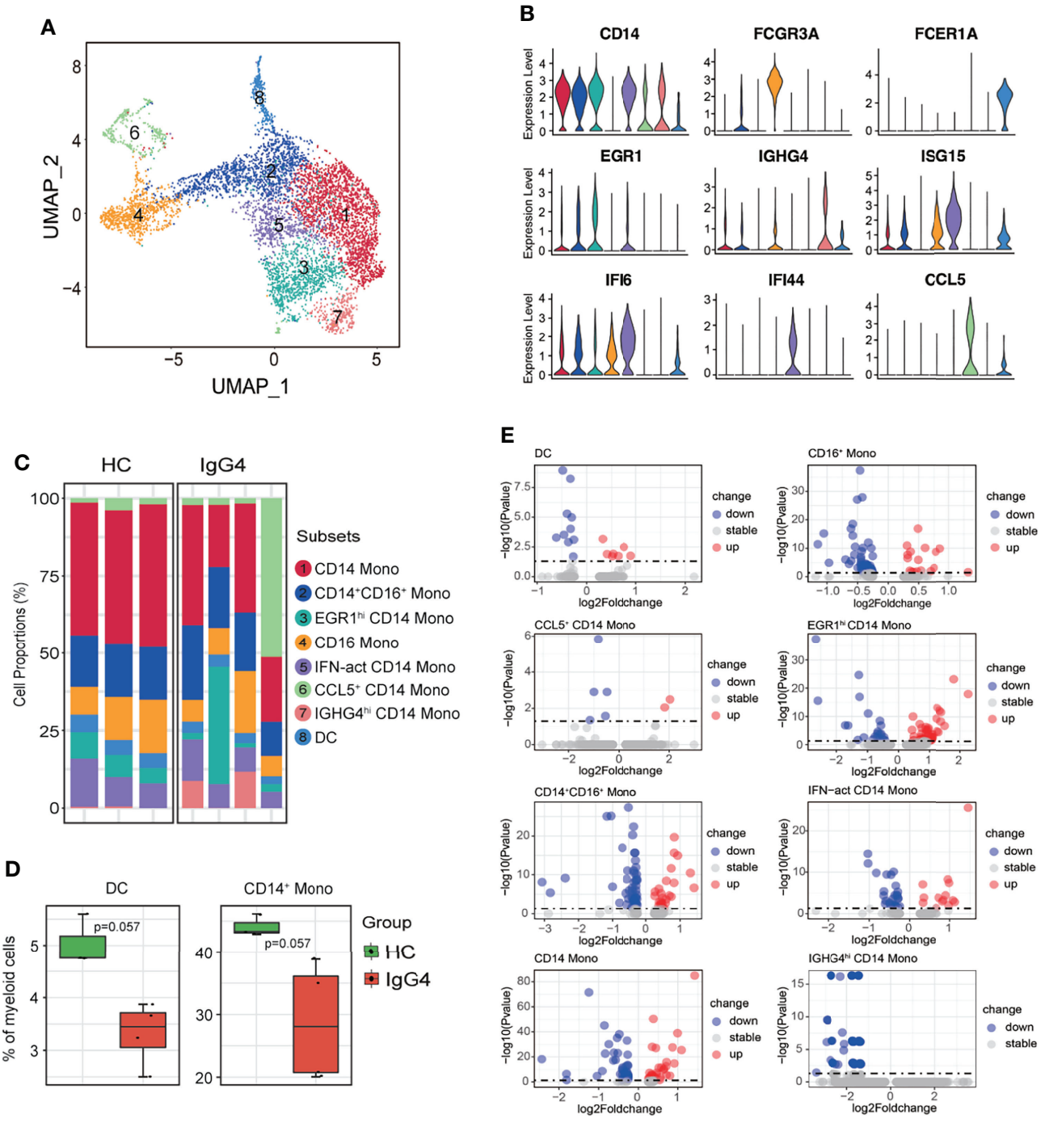

FIGURE 3 | The heterogeneity and transcriptional features of myeloid cells in IgG4-RD. **(A)** UMAP representation of 6324 myeloid cells, showing the formation of 8 clusters. **(B)** Violin plots showing expression distribution of canonical cell markers. **(C)** Bar plot showing cluster abundance of each myeloid cell type across all samples. **(D)** Percentages of DC and $CD14^+$ Mono between HCs and IgG4-RD. The *y*-axis shows the average percentage. Error bars are shown in mean ± SEM. Student *t*-test was used for the analysis, and $P < 0.05$ is considered a significant difference. **(E)** Volcano plot showing the DEGs of myeloid cell subtypes between HCs and patients with IgG4-RD. Data are expressed as mean ± SD.

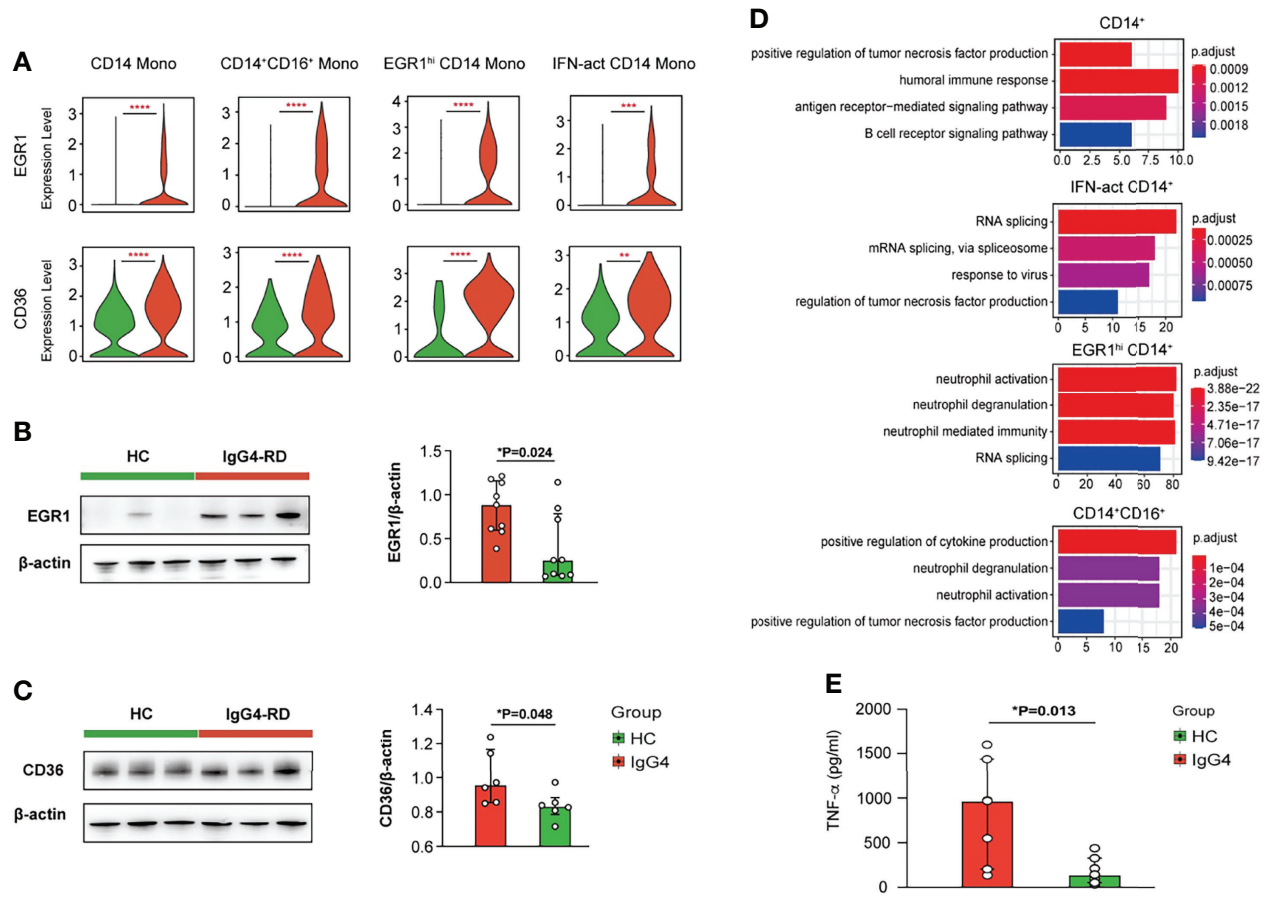

FIGURE 4 | Functional analysis of myeloid cells in IgG4-RD. **(A)** Violin plots showing expression of *EGR1* and *CD36* in different CD14$^+$ mono subtypes. **(B, C)** The comparison of EGR1 and CD36 expressions in purified CD14$^+$ monocytes from HCs and patients with IgG4-RD. **(D)** GO analysis showing the biological process enriched in different CD14$^+$ monocytes of patients with IgG4-RD. **(E)** CD14$^+$ monocytes purified from PBMCs of HCs and patients with IgG4-RD and cultured for 12 h *in vitro*. The TNF-α in the supernatant was measured using ELISA. Data are expressed as mean ± SD, *P < 0.05, **P < 0.01, ***P < 0.001, and ****P < 0.0001.

pathway was the most enriched from CD4$^+$ T cells to CD14$^+$ monocytes (**Figure 7B**). Notably, *CellChat* also predicted that myeloid cells were key sources and mediators for CXCL and TNF signaling pathways (**Figure 7B**). *CellChat* was also used to analyze the communication patterns in different cell groups. Several outgoing effector T/NK cells were characterized by pattern #1, representing multiple pathways, including MIF, ANNEXIN, and CCL signaling pathways (**Figure 7C**). The outgoing of myeloid cells was characterized by pattern #2, representing mainly GALECTIN, RESISTIN, BAFF, and BAG signaling pathways (**Figure 7C**). Moreover, the communication patterns of target cells showed that the incoming effector T/NK cells signaling was dominated by pattern #1, #3, and #5, mainly representing GALECTIN, RESISTIN, IL16, FLT3, and BAG signaling pathways (**Figure 7D**). Most incoming CD14 Mono signaling were dominated by pattern #2, representing ANNEXIN, CCL, TNF, and CD40 signaling pathways (**Figure 7D**). Notably, the incoming B and plasma B signaling were characterized by pattern #4, representing BAFF and CXCL signaling pathways (**Figure 7D**). Together, the interaction analysis highlights the role of myeloid cells in promoting B-cell over-activation through BAFF signaling pathway in patients with IgG4-RD.

DISCUSSION

IgG4-RD is an immune-mediated fibrotic disease. Previous studies have reported the characteristics of immune responses in IgG4-RD disease, enhancing the understanding of potential immune pathogenesis of IgG4-RD disease. However, the cellular and molecular immune responses in IgG4-RD are unclear. Herein, the immunological landscape profiles in patients with IgG4-RD at single-cell resolution were assessed to reveal the critical factors and pathways involved in immune pathogenesis.

We observed reduced B-cell proportions at the single cell level. Our observation was in consistent with our recent published study in which we observed decreased percentage of CD19+ B cells in patients with IgG4-RD by flow cytometry (18). In

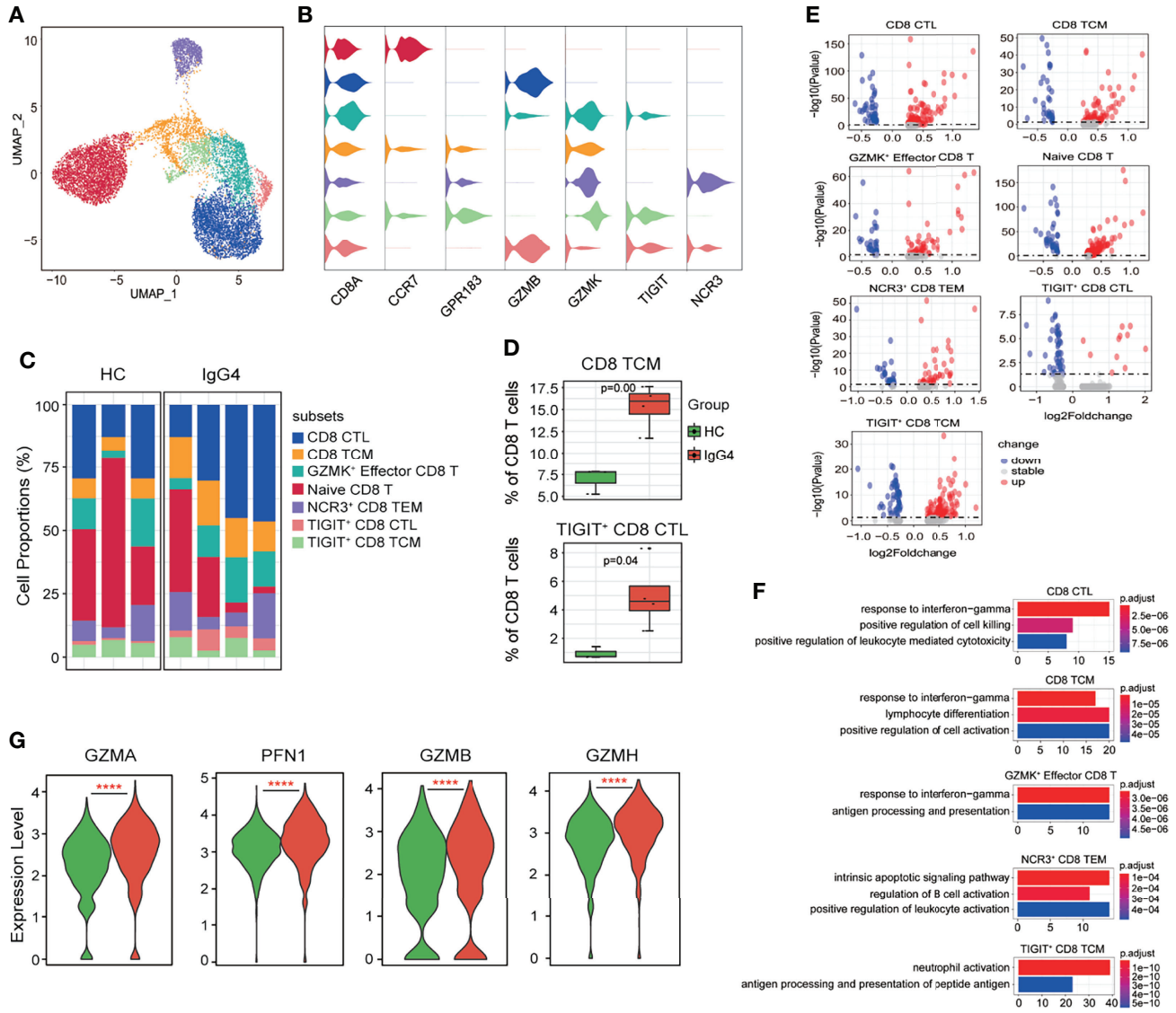

FIGURE 5 | The heterogeneity and transcriptional features of CD8 T-cell subsets in IgG4-RD. **(A)** UMAP representation of 11,864 CD8 T cells, showing the formation of seven clusters. **(B)** Violin plots showing expression distribution of canonical cell markers. **(C)** Bar plot showing cluster abundance of each CD8 T-cell type across all samples. **(D)** Percentages of two types of CD8 T-cell between HCs and IgG4-RD. The *y*-axis shows the average percentage of CD8 T-cell subtypes in total CD8 T cells. Error bars are shown in mean ± SEM. Student *t*-test was used for the analysis, and $P < 0.05$ is considered as a significant difference. **(E)** Volcano plot showing the DEGs of CD8 T-cell subtypes between HCs and patients with IgG4-RD. **(F)** Violin plots showing expression of *GZMA*, *PFN1*, *GZMB*, and *GZMH* in CD8 CTL. **(G)** GO analysis showing the biological process enriched in different CD8 T-cell subtypes of patients with IgG4-RD, ****P < 0.0001.

addition, a previous study by Lanzillotta et al. (19) addressed decreased B cells absolute counts in patients with IgG4-RD compared with HCs. Plasma B-cell levels were increased in patients with IgG4-RD, consistent with previous findings (5, 20). Interestingly, "glycolysis/gluconeogenesis", "protein export", and "protein processing in endoplasmic reticulum" pathways were enriched in plasma B cells from patients with IgG4-RD. A previous study showed that glycolysis activity is correlated with plasmablast differentiation and disease activity (21). However, another study performed by Alvise Berti et al. (22) performed positron emission tomography (PET)/computerized tomography (CT) to measure [18F] Fluorodeoxyglucose (18F-FDG) uptake and found that circulating plasmablasts were inversely correlated with the total lesion glycolysis. Therefore, whether increased glycolysis or gluconeogenesis activity can induce class-switching and differentiation of plasma B cells, promoting antibody processing and production in patients with IgG4-RD needs further investigation.

Notably, the analysis of the incoming signaling *via CellChat* predicted that BAFF signaling pathway, mediated by myeloid cells, was dominant in B and plasma B subsets. BAFF is a key B-cell survival factor. BAFF overexpression is associated with

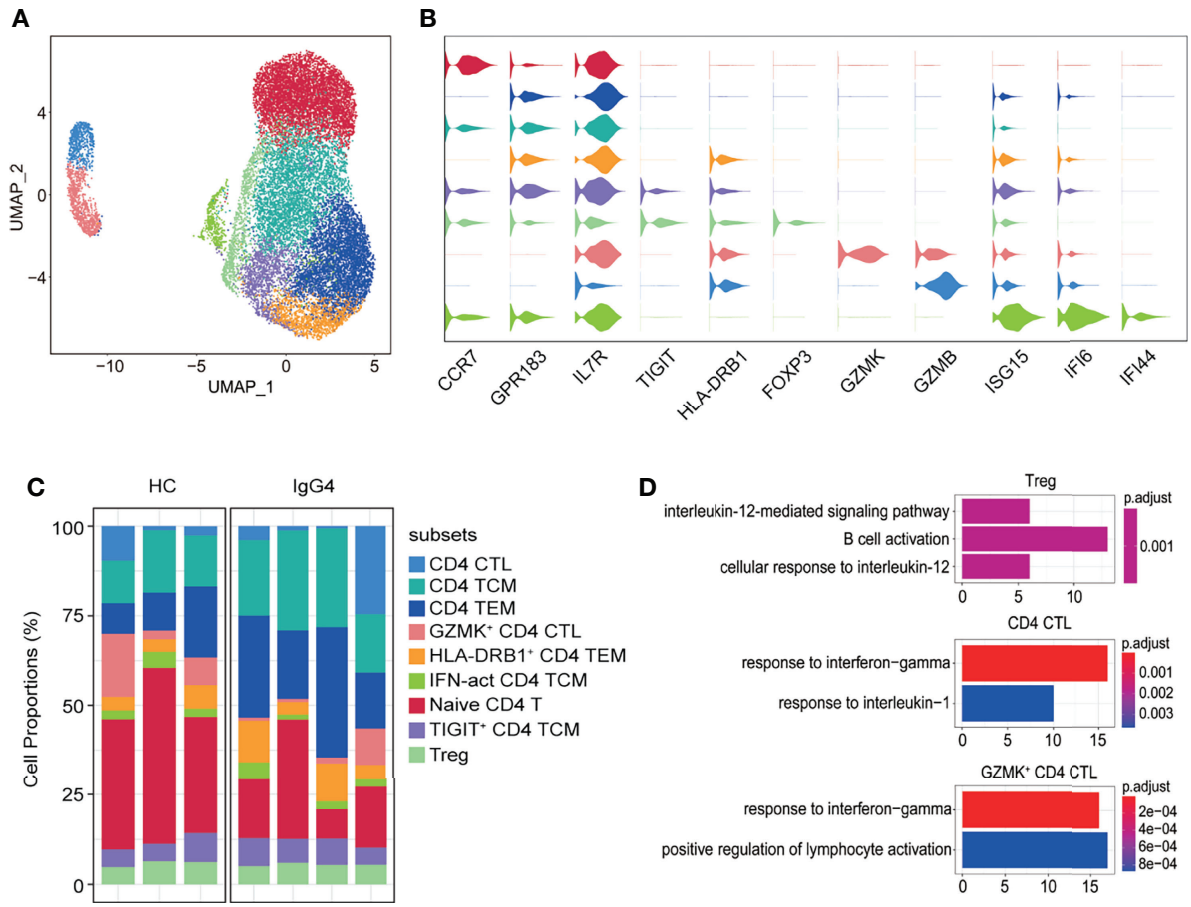

FIGURE 6 | The heterogeneity and transcriptional features of CD4 T-cell subsets in IgG4-RD. **(A)** UMAP representation of 19,629 CD4 T cells, showing the formation of nine clusters. **(B)** Violin plots showing expression distribution of canonical cell markers. **(C)** Bar plot showing cluster abundance of each CD4 T-cell type across all samples. **(D)** GO analysis showing the biological process enriched in Treg, CD4 CTL, and *GZMK*$^+$ CD4 CTL of patients with IgG4-RD.

autoantibody-related autoimmune diseases, such as systemic lupus erythematosus (SLE), primary sjogren's syndrome (pSS) patients, IgA nephropathy, and rheumatoid arthritis (23–25). Clinical trials have used therapeutic monoclonal antibody neutralizing BAFF, belimumab, in recent years. Belimumab can be used as a targeted therapy for SLE (26–28). A previous study showed that the serum levels of BAFF and APRIL are significantly higher in IgG4-RD and pSS than in HCs (29). A recent study also demonstrated that BAFF produced by neutrophils and dendritic cells enhances antibody responses (30). Herein, myeloid cells from BAFF promoted class-switching and differentiation of B cells to IgG4-producing plasma B cells in patients with IgG4-RD. Similarly, a previous study found that IgG4-RD–derived monocytes can induce IgG4 production of HC-derived B cells in a BAFF-dependent and T cell-independent manner (31). Therefore, monoclonal antibody neutralizing BAFF can be used for the clinical treatment of IgG4-RD.

Macrophages play a role in IgG4-RD initiation. Previous studies have shown that CD163$^+$ M2 macrophages are activated by TLR7, accumulated in multiple organs of patients with IgG4-RD, thus promoting fibrotic phenotype by producing CCL18 and IL-10 or activating T helper type 2 (Th2) immune response *via* IL-33 (32–34). Herein, increased TNF production in CD14$^+$ monocytes promoted activation of NK cells and also acted as an autocrine to activate themselves. Moreover, EGR1 and CD36 expressions were significantly higher in CD14$^+$ monocytes from IgG4-RD than those from HCs. A previous study showed that Egr-1 is significantly upregulated in the skin lesions of psoriasis patients and promotes TNF-α production (35). CD36 is a scavenger receptor. Macrophage CD36 can interact with oxidized low-density lipoprotein (oxLDL), trigger signaling cascades for inflammatory response, and is involved in atherosclerosis (36, 37). However, future studies should assess the mechanisms underlying the role of EGR1 and CD36 in promoting TNF production in patients with IgG4-RD.

Moreover, Th2 cells and Tregs play crucial roles in IgG4-RD. The number of Th2 cells is correlated with elevated serum IgG4 levels, IL-4, plasmablast counts, and disease activity (38, 39). PD-1$^+$CXCR5$^-$ circulating Tfh cell populations are significantly

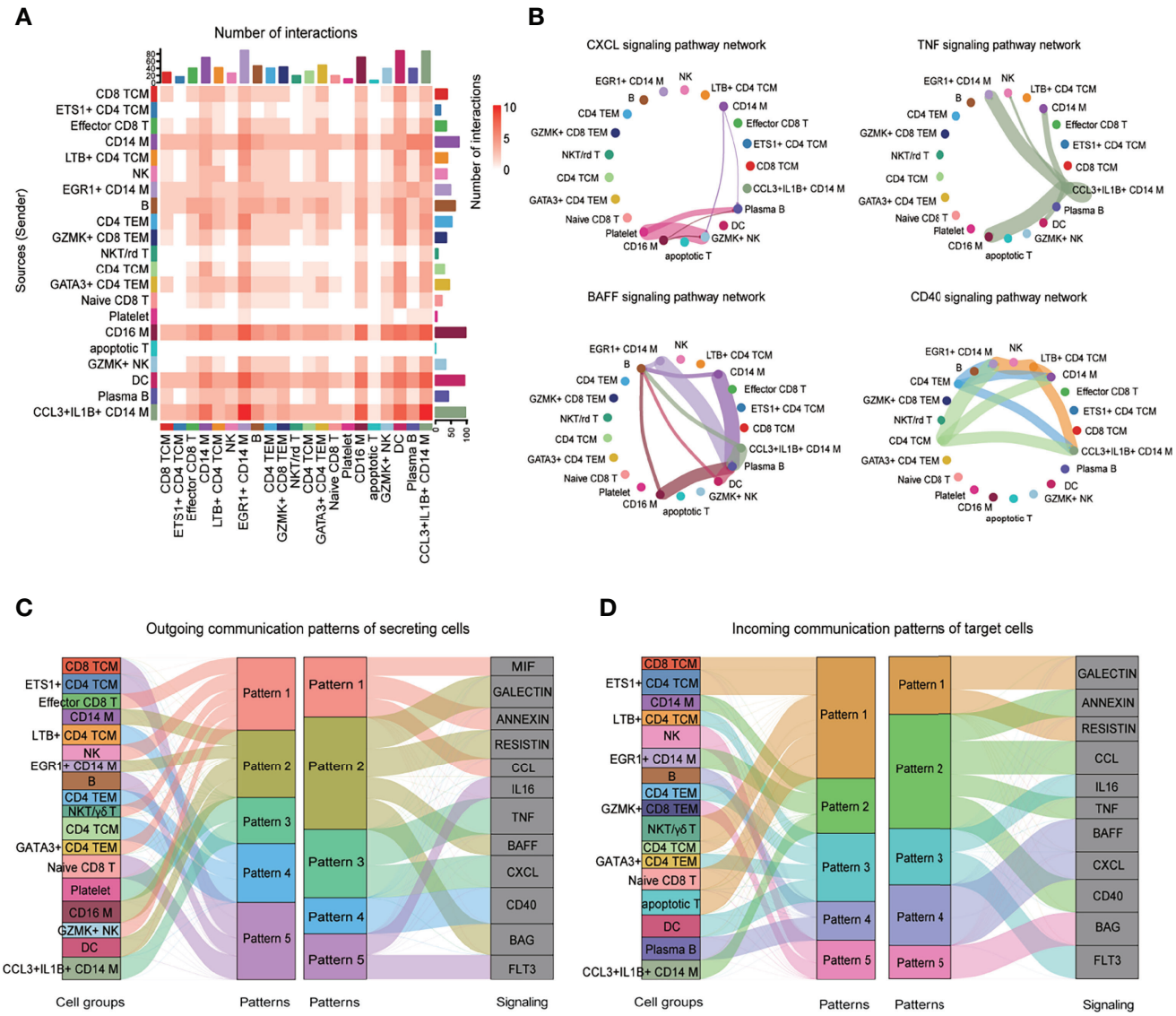

FIGURE 7 | CellChat analysis of the communications among immune cells. **(A)** Heatmap showing the number of interactions of different cell subsets in PBMCs. **(B)** Circle plot showing the inferred intercellular communication network for CXCL, TNF, BAFF, and CD40 signaling among different cell subsets. The number of cells in each cluster is proportional to the circle size, and the line thickness represents the strength of signaling. **(C)** The inferred outgoing communication patterns of secreting cells, which shows the correspondence between the inferred latent patterns and cell groups, and signaling pathways. The thickness of the flow indicates the contribution of the cell group or signaling pathway to each latent pattern. **(D)** The inferred incoming communication patterns of target cells.

increased in patients with IgG4-RD than those in healthy volunteers and are correlated with IgG4 class switching and clinical manifestations of IgG4-RD (40–43). A previous study also found that the frequency of circulating Tfh is increased in the peripheral blood and involved tissue of IgG4-RD. An *in vitro* co-culture study showed that cTfh cells from IgG4-RD can facilitate B-cell proliferation and enhance the differentiation of naïve B cells into switched memory B cells and plasmablast/plasma cells (44). Expanded cytotoxic $CD4^+$ T cells have been detected in patients with IgG4-RD. Moreover, $SLAM7^+$granzyme A^+IL-$1\beta^+$TGF-$\beta1^+$CD4 CTLs secreting IFN-γ are the dominant T cells infiltrating inflamed IgG4-RD tissue site (45, 46). Herein, response to IFN-γ was enhanced in both effector CD4 and CD8 T subsets. Moreover, some T-cell subsets in IgG4-RD activated B cells and neutrophils. Therefore, the role of IFN-γ and the interaction of T cells with neutrophils in patients with IgG4-RD should be assessed.

However, this study had a limited sample size, which may result in low resolution of further subclustering. Therefore, further studies with large samples and fibrotic tissues are needed to explore how immune cells promote fibrotic lesions of patients with IgG4-RD. Moreover, not all mechanistic studies were performed to validate the findings at the single cell level in our

present study. Therefore, further efforts are still needed to validate the phenomenon that we observed at present study, e.g., whether enhanced glycolysis ability promote abnormal B-cell class-switching and antibody production, the role of increased EGR1 expression in monocytes, whether the involved pathways are actually enriched and their role in T/NK cells functions of patients with IgG4-RD.

In summary, this study enhances the understanding of the role of immune cells, thus providing new potential therapeutic targets for the treatment of patients with IgG4-RD.

DATA AVAILABILITY STATEMENT

The datasets presented in this study can be found in online repositories. The name of the repository and accession number can be found below: Genome Sequence Archive of the Beijing Institute of Genomics (BIG) Data Center, BIG, Chinese Academy of Sciences (http://bigd.big.ac.cn/gsa-human); accession code HRA001555.

ETHICS STATEMENT

The studies involving human participants were reviewed and approved by the ethics committee of Peking Union Medical College Hospital (approval number: JS-3389). The patients/participants provided their written informed consent to participate in this study.

AUTHOR CONTRIBUTIONS

XW performed study design, literature search, data analysis, data interpretation, statistical analyses, and manuscript writing. YP performed the experiments, analyzed patients' clinical data, and helped write the manuscript. JL recruited the patients, performed statistical analyses, and helped write the manuscript. PZ, ZL, and HL helped recruit the patients and conducted statistical analyses. LP, JZ, YF, and XZ helped recruit the patients. YZ and WZ conceived the study, provided patient samples, supervised experiments, and revised the manuscript. All authors contributed to the article and approved the submitted version.

FUNDING

This work was supported by the National Natural Science Foundation of China (81771757, 82071839, and 81971544), Capital's Funds for Health Improvement and Research (No. 2020-2-4017), CAMS Innovation Fund for Medical Sciences (CIFMS 2021-1-I2M-003), and Beijing Municipal Science and Technology Commission (No. Z201100005520023).

SUPPLEMENTARY MATERIAL

The Supplementary Material for this article can be found online at: https://www.frontiersin.org/articles/10.3389/fimmu.2022.904288/full#supplementary-material

REFERENCES

1. Wallace ZS, Perugino C, Matza M, Deshpande V, Sharma A, Stone JH. Immunoglobulin G4-Related Disease. *Clin Chest Med* (2019) 40:583–97. doi: 10.1016/j.ccm.2019.05.005
2. Maritati F, Peyronel F, Vaglio A. IgG4-Related Disease: A Clinical Perspective. *Rheumatol (Oxford)* (2020) 59:iii123–31. doi: 10.1093/rheumatology/kez667
3. Perugino CA, Stone JH. IgG4-Related Disease: An Update on Pathophysiology and Implications for Clinical Care. *Nat Rev Rheumatol* (2020) 16:702–14. doi: 10.1038/s41584-020-0500-7
4. Perugino CA, AlSalem SB, Mattoo H, Della-Torre E, Mahajan V, Ganesh G, et al. Identification of Galectin-3 as an Autoantigen in Patients With IgG(4)-Related Disease. *J Allergy Clin Immunol* (2019) 143:736–745.e6. doi: 10.1016/j.jaci.2018.05.011
5. Lin W, Zhang P, Chen H, Chen Y, Yang H, Zheng W, et al. Circulating Plasmablasts/Plasma Cells: A Potential Biomarker for IgG4-Related Disease. *Arthritis Res Ther* (2017) 19:25. doi: 10.1186/s13075-017-1231-2
6. Lanzillotta M, Della-Torre E, Milani R, Bozzolo E, Bozzalla-Cassione E, Rovati L, et al. Increase of Circulating Memory B Cells After Glucocorticoid-Induced Remission Identifies Patients at Risk of IgG4-Related Disease Relapse. *Arthritis Res Ther* (2018) 20:222. doi: 10.1186/s13075-018-1718-5
7. Khosroshahi A, Bloch DB, Deshpande V, Stone JH. Rituximab Therapy Leads to Rapid Decline of Serum IgG4 Levels and Prompt Clinical Improvement in IgG4-Related Systemic Disease. *Arthritis Rheum* (2010) 62:1755–62. doi: 10.1002/art.27435
8. Della-Torre E, Feeney E, Deshpande V, Mattoo H, Mahajan V, Kulikova M, et al. B-Cell Depletion Attenuates Serological Biomarkers of Fibrosis and Myofibroblast Activation in IgG4-Related Disease. *Ann Rheum Dis* (2015) 74:2236–43. doi: 10.1136/annrheumdis-2014-205799
9. Higashioka K, Ota Y, Maehara T, Moriyama M, Ayano M, Mitoma H, et al. Association of Circulating SLAMF7(+)Tfh1 Cells With IgG4 Levels in Patients With IgG4-Related Disease. *BMC Immunol* (2020) 21:31. doi: 10.1186/s12865-020-00361-0
10. Kamekura R, Takahashi H, Ichimiya S. New Insights Into IgG4-Related Disease: Emerging New CD4+ T-Cell Subsets. *Curr Opin Rheumatol* (2019) 31:9–15. doi: 10.1097/BOR.0000000000000558
11. Mattoo H, Stone JH, Pillai S. Clonally Expanded Cytotoxic CD4(+) T Cells and the Pathogenesis of IgG4-Related Disease. *Autoimmunity* (2017) 50:19–24. doi: 10.1080/08916934.2017.1280029
12. Uchida K, Okazaki K. Roles of Regulatory T and B Cells in IgG4-Related Disease. *Curr Top Microbiol Immunol* (2017) 401:93–114. doi: 10.1007/82_2016_41
13. Wallace ZS, Naden RP, Chari S, Choi HK, Della-Torre E, Dicaire JF, et al. The 2019 American College of Rheumatology/European League Against Rheumatism Classification Criteria for IgG4-Related Disease. *Ann Rheum Dis* (2020) 79:77–87. doi: 10.1136/annrheumdis-2019-216561
14. Stuart T, Butler A, Hoffman P, Hafemeister C, Papalexi E, Mauck WM3rd, et al. Comprehensive Integration of Single-Cell Data. *Cell* (2019) 177:1888–1902.e21. doi: 10.1016/j.cell.2019.05.031
15. Subramanian A, Tamayo P, Mootha VK, Mukherjee S, Ebert BL, Gillette MA, et al. Gene Set Enrichment Analysis: A Knowledge-Based Approach for Interpreting Genome-Wide Expression Profiles. *Proc Natl Acad Sci USA* (2005) 102:15545–50. doi: 10.1073/pnas.0506580102
16. Yu G, Wang LG, Han Y, He QY. Clusterprofiler: An R Package for Comparing Biological Themes Among Gene Clusters. *Omics* (2012) 16:284–7. doi: 10.1089/omi.2011.0118
17. Jin S, Guerrero-Juarez CF, Zhang L, Chang I, Ramos R, Kuan CH, et al. Inference and Analysis of Cell-Cell Communication Using CellChat. *Nat Commun* (2021) 12:1088. doi: 10.1038/s41467-021-21246-9

18. Li J, Liu Z, Zhang P, Lin W, Lu H, Peng Y, et al. Peripheral B-Cell Immunophenotyping Identifies Heterogeneity in IgG4-Related Disease. *Front Immunol* (2021) 12:747076. doi: 10.3389/fimmu.2021.747076
19. Lanzillotta M, Della-Torre E, Milani R, Bozzolo E, Bozzalla-Cassione E, Rovati L, et al. Effects of Glucocorticoids on B-Cell Subpopulations in Patients With IgG4-Related Disease. *Clin Exp Rheumatol* (2019) 37 Suppl 118(3):159–66. doi: 10.1136/annrheumdis-2016-209139
20. Heeringa JJ, Karim AF, van Laar JAM, Verdijk RM, Paridaens D, van Hagen PM, et al. Expansion of Blood IgG(4)(+) B, T(H)2, and Regulatory T Cells in Patients With IgG(4)-Related Disease. *J Allergy Clin Immunol* (2018) 141:1831–1843.e10. doi: 10.1016/j.jaci.2017.07.024
21. Torigoe M, Iwata S, Nakayamada S, Sakata K, Zhang M, Hajime M, et al. Metabolic Reprogramming Commits Differentiation of Human CD27(+)IgD(+) B Cells to Plasmablasts or CD27(-)IgD(-) Cells. *J Immunol* (2017) 199:425–34. doi: 10.4049/jimmunol.1601908
22. Berti A, Della-Torre E, Gallivanone F, Canevari C, Milani R, Lanzillotta M, et al. Quantitative Measurement of 18F-FDG PET/CT Uptake Reflects the Expansion of Circulating Plasmablasts in IgG4-Related Disease. *Rheumatology (Oxford)* (2017) 56(12):2084–92. doi: doi:10.1093/rheumatology/kex234
23. Carrillo-Ballesteros FJ, Palafox-Sánchez CA, Franco-Topete RA, Muñoz-Valle JF, Orozco-Barocio G, Martínez-Bonilla GE, et al. Expression of BAFF and BAFF Receptors in Primary Sjögren's Syndrome Patients With Ectopic Germinal Center-Like Structures. *Clin Exp Med* (2020) 20:615–26. doi: 10.1007/s10238-020-00637-0
24. Samy E, Wax S, Huard B, Hess H, Schneider P, Targeting BAFF. And APRIL in Systemic Lupus Erythematosus and Other Antibody-Associated Diseases. *Int Rev Immunol* (2017) 36:3–19. doi: 10.1080/08830185.2016.1276903
25. Vincent FB, Morand EF, Schneider P, Mackay F. The BAFF/APRIL System in SLE Pathogenesis. *Nat Rev Rheumatol* (2014) 10:365–73. doi: 10.1038/nrrheum.2014.33
26. Brunner HI, Abud-Mendoza C, Viola DO, Calvo Penades I, Levy D, Anton J, et al. Safety and Efficacy of Intravenous Belimumab in Children With Systemic Lupus Erythematosus: Results From a Randomised, Placebo-Controlled Trial. *Ann Rheum Dis* (2020) 79:1340–8. doi: 10.1136/annrheumdis-2020-217101
27. Furie R, Petri M, Zamani O, Cervera R, Wallace DJ, Tegzová D, et al. Randomized, Placebo-Controlled Study of Belimumab, a Monoclonal Antibody That Inhibits B Lymphocyte Stimulator, in Patients With Systemic Lupus Erythematosus. *Arthritis Rheum* (2011) 63:3918–30. doi: 10.1002/art.30613
28. Dooley MA, Houssiau F, Aranow C, D'Cruz DP, Askanase A, Roth DA, et al. Effect of Belimumab Treatment on Renal Outcomes: Results From the Phase 3 Belimumab Clinical Trials in Patients With SLE. *Lupus* (2013) 22:63–72. doi: 10.1177/0961203312465781
29. Kiyama K, Kawabata D, Hosono Y, Kitagori K, Yukawa N, Yoshifuji H, et al. And APRIL Levels in Patients With IgG4-Related Disease and Their Clinical Significance. *Arthritis Res Ther* (2012) 14:R86. doi: 10.1186/ar3810
30. Giordano D, Kuley R, Draves KE, Roe K, Holder U, Giltiay NV, et al. And Dendritic Cells Is Regulated Differently and Has Distinct Roles in Antibody Responses and Protective Immunity Against West Nile Virus. *J Immunol* (2020) 204:1508–20. doi: 10.4049/jimmunol.1901120
31. Watanabe T, Yamashita K, Fujikawa S, Sakurai T, Kudo M, Shiokawa M, et al. Involvement of Activation of Toll-Like Receptors and Nucleotide-Binding Oligomerization Domain-Like Receptors in Enhanced IgG4 Responses in Autoimmune Pancreatitis. *Arthritis Rheum* (2012) 64:914–24. doi: 10.1002/art.33386
32. Furukawa S, Moriyama M, Tanaka A, Maehara T, Tsuboi H, Iizuka M, et al. Preferential M2 Macrophages Contribute to Fibrosis in IgG4-Related Dacryoadenitis and Sialoadenitis, So-Called Mikulicz's Disease. *Clin Immunol* (2015) 156:9–18. doi: 10.1016/j.clim.2014.10.008
33. Furukawa S, Moriyama M, Miyake K, Nakashima H, Tanaka A, Maehara T, et al. Interleukin-33 Produced by M2 Macrophages and Other Immune Cells Contributes to Th2 Immune Reaction of IgG4-Related Disease. *Sci Rep* (2017) 7:42413. doi: 10.1038/srep42413
34. Ishiguro N, Moriyama M, Furusho K, Furukawa S, Shibata T, Murakami Y, et al. Activated M2 Macrophages Contribute to the Pathogenesis of IgG4-Related Disease *via* Toll-Like Receptor 7/Interleukin-33 Signaling. *Arthritis Rheumatol* (2020) 72:166–78. doi: 10.1002/art.41052
35. Jeong SH, Park JH, Kim JN, Park YH, Shin SY, Lee YH, et al. Up-Regulation of TNF-Alpha Secretion by Cigarette Smoke Is Mediated by Egr-1 in HaCaT Human Keratinocytes. *Exp Dermatol* (2010) 19:e206–12. doi: 10.1111/j.1600-0625.2009.01050.x
36. Park YM. CD36, a Scavenger Receptor Implicated in Atherosclerosis. *Exp Mol Med* (2014) 46:e99. doi: 10.1038/emm.2014.38
37. Chen Y, Yang M, Huang W, Chen W, Zhao Y, Schulte ML, et al. Mitochondrial Metabolic Reprogramming by CD36 Signaling Drives Macrophage Inflammatory Responses. *Circ Res* (2019) 125:1087–102. doi: 10.1161/CIRCRESAHA.119.315833
38. Akiyama M, Suzuki K, Yamaoka K, Yasuoka H, Takeshita M, Kaneko Y, et al. Number of Circulating Follicular Helper 2 T Cells Correlates With IgG4 and Interleukin-4 Levels and Plasmablast Numbers in IgG4-Related Disease. *Arthritis Rheumatol* (2015) 67:2476–81. doi: 10.1002/art.39209
39. Akiyama M, Yasuoka H, Yamaoka K, Suzuki K, Kaneko Y, Kondo H, et al. Enhanced IgG4 Production by Follicular Helper 2 T Cells and the Involvement of Follicular Helper 1 T Cells in the Pathogenesis of IgG4-Related Disease. *Arthritis Res Ther* (2016) 18:167. doi: 10.1186/s13075-016-1064-4
40. Kamekura R, Yamamoto M, Takano K, Yabe H, Ito F, Ikegami I, et al. Circulating PD-1(+)CXCR5(-)CD4(+) T Cells Underlying the Immunological Mechanisms of IgG4-Related Disease. *Rheumatol Adv Pract* (2018) 2:rky043. doi: 10.1093/rap/rky043
41. Kamekura R, Takano K, Yamamoto M, Kawata K, Shigehara K, Jitsukawa S, et al. Cutting Edge: A Critical Role of Lesional T Follicular Helper Cells in the Pathogenesis of IgG4-Related Disease. *J Immunol* (2017) 199:2624–9. doi: 10.4049/jimmunol.1601507
42. Maehara T, Mattoo H, Mahajan VS, Murphy SJ, Yuen GJ, Ishiguro N, et al. The Expansion in Lymphoid Organs of IL-4(+) BATF(+) T Follicular Helper Cells is Linked to IgG4 Class Switching *In Vivo*. *Life Sci Alliance* (2018) 1(1): e201800050. doi: 10.1101/284737
43. Kubo S, Nakayamada S, Zhao J, Yoshikawa M, Miyazaki Y, Nawata A, et al. Correlation of T Follicular Helper Cells and Plasmablasts With the Development of Organ Involvement in Patients With IgG4-Related Disease. *Rheumatol (Oxford)* (2018) 57:514–24. doi: 10.1093/rheumatology/kex455
44. Chen Y, Lin W, Yang H, Wang M, Zhang P, Feng R, et al. Aberrant Expansion and Function of Follicular Helper T Cell Subsets in IgG4-Related Disease. *Arthritis Rheumatol* (2018) 70:1853–65. doi: 10.1002/art.40556
45. Mattoo H, Mahajan VS, Maehara T, Deshpande V, Della-Torre E, Wallace ZS, et al. Clonal Expansion of CD4(+) Cytotoxic T Lymphocytes in Patients With IgG4-Related Disease. *J Allergy Clin Immunol* (2016) 138:825–38. doi: 10.1016/j.jaci.2015.12.1330
46. Maehara T, Mattoo H, Ohta M, Mahajan VS, Moriyama M, Yamauchi M, et al. Lesional CD4+ IFN-γ+ Cytotoxic T Lymphocytes in IgG4-Related Dacryoadenitis and Sialoadenitis. *Ann Rheum Dis* (2017) 76:377–85. doi: 10.1136/annrheumdis-2016-209139

Conflict of Interest: The authors declare that the research was conducted in the absence of any commercial or financial relationships that could be construed as a potential conflict of interest.

frontiers | Frontiers in Immunology

TYPE Clinical Trial
PUBLISHED 12 August 2022
DOI 10.3389/fimmu.2022.930872

OPEN ACCESS

EDITED BY
Ming Zhao,
Central South University, China

REVIEWED BY
Adolfo Andrade-Cetto,
National Autonomous University of Mexico, Mexico
Dong-Hua Yang,
St. John's University, United States
Ali M Alqahtani,
King Khalid University, Saudi Arabia

*CORRESPONDENCE
Kaijian Hou
kaijianhou@126.com
Fengwu Chen
fengwuchen123@163.com

†These authors have contributed equally to this work and share first authorship

SPECIALTY SECTION
This article was submitted to Autoimmune and Autoinflammatory Disorders, a section of the journal Frontiers in Immunology

RECEIVED 28 April 2022
ACCEPTED 11 July 2022
PUBLISHED 12 August 2022

CITATION
He L, Chen R, Zhang B, Zhang S, Khan BA, Zhu D, Wu Z, Xiao C, Chen B, Chen F and Hou K (2022) Fecal microbiota transplantation treatment of autoimmune-mediated type 1 diabetes mellitus. *Front. Immunol.* 13:930872. doi: 10.3389/fimmu.2022.930872

Fecal microbiota transplantation treatment of autoimmune-mediated type 1 diabetes mellitus

Lina He[1,2†], Rongping Chen[3†], Bangzhou Zhang[4,5†], Shuo Zhang[1,6†], Barkat Ali Khan[7], Dan Zhu[1], Zezhen Wu[1,6], Chuanxing Xiao[4,5,8], Baolong Chen[9], Fengwu Chen[1,6*] and Kaijian Hou[1,6*]

[1]Department of Endocrine and Metabolic Diseases, Longhu People's Hospital, Shantou, China, [2]Key Laboratory for Research on Active Ingredients in Natural Medicine of Jiangxi Province, Yichun University, Yichun, China, [3]School of Laboratory Medical and Biotechnology, Southern Medical University, Guangzhou, China, [4]School of Pharmacy, Fujian University of Traditional Chinese Medicine, Fuzhou, China, [5]School of Basic Medical Science, Central South University, Changsha, China, [6]Department of Endocrine and Metabolic Diseases, The First Affiliated Hospital of Shantou University Medical College, Shantou, China, [7]Drug Delivery and Cosmetics Lab, Good Clinical Practice (GCPS), Faculty of Pharmacy, Gomal University, Dera Ismail Khan, Pakistan, [8]Department of Gastroenterology, The Second Affiliated Hospital of Fujian University of Traditional Chinese Medicine, Fuzhou, China, [9]Center for Research and Development, Xiamen Treatgut Biotechnology Co. Ltd., Xiamen, China

Type 1 diabetes mellitus (T1DM) is an autoimmune-mediated disease characterized by a reduced or absolute lack of insulin secretion and often associated with a range of vascular and neurological complications for which there is a lack of effective treatment other than lifestyle interventions and pharmacological treatments such as insulin injections. Studies have shown that the gut microbiota is involved in mediating the onset and development of many fecal and extrafecal diseases, including autoimmune T1DM. In recent years, many cases of gut microbiota transplantation for diseases of the bowel and beyond have been reported worldwide, and this approach has been shown to be safe and effective. Here, we conducted an experimental treatment study in two adolescent patients diagnosed with autoimmune T1DM for one year. Patients received one to three rounds of normal fecal microbiota transplants (FMT) and were followed for up to 30 weeks. Clinical outcomes were measured, including biochemical indices, medication regimen, and dosage adjustment. Fecal microbiota metagenomic sequencing after transplantation provides a reference for more reasonable and effective microbiota transplantation protocols to treat autoimmune T1DM. Our results suggest that FMT is an effective treatment for autoimmune T1DM.

Clinical Trial Registration: http://www.chictr.org.cn, identifier ChiCTR2100045789.

KEYWORDS

fecal microbiota transplantation (FMT), gut microbiota (GM), autoimmune-mediated, treatment, type 1 diabetes mellitus

Introduction

The development of T1DM is not only associated with genetic factors but also non-genetic factors, and rapidly changing external environmental factors especially play an important role in the pathogenesis of T1DM (1). The incidence of diabetes and impaired glucose tolerance in adults has been increasing worldwide, associated with changes in dietary habits and lifestyle, the use of antibiotics, changes in childbirth practices, and external environmental pollution (2–5). There is an estimated annual growth rate of 3%–4% of newly diagnosed diabetics (4, 6) and the International Diabetes Federation Atlas (IDF) estimates the global prevalence of diabetes to be 10.5% (536.6 million people) among people aged 20–79 years in 2021, rising to 12.2% (783.2 million) in 2045 (7), and 108,300 children under 15 years of age will be diagnosed in 2021, a number that rises to 149,500 if the age range is extended to under 20 years (8). T1DM is currently treated with lifestyle interventions, local insulin injections, and oral hypoglycemic agents. However, the main groups of T1DM sufferers are adolescents and children, and their blood glucose, which is often poorly controlled through diet and exercise, fluctuates. Additionally, long-term insulin use can cause a series of side effects such as obesity, hypoglycemia, hyperinsulinemia, and injection site pain. Importantly, it will also lead to unhealthy psychology in juvenile patients (9). Unhealthy psychology may also be involved in the developmental process of T1DM (10, 11). The diagnosis and management of diabetes also imposes a huge economic burden on the country and families (12). Therefore, novel treatment modalities for autoimmune type 1 diabetes have become an immediate social need, and gut microbiota transplantation is a global research hotspot.

Early in life, the gut microbiota shape the immune system and regulates metabolism, whereas imbalances in the gut microbiota later in life can cause several autoimmune and metabolic disorders (1, 8). Social and lifestyle changes, including the mode of delivery of newborns, dietary structure, and the use of antibiotics in the latter stages of life, have aggravated the imbalance in the type and quantity of fecal microbiota (13). These alterations have stimulated the exploration of the relationship between various internal and external fecal diseases and the change in the structure of fecal microbiota, the incidence of which is gradually increasing worldwide (2). The number of fecal microbiota, the types of dominant microbiota, and the proportion of microbiota were found to change in type 1 diabetic patients compared with normal people (9). Qi et al. (2) studied changes in the microbiota of children with T1D and healthy children (control group) and found that the fecal bacterial content was significantly lower in the T1D group than in the control group; it was also found that Clostridial microbiota IV and XIVa also play an important role in the homeostasis of the immune fecal environment and that their products, short-chain fatty acids, regulate the expression of Foxp3 in CD4+ T cells (3).

At least two mechanisms may explain the fecal microbiota involvement in the occurrence and development of T1DM. By one mechanism, fecal microbiota affect the permeability of fecal mucosa. Fecal microbiota secrete mucus to constitute the fecal mechanical barrier, and the breakdown products of fecal microbiota, short-chain fatty acids, promote the metabolism and repair of fecal epithelial cells and maintain the barrier function of fecal epithelium. Alternatively, fecal microbiota affect autoimmunity. Studies on NOD mice revealed that the interaction between fecal microbiota and the natural immune system is an important factor in the development of type 1 diabetes (4). When the fecal microbiota are dysregulated and the fecal barrier function is reduced, pathogenic microorganisms can invade the mesenteric lymph nodes, causing excessive activation of T and B lymphocytes in the intestine and intestine-associated lymphoid tissues. Since these tissues are connected to the pancreas through the pancreatic lymph nodes and mesenteric lymph nodes, the activated T and B lymphocytes trigger immune- and inflammation-mediated pancreatic β-cell injury (5), which further decreases insulin secretion.

The modulation of the gut microbiota through probiotics, prebiotics, interventions with dietary factors, and fecal microbial transplants all allows beneficial microorganisms to modulate early host–microbiota interactions by exerting their protective potential in patients with T1DM or those at high risk of T1DM (6). Among these therapeutic modifications, the main one is fecal microbiota transplantation (FMT). FMT is a method for regulating or rebuilding fecal microbiota and treating gastrofecal and non-gastrofecal diseases by fabricating a suspension of fecal microbiota from a healthy donor through an intelligent enterobacteria processing system and transplanting it into the gastrofecal tract of the patient by capsule preparation, nasal-fecal tube infusion, gastroscopy, enteroscopy, or intubation. The application of fecal microbiota transplantation has brought hope for the cure of many diseases, including irritable bowel syndrome (7), ulcerative colitis (10), and other fecal diseases, and depression, anxiety disorders (11), and many other diseases outside the fecal tract. Several examples of improved glycemic control in mice by gut microbiota transplantation have been described in rodent models (9–11). Transplantation of gut microbiota from MyD88-deficient non-obese diabetic (MyD88−/−NOD) mice into non-obese diabetic mice reduced the incidence of isletitis and significantly delayed the onset of diabetes (12). Administration of Lactococcus lactis expressing GAD65 and IL-10, combined with a short course of low-dose anti-CD3, stabilized isletitis, preserved functional beta-cell populations, and restored blood glucose to normal levels in recently developed NOD mice (14). Additionally, Dolpady et al. (11) found experimentally that

alterations in the fecal microbiota induced by oral administration of the lactic acid bacteria-rich probiotic VSL#3, alone or along with retinoic acid (RA), protected NOD mice from T1D by affecting the inflammasome at the fecal level. Thus, FMT can adjust the fecal microbiota of transplanted patients and slow down T1MD disease progression.

FMT was found to be safe and effective in several human clinical studies. FMT has significantly altered the composition of the gut microbiota and to affect glycemic control and insulin resistance in subjects with metabolic syndrome based on baseline microbiota (15); therefore, in recent years, greater research attention has been focused on fecal microbiota transplantation for T1DM. Mocanu et al. (16), studied the change in insulin sensitivity (Homa-IR) from baseline to 6 weeks after fecal microbiota transplantation supplemented with high and low fermentable fiber in patients with obesity and metabolic syndrome, and found that FMT combined with low fermentable fiber significantly improved insulin resistance in transplant recipients. The difference was statistically significant, with no cases of adverse effects throughout the transplantation process. In performing lean body donor (allogeneic) versus self (autologous) fecal microbiota transplantation in male subjects with metabolic syndrome, Kootte (17) found a significant improvement in insulin sensitivity after 6 weeks of allogenic fecal microbiota transplantation, accompanied by changes in microbiota composition and changes in plasma metabolites, with no cases of adverse effects during this experiment. In a randomized controlled trial of patients with new-onset T1DM within 6 months, de Groot and colleagues (16) found that fecal microbiota transplantation stabilized residual beta-cell function and optimized glycemic control in patients. These clinical trials show that fecal microbiota have a great biological driving effect in T1DM patients, and FMT is a safe and feasible treatment of T1DM. Microbiota transplantation has also been reported in obese people with type 2 diabetes (18).

To understand clinical strategies to treat T1DM, we initiated an experimental treatment study in two adolescent pediatric patients with autoimmune T1DM. Ianiro et al. (19) conducted a meta-analysis that showed that the overall response rate of capsule FMT was over 90% and was minimally invasive, and Ng et al. (18) found that repeat FMT is safe and facilitates the implantation of the transplanted microbiota. Therefore, we chose to perform multiple clinical nodes of fecal microbiota transplantation, most as oral liquid capsules, in our patients. The number of performed microbiota transplants and the specific clinical pathways differed between the two patients, resulting in different clinical outcomes, as will be discussed.

Materials and methods

At the onset, we took stool specimens from the subjects and mated them with healthy donors who met the criteria. Both patients had signed informed consent for microbiota capsule preparation when they were enrolled. The mated fecal microbiota was introduced into the patients in oral capsules or by nasal-fecal tube infusion, and serum and stool specimens were collected for observation and laboratory analysis before and after each microbiota transplantation was completed. Current research on diabetes has focused on the collection and analysis of serum samples from patients, but it is also important to collect stool samples and correlate a multi-omics approach with the gut microbiota because only then can we reconstruct the bridge from disease parameters to etiology (6]. Therefore, our observational indices are divided into two types: 1) primary observation indices, i.e., changes in insulin and oral hypoglycemic drug use compared with those before microbiota transplantation, glycemic control, insulin resistance, and whether autoantibodies associated with autoimmune T1DM turn negative; and 2) secondary observation indices, by metagenomic analysis of the fecal microecological changes of the patients, fluctuations in inflammatory factors (blood routine, white blood cells, sedimentation, C-reactive protein, calcitoninogen), and linking the serological changes and fecal microbiota changes of the patients to each other. The study procedure is described below.

Note: Research ethics number: LHLL2021001, Ethics Committee of Longhu People's Hospital Shantou, China.

Clinical Registration Number: ChiCTR2100045789, Chinese Clinical Trail Registry: http://www.chictr.org.cn/showprojen.aspx?proj=125179.

Recruitment criteria for study subjects

Recruitment parameters for patients followed the 2019 World Health Organization (WHO) diagnostic criteria for type 1 glucose (T1DM). The inclusion and exclusion criteria are shown in Table 1.

Based on the above recruitment criteria, two patients, designated patient 1 (P1) and patient 2 (P2), were included in this study.

Patient 1 was a 15-year-old male, with a height of 1.55 m, a weight of 37 kg, and a body mass index (BMI) of 15.4 kg/m2, who had been diagnosed with T1DM for more than 1 year. Prior to FMT, the patient required insulin in combination with oral hypoglycemic agents for glycemic control. Under pharmacological treatment, FBG and 2HPG were moderately controlled with a small fluctuation range. The first FMT for this patient was performed by transnasal fecal tube injection of 200 ml of precisely matched bacteriological solution provided by the South China Bacterial Bank, while the second and third FMTs were subsequently performed at the sixth and eighth week after the first transplantation by oral administration of bacteriological solution capsules. Several serum and fecal

TABLE 1 Inclusion and Exclusion criteria for subjects.

Inclusion criteria	Exclusion criteria
1 Have detectable production of autoantibodies that cause impaired islet cell function (ICA or/and IAA or/and GAD antibody positive); 2. after stable glycemic control with intensive insulin therapy, islet function C peptide release levels assessed under stimulation of a mixed diet remain below normal or lower limit of detection; 3. any gender; 4.any age (patients older than 18 years old should voluntarily participate in the trial and have good compliance; 5. younger than 18 years old should obtain informed consent from one and, if necessary, both guardians and have good compliance); 6. any body mass index; and 7. must be able to cooperate with the follow-up of the study team.	1. combination of acute and chronic infectious diseases, gastrofecal diseases, severe cardiac insufficiency, severe hepatic and renal insufficiency, leukopenia or leukopenia, autoimmune disease manifestations or previous diagnosis of autoimmune disease in the past three months, other diseases or complications; 2. other gastrofecal diseases that may affect drug absorption; 3. pregnant and lactating women; 4. patients treated with other hormones or antibiotics in the past three months; 5. new onset of cardiovascular disease within the last three months; and 6. participated in other clinical trials during the same period.

samples were collected, and a 30-week clinical follow-up was performed.

Patient 2 was a 12-year-old male patient diagnosed with T1DM for 1 year. He was 1.51 m tall, weighed 31 kg, and had a BMI of 13.8 kg/m2. We performed two fecal microbiota transplants in the form of oral liquid capsules on 29 July 29 and 2 August 2021, during which multiple serum and stool samples were collected from the patient and a 10-week clinical follow-up was performed. Prior to the microbiota transplantation, the blood glucose of the patient was controlled with insulin and oral hypoglycemic agents, with FBG fluctuating from 7 to 8 mmol/L and 2 HPG fluctuating from 12 to 21 mmol/L. The usual self-life management of the patient was poor, with a wide range of blood glucose fluctuations.

Fecal donor recruitment, randomization, and FMT procedures

Healthy individuals after a comprehensive screening (20) were accepted as donors for fecal microbiota transplantation, and patients meeting the inclusion criteria were designated as recipients. Subjects received the same diet and exercise controls. The dietary principles of both diabetic patients were low salt, low fat, and light during the transplantation period. The two patients followed the guidelines of waiting for 1 h to exercise after meals, with an exercise time of 30 min a day and regular exercise and daily activities for five days a week. Diabetes-related indicators and inflammatory factors were recorded and evaluated before starting treatment (see Table 1). In a study of FMT for intestinal inflammatory diseases (10, 21, 22), it was found that FMT at weeks 1, 6, and 8 could significantly improve the composition of intestinal microbiota, endoscopic disease severity index, and inflammatory index, and frequent intensive regimens were effective (23, 24). Therefore, we chose to give patients three rounds of transplantation at the time points of day 1, week 6, and week 8. Among the two patients included in our study, one patient completed the transplantation at all-time points, and the other patient only completed one round of flora transplantation because of the problem of compatibility. Patient 1 received three fecal microbiota transplants on day 1, week 6, and week 8 of the experiment by one nasal fecal tube injection and two oral capsules, respectively. Patient 2 received two fecal microbiota transplants by oral capsules on days 1 and 4 of the experiment. Both patients were evaluated by collecting stool specimens after each microbiota transplant.

Clinical indicators and relevant laboratory methods applied

Blood (5 ml) was drawn from the elbow vein of the subject before treatment and at the corresponding clinical node after each fecal microbiota transplant treatment in the early morning on an empty stomach, and the samples were collected and centrifuged at 3,000 rpm, and the serum was separated. Fasting glucose (FBG), 2-hour postprandial glucose (2HPG), 2-hour postprandial insulin (2INS), fasting insulin (FINS), fasting C-peptide (FCP), 2-hour postprandial C-peptide (2HCP), white blood cell (WBC), blood sedimentation (ESR), C-reactive protein (CRP), calcitoninogen (PCT), biochemical index, and steady-state model, which included insulin resistance index (Homa IR) and islet cell function index (HOMA-HBCI), where Homa IR = (FINS × FPG)/22.5 and HOMA-HBCI = 20 × FINS/(FPG − 3.5)), glycated hemoglobin was measured by ELISA. Data are expressed as mean values ± standard deviation. Unpaired Student's t-test for categorical variables was applied for comparison between before and after FMT. Results with a two-tailed p-value of <0.05 were considered significant. IBM SPSS Statistics 25 was used for clinical index analyses.

Simultaneously, stool specimens were collected at different time points after each microbiota transplantation treatment. Then the stool specimens were stored in a microbiota stabilizer, EffcGut (25) until DNA extraction. Fecal genomic DNA was extracted using the QIAamp Fast DNA Stool Mini Kit (Qiagen, CA, USA). DNA samples were fragmented to an insert size of 400 bp for library preparation and sequenced by Illumina Nova seq with PE 150 reagents. Raw reads were detected as

having good sequencing quality by FastQC (http://www.bioinformatics.bbsrc.ac.uk/projects/fastqc/) with default parameters. Then reads were trimmed to filter the sequencing adapter, low-quality reads, and the human genome (based on reference hg18) using Trimmomatic and Bowtie2 with default parameters (26, 27).The microbial taxonomic composition at genus, species, and strain levels was processed using default parameters (25). The metagenome sequencing was used to: 1) compare and analyze the alpha diversity (including the abundance (ACE, Chao1, and observed species), diversity (Shannon index and Simpson index), homogeneity (J), and beta diversity of the fecal microbiota of each patient before and after transplantation, the latter transplantation compared with the previous transplantation, and the later long clinical follow-up; 2) compare and analyze the microbiota with the same trend at the species and genus levels for both patients after fecal microbiota transplantation; and 3) make an analysis of blood glucose related indexes and fecal microbiota correlation at the species and genus levels. These analyses were performed using R v3.4.1 (28) and the main R packages were ggplot2 (v3.3.5) (29) and vegan (2.5–7) (30).

Results

Adjustment of drug regimen and changes in serum indices before and after transplantation in two patients

Patient 1: During the transplantation process and the later clinical follow-up, our observation indicators were annotated as follows:

Adjustment of medication regimen. Within one week after the completion of the first FMT, the patient had stopped taking insulin as well as oral hypoglycemic drugs, and no additional hypoglycemic drugs were added during the subsequent FMT and clinical follow-up. Until the end of the follow-up period, the FBG and 2HPG of the patient did not fluctuate significantly and were not significantly different from those under insulin control before transplantation, so FMT brought beneficial changes to the patient (Figure 1).

Blood glucose-related indices. As shown in Figure 1, the FBG and 2HPG of the patient had a large decrease after the first FMT and after each subsequent FMT. After each FMT, FBG and

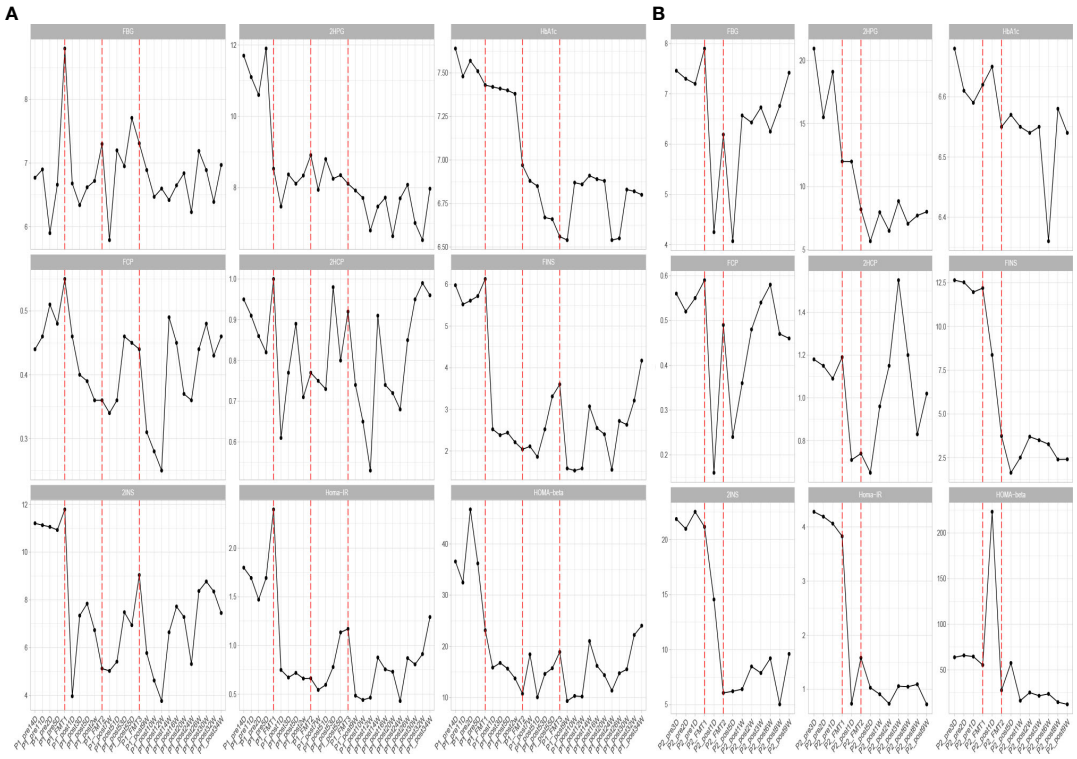

FIGURE 1
Changes in blood glucose before and after transplantation in Patients 1 **(A)** and 2 **(B)**. FBG, fasting blood glucose; 2HPG, 2-hour postprandial blood glucose; HbA1c, glycated hemoglobin; FCP, fasting C-peptide; 2HCP, 2-hour postprandial C-peptide; FINS, fasting insulin; 2INS, 2-hour postprandial insulin; Homa-IR, insulin resistance index; HOMA, islet cell function index. The horizontal coordinates in the figure indicate the different time points before and after transplantation. The vertical coordinates are the corresponding values of glucose-related clinical indicators at different time points.

2HPG decreased, though the decrease was smaller than the first one. Three days after each transplant, the trend of blood glucose fluctuation gradually stabilized, and based on the discontinuation of hypoglycemic drugs, the overall blood glucose of the patient showed a trend of first decrease and then stable change. As shown in Table 2 (Patient 1 blood glucose index), the FBG of the patient after treatment (6.77 ± 0.44 mmol/L) was lower than that before treatment (7.01 ± 1.08 mmol/L), p = 0.056, though this was not statistically significant. However, the 2HPG of the patient was significantly lower after treatment (7.82 ± 0.65 mmol/L after compared to 10.77 ± 1.35 mmol/L before), p = 0.076, though this was not statistically significant. Given that the patient discontinued all hypoglycemic agents, including insulin, after the fecal microbiota transplants, FMT was beneficial to the patient. The glycosylated hemoglobin of the patient decreased to a certain extent after each transplantation, and after about 2 weeks after the completion of all transplants, the glycosylated hemoglobin increased slightly and then stabilized, but the overall level still showed a decreasing trend (Table 2). The mean glycated hemoglobin was significantly better controlled in the patient after transplantation (Table 2). As seen in Figure 1, the C-peptide and insulin secretion levels of the patients showed a decreasing trend after each transplantation, while C-peptide and insulin levels showed an increasing trend about 3 months after the completion of transplantation. Homa-β had a substantial decrease after the first transplantation, which was mainly caused by the discontinuation of exogenous insulin. In the later clinical follow-up, there was a small increase in Homa-β, indicating an upward trend in the own islet secretion function of the patient. Homa-IR decreased substantially to normal (<1) after the first transplantation, and then fluctuated within a small range, but at the follow-up of the 30th week, Homa-IR had increased again to >1. The C-peptide, insulin secretion index, and Homa-IR in the patient were reduced after transplantation compared with those before transplantation (Table 2). This was mainly due to the presence of a large amount of exogenous insulin in the body of the patient before FMT interfered with the before-and-after comparison of these clinical indicators. There is no washout period in this study because insulin withdrawal in type 1 diabetes will lead to a significant increase in blood glucose and may lead to diabetic ketosis or even diabetic ketoacidosis. The patient was observed after FMT and discontinuation of exogenous insulin treatment. The Homa-IR, the index of insulin resistance, was calculated. We found that the value of Homa-IR fluctuated within the normal range (0.75 ± 0.24, <1) after transplantation, and that the insulin resistance of this patient improved obviously, though this was not statistically significant.

Inflammatory indexes. Before FMT, the inflammatory indices such as CRP, WBC, and ESR of the patient were within the normal range, while calcitonin indices were outside the normal range (Figure 2). Some studies have found that inflammatory responses unrelated to infection exist in type 1 diabetic patients, which may be due to an autoimmune disorder (15). After the initial transplantation, the leukocytes in the patient showed an acute increase to 21.2 × 109/L on the first day after transplantation (Table 2), and then decreased to normal after 2 days, while the rest of the inflammatory indices did not change. We considered that the rise of leukocyte indices might be related to the immune response triggered by the initial exposure to the transplanted microbiota in the body of the patient. Likely, the immune system of the patient had already adapted to the implantation of foreign microbiota, and this finding was beneficial for the progress of microbiota transplantation treatment. In the biochemical indices of the patient, these values always fluctuated within the normal range (Figure 3). The biochemical indices of the patient were normal before and after the treatment. These findings suggest that fecal microbiota transplants will not adversely affect the liver and kidneys of the patient.

TABLE 2 Mean values of blood glucose and insulin indexes plus or minus standard deviation at each time point before and after treatment of Patients 1 and 2.

Group	FBG mmol/L	2HPG mmol/L	HbA1c (%)	FCP ng/ml	2HCP ng/ml	FINS mU/L	2INS mU/L	Homa-IR	Homa-β
Patient1 Before fmt	7.01 ± 1.08	10.77 ± 1.35	7.53 ± 0.08	0.49 ± 0.04	0.91 ± 0.07	5.79 ± 0.26	11.22 ± 0.33	1.81 ± 0.35	35.03 ± 8.5
Patient1 After fmt	6.77 ± 0.44	7.82 ± 0.65	6.89 ± 0.29	0.40 ± 0.07	0.79 ± 0.13	2.48 ± 0.71	6.62 ± 1.58	0.75 ± 0.24	15.22 ± 4.11
P value	0.056	0.076	0.126	0.173	0.118	0.137	0.006	0.49	0.115
Patient2 Before fmt	7.47 ± 0.31	16.89 ± 3.96	6.63 ± 0.04	0.56 ± 0.03	1.15 ± 0.04	12.33 ± 0.31	21.64 ± 0.71	4.09 ± 0.2	62.45 ± 4.77
Patient2 After fmt	6.08 ± 1.08	7.90 ± 1.71	6.55 ± 0.07	0.43 ± 0.13	0.99 ± 0.27	3.39 ± 1.88	8.27 ± 2.70	0.97 ± 0.26	44.02 ± 64.24
P-value	0.16	0.026	0.72	0.052	0.047	0.246	0.184	0.619	0.195

FBG, Fasting glucose; 2HPG, 2-hour postprandial glucose; HbA1c, glycated hemoglobin; FCP, fasting C-peptide; 2HCP, 2-hour postprandial C-peptide; FINS, fasting insulin; 2INS, 2-hour postprandial insulin; pre-treatment and post-treatment values were given as mean plus or minus standard deviation; statistical analysis was performed using independent sample t-test with a significance level of p <0.05.

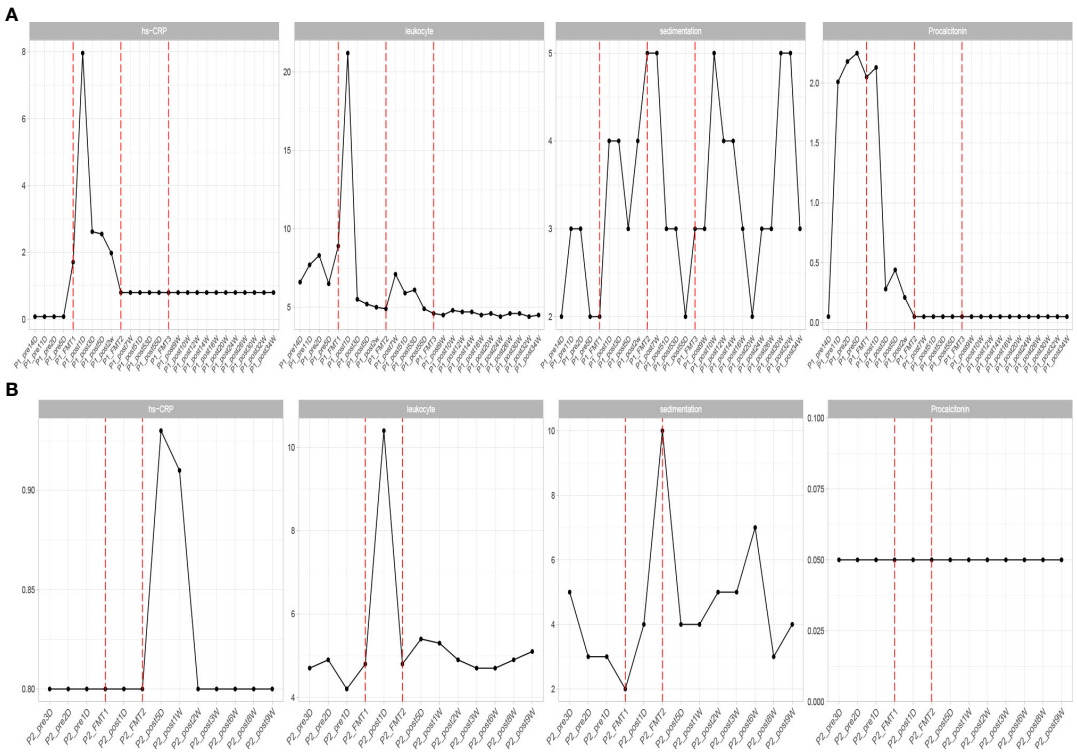

FIGURE 2
Changes in inflammatory indexes in patients before and after transplantation in Patients 1 **(A)** and 2 **(B)**. hs-CRP, C-reactive protein; leukocyte, white blood cells; sedimentation, blood sedimentation; Procalcitonin, calcitonin.

Patient 2: Our observation indices were as follows:

Adjustment of medication. After the first FMT, the patient stopped the use of insulin and only took the oral hypoglycemic drug Repaglinide ligliptin. In the later clinical follow-up, the patient did not use insulin again, and the use of hypoglycemic drugs was as before.

Glycemic indices. The FBG of the patient fluctuated from 8 to 8 mmol/L and 2HPG fluctuated from 12 to 21 mmol/L (Figure 1). The FBG of the patient decreased after each transplant, with a larger decrease after the first transplant, and it rose again 1–2 weeks after completing the transplant, and then maintained at the impaired fasting glucose level (6–7 mmol/L) fluctuation, compared with the better improvement of the 2HPG of the patient (Figure 1). In contrast, the 2HPG of this patient improved, with some decrease in 2HPG after each transplantation and small fluctuations in 2HPG within the normal range after completion of transplantation and during the later clinical follow-up. As shown in Table 2, the post-treatment fasting glucose value (6.08 ± 1.08 mmol/L) of the patient was significantly lower than the pre-treatment fasting glucose value (7.47 ± 0.31 mmol/L) ($p = 0.16$). The post-treatment 2-hour postprandial glucose (7.90 ± 1.71 mmol/L) of the patient was also significantly lower than the pre-treatment 2-hour postprandial glucose (16.89 ± 3.96 mmol/L). As shown in Figure 1, the glycosylated hemoglobin of the patient decreased slightly after each transplantation and remained stable after the completion of transplantation. The glycosylated hemoglobin level after fecal microbiota transplants (6.55 ± 0.07%) of the patient was not significantly different from before fecal microbiota transplants (6.63 ± 0.04%). The C-peptide of the patient decreased after both transplants, and after a large increase, FCP remained basically stable, while 2HCP fluctuated in a wide range. The insulin index of the patient had a large decrease after the first fecal microbiota transplant. The change was related to the discontinuation of insulin, and then fluctuated at a lower level. In the later clinical follow-up, FINS and 2IS had a small upward trend. Homa-β decreased significantly after the first microbiota transplantation and remained stable afterwards. Homa-IR also decreased after the first microbiota transplantation and remained normal afterwards (0.97 ± 0.26), suggesting that the insulin resistance of this patient was greatly improved (Table 2).

Inflammatory indices: the inflammatory indices of the patient, such as C-reactive protein, blood leukocytes, and sedimentation, were within normal limits (Figure 2). As in the previous experimental cases, on the first day after the first

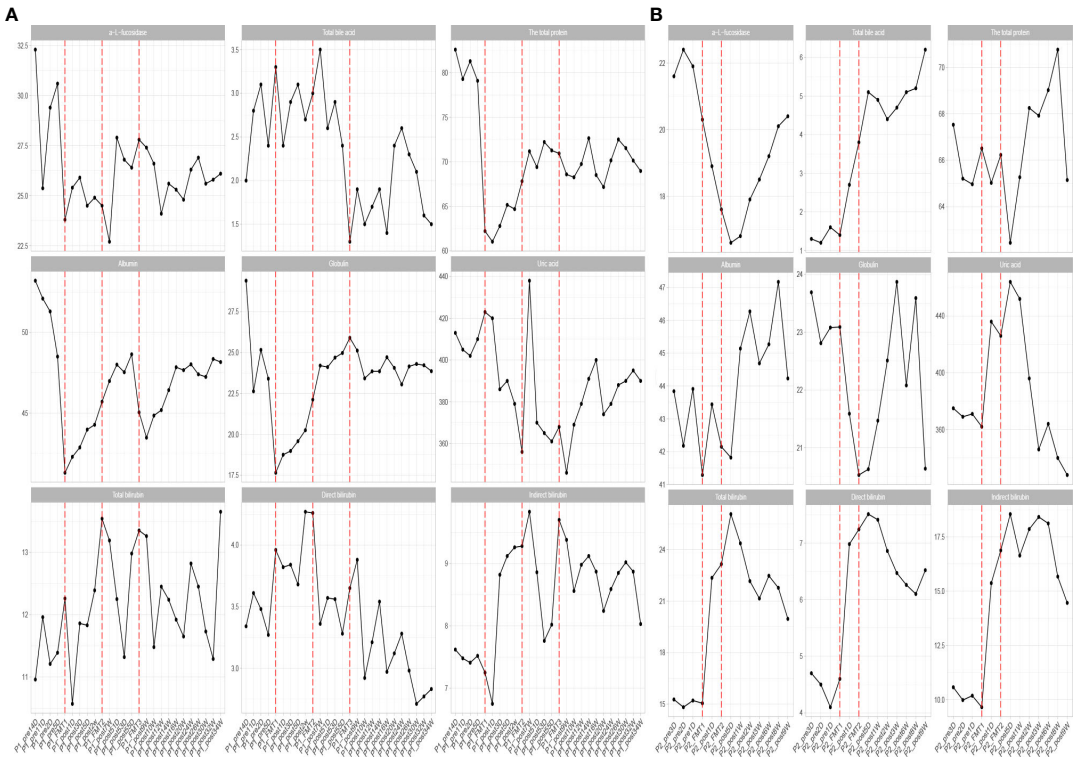

FIGURE 3
Changes in biochemical parameters before and after transplantation in Patients 1 **(A)** and 2 **(B)**. The horizontal coordinates in the graph indicate the different time points before and after the transplantation of the patient. The verticalcoordinates are the corresponding values of biochemical related indexes at different time points.

transplantation, the patient showed an abnormal increase in leukocytes that was not accompanied by an increase in other inflammatory indices, and after 2 days the leukocyte index decreased to normal, and after the second fecal microbiota transplantation there was no abnormal increase in leukocytes. This phenomenon is consistent with our previous conjecture that the initial input of transplanted microbiota induces a transient inflammatory reaction in the patient, who will adapt to the transplanted microbiota and the inflammatory index will gradually decrease to normal. The subsequent transplantation of microbiota did increase the inflammatory index of the patient.

Biochemical indices: The biochemical indices of the patient before and after treatment were both normal (Figure 3), which suggested that the microbiota transplantation did not have adverse effects on the liver, kidneys, and other organs of the patient. In addition to this, both patients had no adverse effects after FMT.

The clinical outcomes of the two patients after transplantation showed that both patients had fair glycemic control during transplantation and later clinical follow-up based on discontinuation of all hypoglycemic agents and discontinuation of insulin, respectively, which indicates the effectiveness of FMT on glycemic control in T1DM and that this effectiveness can be maintained, which is consistent with the study by Mokhtari et al. (18); patients with T1DM who underwent fecal microbiota transplants effectively prolonged the function of residual beta cells. FMT significantly improved insulin resistance in both patients, which provides strong evidence for us to conduct more fecal microbiota transplants for T1DM in the future. The postprandial glucose fluctuation range of Patient 1 was smaller, and the improvement of insulin resistance was more obvious, which may be caused by the following reasons: 1) Patient 1 had more transplants than Patient 2, and the interval was longer, so the multiple transplants with a slightly longer interval may have a "strengthening" effect in improving blood glucose; 2) Patient 1 usually had better personal dietary management than Patient 2.

Analysis of gut microbiota in two patients after transplantation

The altered microbial diversity of patients 1 and 2 is shown in Figure 4. Then, alpha-diversity analysis was used to analyze the complexity of microbial community composition within the samples, including the richness (ACE, Chao1, and observed

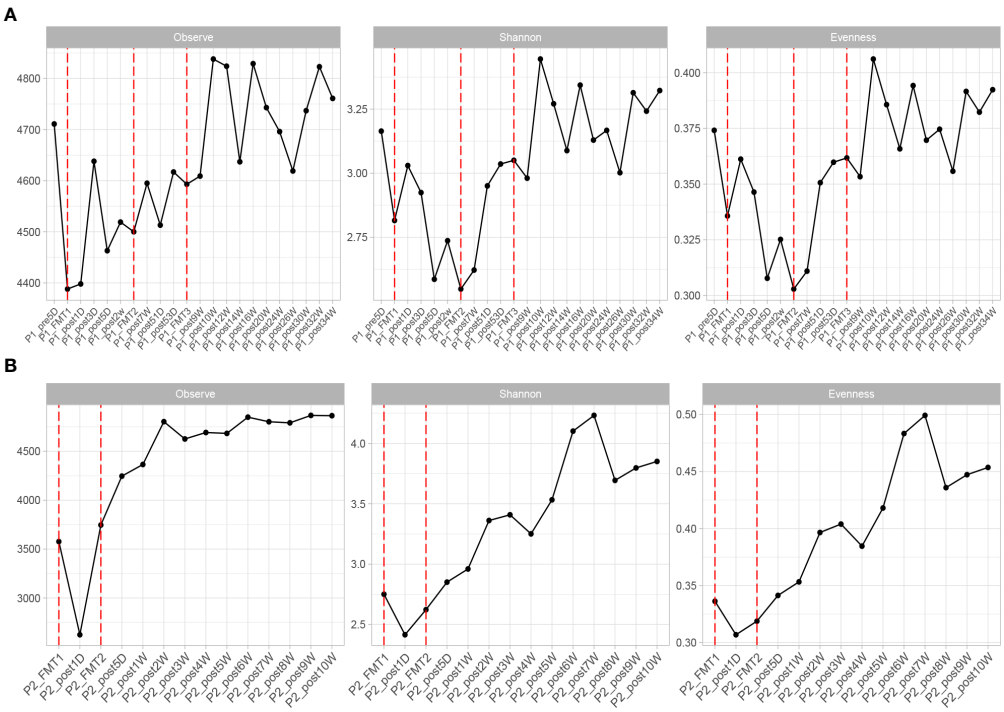

FIGURE 4
Changes in microbial diversity after transplantation in Patient 1 **(A)** and 2 **(B)**, including: Observe, Shannon, and Evenness index.

species), diversity (Shannon and Simpson), and evenness (J) of the microbial community within the sample. The ACE, Chao1, observed species, Shannon and Simpson, and J indices of the fecal microbiota of Patient 2 showed an increasing trend after both transplants and stabilized at 16 days after transplantation, as shown in Figure 4.

The change in microbial diversity in patient 1 and patient 2 is shown in Figure 4. The ACE, Chao1, and observed species indices showed increasing and stabilizing trends. The Shannon and Simpson and J indices fluctuated after the first transplant, but also showed an increasing and stabilizing trend after the second and third transplant. The overall microbial structure changed after FMT and tended to stabilize over time (Figure 5 and Figure S1). Diversity improved with the first, second, and third transplants.

By high-throughput sequencing, we identified microbes that changed consistently after the transplantation of Patients 1 and 2. Both species level and genus level were included. At the species level (Figure 6), the bacteria that increased in both patients after transplantation were Alistipes sp. Marseille-P5997, Bacteroides cellulosilyticus, A. finegoldii, A. shahii, B. caccae, B. thetaiotaomicron, Blautia sp. SC05B48, and Lachnospiraceae bacterium GAM79. The genera (Figure 7) that both increased after transplantation were Butyricimonas, Alistipes, and Parabacteroides, and those that both decreased were Escherichia and Odoribacter.

Additionally, we performed correlation analysis between characteristic bacteria and clinical indicators at the genus level and species level. The correlation analysis of blood glucose related indicators and fecal microbiota at the genus level is shown in Figure 8-1. It can be found that the genera with a significant negative correlation with HOMA-beta are Faecalibacterium and Butyricimonas. Homa-IR was significantly negatively correlated with Butyricimonas and Phascolarctobacterium. 2HCP is significantly positively correlated with Streptococcus and Blautia. 2HCP was significantly negatively correlated with Phascolarctobacterium and Paraprevotella. Fasting C-peptide and Streptococcus were significantly positively correlated.

The correlation analysis of blood glucose related indexes and fecal microbiota at the species level is shown in Figure 8-2, and it can be found that HOMA-beta and L. bacterium GAM79 and B. caeccae were positively correlated, while B. salanitronis and F. prausnitzii were negatively correlated. The bacteria that showed a significant positive correlation with Homa-IR were B. ovatus. L. bacterium GAM79 and 2INS showed a significant positive correlation. L. bacterium GAM79, Ruminococcus. gnavus, L. bacterium Choco8, A. shahii, and B. ovatus were significantly

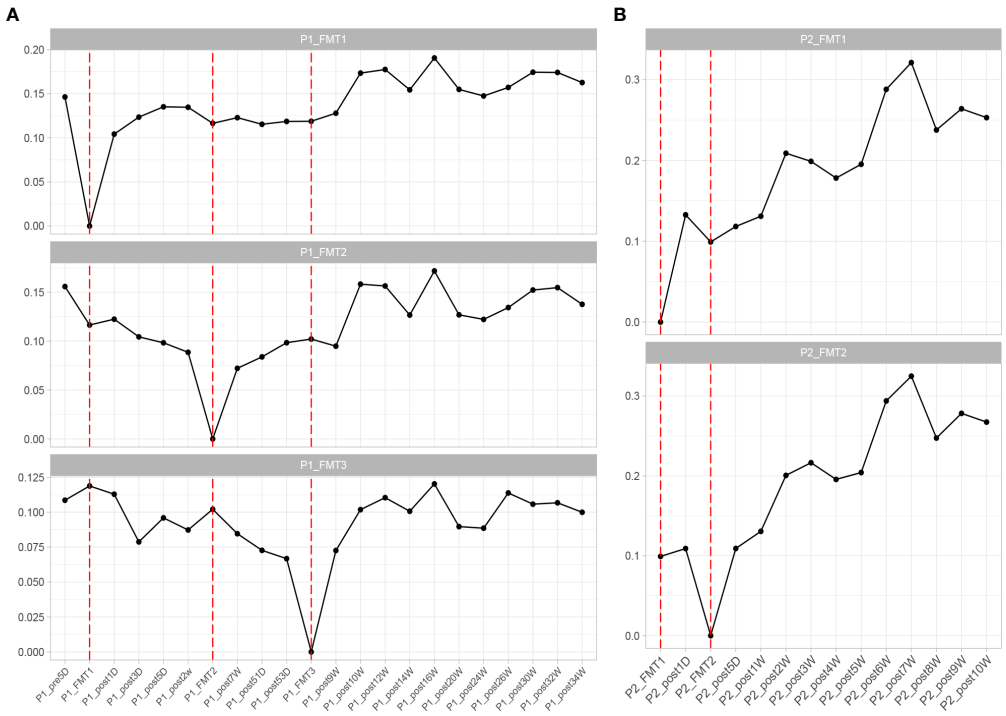

FIGURE 5
Changes in overall microbial composition of Patient 1 **(A)** and Patient 2 **(B)** after each transplant, measured by Bray–Curtis distance.

positively correlated with 2HCP. P. succinatutens, P. faecium, and 2HCP were significantly negatively correlated. L. bacterium GAM79, Clostridium boleae, and B. caccae were significantly and negatively correlated with FBG. The correlation analysis between other clinical indicators and fecal microbiota was positive for A. finegoldii and ALP, total bile acid, and cystatin.

The correlation analysis of clinical indicators and microbiota at genus and species levels indicates that improvement of clinical indicators is associated with altered microbiota diversity.

Discussion

T1DM is a metabolic disease characterized by insulin deficiency and disorders of glucose metabolism caused by autoimmune-mediated selective islet beta cell damage (34). The association between gut microbiota and autoimmune diseases is well known. Disruption of the microbiome microbiota balance can induce autoimmune diseases in people with certain genetic backgrounds and environmental factors (31). Many studies have found that dysbiosis is also involved in the pathogenesis of T1DM. In a Chinese study, children with T1 diabetes had a lower abundance of microbiota in stool samples compared to healthy controls, particularly the newly isolated gram-positive and butyric acid-producing anaerobic bacterium Inestinimonas (3). In contrast, increased glaucoma was found in these patients. In addition, early supplementation with probiotics has been shown to reduce the risk of islet autoimmunity in children at higher genetic risk for T1DM in a multicenter prospective cohort study (32). This means that the pathogenesis and development of T1D is driven by a combination of genetic susceptibility and environmental factors. The gut microbiota is one of the potential environmental influences involved in the pathophysiological processes of T1DM. Gut microbes mediate the development of diabetes by altering fecal permeability and modulating fecal immunity and molecular mimicry. Compared to healthy individuals, T1DM patients have significantly altered gut microbial diversity, taxonomic profile, and functional potential (33). In this study, two patients with T1DM received FMT, and after transplantation, both patients showed significant improvement in diabetes-related clinical indicators. Moreover, the diversity and abundance of fecal microbiota increased relative to pre-transplantation. Our study also found a correlation between the improvement of some clinical indicators of diabetes and the change of fecal microbiota and identified the genus and species of bacteria that increased and decreased in both patients after transplantation. Identification of the role of related bacteria in the development and progression of T1DM can help guide early screening and diagnosis of T1DM

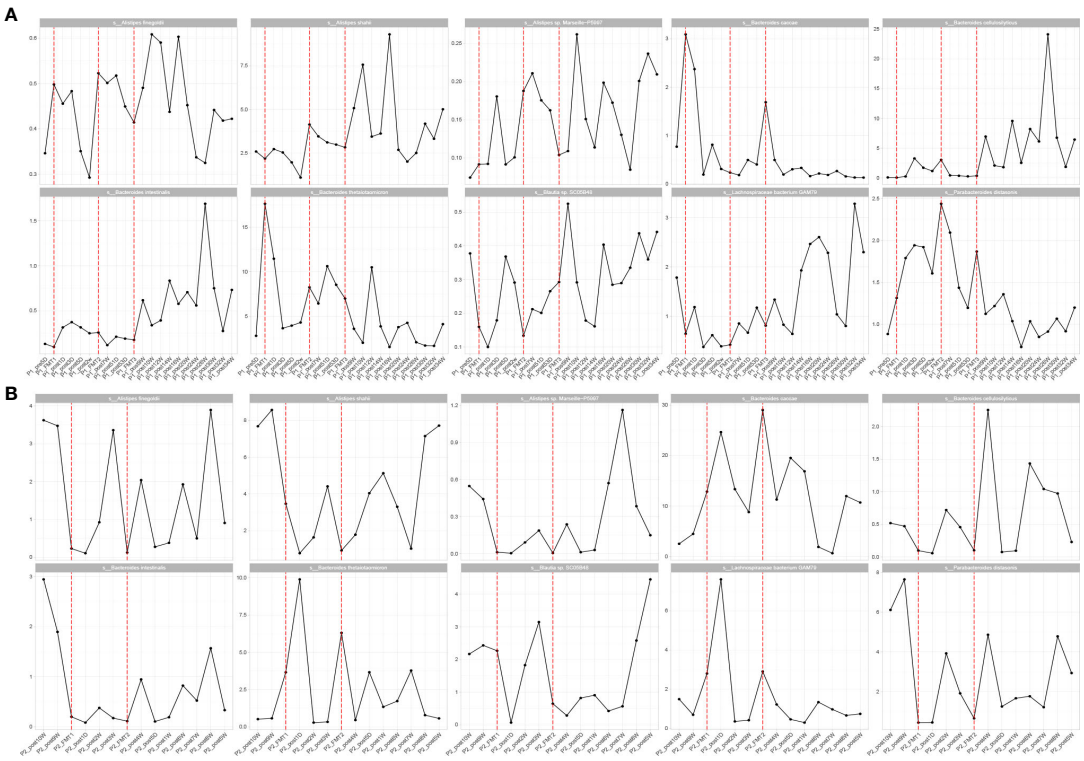

FIGURE 6
Patients 1 **(A)** and 2 **(B)** transplanted with consistent changes in microbial species level.

and the development of new target therapies for T1DM based on microecological reconstruction.

The bacteria that were reduced at the species level in both patients after transplantation were A. caccae, B. thetaiotaomicron, Blautia sp. SC05B48, and L. bacterium GAM79. A. caccae is a ubiquitous anaerobic bacterium. Patients with diabetes are at an increased risk of anaerobic infections. It has been shown that L. bacterium is a fecal conditionally pathogenic bacterium. It can invade the fecal mucosa and cause various abdominal septic infections (35). This study shows that the abundance of A. caccae can be reduced by microbiota transplantation, which also reduces the risk of A. caccae infection in diabetic patients. B. thetaiotaomicron has two key aspects in the human fecal symbiotic lifestyle: extensive digestion of dietary fiber and host polysaccharides, and dynamic cell surface structures that promote interaction and evasion with the host immune system. Like other fermentative gut microbes, polymorphic bacilli produce host-absorbable short chains and organic acids, both of which can be absorbed by the host as energy sources. The L. bacterium GAM79 decreased after transplantation in the two patients. The presence of lipopolysaccharide (LPS) in the intestine is necessary but insufficient for developing diabetes. The investigators hypothesized that Trichophyton spp. AJ110941 may help translocate LPS from the intestine to the bloodstream. It has been proposed that colonization by AJ110941 may promote pancreatic β-cell dysfunction. Trichoderma spp. AJ110941 may be one of the important pathogenic bacteria of T2DM (36). Our study concluded that the abundance of L. bacterium GAM79 could be reduced by fecal microbiota transplants, which may be beneficial for diabetic patients.

The genera with increased levels in both patients after transplantation were Vibrio butyricus, Vibrio aliens, and Vibrio parapsilosis. V. butyric acid generates butyric acid by fermenting glucose, which in turn synthesizes short-chain fatty acids that protect the structural and functional stability of the fecal epithelium and act to inhibit inflammation. The presence of V. butyricus spp. enhances fecal immunity, broad-spectrum antibacterial, and inhibits inflammatory responses. Children with T1DM have dysbiosis of the fecal microbiota and small numbers of P. aeruginosa and V. butyricus spp (37). In the case report of this study, both type 1 diabetic patients had an increase in V. butyricus spp. after microbiota transplantation, which is beneficial for type 1 diabetic patients. Both patients also had an increase in V. paraquaternus spp. after transplantation. Previously, the metabolic benefit of Dictyostelium paraquaternum was observed in reducing hyperglycemia in T1DM rats (38, 39). Treatment with Dictyostelium parapsilosis significantly altered the bile acid

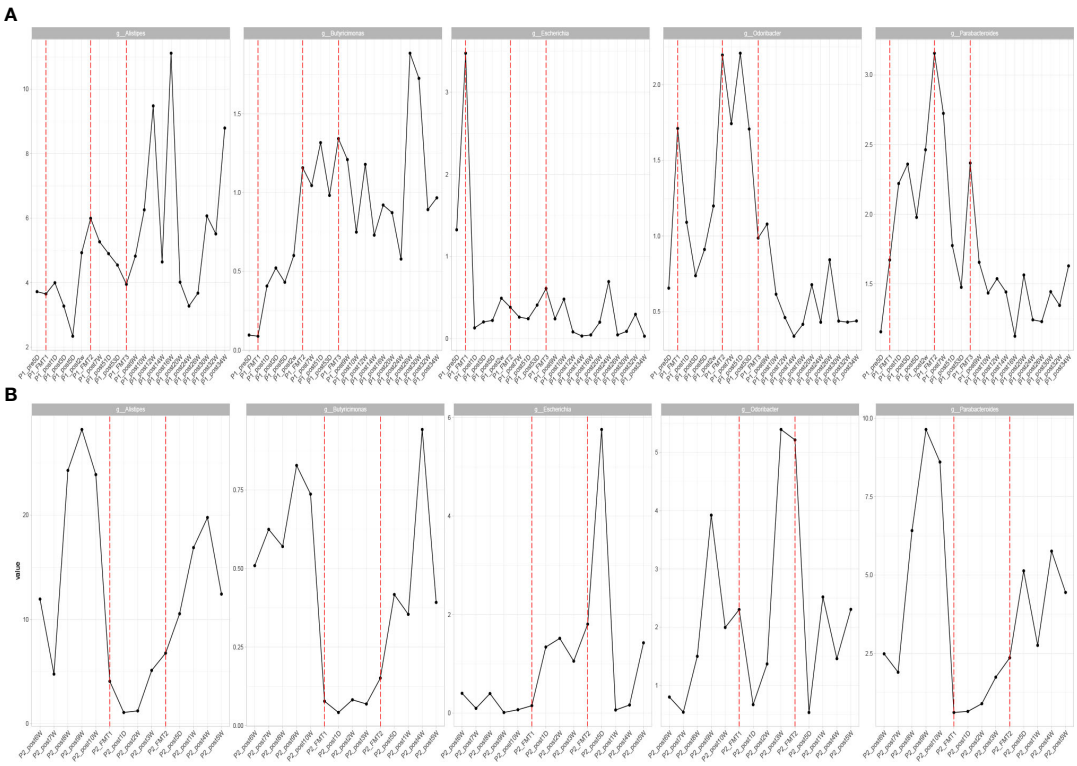

FIGURE 7
Patients with consistent changes in genus level after transplantation in Patient 1 **(A)** and Patient 2 **(B)**.

profile with elevated lithodeoxycholic acid and ursodeoxycholic acid and increased fecal succinic acid levels. In vitro cultures of D. parapsilosis have demonstrated its ability to convert bile acids and produce succinate. Supplementation with succinate in the diet reduced hyperglycemia in obese mice by activating fecal gluconeogenesis. This means that the bacterium reduces obesity and metabolic disorders by producing succinate and secondary bile acids (40). The genera in which the levels in both patients decreased after transplantation are Ehrlichia spp. and Bacillus odoratum spp. Ehrlichia spp. are pathogenic under normal microbiota conditions and can also cause many diseases, with urinary tract infections being common (12). It has been shown that butyric acid producing bacteria and Streptococcus spp. are reduced and Escherichia spp. are increased in diabetic patients compared with healthy individuals (14). Ehrlichia spp. can be reduced by microbiota transplantation. This is beneficial for patients with T1DM.

After transplantation, changes were found in common between the microbiota of both patients. Both showed an increase in B. cellulosilyticus, which plays an important role in the degradation of cellulose in the human microbiota. Cellulose is a polysaccharide found in plant cell walls and is an important source of dietary fiber. Most bacteria in the human gut are unable to break down plant polysaccharides, and B. cellulosilyticus is the star strain for studying the molecular mechanisms of metabolism of complex plant polysaccharides in fecal microbes (41). Of note, the risk of diabetes is two times higher in people who eat high-fat, low-fiber foods than in people who eat low-fat, high-fiber foods, which shows that dietary fiber has a significant effect on reducing the risk of diabetes (42). The abundance of A. shahil also increased in both patients after transplantation. In patients with compensated and decompensated cirrhosis, fresh fecal metagenome sequences from healthy volunteers and patients with various types of cirrhosis showed a reduction in A. shahil compared to healthy controls (43). In addition, a study conducted in mice with liver cancer showed the potential anti-inflammatory effects of healthy probiotics. Alistipes increased in abundance in the group of mice receiving probiotics. At the species level, A. shahil was shown to be significantly increased in the probiotic group. Some investigators speculate that A. shahil plays a role in tumor suppression like that seen in cancer immunotherapy (44). D. parapsilosis was elevated in both patients after transplantation, the correlation analysis (11) showed that Parabacteroides distasonis is one of the core species in the human microbiota, and its level significantly negatively correlates with disease states

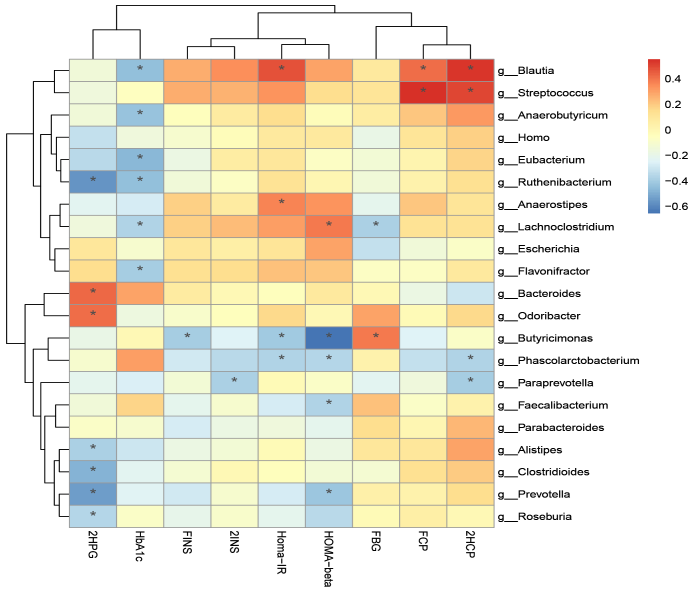

FIGURE 8-1
Correlation analysis of clinical indicators and genus level difference bacteria after transplantation in Patients 1 and 2 *P-value <0.05.

such as obesity, NAFLD, and diabetes, suggesting that it may play a positive regulatory role in glucolipid metabolism. This is consistent with our study, in which D. parapsilosis was elevated in both patients with improved glycemic control after transplantation.

We found a significant negative correlation between the genus Faecalibacterium and HOMA-beta. A. muciniphila and Prevotella faecalis have also been shown to be highly abundant human fecal microorganisms in healthy individuals, and reduced levels are associated with inflammation and altered metabolic processes involved in the development of type 2 diabetes (45). Studies have shown that impaired fecal barrier structure and function has been shown to be an important pathogenic process in type 2 diabetes mellitus (T2DM). Dysbiosis of the fecal microbiota is a key factor in the pathogenesis of the diabetic gut. As the most abundant commensal bacterium, Pseudomonas putida plays an important role in fecal homeostasis. One metabolite of P.

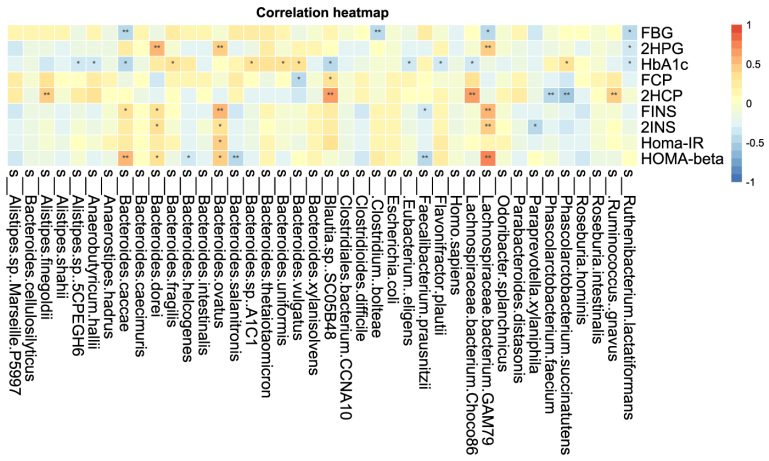

FIGURE 8-2
Correlation analysis of clinical indicators and species level difference bacteria after transplantation in Patients 1 and 2 *P-value <0.05, **P-value <0.01.

procumbens has anti-inflammatory potential in inflammatory bowel disease (46). Butyricimonas and Phascolarctobacterium were significantly negatively correlated with Homa-IR. Children with multiple islet autoantibodies (≥−2IA) or T1DM had dysbiosis of the fecal microbiota with lower amounts of Prevotella and Butyricimonas (39). Although this is an interesting finding, studies and trials with more patients are needed to verify the results and to further understand the correlation and potential mechanism for the improvement of insulin resistance by gut microbes.

2HCP was significantly and positively correlated with Streptococcus and Blautia and was significantly and negatively correlated with Phascolarctobacterium. Fasting C-peptide and Streptococcus were significantly positively correlated. A randomized, placebo-controlled trial of T1DM children aged 8 to 17 years treated with placebo or oligofructose-enriched probiotic inulin for 12 weeks revealed a significant increase in C-peptide levels in the group receiving probiotics at 3 months, accompanied by a mild improvement in fecal permeability. The relative abundance of Bifidobacteria in the probiotic group was significantly increased at 3 months but was no longer present after 3 months of washing. At 3 months, the relative abundance of Streptococcus, Roseburia inulinivorans, Terrisporobacter, and Faecalitalea in the placebo group compared to the probiotic group was significantly higher (47). This is in agreement with our study that the 2-hour postprandial C-peptide (2HCP) is significantly and positively correlated with Streptococcus.

One study reported a significant reduction of Blautia in colorectal cancer patients, with potential probiotic properties such as preventing inflammation and promoting SCFA production and other activities to maintain fecal homeostasis (34). Blautia spp. may optimize glycemic control by increasing tolerance to metformin in diabetic patients (48). AMC showed better results in improving homeostatic model assessment of HOMA-IR and plasma triglycerides and had a greater effect on the gut microbiota, and growing evidence suggests that the composition of the gut microbiota is highly correlated with the outcome of T2DM treatment (49).

It has been demonstrated that ferulose oligosaccharides (FOs) and ferulic acid (FA) reduced symptoms in diabetic rats, and that oligofructose reduced the abundance of Lactobacillus, Rumex, Oscillibacter, and Desulfovibrio, while increasing the abundance of Acinetobacter, Phascolarctobacterium, and Turicibacter (50). A. muciniphila and F. prausnitzii are highly abundant human fecal microorganisms in healthy individuals, and their reduced levels are associated with inflammation and altered metabolic processes, which are involved in the development of type 2 diabetes. A. muciniphila and F. prausnitzii are human fecal microorganisms highly abundant in healthy individuals, and their reduced levels are associated with inflammation and alterations in metabolic processes (45).

Metformin can alter the fecal microbiota in type 2 diabetic patients, and gastrofecal tolerance to metformin may be mediated by fecal microbiota. It was found that the early tolerant group had higher abundance of Subdoligranulum, while the intolerant group had higher levels of Subdoligranulum. The tolerant group exhibited an enrichment of Megalomonas and Streptococcus shortum, with lower levels of ruminal cocci in the longitudinal analysis. At the endpoint, the relative abundance of Megamonas, Megamonas rupellensis, and Phascolarctobacterium spp. R. gnavus was higher in the tolerant group than in the non-tolerant group. The numbers of Megamonas, M. rupellensis, Phascolarctobacterium spp., and R. gnavus were higher in the non-tolerant group. PICRUST analysis showed that the activity of the amino acid biosynthesis pathway was lower, and the sugar degradation pathway was higher in the non-tolerant group (48).

It has also been shown that anthocyanin extracts can modulate fecal microbiota in diabetic patients with a decreased abundance of R. torques and L. bacterium 4_1_37FAA and increased oxidative phosphorylation (51).

There has been a dramatic increase in the incidence of the autoimmune disease T1DM. In addition to genetic susceptibility, environmental factors are thought to play a key role in this increase. As with other autoimmune diseases, the gut microbiome is thought to play a potential role in controlling the progression to T1DM in children at a high genetic risk. It has been shown that a high abundance group consisting of two closely related species (B. dorei and B. vulgatus) was significantly higher in the T1DM group than in the control group. Metagenomic sequencing of samples with higher abundance in the B. dorei/Common Bacteroides group prior to seroconversion and longer 16S rRNA sequencing identified this group as B. dorei. The abundance of B. dorei peaked at 7.6 months, 8 months before the appearance of the first islet autoantibodies, suggesting that early changes in the microbiome may help predict T1D autoimmunity in genetically susceptible infants. The reason for the increased abundance of B. dorei in these cases is unclear, but its timing seems to coincide with the introduction of solid foods (52). This is consistent with the results obtained in our study. B. dorei showed a significant positive correlation with FBG.

In conclusion, we found some characteristic bacteria related to clinical indicators of diabetes. More in-depth studies will need to be performed.

Prospect

Current research on FMT has allowed us to recognize the important role of fecal microbiota in the development of the disease, providing new hope and research basis for the treatment of autoimmune T1DM mellitus by this modality. Many selective and divergent issues still need to be resolved.

About microbiota donor

Whether the microbiota donor should be selected from healthy allogeneic or autologous donors. autoimmune T1DM mellitus by this modality. Many selective and divergent issues still need to be resolved:

1). Whether the microbiota donor should be selected fromhealthy allogeneic or autologous donors.
2). Whether the duration of stool storage affects the therapeutic efficacy of microbiota transplantation.
3). Whether the stool should be stored frozen or freeze-dried.
4). Whether patients need to adjust their own fecal microbiota by adjusting their diet, taking probiotics, prebiotics, or antibiotics before the treatment.
5). Which part of the intestine should be selected for microbiota injection in order to cause less immune rejection and other side effects and better adjust the autoimmune status of the patient. This is necessary because, compared with the small intestine, the large intestine has a larger variety and number of microbes, and the metabolic and immune reactions that occur are more frequent.
6). Whether the length of the treatment period, the number of treatments, and the interval between treatments are closely related to the clinical cure rate of patients.

At present, when patients receive fecal microbiota, the donors are mostly randomized, and the transplantation process is not precise, resulting in low efficiency of microbiota transplantation therapy. Moreover, some microbiota that are not in the demand range of the patient also enter the intestine of the transplanted person, and these microbes may be harmful. The input of harmful bacteria also increases the permeability of the intestine, which requires us to combine the detection of fecal microbiota of patients, analyze the differences in the composition of their fecal microbiota and normal human fecal microbiota, as well as their fecal specific microbiota, beneficial bacteria, harmful bacteria, and other factors.

In addition, there are still many technical problems that need to be solved in FMT. During the process of microbiota transplantation, accidental infections and the input of harmful bacteria will instead reduce the permeability of the fecal mucosa, trigger autoimmune reactions, and accelerate the progress of autoimmune T1DM. It is necessary to improve the development of microbiota injection technology.

Conclusion

Additionally, although the pre-transplant baseline glycemia was not identical between the two patients, we showed that the number of transplants and the time interval between transplants impacted clinical outcomes; multiple transplants at slightly longer intervals may have an “enhancing” effect in terms of glycemic improvement.

Data availability statement

The raw sequencing data supporting the conclusions of this article were deposited in the NCBI Sequence Read Archive (SRA) database under bioproject number PRJNA833152 (https://www.ncbi.nlm.nih.gov/sra/PRJNA833152).

Ethics statement

This study was reviewed and approved by Note: Research ethics number: LHLL2021001, Ethics committee of Longhu People’s Hospital Shantou, China. Written informed consent to participate in this study was provided by the participants’ legal guardian/next of kin. Written informed consent was obtained from the minor(s)’ legal guardian/next of kin for the publication of any potentially identifiable images or data included in this article.

Author contributions

Conceived and designed the study: KH, FC, LH, and BZ. Participated in investigation: RC, SZ, and LH. Performed formal analysis: BK, DZ, ZW, CX, and BC. Curated the data: BZ, FC, and KH. Wrote the manuscript: FC, RC, SZ, and LH. Supervised the study: KH and BZ. All authors listed have made a substantial, direct, and intellectual contribution to the work and approved it for publication.

Funding

This work was supported by grants from the Guangdong Science and Technology Special Fund (No.210629086900260), Longhu People’s Hospital, Shantou, China.

Conflict of interest

Author BC was employed by the Xiamen Treatgut Biotechnology Co., Ltd.

The remaining authors declare that the research was conducted in the absence of any commercial or financial relationships that could be construed as a potential conflict of interest.

The handling editor MZ declared a shared parent affiliation with the authors BZ, CX, and KH at the time of review.

Publisher's note

Supplementary material

The Supplementary Material for this article can be found online at: https://www.frontiersin.org/articles/10.3389/fimmu.2022.930872/full#supplementary-material

SUPPLEMENTARY FIGURE 1
PCA samples from patient1 **(A)** and patient 2 **(B)** shown by changes in the microflora at each time visiting point.

References

1. Blaser MJ. The theory of disappearing microbiota and the epidemics of chronic diseases. *Nat Rev Immunol* (2017) 17(8):461–3. doi: 10.1038/nri.2017.77

2. Ianiro G, Gasbarrini A, Cammarota G. Autologous faecal microbiota transplantation for type 1 diabetes: a potential mindshift in therapeutic microbiome manipulation? *Gut* (2021) 70(1):2–3. doi: 10.1136/gutjnl-2020-323252

3. Qi CJ, Zhang Q, Yu M, Xu JP, Zheng J, Wang T, et al. Imbalance of Fecal Microbiota at Newly Diagnosed Type 1 Diabetes in Chinese Children. *Chin Med J* (2016) 129(11):1298–304. doi: 10.4103/0366-6999.182841

4. Bulgart HR, Neczypor EW, Wold LE, Mackos AR. Microbial involvement in Alzheimer disease development and progression. *Mol neurodegeneration* (2020) 15 (1):42. doi: 10.1186/s13024-020-00378-4

5. Li X, Atkinson MA. The role for gut permeability in the pathogenesis of type 1 diabetes–a solid or leaky concept? *Pediatr Diabetes* (2015) 16(7):485–92. doi: 10.1111/pedi.12305

6. Gradisteanu Pircalabioru G, Corcionivoschi N, Gundogdu O, Chifiriuc MC, Marutescu LG, Ispas B, et al. Dysbiosis in the Development of Type I Diabetes and Associated Complications: From Mechanisms to Targeted Gut Microbes Manipulation Therapies. *Int J Mol Sci* (2021) 22(5):2723. doi: 10.3390/ijms22052763

7. El-Salhy M, Casen C, Valeur J, Hausken T, Hatlebakk JG. Responses to faecal microbiota transplantation in female and male patients with irritable bowel syndrome. *World J Gastroenterol* (2021) 27(18):2219–37. doi: 10.3748/wjg.v27.i18.2219

8. Que Y, Cao M, He J, Zhang Q, Chen Q, Yan C, et al. Gut Bacterial Characteristics of Patients With Type 2 Diabetes Mellitus and the Application Potential. *Front Immunol* (2021) 12:722206. doi: 10.3389/fimmu.2021.722206

9. Hou K, Zhang S, Wu Z, Zhu D, Chen F, Lei ZN, et al. Reconstruction of intestinal microecology of Type 2 diabetes by fecal microbiota transplantation: Why and how. *Bosn J Basic Med Sci* (2022) 22(3):315–25.

10. Costello SP, Hughes PA, Waters O, Bryant RV, Vincent AD, Blatchford P, et al. Effect of Fecal Microbiota Transplantation on 8-Week Remission in Patients With Ulcerative Colitis: A Randomized Clinical Trial. *JAMA* (2019) 321(2):156–64. doi: 10.1001/jama.2018.20046

11. Chinna Meyyappan A, Forth E, Wallace CJK, Milev R. Effect of fecal microbiota transplant on symptoms of psychiatric disorders: a systematic review. *BMC Psychiatry* (2020) 20(1):299. doi: 10.21203/rs.3.rs-16542/v1

12. Peng J, Narasimhan S, Marchesi JR, Benson A, Wong FS, Wen L. Long term effect of gut microbiota transfer on diabetes development. *J autoimmunity* (2014) 53:85–94. doi: 10.1016/j.jaut.2014.03.005

13. Hou K, Wu ZX, Chen XY, Wang JQ, Zhang D, Xiao C, et al. Microbiota in health and diseases. *Signal Transduct Target Ther* (2022) 7(1):135. doi: 10.1038/s41392-022-00974-4

14. Robert S, Gysemans C, Takiishi T, Korf H, Spagnuolo I, Sebastiani G, et al. Oral delivery of glutamic acid decarboxylase (GAD)-65 and IL10 by Lactococcus lactis reverses diabetes in recent-onset NOD mice. *Diabetes* (2014) 63(8):2876–87. doi: 10.2337/db13-1236

15. de Groot PF, Nikolic T, Imangaliyev S, Bekkering S, Duinkerken G, Keij FM, et al. Oral butyrate does not affect innate immunity and islet autoimmunity in individuals with longstanding type 1 diabetes: a randomised controlled trial. *Diabetologia* (2020) 63(3):597–610. doi: 10.1007/s00125-019-05073-8

16. Mocanu V, Zhang Z, Deehan EC, Kao DH, Hotte N, Karmali S, et al. Fecal microbial transplantation and fiber supplementation in patients with severe obesity and metabolic syndrome: a randomized double-blind, placebo-controlled phase 2 trial. *Nat Med* (2021) 27(7):1272–9. doi: 10.1038/s41591-021-01399-2

17. Kootte RS, Levin E, Salojarvi J, Smits LP, Hartstra AV, Udayappan SD, et al. Improvement of Insulin Sensitivity after Lean Donor Feces in Metabolic Syndrome Is Driven by Baseline Intestinal Microbiota Composition. *Cell Metab* (2017) 26 (4):611–9 e6. doi: 10.1016/j.cmet.2017.09.008

18. Ng SC, Xu Z, Mak JWY, Yang K, Liu Q, Zuo T, et al. Microbiota engraftment after faecal microbiota transplantation in obese subjects with type 2 diabetes: a 24-week, double-blind, randomised controlled trial. *Gut* (2022) 71 (4):716–23. doi: 10.1136/gutjnl-2020-323617

19. Ianiro G, Maida M, Burisch J, Simonelli C, Hold G, Ventimiglia M, et al. Efficacy of different faecal microbiota transplantation protocols for Clostridium difficile infection: A systematic review and meta-analysis. *United Eur Gastroenterol J* (2018) 6(8):1232–44. doi: 10.1177/2050640618780762

20. He J, He X, Ma Y, Yang L, Fang H, Shang S, et al. A comprehensive approach to stool donor screening for faecal microbiota transplantation in China. *Microbial Cell factories* (2021) 20(1):216. doi: 10.1186/s12934-021-01705-0

21. Sokol H, Landman C, Seksik P, Berard L, Montil M, Nion-Larmurier I, et al. Fecal microbiota transplantation to maintain remission in Crohn's disease: a pilot randomized controlled study. *Microbiome* (2020) 8(1):12. doi: 10.1186/s40168-020-0792-5

22. Rossen NG, Fuentes S, van der Spek MJ, Tijssen JG, Hartman JH, Duflou A, et al. Findings From a Randomized Controlled Trial of Fecal Transplantation for Patients With Ulcerative Colitis. *Gastroenterology* (2015) 149(1):110–8 e4. doi: 10.1053/j.gastro.2015.03.045

23. Paramsothy S, Kamm MA, Kaakoush NO, Walsh AJ, van den Bogaerde J, Samuel D, et al. Multidonor intensive faecal microbiota transplantation for active ulcerative colitis: a randomised placebo-controlled trial. *Lancet* (2017) 389 (10075):1218–28. doi: 10.1016/S0140-6736(17)30182-4

24. Moayyedi P, Surette MG, Kim PT, Libertucci J, Wolfe M, Onischi C, et al. Fecal Microbiota Transplantation Induces Remission in Patients With Active Ulcerative Colitis in a Randomized Controlled Trial. *Gastroenterology* (2015) 149 (1):102–9 e6. doi: 10.1053/j.gastro.2015.04.001

25. Yang L, Hou K, Zhang B, Ouyang C, Lin A, Xu S, et al. Preservation of the fecal samples at ambient temperature for microbiota analysis with a cost-effective and reliable stabilizer EffcGut. *Sci Total Environ* (2020) 741:140423. doi: 10.1016/j.scitotenv.2020.140423

26. Wood DE, Lu J, Langmead B. Improved metagenomic analysis with Kraken 2. *Genome Biol* (2019) 20(1):257. doi: 10.1186/s13059-019-1891-0

27. Bolger AM, Marc L, Bjoern UJB. Trimmomatic: a flexible trimmer for Illumina sequence data. *Bioinformatics* (2014) 15):2114–20. doi: 10.1093/bioinformatics/btu170

28. Null R, Team R, Null R, Writing TC, Null RTeam R. R: A language and environment for statistical computing. *Computing* (2011) 1:12–21.

29. Wickham H, Chang W. Abstracts RJBo. ggplot2: Create Elegant Data Visualisations Using the Grammar of Graphics. (2016).

30. Dixon PJJoVS. VEGAN, a package of R functions for community ecology. *J Veg Sci* (2003) 14(6):927–30.

31. Mokhtari P, Metos J, Anandh Babu PV. Impact of type 1 diabetes on the composition and functional potential of gut microbiome in children and adolescents: Possible mechanisms, current knowledge, and challenges. *Gut Microbes.* (2021) 13(1):1–18. doi: 10.1080/19490976.2021.1926841

32. Dayan CM, Besser REJ, Oram RA, Hagopian W, Vatish M, Bendor-Samuel O, et al. Preventing type 1 diabetes in childhood. *Science* (2021) 373(6554):506–10. doi: 10.1126/science.abi4742

33. De Luca F, Shoenfeld Y. The microbiome in autoimmune diseases. *Clinical and experimental immunology* (2019) 195(1):74–85. doi: 10.1111/cei.13158

34. Uusitalo U, Liu X, Yang J, Aronsson CA, Hummel S, Butterworth M, et al. Association of Early Exposure of Probiotics and Islet Autoimmunity in the TEDDY Study. *JAMA pediatrics* (2016) 170(1):20–8. doi: 10.1001/jamapediatrics.2015.2757

35. Cheng Z, Huang Y, Wie W, Wang Y, Wang Z. Bloodstream Infection Caused by Bacteroides caccae in a Diabetic Patient: a Case Report and Review of the Literature. *Clin Lab* (2019) 65(12). doi: 10.7754/Clin.Lab.2019.190534

36. Kameyama K, Itoh K. Intestinal colonization by a Lachnospiraceae bacterium contributes to the development of diabetes in obese mice. *Microbes environments* (2014) 29(4):427–30. doi: 10.1264/jsme2.ME14054

37. Harbison JE, Roth-Schulze AJ, Giles LC, Tran CD, Ngui KM, Penno MA, et al. Gut microbiome dysbiosis and increased intestinal permeability in children with islet autoimmunity and type 1 diabetes: A prospective cohort study. *Pediatr diabetes* (2019) 20(5):574–83. doi: 10.1111/pedi.12865

38. Ma Q, Li Y, Wang J, Li P, Duan Y, Dai H, et al. Investigation of gut microbiome changes in type 1 diabetic mellitus rats based on high-throughput sequencing. *BioMed Pharmacother* (2020) 124:109873. doi: 10.1016/j.biopha.2020.109873

39. Wang Z, Wang J, Hu J, Chen Y, Dong B, Wang Y. A comparative study of acarbose, vildagliptin and saxagliptin intended for better efficacy and safety on type 2 diabetes mellitus treatment. *Life Sci* (2021) 274:119069. doi: 10.1016/j.lfs.2021.119069

40. Wang K, Liao M, Zhou N, Bao L, Ma K, Zheng Z, et al. Parabacteroides distasonis Alleviates Obesity and Metabolic Dysfunctions *via* Production of Succinate and Secondary Bile Acids. *Cell Rep* (2019) 26(1):222–35.e5. doi: 10.1016/j.celrep.2018.12.028

41. Flint HJ, Bayer EA, Rincon MT, Lamed R, White BA. Polysaccharide utilization by gut bacteria: potential for new insights from genomic analysis. *Nat Rev Microbiol* (2008) 6(2):121–31. doi: 10.1038/nrmicro1817

42. Reynolds AN, Akerman AP, Mann J. Dietary fibre and whole grains in diabetes management: Systematic review and meta-analyses. *PloS Med* (2020) 17 (3):e1003053. doi: 10.1371/journal.pmed.1003053

43. Rau M, Rehman A, Dittrich M, Groen AK, Hermanns HM, Seyfried F, et al. Fecal SCFAs and SCFA-producing bacteria in gut microbiome of human NAFLD as a putative link to systemic T-cell activation and advanced disease. *United Eur Gastroenterol J* (2018) 6(10):1496–507. doi: 10.1177/2050640618804444

44. Iida N, Dzutsev A, Stewart CA, Smith L, Bouladoux N, Weingarten RA, et al. Commensal bacteria control cancer response to therapy by modulating the tumor microenvironment. *Sci (New York NY)* (2013) 342(6161):967–70. doi: 10.1126/science.1240527

45. Verhoog S, Taneri PE, Roa Díaz ZM, Marques-Vidal P, Troup JP, Bally L, et al. Dietary Factors and Modulation of Bacteria Strains of Akkermansia muciniphila and Faecalibacterium prausnitzii: A Systematic Review. *Nutrients* (2019) 11(7). doi: 10.3390/nu11071565

46. Xu J, Liang R, Zhang W, Tian K, Li J, Chen X, et al. Faecalibacterium prausnitzii-derived microbial anti-inflammatory molecule regulates intestinal integrity in diabetes mellitus mice *via* modulating tight junction protein expression. *J diabetes* (2020) 12(3):224–36. doi: 10.1111/1753-0407.12986

47. Ho J, Nicolucci AC, Virtanen H, Schick A, Meddings J, Reimer RA, et al. Effect of Prebiotic on Microbiota, Intestinal Permeability, and Glycemic Control in Children With Type 1 Diabetes. *J Clin Endocrinol Metab* (2019) 104(10):4427–40. doi: 10.1210/jc.2019-00481

48. Diaz-Perdigones CM, Munoz-Garach A, Alvarez-Bermudez MD, Moreno-Indias I, Tinahones FJ. Gut microbiota of patients with type 2 diabetes and gastrointestinal intolerance to metformin differs in composition and functionality from tolerant patients. *BioMed Pharmacother* (2022) 145:112448. doi: 10.1016/j.biopha.2021.112448

49. Tong X, Xu J, Lian F, Yu X, Zhao Y, Xu L, et al. Structural Alteration of Gut Microbiota during the Amelioration of Human Type 2 Diabetes with Hyperlipidemia by Metformin and a Traditional Chinese Herbal Formula: a Multicenter, Randomized, Open Label Clinical Trial. *mBio* (2018) 9(3). doi: 10.1128/mBio.02392-17

50. Song Y, Wu MS, Tao G, Lu MW, Lin J, Huang JQ. Feruloylated oligosaccharides and ferulic acid alter gut microbiome to alleviate diabetic syndrome. *Food Res Int (Ottawa Ont)* (2020) 137:109410. doi: 10.1016/j.foodres.2020.109410

51. Chen K, Wei X, Kortesniemi M, Pariyani R, Zhang Y, Yang B. Effects of acylated and nonacylated anthocyanins extracts on gut metabolites and microbiota in diabetic Zucker rats: A metabolomic and metagenomic study. *Food Res Int (Ottawa Ont)* (2022) 153:110978. doi: 10.1016/j.foodres.2022.110978

52. Davis-Richardson AG, Ardissone AN, Dias R, Simell V, Leonard MT, Kemppainen KM, et al. Bacteroides dorei dominates gut microbiome prior to autoimmunity in Finnish children at high risk for type 1 diabetes. *Front Microbiol* (2014) 5:678. doi: 10.3389/fmicb.2014.00678

Advantages of publishing in Frontiers

OPEN ACCESS
Articles are free to read for greatest visibility and readership

FAST PUBLICATION
Around 90 days from submission to decision

HIGH QUALITY PEER-REVIEW
Rigorous, collaborative, and constructive peer-review

TRANSPARENT PEER-REVIEW
Editors and reviewers acknowledged by name on published articles

Frontiers
Avenue du Tribunal-Fédéral 34
1005 Lausanne | Switzerland

Visit us: www.frontiersin.org
Contact us: frontiersin.org/about/contact

REPRODUCIBILITY OF RESEARCH
Support open data and methods to enhance research reproducibility

DIGITAL PUBLISHING
Articles designed for optimal readership across devices

FOLLOW US
@frontiersin

IMPACT METRICS
Advanced article metrics track visibility across digital media

EXTENSIVE PROMOTION
Marketing and promotion of impactful research

LOOP RESEARCH NETWORK
Our network increases your article's readership